Emulated Inertia and Frequency Support from Fast Acting Reserves

Rezkalla, Michel Maher Naguib

Publication date:
2018

Document Version
Publisher's PDF, also known as Version of record

Technical University of Denmark

Michel Maher Naguib Rezkalla

Emulated Inertia and Frequency Support from Fast Acting Reserves

Comparative assessment and experimental validation

Ph.D. Thesis, March 2018

Risø, Roskilde, Denmark

Center for Electric Power and Energy
Department of Electrical Engineering

DANMARKS TEKNISKE UNIVERSITET
Center for Electric Power and Energy (CEE)
DTU Electrical Engineering

Emulated Inertia and Frequency Support from Fast Acting Reserves

Syntetisk inerti og frekvensregulering fra hurtige reserver

Ph.D. Thesis, by Michel Maher Naguib Rezkalla

Supervisors:
Associate Professor Mattia Marinelli, Technical University of Denmark
Senior Researcher Henrik W. Bindner, Technical University of Denmark
Assistant Professor Kai Heussen, Technical University of Denmark

DTU - Technical University of Denmark, Risø - March 2018

Emulated Inertia and Frequency Support from Fast Acting Reserves

This thesis was prepared by:
Michel Maher Naguib Rezkalla

Supervisors:
Associate Professor Mattia Marinelli, Technical University of Denmark
Senior Researcher Henrik W. Bindner, Technical University of Denmark
Assistant Professor Kai Heussen, Technical University of Denmark

Dissertation Examination Committee:
Professor Poul Ejnar Sørensen (Chairman)
Department of Wind Energy, Technical University of Denmark, Denmark

Professor Kjetil Uhlen
Department of Electric Power Engineering, Norwegian University of Science and Technology, Norway

Professor Fabrizio Pilo
Department of Electrical and Electronic Engineering, University of Cagliari, Italy

Center for Electric Power and Energy (CEE)
DTU Electrical Engineering
Elektrovej, Building 325
DK-2800 Kgs. Lyngby
Denmark

Tel: (+45) 4525 3500
Fax: (+45) 4588 6111
E-mail: cee@elektro.dtu.dk

Release date: March 2018

Class: Public

Field: Electrical Engineering

Remarks: This thesis is presented to the Department of Electrical Engineering of the Technical University of Denmark in partial fulfillment of the requirements for the degree of Doctor of Philosophy.

Everything should be made as simple as possible, but not simpler.

— Albert Einstein

To my parents and my fiancée

Preface

This thesis has been prepared at the Department of Electrical Engineering, Technical University of Denmark in partial fulfilment of the requirements for acquiring the degree of Doctor of Philosophy in Engineering. This PhD project was funded by the EU FP7 project ELECTRA (grant: 609687) and the Danish Research Project ELECTRA Top-up (grant: 3594756936313).

This thesis summarizes the work carried out by the author during his PhD project, which started on 1st April 2015 and was completed on 30th March 2018. During this period, the author was hired by the Technical University of Denmark as a PhD student at the Center for Electric Power and Energy (CEE).

The thesis is composed of six chapters and eight attached scientific papers, six of which have been peer-reviewed and published, whereas the remaining two are currently in review.

Michel Maher Naguib Rezkalla
March 2018

Acknowledgements

As everything in life, the completion of this thesis was characterised by hard and long journey, full of ups and downs. However, I would have not arrived to this stage without the help of several people. I would like to express my sincere gratitude to all of them.

First of all, I am extremely grateful to my thesis supervisors Mattia Marinelli, Henrik W. Bindner and Kai Heussen for giving me this opportunity and guiding me through my PhD studies. I am grateful to Mattia for all his help, from the first day I arrived to Denmark. Thank you for all the scientific discussions and the time you spent for supporting me in my work, thanks for the help in adapting to life in Denmark and for the useful advice on where I should buy my wedding ring! I am also grateful to Henrik, thank you for being always available when needed, thanks for the very helpful scientific comments and for being a very good manager, which made my life much easier. I am also grateful to Kai, thank you for supporting me during the last three years and a special thanks for helping me at the beginning of my PhD to find and formulate the topic on which I worked during my PhD studies.

I would also like to thank all my colleagues at 776 at Risø- campus who made this journey very enjoyable and joyful. I am thankful to all of my colleagues, in particular Alex, Andreas, Angelina, Antonio, Carsten, Esteban, Eva, Haris, Helle, Oliver, Serafym and Tue. Thanks for the very friendly working environment with the weakly Friday breakfast, countless cakes and the traditional Danish Christmas party. I am thankful to all my colleagues for all the discussions we had, both work and non-work related. In addition, my special thanks go to Michael, my PhD companion who started his PhD two months before me on the same project. Thanks Michael for sharing the same office for the last three years and of for the nice and fun talks we had, thanks my friend!

Moreover, I want to thank all my friends in Denmark for all the support and the fun time we had together during the past years. A special thanks goes to Lucia, my Danish course companion, to my Danish friend Katrine and to my Egyptian friends from the Coptic church in Denmark, namely Andrew, John, Sherif and John.

Furthermore, I am very grateful to my parents Maher and Mervet, thanks for your support during my entire life! I am grateful to my brother Abanoub, my sister Marie and her husband Bassem, thanks for all your support and for the funny moments spent with my nephews Pierre and Daniel. I would like to thank also my uncle Sami, thank you for your words of encouragement.

Last, but not least, I am particularly grateful to my lovely fiancée Mariam, who shared with me the happy and stressful moments of my PhD. Thank you also for drawing some of the figure in this PhD thesis (e.g. Figure 2.3)!

Michel

Risø, Denmark, 2018

Table of Contents

List of Figures

List of Tables

Abstract

Environmental concerns are increasingly driving the evolution of the energy sector. A high share of renewable energy sources (RES) into the power system will potentially support the reduction of CO2 emissions; however, this presents considerable challenges for the power system operators. Currently, transmission system operators (TSOs) and distribution system operators (DSOs) are facing substantial change in the power system architecture, moving from centralized architecture, where electricity is generated from large power plants by conventional synchronous generators, centrally located and connected to the transmission network into a distributed architecture, where electricity is generated by distributed energy resources (DER) converter connected to distribution networks. The transition towards a higher share of DER replacing conventional power plants, brings to the DSO new responsibilities and also new challenges to TSOs. The TSOs are no longer able to monitor the total generation because the majority of DERs are connected to the distribution network. Therefore, new requirements on control and supervision functionality to be integrated into distribution management systems (DMS) need to be identified. Moreover, the displacement of conventional generation by inertia-less resources (i.e. converter connected) entails an upsurge in the requirement for balancing and system stabilization services. The reduction of system inertia is leading to faster rate of change of frequency (RoCoF), resulting in possible cascade tripping of embedded renewable generation and also higher frequency deviations (nadirs/zeniths), which can potentially lead to load shedding and, in the worst case, system collapse.

This thesis deals with the requirements and challenges that TSOs and DSOs are facing due to the high integration of distributed and inertia-less resources, and it sets out the various solutions. Some of the new requirements and related functions to be integrated into the DMS platform to cope with these challenges are summarized. This thesis focuses on the challenges and solutions of the reduction of system inertia and the potential benefits of specialized control schemes to utilize fast acting reserves (FAR) to compensate for the lack of inertia. State-of-the-art of control schemes and technologies that could potentially compensate for reduction in system inertia and assist the transition toward a RES based power system are presented and analyzed, emphasizing the benefits and drawbacks of each solution. The two main control schemes that will be analyzed during the course of the thesis are synthetic inertia control (SIC) (i.e. RoCoF based control) and fast frequency control (FFC) (i.e. frequency deviation based control).

A trade-off analysis between SIC and FFC in a converter dominated network employing energy storage systems is presented, using the power system simulation software PowerFactory. This aims to define the constraints and abilities of the two controllers to improve the frequency performance, in general, and limiting the RoCoF, in particular. Moreover, the potential benefits and drawbacks of providing such services from electric vehicles (EVs) are investigated and analyzed.

Experimental activities were conducted to validate the technical feasibility of series produced EVs to provide these frequency services, namely, SIC and FFC. Emphasis was placed on assessing the two controllers' ability to mitigate the RoCoF and improve the frequency performance, including

assessing several EVs' parameters, such as EVs'response time and EVs' accuracy in following the desired set-point.

Adopting the All Island Power System (AIPS) of Ireland as a test case, and employing the TSO's data and models, the ability of SIC and FFC to mitigate the RoCoF and compensate for the reduction in system inertia is investigated. Exploiting more than 700 simulated dispatches of the all island power system, a model based approach is proposed to quantify the relationship between FAR (employing SIC or FFC) and synchronous inertia. The application of this methodology will assist the system operator in increasing the penetration of converter connected resources while respecting the grid code constraint of maximum RoCoF.

Overall it is shown that SIC or FFC can help to mitigate the RoCoF. It was demonstrated that SIC does provide a slightly better performance in terms of RoCoF compared to FFC. Meanwhile, the FFC performed better in terms of frequency nadir and steady state values. Moreover, it was shown that SIC was more sensitive to time delays in low inertia systems, which can easily lead to system oscillation.

Resumé

Der sker store ændringer i energisektoren på grund af den øgede miljømæssige bekymring i samfundet. En stor andel af vedvarende energikilder (RES) i elsystemet kan potentielt understøtte reduktionen af CO2-udledninger, men den udgør en stor udfordring for elsystemets drift.

Faktisk står operatørerne af transmissionsnettet (TSO) distributionsnettet (DSO) over for en væsentlig ændring i strukturen af hele el-systemet. Det går fra en centraliseret arkitektur, hvor elektriciteten produceres på store kraftværker med konventionelle synkrone generatorer, centralt beliggende og forbundet med transmissionsnettet til en mere distribueret arkitektur, hvor elektricitet produceres af distribuerede energiressourcer (DER) der er forbundet til distributionsnettet via konvertere. Overgangen til et system hvor en højere andel af konventionelle kraftværker erstattes af DER, skaber nye ansvarsområder for DSO'en og nye udfordringer for TSO'en. TSO'erne er faktisk ikke længere i stand til at overvåge den samlede produktion, da størstedelen af DER er forbundet til distributionsnettet. Derfor er det nødvendigt at identificere hvilke nye krav der skal stilles til kontrol- og overvågnings-systemer, integreret i distributionsstyringssystemet (DMS). I takt med, at færre synkrongeneratorer er forbundet til systemet vil systemets samlede inerti blive reduceret, hvilket sætter meget højere krav til leverandørerne af balancerende og stabiliserende ydelser. Reduktionen af systemets inerti fører til hurtigere frekvensændring (RoCoF), hvilket resulterer i en mulig serie-afkobling af kraftværker, samt højere frekvensafvigelser (nadirs / zeniths), der potentielt fører til afkobling af forbrugere og i værste fald systemkollaps. Denne afhandling beskriver de krav og udfordringer, som TSO og DSO står overfor på grund af den store integration af distribuerede ressourcer med mindre inerti, og de mulige løsninger. Nogle af de nye krav og relaterede funktioner, der skal integreres i DMS-platformen for at klare disse udfordringer er her opsummeret. Afhandlingen fokuserer primært på udfordringerne og løsningerne ved reduktion af systemets inerti og de potentielle fordele ved specialiserede kontrolordninger til at udnytte hurtigvirkende reserver (FAR) til kompensation for den manglende inerti.

De mest moderne reguleringssystemer og teknologier, der potentielt kan kompensere for en reduktion af systeminerti og afhjælpe overgangen til et RES-baserede elsystem, præsenteres og analyseres under henvisning til fordele og ulemper ved hver løsning. De to vigtigste reguleringssystemer, der vil blive analyseret i afhandlingen, er syntetisk inerti (SIC) (dvs. RoCoF-baseret regulering) og hurtig frekvens regulering (FFC) (dvs. baseret på frekvensafvigelsen). En analyse af fordele of ulemper af SIC og FFC i et netværk domineret af enheder forbundet til el-nettet med en konverter og med net-forbundne batteri-systemer er lavet ved hjælp af simuleringsværktøjet PowerFactory. Det sigter mod at definere de to regulatorers begrænsninger og evner til at forbedre frekvensen generelt og særdeles til begrænsning af RoCoF. Desuden undersøges og analyseres de potentielle fordele og ulemper ved at levere sådanne ydelser med elbiler. Eksperimentelle aktiviteter blev udført for at validere den tekniske kunnen af serieproducerede elbiler til at levere de ovennævnte frekvensregulerings ydelser, SIC og FFC.

Der lægges vægt på at vurdere de to regulatorers evne til at minimere RoCoF og forbedre kvaliteten af frekvensen samt vurdere forskellige EV-parametre, såsom responstid og nøjagtighed i forhold til at følge den ønskede reference.

Ved at vælge Irlands el-system som test case og anvende af TSO'ens data og modeller er SIC og FFC evne til at afbøde RoCoF og kompensere for reduktionen i systeminertien undersøgt. Ved at udnytte 700 simulerede producerende enheder på hele øen foreslås en modelbaseret tilgang til at kvantificere forholdet mellem FAR (ved brug af SIC eller FFC) og synkron inerti. Anvendelsen af den præsenterede metode kan hjælpe systemoperatøren med at øge delen af konverter-tilsluttede ressourcer uden at bryde de tekniske forskrifter for begrænsning af maksimum RoCoF. Samlet set er det fundet, at både SIC og FFC kan hjælpe med at reducere RoCoF. Det blev påvist, at SIC giver en lidt lavere RoCoF i forhold til FFC. På den anden side viste FFC sig mere effektiv med hensyn til frekvens nadir og steady-state. Desuden blev det vist, at i systemer med lav inerti er SIC mere følsom overfor tidsforsinkelser, som kan føre til systemoscillation.

Acronyms

AIPS All Island Power System

CAES compressed air energy storage

DER distributed energy resources

DG distributed generators

DMS distribution management systems

DSM demand side management

DSO distribution system operator

EIC emulated inertia control

EMS energy management system

ESS energy storage system

EV electric vehicle

EVSE electric vehicle supply equipment

FAR fast acting reserves

FCR frequency containment reserves

FFC fast frequency control

FRR frequency restoration reserves

GIS load geographical information system

HQT Hydro-Quebec TransÉnergie

HVDC high-voltage DC

ICT information and communication technology

LSI largest single infeed

LV low voltage

PFC primary frequency control

PFR primary frequency reserve

PHS pumped hydroelectric storage

PV photovoltaic

RES renewable energy sources

RoCoF rate of change of frequency

RR replacement reserves

RTU remote terminal units

SC synchronous condensers

SCADA supervisory control and data acquisition

SD standard deviations

SFM single frequency model

SG synchronous generator

SIC synthetic inertia control

SOC state of charge

TSO transmission system operator

V2G Vehicle-to-Grid

VRB vanadium redox battery

VSM virtual synchronous machines

CHAPTER 1

Introduction

1.1 Background

The scientific evidence is now overwhelming: climate change is a serious global threat and it demands an urgent global response [5]. Climate change has the potential to raise average temperatures by over 5° C from pre-industrial levels. These changes would transform the physical and human geography of our planet, including how and where we live our lives. Climate change will affect the basic elements of life for people around the world, including access to water, food production, health, and the environment. Hundreds of millions of people could suffer hunger, water shortages, and coastal flooding as the world warms. CO_2 emissions can be reduced through increased energy efficiency and through the adoption of renewable energy resources, the so called clean energy. Many countries and regions are taking action already and the EU is among those with the most ambitious policies to reduce greenhouse gas emissions [5]. The 2030 framework proposes new targets and measures to make EU's energy system more secure and sustainable. This includes targets for reducing greenhouse gas emissions and increasing the use of renewable energies (e.g a renewable energy target of at least 27% of energy consumption in 2030) [6] Simultaneously, some countries have set an interim and more ambitious goal to reduce CO_2 emissions. For example, the current Danish government platform includes a target of at least 50% renewable energy by 2030 and a long term goal of a fossil-free economy, meaning that the entire energy supply, electricity, heating, industry and transportation is to be covered by renewable energy by 2050 [7].

The integration of renewable energy sources is growing at a tremendous pace. However, this development presents a number of challenges for system operators to maintain and operate the power system in a secure state. To understand the challenges of renewable energy integration and the relevance of this research project, it is important to understand how the electric power system is currently operated and how it is evolving. The following subsections will provide an overview of how the power system is traditionally operated, the effects of replacing conventional plant by renewable energy resources, and the system operator's changing roles.

1.2 The electric power system

Traditionally, electric power systems have been designed to follow consumption by generating electricity centrally through bulk power plants. The electricity is then transported through the high voltage transmission network and distributed to the consumers through the medium and low voltage distribution network, which is characterized by its unidirectional power flows, as shown in Figure 1.1. Among the most important entities in the present power system configuration are transmission system operator (TSO) and distribution system operator (DSO), who have pre-established roles to maintain and operate the power system in a secure state. TSOs are responsible for operating the power system in a secure state by maintaining a balance at all times between supply and demand.

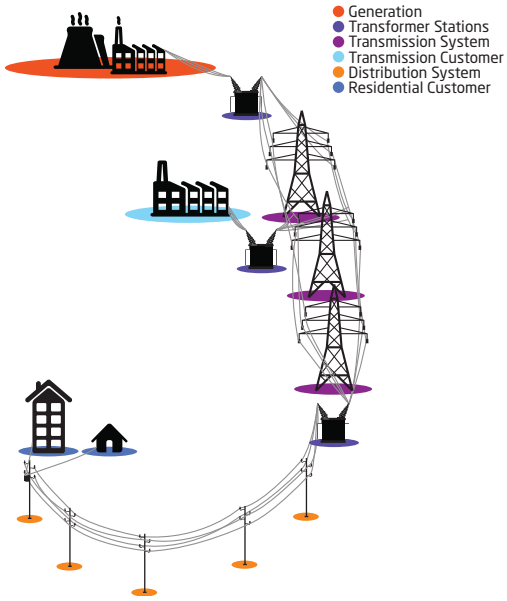

Figure 1.1: The traditional electric power system. Used with permission from the author in [1]

System frequency is used as a metric for evaluating imbalances between generation and consumption. To deal with these imbalances, TSOs must procure ancillary services that maintain the system frequency at nominal value to ensure stable and reliable power system operation [8]. The classification of frequency ancillary services varies among countries; however, it is generally divided into primary, secondary, and tertiary frequency control, as shown in Figure 1.2. Following a large disturbance, which causes the frequency to significantly deviate from its nominal value, and before the activation of ancillary services, the synchronous generators (SGs) releases the kinetic energy that is stored in their rotating masses as an inertia response. The system's total inertia is a physical characteristic of the system and it has played a fundamental role in limiting frequency changes caused by imbalances between supply and demand [9]. However, inertia response has always been considered as an inherent characteristic of the system and it is proportional to the number of connected conventional power plants and their inertia.

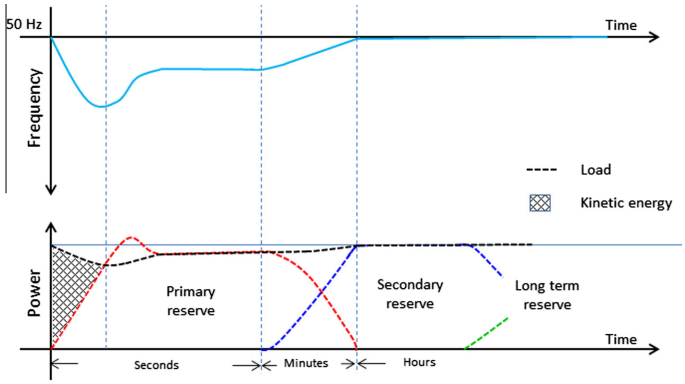

Figure 1.2: Primary, secondary, and tertiary control. Used with permission from the author in [2]

Primary frequency control occurs within the first few seconds following a change in system

frequency to ensure that the balance between consumption and production is restored, stabilizing the frequency close to, but deviating from nominal value. Primary reserve regulation is automatic and it is usually provided by large generators that are equipped with droop control capabilities, in which the power output change is proportional to the grid frequency deviations. Meanwhile, secondary frequency control is a slower control that is used to restore frequency to a nominal value following the stabilization of the frequency by means of primary regulation. Secondary frequency control is automatically actuated by the central grid controller and it is usually provided by generation or consumption units consisting of upward and downward regulation reserves [8, 10]. Finally, tertiary control is used for the relief of the secondary control reserve to restore a secondary control volume and they are usually manually activated.

While various terminology and implementation details (e.g. activation time frames) may be used in relation to frequency control among the different synchronous areas, the same control structure is valid. In the European synchronous area, primary, secondary, and tertiary control reserves are referred to as frequency containment reserves (FCR), frequency restoration reserves (FRR), and replacement reserves (RR), respectively [11].

1.3 Challenges introduced by converter connected resources

In recent years, the electric power system has started to face radical changes due to the high integration of distributed energy resources (DER), such as photovoltaic (PV) and wind turbines. For example, the total global wind power capacity by the end of 2016 was nearly 487 GW. Similarly, during 2016, at least 75 GW of PV capacity was added worldwide, which is equivalent to the installation of more than 31000 solar panels every hour. The global solar PV capacity totaled nearly 303 GW by the end of 2016 [12].

The reliability of the power system operation is threatened by the shift towards a high share of DER replacing conventional power plants. This leads to a new-generation of electrical power system, which is generally known as the smart grid. This system is characterized by the increased use of communication and information technology, and by producers of electric energy connected to the distribution grid [13], as shown in Figure 1.3.

The transition towards the smart grid brings new responsibility to the DSOs, in addition to new challenges to TSOs. For example, frequency ancillary services will be also provided by resources connected to the distribution grid. This will raise new control objectives from the DSOs's perspective and require new functionality in the distribution management systems (DMS), it will also require higher observability to provide effective support to the operator.

Moreover, the displacement of conventional generation by inertia-less resources (i.e. converter connected) entails an increasing upsurge in the requirement for balancing and system stabilization services. Conventional power systems rely on electricity generation from large rotating SGs. Due to the continuous exchange of energy between the rotating masses of the SGs and the grid, the dynamics of the grid frequency are limited and the frequency is maintained within an admissible range. Following a large disturbance, which causes the frequency to significantly deviate from its nominal value, the SGs release the kinetic energy that is stored in their rotating masses as an inertia response. Additionally, the SGs participate in primary and secondary frequency control by increasing/decreasing their active power generation [14]. The reduction of system inertia has two implications for system frequency stability, namely: 1) faster rate of change of frequency (RoCoF),

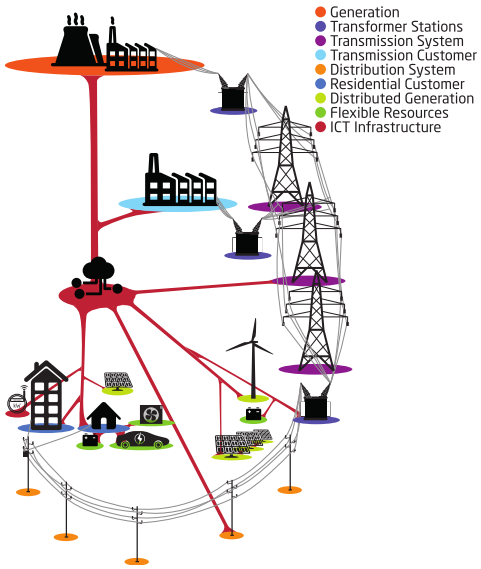

Figure 1.3: The future smart grid paradigm. Used with permission from the author in [1].

which results in possible tripping of grid components, especially embedded renewable generation, conventional generation pole slipping and cascade tripping; and, 2) higher frequency deviations (nadirs/zeniths), potentially leading to load shedding and, in the worst case, system collapse [15]. Moreover, the high volatility of renewable energy sources (RES) contributes to the frequency stability issue by changing the grid inertia over time and increasing the need for better planning due to higher uncertainty.

The growing number of electric vehicles (EVs) has concerned the DSOs. The uncertainty of EV driving patterns, high penetration levels, and charging in the distribution network could result in new system peaks and negative distribution system impacts, exceeding the load capacities of the distribution lines and transformers [16, 17]. Given that EVs are essentially battery storage devices with seconds range response time, the TSO can greatly benefit from EVs participation in frequency service provision.

The EU ELECTRA Integrated Research Program on Smart Grids has been established to reinforce and accelerate Europe's transition towards a clean energy system with a high share of renewable electricity production. ELECTRA proposes novel frequency and voltage control concepts to maintain and operate the power system in a secure state [18]. Within the ELECTRA project, the PhD project "Validation of decentralized and coordinated operation of frequency and voltage control systems in the control room", which is part of this thesis, was formed to focus on the challenges of system inertia reduction and its various solutions. Analytical investigation, simulations, and experimental field test validation were carried throughout the project to asses and validate the proposed solutions.

1.4 Research objectives

This thesis deals with the requirement and challenges that TSOs and DSOs are facing due to the high integration of distributed and inertia-less resources, including the various solutions. It focuses on synthetic inertia and fast frequency control services provided from fast acting reserves (FAR).

In this thesis, different power system models with different degrees of complexity have been used. Throughout this study, three main power system models have been used. First, a quasi mono-bus representative network that is useful for providing first analysis of small power systems' dynamics was used. Second, experiments were executed in the experimental infrastructure SYSLAB, which represents a small-scale low-voltage power system with a number of interconnected real power components. Finally, an equivalent model of the All Island Power System (AIPS) of the Republic of Ireland and Northern Ireland was used, which employs model, system parameters and dispatches provided by the Irish TSO EirGrid.

The main research question that this thesis seeks to answer is: **What are the effects of reduced system inertia on a secure power system operation? And, how can we compensate for this reduction?** This question can be divided into the following sub-questions:

[Q1] *What are the state-of-the-art of control schemes and technologies that could potentially compensate for the effects of the reduction in system inertia and assist in the transition toward a RES-based power system?*

The current transition toward high share of RES is altering the power system's characteristics, imposing various challenges to maintain and operate the power system in a secure state. One of these challenges is fast frequency dynamics and consequently faster RoCoF, due to the reduction in system inertia. A literature review is required to summarize the most prominent control approaches and technologies that are suitable to compensate for this reduction as well as emphasizing the benefits and drawbacks of each solution.

[Q2] *What are the properties of synthetic inertia and fast frequency control on the frequency dynamics?*

Future frequency ancillary services, such as synthetic inertia and fast frequency control, are gaining interest among system operators and power system components manufacturers, such as wind turbine manufacturers. Therefore, an investigation of the trade-off analysis of these control solutions, including their effects on the system's stability, is required. Moreover, it is of interest to analyze the technical limitations of the devices providing these services.

[Q3] *What are the capabilities and limitations of series-produced EVs in providing frequency services in terms of synthetic inertia and fast frequency control?*

Electric vehicles can represent an effective and distributed solution to enhance frequency stability due to their ability to respond quickly and their ability to provide a large amount of aggregated power units. Therefore, an investigation of how the system could benefit from this capability, including the possible detrimental impacts that it could have, is necessary.

[Q4] *How to asses the equivalent amount of synchronous inertia replaced by fast acting reserves (FAR)?*

FARs are seen as a possible solution that can improve the frequency dynamics. There is, however, a lack of clarity regarding the volume of FARs that can potentially compensate for the reduction in system inertia. During the dispatch phase, control room operators need to guarantee the availability of a minimum amount of inertia (i.e. synchronous or emulated inertia) to maintain and operate the system in a secure state. Therefore, a definition of the quantitative relationship between MW of FAR and MWs of inertia is required.

1.5 Thesis outline and research contributions

This thesis is organized in six chapters: an introduction, four self-contained technical chapters and a conclusion. The eight scientific core publications Pub. [A] through Pub. [H] are attached to this thesis. The main results are published in these scientific papers and they are referenced throughout this thesis as needed. However, they may also be read independently of this thesis. The description of each chapter is as follows.

Chapter 2 explains the current requirements and challenges that system operators are currently facing due to the high integration of inertia-less resources. It defines the analytical inter-dependency among synthetic inertia, fast frequency control, and frequency gradient, and it summarizes the various solutions and technologies that could potentially compensate for the reduction in system inertia. Moreover, new DMS functionality that could support system operators during the transition toward higher share of RES is discussed. This chapter includes contents of Pub. [A] and Pub. [B]

Chapter 3 focuses on the properties of synthetic inertia control (SIC) and fast frequency control (FFC) to improve the frequency dynamics, in general, and limit the frequency gradient, in particular, by employing energy storage to provide these services. Additionally, by exploiting the EVs, which are treated as distributed energy storage systems, this chapter presents the key requirements and capabilities of EVs to flexibly provide SIC and FFC. This chapter also includes several recommendations for overcoming the technical limitations. This chapter includes contents of Pub. [C], Pub. [D] and Pub. [E].

Chapter 4 focus on validating the technical feasibility of series-produced EVs to provide frequency support in terms of SIC and FFC through a set of field and laboratory experiments, which are presented in Pub. [F] and Pub. [G]. Moreover, this chapter investigates the impact of the system's characteristics, such as system inertia, primary frequency control reserves and EV's response, time on the frequency stability and the performance of the provided service.

Chapter 5 investigates the ability of mitigating the RoCoF by SIC and FFC in an equivalent model of the AIPS. This study employs an equivalent model of the Republic of Ireland and Northern Ireland power system, which is provided by the Irish TSO, and it uses simulated system dispatches. Additionally, this chapter focuses on implementing a methodology that can define the quantitative relationship between FAR (using SIC or FFC) and conventional inertia, characterizing each unit by an equivalent inertia value in MWs. although the proposed methodology has been tested on an equivalent model of AIPS, that does not limit its applicability on other systems because no direct connection between the equivalent model and the methodology is present. This chapter includes contents of Pub. [H].

1.6 List of publications

The relevant publications that are the core of this thesis are listed as follows:

[A] M. Rezkalla, M. Pertl and M. Marinelli, "Electric Power System Inertia: Requirements, Challenges and Solutions", in Springer Electrical Engineering, under review.

[B] M. Rezkalla, K. Heussen, M. Marinelli, J. Hu and H. W. Bindner, "Identification of Requirements for Distribution Management Systems in the Smart Grid Context", in *Power Engineering Conference (UPEC), International Universities.* Stoke on Trent, United Kingdom, Sep. 2015.

[C] M. Rezkalla, M. Marinelli, M. Pertl and K. Heussen, "Trade-off Analysis of Virtual Inertia and Fast Primary Frequency Control During Frequency Transients in a Converter Dominated Network", *in IEEE PES Innovative Smart Grid Technologies Conference Asia (ISGT).* Melbourne, Australia, 2016.

[D] M. Rezkalla, A. Zecchino, M. Pertl and M. Marinelli, "Grid Frequency Support by Single-Phase Electric Vehicles Employing an Innovative Virtual Inertia Controller", in *Power Engineering Conference (UPEC), International Universities.* Coimbra, Portugal, 2016.

[E] A. Zecchino, M. Rezkalla and M. Marinelli, "Grid Frequency Support by Single-Phase Electric Vehicles: Fast Primary Control Enhanced by a Stabilizer Algorithm", in *Power Engineering Conference (UPEC), International Universities.* Coimbra, Portugal, 2016.

[F] M. Rezkalla, A. Zecchino, S. Martinenas, A. M. Prostejovsky and M. Marinelli, "Comparison Between Synthetic Inertia and Fast Frequency Containment Control Based on Single Phase EVs in a Microgrid", in Applied Energy, vol. 210, pp. 764-775,2018.

[G] M. Rezkalla, S. Martinenas, A. Zecchino, M. Marinelli and E. Rikos, "Implementation and Validation of Synthetic Inertia Support Employing Series Produced Electric Vehicles", in CIRED - Open Access Proceedings Journal, vol. 2017, no. 1, pp. 1197-1201, 2017.

[H] M. Rezkalla, M. Marinelli, H. Qazi and J. O'Sullivan, "Augmenting System Inertia Through Fast Acting Reserve - A Power System Case Study with High Penetration of Wind Power", in *IEEE Transaction on Sustainable Energy*, under review.

The following publications have also been prepared during the course of my PhD study but have been omitted from this thesis because they are not directly related to the primary objective or they are partially covered by other presented papers.

Peer-reviewed journal papers

[I] A. M. Prostejovsky, M. Marinelli, M. Rezkalla, M. H. Syed and E. Guillo-Sansano, "Tuningless Load Frequency Control Through Active Engagement of Distributed Resources," IEEE Trans. Power Syst., 2017.

[J] M. Pertl, T. Weckesser, M. Rezkalla, K. Heussen and M. Marinelli, "A decision support tool for transient stability preventive control," Electr. Power Syst. Res., vol. 147, 2017.

[K] M. Pertl, T. Weckesser, M. Rezkalla and M. Marinelli, "Transient Stability Improvement: A Review and Comparison of Conventional and Renewable-based Techniques for Preventive and Emergency Control," Electr. Eng., 2017.

[L] E. Rikos, M. Syed, C. Caerts, M. Rezkalla, M. Marinelli and G. Burt, "Implementation of Fuzzy Logic for Mitigating Conflicts of Frequency Containment Control," CIRED - Open Access Proc. J., vol. 2017, no. 1, pp. 1206-1210, 2017.

Peer-reviewed conference papers

[M] M. Pertl, M. Rezkalla and M. Marinelli, "A Novel Grid-wide Transient Stability Assessment and Visualisation Method for Increasing Situation Awareness of Control Room Operators," in IEEE PES Innovative Smart Grid Technologies Conference Europe, 2016.

[N] V. T. Sæmundsson, M. Rezkalla, A. Zecchino and M. Marinelli, "Aggregation of Single-phase Electric Vehicles for Frequency Control Provision Based on Unidirectional Charging," in 52nd International Universities Power Engineering Conference (UPEC), 2017, pp. 1-6.

[O] M. Pertl, K. Heussen, O. Gehrke and M. Rezkalla, "Voltage Estimation in Active Distribution Grids Using Neural Networks," in IEEE Power and Energy Society General Meeting, 2016.

[P] M. Marinelli, M. Pertl, M. Rezkalla, M. Kosmecki, S. Canavese, A. Obushevs and A. Z. Morch, "The Pan European Reference Grid Developed in ELECTRA for Deriving Innovative Observability Concepts in the Web of Cells Framework," in International Universities Power Engineering Conference UPEC, 2016, pp. 1-6.

ELECTRA reports and deliverables

[Q] M. Marinelli, K. Heussen, T. Strasser, R. Schwalbe, J. Merino-Fernandez, S. Riano, A. M. Prostejovsky, M. Pertl, M. Rezkalla, J. Croker, B. Evenblij, V. Catterson and M. Chen, "ELECTRA Deliverable 8.1: Future Control Room Functionality: Demonstration of Visualisation Techniques for the Control Room Engineer in 2030", tech. report, The ELECTRA Consortium, 2017.

[R] K. Visscher, K. Heussen, J. Hu, S. Hänninen, M. Rezkalla, R. D'hulst, J. Merino,E. Rodríguez, E. Rikos and M. Kosmecki, "ELECTRA Deliverable 6.1: Functional Specification of the Control Functions for the Control of Flexibility Across the Different Control Boundaries ", tech. report, The ELECTRA Consortium, 2015.

[S] T. Strasser, A. Latif, F. Leimgruber, M. Syed, E. Guillo, G. Burt, M. Marinelli, A. Prostejovsky, M. Rezkalla, J. Merino, E. Rikos, R. Ciavarella, M. Nuschke, A. Coelho, A. Guagliardi, M. Cabiati, A. Morch, M. Degefa, S. Hanninen, R. Pasonen, "ELECTRA Deliverable 7.1: Report on the evaluation and validation of the ELECTRA WoC control concept ", tech. report, The ELECTRA Consortium, 2018.

CHAPTER 2

Requirements and State-of-the-Art

This chapter opens by highlighting the necessity of defining new functions and control algorithms because of the high share of distributed energy resources (DER), which will support the control room operators in maintaining and operating the power system in a secure state. Next, identification of new requirements for distribution management systems (DMS) in the smart grid context are summarized. Moreover, focusing on one of the new required functions within the DMS, namely emulated inertia control (EIC), a comprehensive summary of the state-of-the-art of the power system inertia requirements, challenges and solutions are presented. This chapter includes results of papers Pub. [A] and Pub. [B].

2.1 Overview

Power system operators need to maintain the power system in a secure state under increasingly complex conditions. The increasing share of renewable energy sources (RES) over the distribution and transmission grid, and the introduction of new components and services, such as energy storage, electric vehicles (EVs) and demand side management (DSM), introduce further complexity and challenges to the system's operation. The current monitoring, analysis and control room functionalities of transmission system operators (TSOs) and distribution system operators (DSOs) are unable to meet these increasingly diverse challenges. Consequently, it is necessary to enhance these functionalities to maintain and operate the power system in a secure and reliable manner.

The future power system, which is usually addressed as the smart grid, will accommodate a large share of weather dependent RES, such as wind and solar energy sources, which will be both centralized and distributed [19]. At the moment, one of the main challenges is the shift from centralized conventional power plants that are connected to the transmission grid, to distributed converter-based resources that are connected to the distribution grid. This paradigm shift imposes considerable challenges for today's control centers, where the TSOs is no longer able to monitor the total power generation through the energy management system (EMS) because a large share of the generation is connected to the distribution grid. Meanwhile, the DSOs are required to introduce new functionalities into the DMS to observe and control these units.

This chapter will present some of the future control room functionalities, in general, and the DMS future requirements, in particular. It also focuses and details one of the control centers functionalities that are required due to the of high share of converter-based resources, namely EIC. This function can be included in the DMS and/or the EMS.

2.2 Future control room functionality

The control centre has been described as the "central nervous system" of a power system [19]. It supervises, controls, optimizes and manages generation to balance electricity demand, and to ensure the system's security and reliability. Due to the increased flexibility within the power system, the increased market influence and automation, among others, significantly improved information and visualization techniques are essential for future control rooms [20].

The ELECTRA IRP EU FP7 project has investigated several innovative approaches for real-time operation to accommodate a higher share of DER [21]. One entire work package, namely WP8, focused on the development of the functionalities and requirements for future control rooms. The full results of the work package are presented in [20] and [22]. This package aims to derive new metrics and associated visualizations for future control rooms. The existing trends from vendors were examined by focusing on the experience in updating an actual DMS and in understanding the current landscape. Simultaneously, support for the final set of requirements for future control centers has been received from various European DSOs, who answered the questionnaire that was developed within WP8 and which described the experiences they are having with smart grid demo projects. The main requirements are categorized as follows:

1. **Distributed local controllers**

   From the various analyzed sources, the future power system will be characterized by the presence of distributed local controls that are applied on parts of the distribution network. The control room operator needs to have an overview of the status of the local controllers and a topological view of the distribution system with a clear indication of the network managed by each local controller.

2. **ICT network status**

   Due to the distributed nature of the control system and the importance of the information and communication technology (ICT) network in this frame, control centers will need to have access to the status of the ICT network. The status of the distributed controllers will include indicators related to the health status of the associated ICT infrastructure. In case of errors or the anomalous operation of one controller, the control room operator should be able to switch off the automatic controller and control the unit remotely. Further, he or she should be able to access the controller input/output data useful to diagnose the controller and to apply corrective actions in the event of malfunction. When employing adaptive control algorithms, the operator should be informed of the currently active mode and they should be alerted in case of any change in the control mechanisms.

3. **Distributed resource flexibility**

   The direct involvement of flexible regulating resources in the network management will require the control systems to interact with them by exchanging measurements and set-points. The control room operators need to be aware of the forecast and actual behaviour of the connected resources and the available flexibility. Therefore, a set of observables for each controlled area should be made available for the operator, including load and generation forecasts in addition to available flexibility in terms of inertia, active and reactive power

4. **System architecture and modularity**

   In the forecast dynamic evolution of the future energy scenarios, and with the increasing involvement of new services, resources, and actors in the control of the power system, it is crucial to enable fast and seamless upgrading of control centers. Consequently, open and modular control room architectures are highly recommended. This will allow an agile integration of new applications and/or visualization modules to replace the existing ones. Similarly, standard protocols and interfaces must be used to facilitate the maintenance and update of the various applications.

2.3 Requirements for control room management systems

Controlling many small and distributed generation units instead of controlling few large generation units is a considerable challenge. The system has to be kept stable and balanced using a centralized control action, as it is currently from TSOs. In this case, an advanced ICT infrastructure with a huge amount of data to be centrally transmitted to the TSO will be needed. An alternative solution is the transition towards distributed and decentralized control actions where distributed units could be locally or remotely controlled. System operators need to address these challenges. Meanwhile, increased collaboration between TSO and the various DSOs needs to be established because many of the DER units are connected to the distribution grid but are not sufficiently observed. When implementing a distributed architecture, it is expected that the DSOs will also be responsible for local active power balancing and voltage control, and will share some of the TSOs's roles. Therefore, it is expected that there will be a core change in the TSOs and DSOs control rooms, in general, and in the EMS and DMS, in particular, to better serve the new requirements. Figure 2.1 presents a graphical representation of how the DMS and EMS are expected to change. In the following, some of the current DMS's functionalities are presented, including some of the future requirements that could also be included in the EMS.

2.3.1 DMS functionalities

DMS coordinates real-time functions within the distribution network with the non-real-time (manually operated devices) information needed to properly control and manage the network on a regular basis. The key to a DMS is the organization of the distribution network model database, access to all supporting ICT infrastructure, and providing the applications that are necessary to populate the model and support the other daily operating tasks. DMS functionalities can be divided into the following three categories, as shown in Figure 2.2.

1. System monitoring,
2. Control actions,
3. Decision support.

System monitoring provides an accurate state of the system using a significant number of real-time and near real-time information about the current status. Real-time information includes data from remote terminal units (RTU) in substations and feeders. Near real-time information includes the measurement equipment (e.g. distribution substation transformers, load tap changers and distributed generating resources).

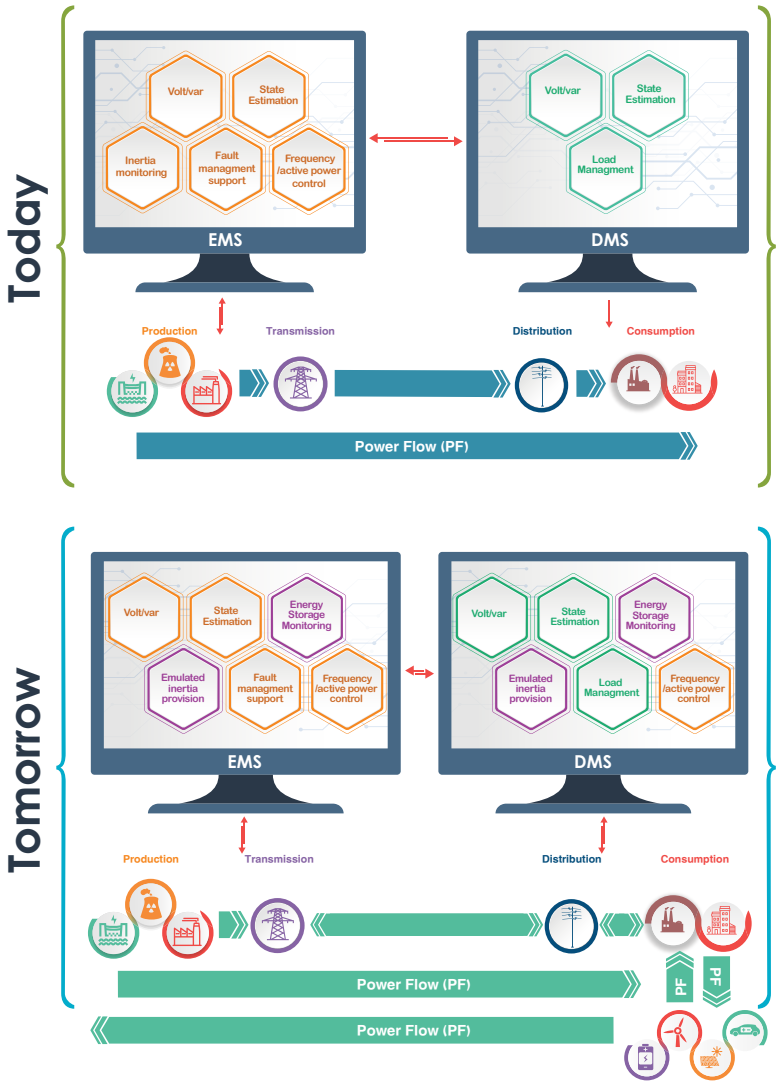

Figure 2.1: DMS and EMS's current and future requirements

The control action is able to control the power system apparatus that is located at distribution substations and field locations. The DMS platform makes available different control actions, such as automated control and operator control. The automated control action is realized directly by the DMS without the need for operator intervention, for example opening a switch breaker to interrupt a fault. Meanwhile, the operator control functions can be divided into two categories: remote control and manual control. Remote control allows the operator to remotely control the various apparatus using the supervisory control and data acquisition (SCADA) system. Manual control enables the operator to call the field crew to open or close a switch that is not remotely controlled [23]. Decision support provides the operator with a set of solutions to enhance the system's reliability and efficiency. This provides decision support solutions and also appropriate control actions.

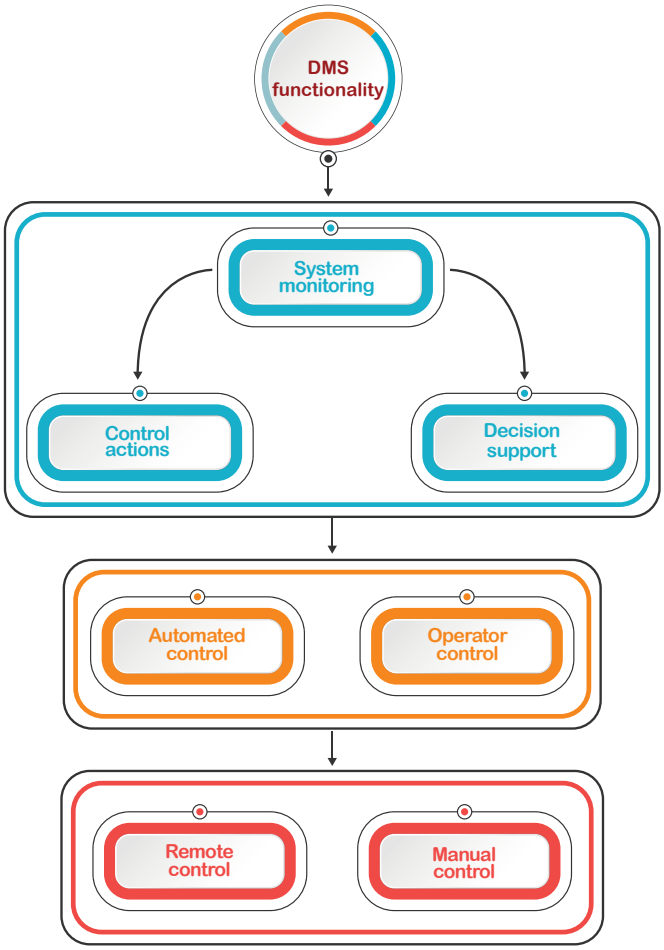

Figure 2.2: DMS functionalities

The DMS platform is provided by various vendors with different functions. The common and main functions can be regrouped under the previously mentioned categories:

1. System monitoring: State estimation, Power flow.
2. Control actions: Volt / Var control.
3. Decision support: Fault management and system restoration, Short circuit analysis, Load management.

2.3.2 DMS future requirements

Based on different EU projects, it is expected that by 2030 between 52% and 89% of electricity production will be generated by renewable energy resources, mainly connected to the distribution grid [24, 25]. To provide solutions for the different challenges that DSOs are facing today, advanced DMS functions are needed. Figure 2.3 presents some of the current and future requirements to be integrated into the DMS.

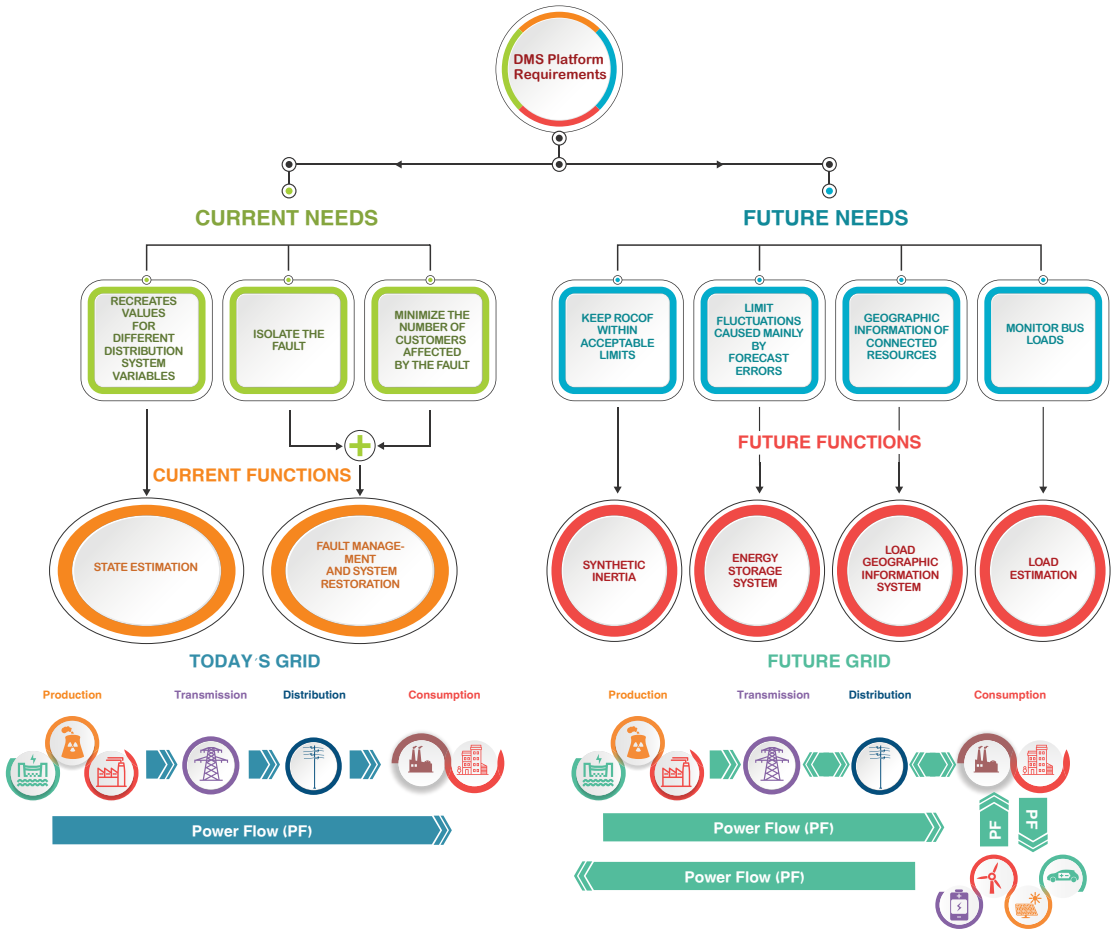

Figure 2.3: DMS current and future requirements.

In the following, an overview of the different functions to be integrated into the DMS are presented.

1. **Emulated inertia control:**

   The system inertia in the power system limits frequency fluctuations after a disturbance, keeping the rate of change of frequency (RoCoF) within acceptable limits. The system RoCoF is mainly limited by the amount of kinetic energy that is stored in the rotating mass at conventional power plants. Due to the high integration of converter connected resources replacing conventional plants, system operators are currently facing many different challenges in maintaining the RoCoF within tolerable values, leading in some cases to cascade tripping of DER. Various system operators, such as EirGrid and National Grid, have identified this issue to be of a critical significance and they have initiated mitigating measures and established new requirements [26, 27]. Wind turbine manufactures, such as General Electric and ENERCON, have started to integrate controllers on modern wind turbine generators to emulate the inertia response [28, 29]. Therefore the DMS should include a new function to provide the operator with the available amount of inertia response and also the capability of activating emulated inertia services.

2. **Energy storage monitoring:**

   Electrical storage prices are projected to drop according to the recommendations of the European energy storage technology development road-map [30]. Therefore, energy storage will become a cost effective solution for dealing with the power fluctuations that are mainly caused by forecast errors and renewable resources intermittency, they can also offer ancillary services. The DMS should provide the operator with the energy storage schedules, location, and the related energy prices in such a way to enable the operator to activate the desired service from the desired energy storage.

3. **Load estimation:**

   Because the distribution system was mainly passive, there was no need to measure and monitor the different bus loads. Nowadays, with the integration of active consumers, such as EVs and residential photovoltaic (PV) systems, load estimation and forecasting has become a complicated but a more fundamental function for operational planning and real time control of the grid. Hence, advanced ICT and new measurement devices need to be installed and integrated within the DMS platform to support the load estimation function.

4. **Load geographical information system:**

   The high share of RES that is directly connected to the distribution grid requires the DSOs to know the location of the DER units and to identify any vulnerabilities that might cause outages. The load geographical information system (GIS) can serve as a solution for this purpose. It can also assist distribution utilities in determining the right location for the installation of new RES and new devices, such as smart grid sensors and smart meters.

2.4 Electric power system inertia and grid requirements

Conventional power systems rely on electricity generation from large rotating synchronous generators (SGs). Due to the continuous exchange of energy between the rotating masses of the SGs and the grid, the dynamics of the grid frequency are limited and the frequency is maintained within an admissible range. Following a large disturbance, which causes the frequency to significantly deviate from its nominal value, the SGs releases the kinetic energy that is stored in their rotating masses as an inertia response.

Traditionally, inertia response has not been considered to be an ancillary service but has instead been considered as a natural characteristic of the power system. Due to the high integration of converter connected resources, which replace SGs, several TSOs in different countries have begun to recognize the value of the inertia response that can be provided by wind power plants, synchronous condensers, and emulated inertia [31–34].

To better comprehend the role of system inertia, Figure 2.4 shows how the system frequency could change after a contingency event in high and low inertia cases. The key parameters involved are: 1) RoCoF, 2) frequency nadir, and 3) steady state frequency.

Because the capacity of the primary frequency reserve (PFR) is the same in both inertia cases, the steady state frequency after the event settles at the same value. However, the lower inertia in the system exhibits a lower frequency nadir and a faster RoCoF.

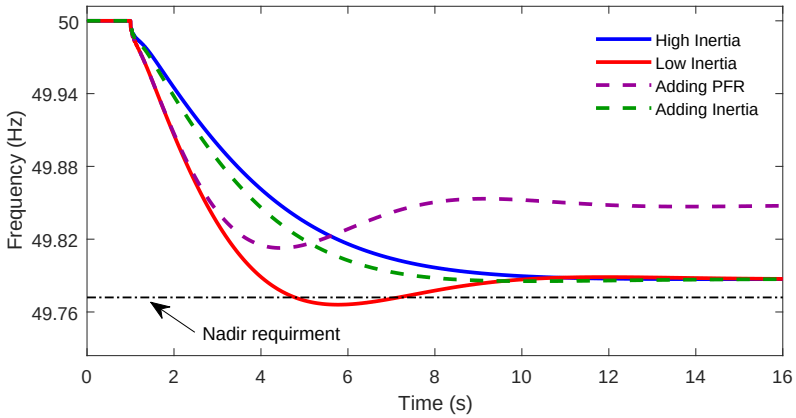

Figure 2.4: Effects of lower inertia on system frequency performance

To maintain and operate the power system in a secure state, the three parameters that characterize the system frequency should be constrained to avoid further implications, such as load shedding, cascade tripping, and, in the worst case, system collapse. The secure operation area for a given operating point can be represented by considering the previously mentioned frequency constraints. The authors in [3] represent the secure operation area by combining the PFR and inertia requirements, as shown in Figure 2.5. The secure area is delimited by the maximum allowed RoCoF (vertical line), the steady state frequency requirement (horizontal line), and the frequency nadir (red curve).

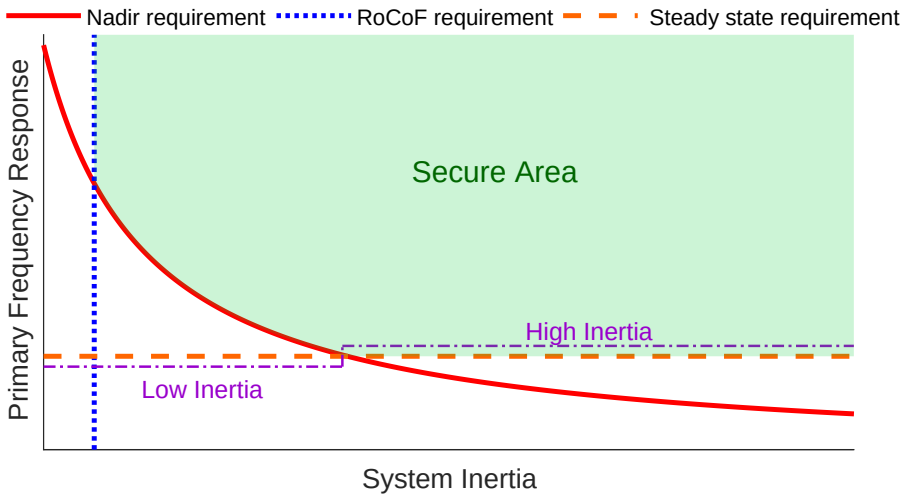

Figure 2.5: Frequency response requirements, adopted from [3]

Figure 2.5 shows that for high inertia cases, the PFR requirement is prevalent on the frequency nadir. In fact, due to the high inertia and the PFR reserve that is required to satisfy the steady state limit, the frequency nadir constraint will automatically be respected. This is also shown by the blue curve in Figure 2.4, where the steady state frequency is lower than the frequency nadir. In other words, due to the high inertia, the steady state requirement is reached before the nadir constraint.

Nevertheless, moving towards low inertia system, the frequency nadir requirement starts to dominate on the steady state requirement. This requirement can be respected by acting on both

PFR and/or system inertia, as shown by the dashed curves in Figure 2.4. Indeed, the frequency nadir can be improved by adding PFR (purple dashed curve) and/or by augmenting system inertia (green dashed curve). The lower the system inertia, the faster the frequency will decline following an event (e.g. the loss of a generator). Hence, a faster primary reserve response is needed. In contrast, in high inertia grids, slower-acting primary reserves are adequate to cope with the imbalance. Figure 2.5 also shows that for low inertia cases, the RoCoF requirement starts to dominate on the frequency nadir. This is an indicator of how the grid requirements are evolving towards a new paradigm due to the high penetration of inertia-less resources.

2.4.1 Grid requirements

From the system operator's perspective, the reduction of system inertia has two implications with regards to system frequency stability:

1. Faster RoCoF increases the likely-hood of tripping of grid components. In particular, embedded renewable generation.
2. Higher frequency deviations (nadirs/zeniths) potentially leading to unintentional load shedding.

Various system operators have identified these issues to be of critical significance and they have consequently initiated mitigating measures and established new requirements. In the following, an overview of some of the new requirements and grid code modifications is presented.

National Grid, which is UK's TSO, started to procure fast reserves to provide the rapid delivery of active power through either increased output from a generator or the reduction of the demand to control frequency changes [27]. The applied control mechanism is a frequency deviation based control, and it is further addressed in this thesis as fast frequency control (FFC).

EirGrid, the Republic of Ireland's TSO , has proposed a RoCoF modification in the grid code to facilitate the delivery of the 2020 renewable targets while maintaining operational security on the power system. Generators are required to withstand a RoCoF event of 1 Hz/s over 500 ms instead of 0.5 Hz/s [35]. Within the DS3 program and the RoCoF alternative studies, EirGrid and SONI (TSO of Northern Ireland) investigate the deployment of synchronous and non-synchronous inertia to maintain the RoCoF at 0.5 Hz/s for a non-synchronous penetration of up to 75 % [26]. EirGrid and SONI have established a minimum value of rotational kinetic energy as an operational constraint during the dispatch phase, namely 20000 MWs [36]. The total rotational energy of the system, which is generally addressed as the system inertia floor [37], is defined as the sum of each machine's rated power multiplied with the relative inertia constant and can be written as:

$$E_{kin}^{sys} = \sum_{i=1}^{n} H_i S_{r,i} \tag{2.1}$$

where H_i is the inertia constant of the i-th generator, $S_{r,i}$ is the rated apparent power of the i-th generator, E_{kin}^{sys} is the total rotational kinetic energy of the system and n is the number of generators.

The Hydro-Quebec TransÉnergie (HQT)'s transmission connection requirement stipulates in detail that wind power plants must be equipped with an inertia emulation system. HQT is now in the process of procuring and validating the manufacturers' models integrating inertia emulation features [38, 39]. This control mechanism is a RoCoF based control and is addressed further as synthetic inertia control (SIC).

2.4.2 Synchronous inertia and mathematical background

Traditionally, the total inertia of a power system was determined by the large rotating masses of conventional power plants; that is, the generator and turbine connected to the same shaft. Due to the synchronous coupling of the machines with the grid, their rotational speed (i.e. ω_m) was linked with the angular velocity of the electromagnetic field (i.e. ω_e). During a disturbance that causes an imbalance between the two opposing torques, the net torque on the rotor is different from zero and this leads to an acceleration or deceleration according to the electro-mechanical swing equation:

$$J\frac{d\omega_m}{dt} = T_m - T_e = T_a \tag{2.2}$$

where J is the combined moment of inertia of the generator and the turbine, T_m and T_e are the mechanical and electrical torque, respectively, and T_a is the acceleration/deceleration torque.

SGs are characterized by their inertia constant H, which is defined as the kinetic energy E_{kin} that is stored in the rotating mass at rated speed, divided by the machine rating power S_r, as follows:

$$H = \frac{E_{kin}}{S_r} = \frac{J\omega_{m,0}^2}{2S_r} \tag{2.3}$$

where $\omega_{m,0}$ is the rated mechanical angular velocity.

$\omega_e = p\omega_m$, where p is the number of pole pairs. Assuming p=1, equation (2.2) and (2.3) can be reformulated as:

$$P_m - P_e = \omega_m \frac{2HS_r}{\omega_{m,0}^2}\frac{\mathrm{d}\omega_m}{\mathrm{d}t} \tag{2.4}$$

where ω_e is the angular velocity of the electromagnetic field and P_m and P_e are the mechanical and electrical power, respectively.

For limited angular velocity variation, one can assume $\omega_m = \omega_{m,0}$, thus (2.4) can be rewritten as:

$$P_m - P_e = \frac{2HS_r}{\omega_{m,0}}\frac{\mathrm{d}\omega_m}{\mathrm{d}t} \tag{2.5}$$

Assuming that P_m is constant and that the frequency regulation is only from the load side, then one can consider that P_e is composed of frequency dependent loads (P_D), devices participating in FFC (P_{FFC}) and devices participating in SIC (P_{SIC}):

$$P_e = P_D + P_{FFC} + P_{SIC} \tag{2.6}$$

Where each is composed by a base value and frequency dependent value:

$$P_D = P_{D_0} + K_D(\omega_e - \omega_{m,0}) \tag{2.7}$$

$$P_{FFC} = P_{FFC_0} + K_{FFC}(\omega_e - \omega_{m,0}) \tag{2.8}$$

$$P_{SIC} = P_{SIC_0} + K_{SIC}\frac{\mathrm{d}\omega_e}{\mathrm{d}t} \tag{2.9}$$

P_{D_0}, P_{FFC_0} and P_{SIC_0} represent the base electric power in steady state and addressed further as $P_{e_0} = P_{D_0} + P_{FFC_0} + P_{SIC_0}$. K_D is a damping factor, which considers the electrical loads that change their active power consumption due to frequency changes. $K_{FFC} = K_{FFC}(t - t0)$ is the FFC proportional control coefficient. $K_{SIC} = K_{SIC}(t - t0)$ is the SIC proportional control coefficient. K_{FFC} and K_{SIC} are represented as function of the time to represent the time required

from those devices to get activated (i.e. time delay). Therefore, the electric power P_e can be expressed as:

$$P_e = P_{e_0} + (K_D + K_{FFC})(\omega_e - \omega_{m,0}) + K_{SIC}\frac{\mathrm{d}\omega_e}{\mathrm{d}t} + \Delta P_e \tag{2.10}$$

where ΔP_e is the perturbation and in the steady state the P_m is equal to P_{e_0}.

The swing equation can be reformulated as:

$$\frac{2H\frac{\mathrm{d}\omega_e}{\mathrm{d}t}}{\omega_{m,0}} = -(K_D + K_{FFC})(\omega_e - \omega_{m,0}) - K_{SIC}\frac{\mathrm{d}\omega_e}{\mathrm{d}t} - \Delta P_e \tag{2.11}$$

Solving the differential equation (2.11) yields:

$$\omega(t) = \omega_{m,0} + \left(\frac{e^{-\frac{(K_D+K_{FFC})\omega_{m,0}}{K_{SIC}\omega_{m,0}+2HS_r}t}}{K_D + K_{FFC}} - \frac{1}{K_D + K_{FFC}}\right)\Delta P_e \tag{2.12}$$

$$\frac{\mathrm{d}\omega(t)}{\mathrm{d}t} = -\omega_{m,0}\frac{e^{-\frac{(K_D+K_{FFC})\omega_{m,0}}{K_{SIC}\omega_{m,0}+2HS_r}t}\Delta P_e}{k_{SIC}\omega_{m,0} + 2HS_r} \tag{2.13}$$

It can be observed that both FFC and SIC affect the RoCoF variation during the transient. This turns out to be a complex time-variant term because of the response time of FFC and SIC and the power ramp-rate limitations of the used resource (e.g. battery ramp-rate). Nevertheless, the presented swing equation shows that mitigating the impact of power imbalances in terms of RoCoF can be achieved by increasing the system rotational inertia H and/or employing fast reserves with EIC approaches.

2.5 Emulated inertia control

Emulated inertia control approaches can be distinguished into three categories, namely: virtual synchronous machines (VSM), SIC and FFC. Figure 2.6 presents an overview of the different solutions that are capable in mitigating the RoCoF.

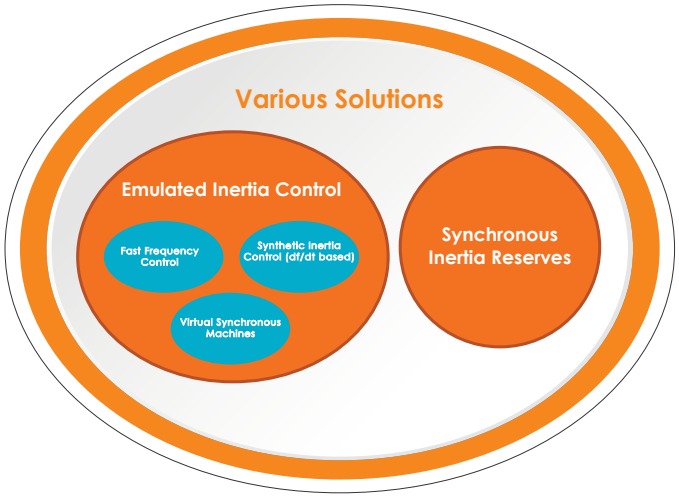

Figure 2.6: Various solutions that are capable of mitigating the RoCoF

Energy resources connected to the grid by means of power electronics could provide artificial inertia if the active power absorbed or generated is achieved through a control strategy that is based

on the frequency variation over time ($\frac{\Delta f}{\Delta t}$), which emulates the synchronous inertia behaviour. Emulated inertia is a combination of control algorithms, renewable energy resources, energy storage systems and power electronics that emulate the inertia of a conventional power system [40]. The general concept of the EIC is presented in Figure 2.7. The core of the system is the emulated inertia algorithm, which varies among the different solutions, based on the application and the desired level of model sophistication [41]. Some typologies try to mimic the exact behaviour of the SG through a detailed mathematical model that represents the SG's dynamics, which are generally addressed as VSM. Meanwhile, other approaches have tried to simplify this by using just the swing equation, which is further indicated as SIC.

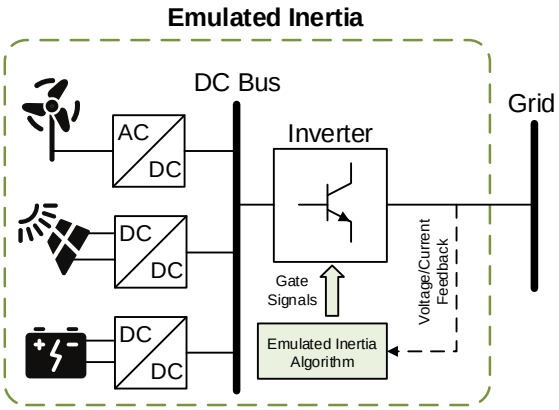

Figure 2.7: Emulated inertia concept

2.5.1 Virtual synchronous machines

The first proposal of a VSM was published by Beck and Hesse in 2007, who labeled as VISMA [42]. The underlying idea behind the VSM concept is to emulate the essential behaviour of a real SG by controlling a power electronic converter. The inertia emulation is a common feature for every VSM control scheme and it is based on the desired degree of accuracy in reproducing the SG dynamics, while additional aspects can be included or neglected (e.g transient and sub-transient dynamics). If the purpose of VSM is to accurately replicate the dynamic behaviour of a SG, then a full order model of the SG has to be included in the converter control system, which results in a 7^{th} order model [43, 44]. An example of a VSM type is presented in Figure 2.8 [45, 46].

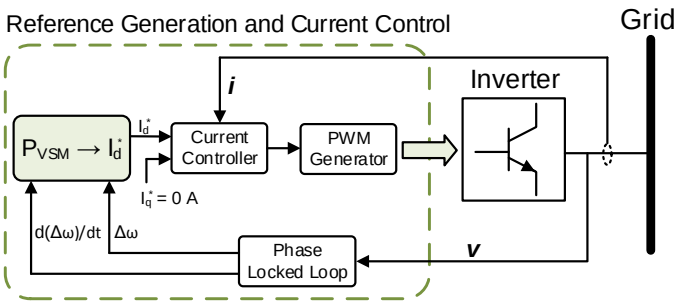

Figure 2.8: **V**irtual **s**ynchronous **m**achine type

Various control schemes for VSM, which represents the interface between the SG models and the power electronic converter, have been presented and discussed in the literature [41–44, 47]. The

control schemes proposed in literature can be categorized into two main groups based on the nature of the output reference from the SG model, namely: voltage reference and current reference models.

- **Voltage reference**: This control scheme is configured to provide a voltage reference output [48]. If a reduced order model of the SG is applied, then the power flow will be mainly related to the inertia emulation and the phase angle resulting from the swing equation. However, protections can be implemented at the hardware level or as parallel loops, over-riding the references from the VSM; however, their interaction with the inertia emulation and the resulting behaviour can be difficult to predict [47].
- **Current reference**: This control approach generates a current reference. This scheme allows the implementation of high order electrical models for the SG [42]. Nevertheless, in practical implementations, this scheme can lead to numerical instability, especially with high order SG models [49].

2.5.2 Synthetic inertia control

The inertia response can be also emulated by tracking the RoCoF and representing the SG only by the swing equation, as shown in (2.9). The control structure is shown in Figure 2.9-a and is only emulating the inertia effect with respect to the response to changes in the frequency gradient. A key parameter in this controller is the RoCoF measurement, which will be discussed in further detail later on.

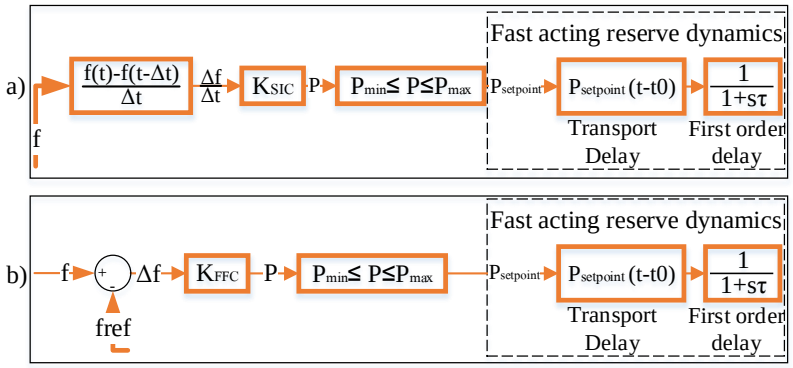

Figure 2.9: a) SIC control diagram, b) FFC control diagram

2.5.3 Fast frequency control

Fast frequency control is frequency deviation based control. It employs the same control mechanism as the currently applied primary frequency control (PFC) to conventional power plants, which is generally achieved using droop controllers, so that governors operating in parallel can share the load variation according to their rated power [4]. The frequency variation, $\Delta f = f - f_{nom}$, which is referred to the nominal frequency of the system, is therefore given as a function of the relative power change ΔP, as reported to the nominal machine power, as shown in Figure 2.10 and mathematically expressed as follows:

$$R = -\frac{\Delta f / f_{nom}}{\Delta P / P_{nom}} \tag{2.14}$$

where R is generally addressed as speed regulation or droop. However, the governors' dynamics (e.g. time response and ramping rate) limit the PFR's capability in improving the RoCoF. By employing fast acting reserves (FAR) such as energy storage, it is possible to mitigate the RoCoF by applying the same control approach as in PFC [50]. The FFC control diagram is presented in Figure 2.9-b and (2.14) can be rewritten as:

$$R = \frac{1}{K_{FFC}} = -\frac{\Delta f / f_{nom}}{\Delta P / P_{nom}} \tag{2.15}$$

where K_{FFC} is the proportional control's gain value.

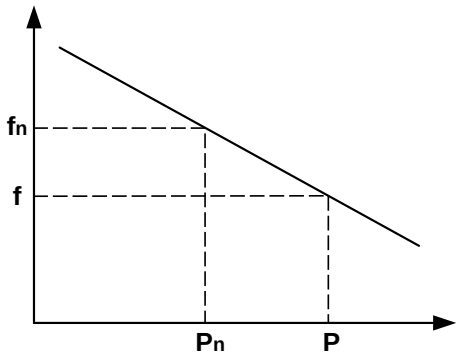

Figure 2.10: Frequency control droop characteristic

Table 2.1 highlights the key features and weaknesses of the various inertia control schemes previously presented.

Table 2.1: Overview of the various control schemes

Control schemes	Key features	Weaknesses
VSM	• Accurate representation of SG model • Frequency derivative not required • Black-start capability	• Can lead to numerical instability • Protections of the voltages and currents of the converter cannot be easily included
SIC	• Simple implementation compared to VSM	• Frequency derivative required • No black-start capability • System susceptible to noise
FFC	• Control type similar to conventional droop control in SGs • Local control (i.e. communication-less) • Stable performance	• Slow transient compared to the previous solutions • No black-start capability

2.5.4 Key parameters and challenges

Emulated inertia services are mainly characterized by the controller and the device dynamics. Different parameters can radically change the units response and can also present a challenge in

applying EIC and, therefore, limit their ability in delivering such services. The key parameters can be divided into four groups: 1) signal measurement, 2) response time, 3) deadband and 4) quantitative relationship between MW and MWs.

2.5.4.1 Signal measurement and processing

Conventionally, utilities have used the speed of SGs as a proxy for the grid frequency because it is relatively easy and accurate to measure. In contrast, converter connected resources delivering frequency support and also protection relays (e.g. under-frequency and RoCoF relays) need to measure the frequency directly from the grid. In the following, an overview of the most common methods to measure the system frequency and the RoCoF, including the associated key challenges, are presented:

- **Frequency measurement:** The system frequency indicates the dynamic balance between power generation and consumption, and it is measured from voltage or current signals, which originate from the synchronous machines whose rotating speed are proportional to the frequency of the generated voltage. The zero crossing algorithm which uses a pulse counting between zero crossings of the signal was the mostly commonly adopted method [51]. Nowadays, with the technological progress in microprocessors and cheaper computational power, many numerical methods for frequency measurement are applied and proposed (e.g. digital Fourier transformation, least square optimization, artificial intelligence etc.) [52–57] Most frequency estimation algorithms employ a window of data to derive the frequency, which causes estimation delay because the frequency is time-varying. On the one hand, a small window of data will reduce the estimation delay while, on the other hand, it reduces the measurement accuracy due to the presence of noise and harmonics. One can see that frequency measurement is quite a challenging task and measurement errors or latency can lead to malfunction of protection or control schemes.

- **RoCoF measurement:** The RoCoF measurement is one of the most critical parameters in delivering synthetic inertia. The RoCoF is the time derivative of the power system frequency (df/dt), which varies in function of the chosen measurement window. A key issue in the measurement of RoCoF across the system is that the frequency measured at different points in the system can vary significantly under transient conditions. To obtain a consistent system wide measurement of RoCoF, the electrical transients need to be removed from the analysis and only the mechanical transients on the system should be considered [37]. By extending the measurement window, the electrical transients can be removed from the RoCoF measurement, allowing for a more consistent system RoCoF to be determined [58]. Meanwhile, relatively large measurement windows might also eliminate the mechanical transients leading to false RoCoF values. Figure 2.11 illustrate the effect of using different measuring windows on the RoCoF value. For example, employing a measuring window of 100 ms, the calculated RoCoF is 2.1 Hz/s versus 0.9 Hz/s for a 500 ms measuring window. Therefore, the chosen measuring window, over which the RoCoF is calculated, is just as important as the RoCoF value itself.

  This issue is also of concern for various system operators because the DERs employs protection schemes for loss-of-mains to ensure that, should a part of the distribution network become islanded from the rest of the distribution system, that there is no generation left operating on that local system, keeping it live [59]. Many of these schemes utilize under and over-frequency relays, in addition to RoCoF relays.

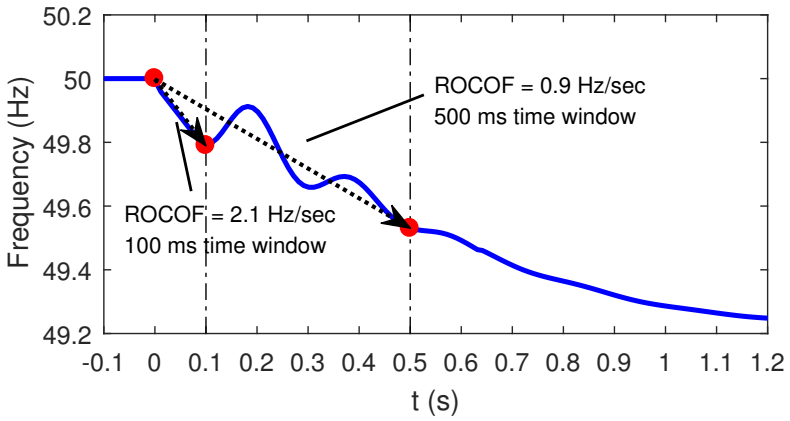

Figure 2.11: Illustration of frequency change and the effect of using different measuring windows

From the TSO perspective, "false" RoCoF values that are influenced by the electrical transients might lead to unintended cascade tripping of distributed energy resources connected by means of RoCoF relays [60, 61]. Moreover, different studies have shown that commercially available RoCoF relays from different manufacturers respond differently to the same event, even when they are configured with the same settings [62–64]. This phenomenon is most likely due to the different measurement techniques that are employed by these relays.

Generally, the grid code establishes the required RoCoF relays' characteristics (e.g. measurement window and threshold), which varies among countries. For example, the Irish grid code defines 1 Hz/s as the RoCoF relays' threshold measured over 500 ms moving window. EirGrid determined that 1 Hz/s would be sufficient to cover for the loss of the current largest single infeed (i.e. East-West interconnector exporting 500 MW) [59].

2.5.4.2 FAR response time

The response time is defined as the total time required from the unit to actively supply the grid with its service. Converter connected technologies delivering emulated inertia are characterized by a delay between the event and the device's response [65]. The response time can be represented by a combination of the following four different parameters:

- **Measurement time**, which is the time needed to detect and measure the desired control parameter (e.g. RoCoF).
- **Signal time**, which is the time required to get the activation signal from the measurement device to the FAR device.
- **Activation time**, which is the time required from the FAR to deliver the initial power response once it received the activation signal.
- **Ramping time**, which is the time required from the FAR to ramp up to the required active power set-point.

2.5.4.3 Deadband

Deadbands are generally categorized into unintentional and intentional deadbands. Unintentional deadband terminology is used to describe the inherent effect of a unit; for example, to describe the

mechanical effect of a turbine-governor system, such as sticky valves, loose gears, and hydraulic system non-linearity, which are unavoidable and unadjustable [66].

In contrast, an intentional deadband is commonly applied for control purposes. For example, in the case of PFC, an intentional deadband is applied to the governor control systems to reduce excessive controller activities for acceptable frequency fluctuations. Deadband values are generally established by the grid code [67]. However, one should differentiate between contingency based and regulation based services. When employing EIC for regulation based services, the controller should employ the same deadband established by the grid code for the governors control system. In the case of contingency based services, defining a deadband is a more complicated task, which depends on the system' characteristics (such as the system inertia).

2.5.4.4 The quantitative relationship between MW and MWs

One of the main challenges in applying EIC to compensate for the reduction in system inertia is to establish a quantitative relationship between MW of FAR and MWs of synchronous inertia, which take into account the FAR dynamics and measurements delays. For example, how much MW of FAR will compensate for the reduction of 1 MWs of synchronous inertia?

2.6 Suitable technologies for inertia support

This section will assess the different technologies suitable to mitigate the RoCoF. The various technologies can be distinguished into two groups: synchronous inertia and emulated inertia employing fast acting reservess (FARs). The synchronous reserves are characterized by their inherent inertia response, which does not require any measurement or control schemes. The assessment is based on the following criteria: 1) geographic limitation, 2) additional system services (e.g. voltage control and black start), 3) type of inertia service provided, 4) inertia constant H (s) and the typical power capacity (MW), and 5) capital cost.

1. **Synchronous condensers**

   synchronous condenserss (SCs) are machines that are synchronized with the power system and which operate as free spinning motors. SCs have played an important role in reactive power compensation and they have contributed to voltage stability in power systems for more than 50 years [68, 69]. Currently, several TSOs have started to investigate SCs effect in mitigating the RoCoF and enhancing the frequency stability [70]. Nevertheless, SCs are characterized by a lower inertia compared to conventional plants because the prime mover's mass is missing. However, in some cases, SCs can be equipped with additional masses to increase the inertia.

   - Geographic limitation: SCs are not influenced by the geographic location and, in principle, are flexible to install. Moreover, existing power plants can be converted to synchronous condensers.
   - Additional system services: As previously mentioned, SCs have been used for many years for reactive power compensation to improve voltage stability.
   - Type of the inertia response: Due to grid connection without power converters, they are able to provide an inherent inertia response without the need for measurements and controls.

- Inertia constant and power capacity range: Typical inertia constant $2H = \{2 - 3\}$ s and power capacity range of $\{50 - 250\}$ MVA [37].
- Capital cost: SCs have a large cost range, which depends on the installation of new SC or converting exiting power plants into SC. However, an average cost for an SCs varies between $\{9 - 35\}$ EUR/kVAr [71].

2. **Pumped storage hydro**

   Although utility-sized energy storage systems are a small percentage of the total generating capability of the power system, they are increasingly gaining attention for their role in enabling higher penetrations of variable renewable resources into the grid [72]. Currently, pumped hydroelectric storage (PHS) is the most common type of utility-scale storage [73]. The authors of a 2012 white paper by the *National Hydro power Association's Pumped Storage Development Council* indicated that the development of new PHS, particularly in areas with increased wind and solar capacity, would significantly improve system reliability while reducing the need to construct new fossil-fuel generation [74]. Simultaneously, the power range of pumped storage devices are suitable for delivering sufficient synchronous inertia, although significantly lower than that of a gas or coal fired power plant [73]. However, this technology requires the construction of an upper and a lower basin, which delimits its application in some countries due to geographical limitations.

   - Geographic limitation: The geographical circumstance is a key requirement to be able to employ this technology. It requires the construction of an upper and a lower basin, which delimits its application to areas which fulfill these requirements.
   - Additional system services: PHS is able to provide various system services as conventional power plants. Additionally, pumped hydro power plants can also consume active power from the grid to pump water from the lower basin to the higher basin.
   - Type of the inertia response: Synchronous inertia response due to direct grid connection.
   - Inertia constant and power capacity range: Inertia constant in the range of $2H = \{2-4\}$ s and power capacity of $\{1 - 3000\}$ MW [75, 76].
   - Capital cost: Capital costs for PHS differ widely. Reliable, experimentally confirmed numbers are only available for traditional geographically determined installations and are reported to be in the range of $\{800 - 1000\}$ EUR/kW [77].

3. **Compressed air energy storage**

   Energy storage systems are effective for supporting the integration of renewable energy and delivering system services. Compressed air energy storage (CAES) is a promising energy storage technology due to its high efficiency, cleanness and long service life [78]. CAES makes use of underground caverns where air is compressed for storage and later decompressed to release the stored energy. A CAES plant consists of a large volume that can store the compressed air (the battery) and, what is in principle, a gas turbine. The plant stores the compressed air underground in caverns or rock formations [79].

   - Geographic limitation: Geology plays a significant role for this technology because it requires an underground cavern, which limits its applicability.
   - Additional system services: CAES is capable of providing multiple system services, such as frequency and voltage support.

- Type of the inertia response: CAES is characterized by its synchronous inertia response.
- Inertia constant and power capacity range: Inertia constant in the range of $2H = \{3-4\}$ s and power capacity that range between $\{15 - 600\}$ MW [75].
- Capital cost: Based on the analysis on 2^{nd} generation CAES, estimated capital costs range between $\{750 - 1000\}$ EUR/kW [77].

4. **AC Interconnection**

   An AC interconnection between two power systems, by means of overhead lines or cables, will lead to a single synchronous network. In case of loss of generation, the inertia of both power systems will start to supply the power imbalance, leading to lower RoCoF and better frequency performance [37, 80].

   - Geographic limitation: Geographical flexibility and large distance play a significant role regarding AC interconnectors installation. For example, if an interconnector was to be built between the Island of Ireland and United Kingdom, the distance would be one of the world's longest sub-marine AC cables, which is likely to challenge current technology.
   - Additional system services: The power system will be strengthened due to the connection of the two subsystems. However, due to the long high voltage cables, the charging current limits the power transfer capability [81].
   - Type of the inertia response: The inherent inertia response improves the overall frequency performance.
   - Inertia constant and power capacity range: For AC inerterconnectors, the inertia constant depends on the inertia of the two interconnected systems. The power capacity depends on the interconnecting link.
   - Capital cost: AC interconnection depends on the distance of the two connected systems and on the geography, which determines the possibility of using overhead lines or cables.

5. **Power plant technical minimum reduction**

   One possible solution for maintaining the same inertia level while allowing greater headroom for non-synchronous generation is by operating SGs at low power set-points. Most conventional power plants are designed to run in the upper capacity range closer to the rated power with a minimum low power set-point. Reducing the minimum set-point value is another option that has the same benefits. However, the power plant type plays a fundamental role for the provision of this service. For example, thermal power plants operating in the lower output range are characterized by high CO_2 emissions [82].

   - Geographic limitation: There are no location restrictions because it uses existing power plants.
   - Additional system services: The same system services of a conventional plant operating in normal conditions but reduced down-regulation reserves.
   - Type of the inertia response: Synchronous inertia response.
   - Inertia constant and power capacity range: The inertia time constant is not altered and is the same as for conventional plants, which is in the range of $2H = \{2 - 9\}$ s and power capacity of $\{0.1 - 1\}$ GW [75].

- Capital cost: This depends on the type of plant and if a refurbishment is needed.

6. **Wind turbines**

   Wind Turbines are generally classified into Type 1, Type 2, Type 3 and Type 4 [83, 84]. Early wind turbines of Type 1 and Type 2 were used with a constant speed asynchronous generator, which is directly connected to the power system and, thus, capable of providing synchronous inertia. Modern wind turbines (i.e. Type 3 and Type 4) are designed to operate at a wider range of rotor speeds. Their rotor speed varies with the wind speed or other system variables, based on the design employed. Additional speed and power controls allow variable-speed turbines to extract more energy from a wind regime than fixed-speed turbines. Nevertheless, for Type 3 and Type 4 turbines, power converters are required to interface the wind turbine with the grid and, thus, do not provide any inherent inertia response [85]. However, several wind turbines manufacturers offer synthetic inertia response control for their Type 3 and Type 4 wind turbines (e.g. ENERCON inertia emulation control and General Electric WindINERTIA) [29, 86].

   - Geographic limitation: Location plays a significant role for the presence of the wind turbine itself. However, for existing wind turbines the geographic location should not present any limitation for providing these services.
   - Additional system services: Wind turbines of Type 3 and Type 4 are capable of providing a wide range of system services thanks to their controllability. Nevertheless, they can only provide system services if sufficient wind is present.
   - Type of the inertia response: Wind turbines of Type 1 and Type 2 provide inherent inertia response while Type 3 and Type 4, in principal, can only provide emulated inertia.
   - Inertia constant and power capacity range: Wind turbines of Type 1 and Type 2 with rated power more than 1 MW have values of inertia constant in the range of $2H = \{3 - 5\}$ s [87]. Meanwhile, in Type 3 and Type 4 turbines, the mechanical inertia is decoupled from the grid. The machine power capacity spans between $\{1 - 10\}$ MW [75].
   - Capital cost: The capital cost of wind turbines varies among technologies. However, for onshore installation capital cost varies between $\{1100 - 1950\}$ EUR/kW while for offshore wind turbines, the capital cost varies between $\{2300 - 4300\}$ EUR/kW [88].

7. **HVDC interconnectors**

   High-voltage DC (HVDC) transmission links provide a means of non-synchronously connecting two (or more) AC power systems whilst maintaining control of the power flow over the HVDC-link. An HVDC-link is an economical way of transferring electrical power over long distances [89]. Due to the asynchronous interconnection between the interconnected power systems, no inherent inertia response is available because the DC connection fully decouples the two areas. Nevertheless, several studies have investigated the ability of HVDC to provide frequency control services, including inertia emulation and primary frequency control [90–92]. Frequency control can be achieved by including frequency control loop, either in the active power controller or the DC voltage controller [93].

   - Geographic limitation: The location of the HVDC interconnectors plays a fundamental role in its applicability. Generally, the main challenge is related to the long distance and high costs.

- Additional system services: HVDC interconnectors are able to provide a large number of system services, depending on the employed converter technology.
- Type of the inertia response: Due to the decoupling between the two subsystems, only emulated inertia can be provided.
- Inertia constant and power capacity range: HVDC interconnectors do not provide an inherent inertia response. HVDC power capacity depends from the employed technology. The current installed HVDC links are characterised by a power capacity in the range of $\{3 - 8000\}$ MW [75].
- Capital cost:HVDC capital cost depends on the applied technology and the distance over which the two areas are connected.

8. **Various Energy Storage Technologies**

   Batteries are energy storage units that store electrical energy and which operate at direct current. Thus, power electronic converters are needed to interface the batteries with the grid. Batteries can provide multiple benefits to the power system in terms of ancillary services and RoCoF enhancement. Nevertheless, the battery's technology plays a fundamental role in deciding the suitability in providing such services. For example, Sodium-Sulfur batteries (NaS) are characterized by their fast response time and, as claimed by certain manufacturers, the response time is within 1 ms [94], allowing the provision of synthetic inertia services and/or fast frequency control services. Meanwhile, hydrogen storage system and synthetic natural gas have a relatively slow response time (i.e. in the range of seconds), which limits their capabilities for synthetic inertia services [95, 96].

   - Geographic limitation: Generally, battery technologies do not have locational restrictions and are flexible to install. However, some minor exceptions might occur for flow batteries due to the additional space required for the auxiliary services and for the more complex technology.
   - Additional system services: Due to their controllability, batteries are able to offer multiple system services.
   - Type of the inertia response: In principal, they can provide only emulated inertia.
   - Inertia constant and power capacity range: Batteries do not have any inherent inertia response. Batteries' power capacity depends on the applied technology, however, typical power capacity is generally up to several MW.
   - Capital cost: The capital coast of batteries varies among the applied technologies. However, it can range between $\{250 - 2600\}$ EUR/kW [76].

9. **Demand side management**

   In theory, demand and generation can participate in frequency control. In the current control schemes, adopted by the majority of TSOs, demand is used to restore severe power imbalance that cannot be alleviated by fast acting generators (i.e. load shedding). Nevertheless, demand capability to contribute to frequency control has previously been underestimated due to the complexity involved in the real-time monitoring and control of aggregated loads [97]. In contrast, with the advancements in measuring and monitoring techniques, DSMs have started to gain more consideration and application from various TSOs in managing the power system efficiently and in accommodating a higher share of renewable energy generation [98].

Simultaneously, different projects and studies are investigating the use of DSM technology to provide additional system services as fast primary frequency control and SIC from aggregated loads. Various studies have conducted simulations and field tests to analyze the ability of electric vehicles to deliver frequency support and system services [50, 99].

- Geographic limitation: Location plays a crucial role in allowing the aggregation of a number of loads to provide adequate response power.
- Additional system services: DSM is able to provide multiple system services such as frequency and voltage control, which depends from the nature and capability of the aggregated units.
- Type of the inertia response: DSM is able to provide regulating power in terms of emulated inertia.
- Inertia constant and power capacity range: DSM does not provide inherent inertia response and, therefore, an inertia constant cannot be provided. Similarly, a power capacity range cannot be provided because it depends on the number of the aggregated electrical loads.
- Capital cost: DSMs have a large range of cost depending on the applied technology and infrastructure

10. **Flywheel**

    Flywheels store kinetic energy in the rotation of a wheel. The moving mass is accelerated and decelerated by a motor/generator and, therefore, can charge or discharge the system [37]. High speed flywheels are interfaced with the grid through power electronics and, thus, are only capable of delivering synthetic inertia. Flywheels energy storage systems are characterized by their fast ramping ability and long-term durability. Due to their fast response time (i.e. in order of milliseconds), flywheels can provide ancillary services, including synthetic inertia and frequency response to power grids [100].

    - Geographic limitation: Flywheels do not have location restrictions and can easily be installed.
    - Additional system services: Flywheels are able to provide frequency support in terms of regulating power.
    - Type of the inertia response: Due to the connection to the grid through power electronics, flywheels are only able to provide emulated inertia.
    - Inertia constant and power capacity range: Flywheels are not characterized by an inertia constant due to the connection to the grid through power electronics. Their typical power capacity range between $\{0.1 - 20\}$ MW [75, 76].
    - Capital cost: Flywheels have a capital cost that ranges between $\{210 - 300\}$ EUR/kW [76].

An overview of these technologies discussed is presented in Table 2.2. This table reports the inertia typology, the average relative inertia value for synchronous inertia, power capacity, geography limitations, possible additional services and capital cost.

Table 2.2: Overview of the various technologies

Technology	Synch. / EIC	Inertia (H)	Power capacity	Geographic limitations	Additional services			Capital cost
					Voltage support	Energy supply	Black start	
Synchronous condensers	synch.	{2 - 3} s	{50 - 250} MVA	Low	YES	NO	NO	{9- 35} EUR/kVAR
Pumped storage hydro	synch.	{2 - 4} s	{1 - 3000} MW	High	YES	Limited	YES	{800-1000} EUR/kW
Compressed air energy storage	synch.	{3 - 4} s	{15 - 600} MW	High	YES	Limited	YES	{750-1000} EUR/kW
AC interconnection	synch.	Depends on the interconnected systems	Depends on the line rating	Medium	Limited	YES	Limited	-
Parking or reduction of the minimum MW generation	synch.	{2- 9} s	Plant dependent	Low	YES	YES	Limited	-
Wind turbines (Type 1 & 2)	Synch. & EIC	{3 - 5} s	0.5 -2	Medium	Limited	YES	NO	Onshore: {1100 - 1950} EUR/kW
Wind turbines (Type 3 & 4)	Synch. & EIC	-	0.5 -2	Medium	YES	YES	NO	Offshore: {2300 - 4300} EUR/kW
HVDC interconnectors (VSC-based)	EIC	-	{100 - 1000} MW	Average	YES	YES	YES	
Electrochemical and chemical batteries	EIC	-	0.1 - 100 MW	Low	YES	Limited	YES	{250 - 2600} EUR/kW
Demand side management	EIC	-	Depends on the aggregated units	Low	Limited	NO	NO	-
Flywheels	EIC	-	{0.1 - 20} MW	Low	YES	NO	NO	{210 - 300} EUR/kW

2.7 Summary

This chapter gives a general overview of future control room requirements and functionalities to facilitate and support the increasing share of RES. Based on different EU projects, in general, and on the EU ELECTRA IRP project, in particular, focus was given to the DMS functionalities. This choice is motivated by the fact that it is expected that by 2030 between 52% and 89% of electricity production will be generated by RES, mainly connected to the distribution network [24, 25]. However, this chapter focuses on emulated inertia services, which is one of these functionalities. To better comprehend the need for this new function, a detailed and analytical analysis of the consequences of reduction in system inertia and employment of emulated inertia have been presented. This chapter has demonstrated the ability of EIC to mitigate the RoCoF and improve the frequency performance. This chapter has provided an overview of the currently available EIC schemes, including their key features and weaknesses. Finally, the key parameters and challenges in applying such services have been detailed.

CHAPTER 3

Frequency support from converter connected units

The focus of this chapter is twofold. It begins by presenting the trade-off analysis between synthetic inertia control (SIC) and fast frequency control (FFC) employing converter connected units, which is further addressed as fast acting reserves (FAR). Emphasis is placed on the energy storage's response time and its effect on the two controllers performance and, consequently, on the frequency performance. The focus is then moved toward analyzing the capabilities and limitations of electric vehicles (EVs) in providing such services. This chapter presents a simulation analysis, which will be further complemented in Chapter 4 by experimental validation. It should be noted that this chapter includes results from the following papers: Pub. [C], Pub. [D] and Pub. [E].

3.1 Overview

As pointed out in Chapter 2, the large scale deployment of inertia-less generation displacing conventional generators will have a considerable impact on the system frequency. Reduced system inertia is a core issue regarding frequency stability. This will lead to faster rate of change of frequency (RoCoF) and lower frequency nadir values, which presents a challenge in hosting higher share of renewable energy sources (RES).

With the increased penetration of RES, the regularity and severity of frequency events is expected to increase as high share of RES leads to more variable and less predictable supply [101]. However, energy storage systems (ESSs) are expected to play a crucial role in the ancillary services market. The fast development of ESSs creates an opportunity to provide a frequency response that is significantly faster than conventional primary frequency reserves (PFRs), which can mitigate the increasing challenges in maintaining the grid reliability and will also enable a higher share of RES [102].

Similarly, EVs could play a significant role in the ancillary services market due to their high degree of flexibility. In fact, EVs should not be considered only as passive assets but rather should be seen as an integrated active resource [99]. EVs could adapt their active power consumption to improve the grid conditions and support further integration of RES. They are a quick-response unit with an attached storage and potentially bi-directional power flow capabilities [103].

This chapter focuses on the ability to mitigate the RoCoF and limiting the frequency nadir by investigating the trade-off analysis between the following two controllers: SIC and FFC. It will employ energy storage systems and then series produced EVs models.

3.2 SIC and FFC employing energy storage systems

This analysis aims to investigate the impact of the high penetration of converter connected resources on frequency dynamics. The abilities and limitations of SIC and FFC in mitigating the RoCoF are presented and discussed. The system is studied with different levels of converter connected resources, namely, 0%, 27% and 55% of the total load.

3.2.1 Controller specifications

This section will give a detailed explanation of the two implemented controllers. The two controllers and also the network model have been implemented in the power system simulation software DIgSILENT-PowerFactory.

3.2.1.1 Synthetic inertia controller

When active power consumption exceeds the active power generation, due for example to the loss of a generation unit, the system frequency will decline. Simultaneously, synchronous rotating machines will release the kinetic energy stored in their rotating mass, which limits the frequency gradient. The developed SIC attempts to emulate the same effect in connection with an energy storage system and the block diagram is shown in Figure 3.1.

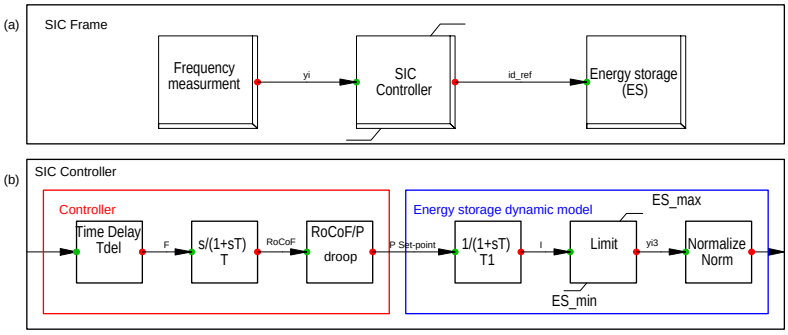

Figure 3.1: Synthetic inertia control block diagram: (a) the SIC frame, and (b) the SIC control algorithm, including the energy storage dynamics.

The controller consists of three main blocks: a frequency measurement device, a SIC controller (i.e. control algorithm), and energy storage. Energy storage is represented by a simplified model of an energy source. For simplicity, the energy storage dynamics (e.g. time response) are included in the control algorithm block. The control algorithm block includes the following functions: a time delay function, a RoCoF calculation function, a RoCoF-power droop function, a first order filter function, a limiter function to represent the energy storage's rated power limitation and finally a normalization block function. The time delay function takes into account various delays, such as communication delay, measurement delay, and activation delay. A time delay of 100 ms is applied. The value is inspired by different studies; for example, the Hawaiian Electric Companies have proposed a fast frequency regulation service with a total reaction time of 100 ms [104, 105]. In this study, the RoCoF is measured over 4 ms as the sampling time of the simulation platform and a low-pass filter of T=10 ms is used to eliminate high-frequency transients. It should be noted that the 4 ms measuring window is very small and might include electrical transients. However, the measuring window and the low-pass filter are inspired by the RoCoF relay parameters that are used for islanding detection [106]. The analytical relationship between RoCoF and active power can be expressed as:

$$\Delta P = K\frac{\Delta f}{\Delta t} \tag{3.1}$$

where ΔP is the active power variation from the participated unit, K is proportional gain, and $\frac{\Delta f}{\Delta t}$ is the RoCoF. Nevertheless, it is not possible to define an univocal analytical formulation of a RoCoF-power droop because the $\frac{\Delta f}{\Delta t}$ reference cannot be defined univocally as the case with

the frequency-power droop, where $f_n = 50$ Hz. Furthermore, a simplification of energy storage model to a first order system has been used in many studies [107–110]. In this study, a T1=200 ms is used. However, this value varies among the different technologies. The various parameters are summarized in Table 3.1.

Table 3.1: SIC block diagram parameters

Time delay (Tdel)	RoCoF window	RoCoF filter (T)	ESS dynamics (T1)
100 ms	4 ms	10 ms	200 ms

3.2.1.2 Fast frequency control

Conventionally, PFR is provided by conventional power plants and it aims to contain the system frequency deviation after an incident within a pre-defined range [11]. The activation is done locally in a decentralized manner by applying a droop control in every participating unit. The analytical relationship between frequency control and active power was shown in Chapter 2, and is reported here for convenience:

$$R = -\frac{\Delta f / f_{nom}}{\Delta P / P_{nom}} \tag{3.2}$$

where R is the speed regulation or droop constant, and ΔP and P_{nom} are the generator's active power variation and nominal power, respectively. Similarly, Δf and f_{nom} are frequency variation and nominal frequency, respectively. However, due to the slow dynamics of prime movers of the participating generators, primary frequency control (PFC) is unable to mitigate the RoCoF in the first instance following a contingency or at least has a very limited effect. On the one hand FFC employs the same control approach as PFC, namely a decentralized droop control approach based on frequency deviation from the nominal value [4]. On the other hand, FFC uses FAR; for example, in this study, energy storage systems have been used. Also in this case, the controller is implemented in DIgSILENT-PowerFactory, the block diagram is shown in Figure 3.2 This consists of three main blocks: a frequency measurement device, a FFC controller (i.e. control algorithm), and energy storage. While the frequency measurement device and the energy storage blocks are similar to the SIC case, the core concept of the control algorithm is different. In fact, RoCoF calculation is not needed and a frequency-power droop is applied. The same time delay and energy storage first order system parameters are used and summarized in Table 3.2

Table 3.2: FFC block diagram parameters

Time delay (Tdel)	ESS dynamics (T1)
100 ms	200 ms

3.2.1.3 Network model

The modelled power system in which the two controllers are analyzed is shown in Figure 3.3, which includes the following components: a constant power load equal to 180 MW, which is divided into 60% of asynchronous machines and 40% of static loads as recommended in [111].

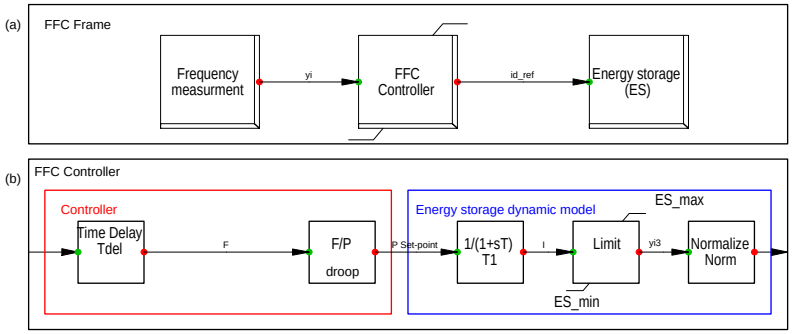

Figure 3.2: Fast frequency control block diagram: (a) the FFC frame, and (b) the FFC control algorithm, including the energy storage dynamics.

A total of 13 transformers with rated power 120 MVA and 220/33 kV rated voltage, 24 transformers with rated power 7 MVA and 33/6.6 kV rated voltage, a photovoltaic (PV) farm with 100 MW rated power, an energy storage system with 1 MW rated power, and six conventional generation units. Table 3.3 summarizes rated power of the generation units together with their relative inertia values.

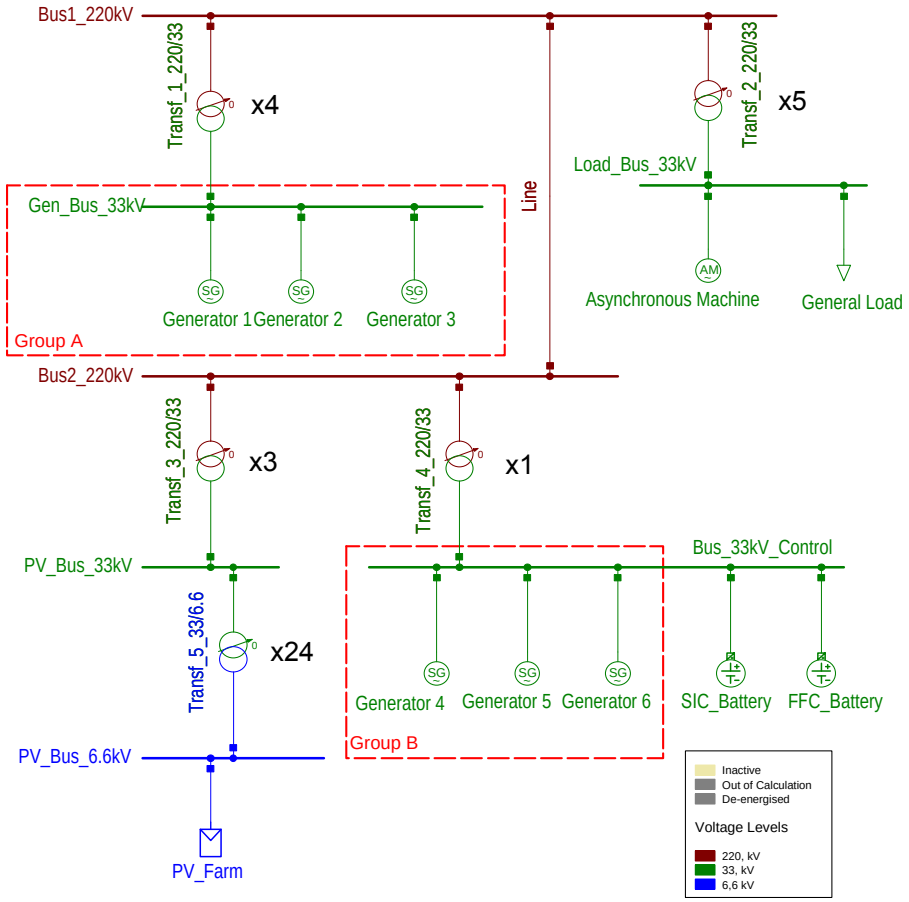

Figure 3.3: Power system network

Table 3.3: Generators' rated power

Generation	Gen. 1	Gen. 2	Gen. 3	Gen. 4	Gen. 5	Gen. 6	PV
Rated power	120 MVA	60 MVA	60 MVA	30 MVA	30 MVA	3 MVA	100 MW
Inertia 2H (s)	4	2	2	2	2	2	-

It is assumed that all conventional generators are equipped with the following IEEE standard models [112]:

- Governor: gov_TGOV2, steam turbine gov. with fast valving.
- Excitation system: avr_IEEET1, 1968 IEEE type 1 excitation system.
- Power system stabilizer (only Generator 1): PSS2A, 1992 IEEE type PSS2A dual input signal stabilizer.

3.2.1.4 Analyzed scenarios

Three different scenarios are analyzed. In these three scenarios, the system response is triggered by the loss of one of the synchronous generators of group B (i.e. Generator 6), determining around 1% loss of the production related to the total consumption. The loss of 1% of generation is inspired by the ENTSO-E network guidelines [11]. The system is studied with different levels of PV penetration: 0%, 27% and 55% PV generation of the total load. Table 3.4 shows the generators set points for the three levels of PV penetration.

Table 3.4: Generator set points

Generation	0%PV	27%PV	55%PV
Generator 1	50 MW	50 MW	50 MW
Generator 2	50 MW	50 MW	disconnected
Generator 3	50 MW	disconnected	disconnected
Generator 4	15 MW	15 MW	15 MW
Generator 5	15 MW	15 MW	15 MW
Generator 6	1.8 MW	1.8 MW	1.8 MW
PV	-	50 MW	100 MW

An overview of the three scenarios follows:

- The first scenario highlights the impact of converter connected resources on frequency dynamics (i.e. RoCoF, frequency nadir and steady-state value). This shows the effects of the reduced system inertia and the PFR provided by conventional power plants.
- The second scenario carries out a sensitivity analysis of the response time of the two analyzed controllers. In this case, the PV penetration level is set to 55% of the total load. The following response times have been considered: 10 ms, 100 ms, 1 s and 2 s.
- The third scenario presents a performance analysis of the FFC versus the SIC on the frequency behaviour. This highlights the effects of the two controllers on the frequency gradient, nadir, and steady-state value.

3.2.1.5 Results and discussion

This section will present and discuss the results of the previously detailed scenarios. As previously mentioned, the first scenario aims to investigate the frequency behaviour after the loss of a conventional generator, namely Generator 6. The conventional unit is tripped at 0 seconds of the simulation. It should be noted that in case of replacement of a conventional plant providing PFR by RES (e.g. PV production), the same amount of reserve should be covered by another plant. However, it has been decided not to compensate for the reduced PFR. This choice is also done to highlight the future need for reserves that provide primary frequency support. Figure 3.4 illustrates how the system frequency behaves after a sudden event when the amount of kinetic energy in the system and also PFR are reduced. As analytically demonstrated and explained in Chapter 2, the reduced system inertia imposes an increase in the frequency gradient, leading to larger frequency variation, as shown by the green curve versus the red curve. Similarly, due to the reduced amount of PFR, the frequency nadir and steady-state values are reduced. However, as analytically presented in Chapter 2, and graphically shown in Figure 2.4 and Figure 2.5, a direct correlation among frequency nadir, gradient, PFR, and system inertia is present. In other words, the lower nadir value is partially due to the reduced inertia and is partially due to the reduced PFR.

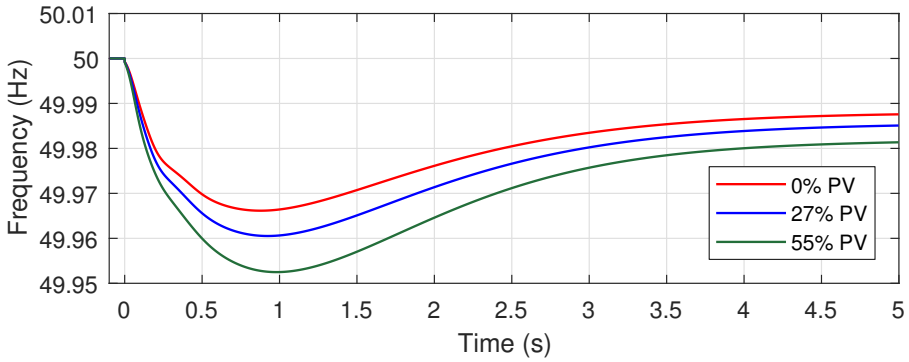

Figure 3.4: Frequency behaviour with different levels of PV penetration

The second scenario aims to highlight the effects of response time due to unavoidable delays on the controllers' performance. It should be noted that the response time includes the measurement time, activation time, and communication time. The following delay values are analyzed: 10 ms, 100 ms, 1 s and 2 s. The chosen values are drawn from the datasheets of energy storage manufacturers [94–96]. The droop parameters of each controller are not constant among the different delays. The gain of each controller is determined using the Ziegler-Nichols method, which is a heuristic method for tuning PID controllers. In this method, the system is made to oscillate by increasing the proportional gain until it reaches the ultimate gain K_u at which the output frequency of the system begins to oscillate with ultimate period T_u. The final proportional gain is calculated as $K_p = 0.5\, K_u$ [113].

The following droops have been considered for SIC: ϵ (the RoCoF limits are ± 0.0125 Hz/s), ζ (± 0.075 Hz/s), ι (± 0.25 Hz/s), and λ (± 0.75 Hz/s). If the RoCoF exceeds the limits, then the active power limits of the energy storage are set (± 1 MW). The different droops are presented in Figure 3.5a. Similarly, four droops have been considered for FFC: 0.0025% (frequency limits of 49.99875-50.00125 Hz), 0.015% (frequency limits of 49.9925-50.0075 Hz), 0.25% (frequency limits of 49.875-

50.125 Hz) and 0.4% (frequency limits of 49.8-50.2 Hz). The different droops are presented in Figure 3.5b. It was possible to apply these steep droops (i.e. high gain parameter) because of the limited energy storage flexibility versus the total installed power, namely 1 MW versus 181.8 MW, respectively. When using a 180 MW machine, the equivalent required four droops will be 0.45%, 2.7%, 45 % and 72%. The frequency performance following the event for SIC and FFC is shown in Figure 3.6a and Figure 3.6b, respectively.

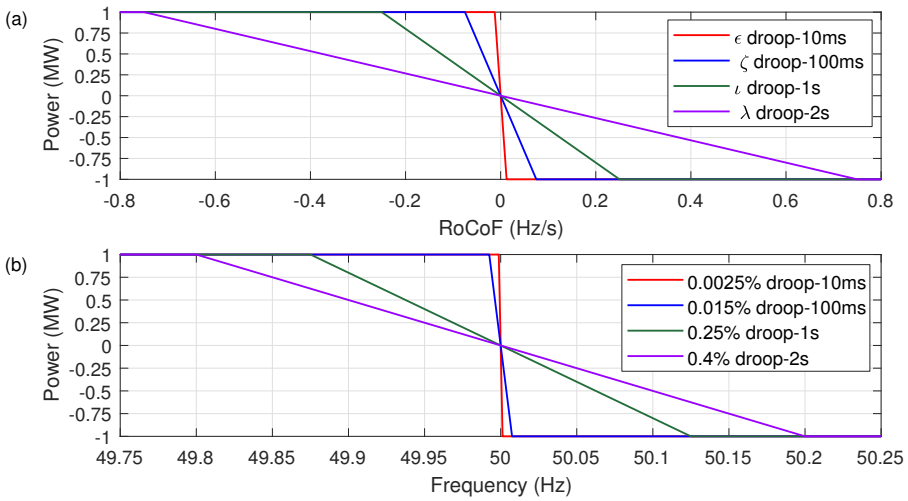

Figure 3.5: (a) RoCoF-power droop employed in the SIC controller for each response time, and (b) frequency-power droop employed in the FFC controller for each response time.

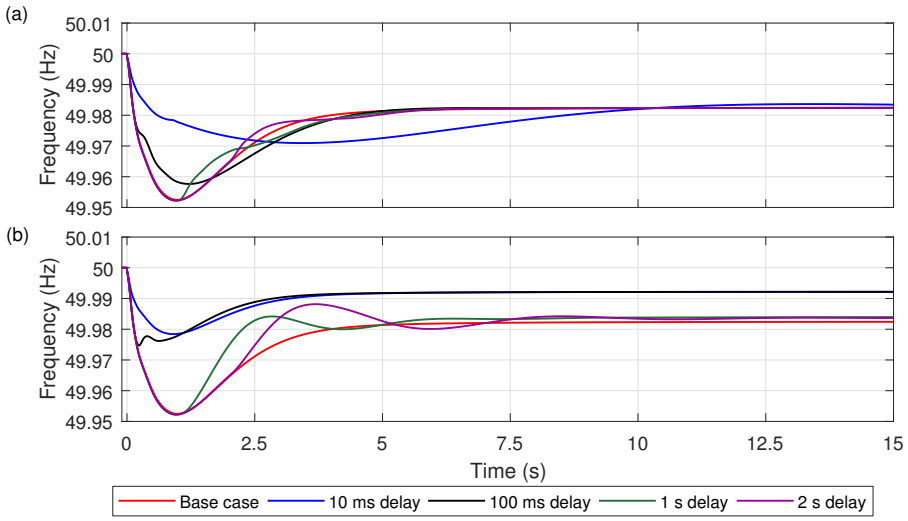

Figure 3.6: Sensitivity analysis of the different time response: (a) the frequency curves for the SIC with RoCoF window 4 ms, and (b) the frequency curves for the FFC.

Because the SIC is a RoCoF based control, one can notice that its implementation is useless for relatively large delays. In fact, it does not influence the steady-state value and has a limited effect on the frequency nadir. Similarly, the large delay reduced the FFC performance; however, it still contributing positively to the steady-state value because it is acting on the frequency deviation from the nominal value.

The third scenario carries on a performance analysis of SIC and FFC. In this scenario, a total delay of 100 ms with its corresponding droop characteristic have been considered, as shown in Figure 3.5, namely ζ droop and 0.03% droop for SIC and FFC, respectively. The main objective is to analyze and compare the impacts of the two controllers on the system frequency after the loss of the same conventional unit as in the previous scenarios. The frequency trend and the produced active power from the energy storage are shown in Figure 3.7.

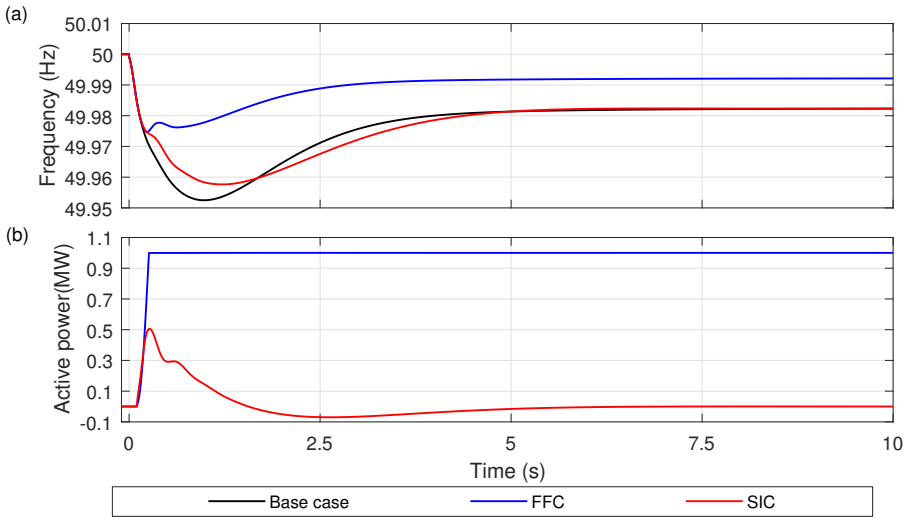

Figure 3.7: Frequency and active power output from the battery during both SIC and FFC. 100 ms time delay is used and RoCoF window 4 ms for SIC.

It is observed from the active power output of the energy storage that SIC is participating marginally faster than the FFC around the first 200 ms following the event. Meanwhile, FFC is performing much better in terms of frequency nadir and steady-state values. The SIC's active power curve is similar to the inertia response of synchronous machines. This behaviour could be explained as follows: after an active power imbalance between generation and consumption, synchronous rotating machines start to release the stored kinetic energy in their rotated mass. Once the maximum instantaneous frequency deviation is reached, the lost kinetic energy needs to be recovered, which explains the reason to absorb active power in the case of SIC and also the longer time needed for the frequency to reach the steady-state value. This negative side effect can be avoided by implementing a control algorithm that limits the energy storage from absorbing active power in these circumstances. However, this behaviour cannot be eliminated when providing inertia support by wind turbines because the controllers aim to extract the stored inertial energy from the moving parts of the wind turbine generator [114]. Table 3.5 shows the maximum RoCoF calculated over the first 200 ms, the frequency nadir, and the steady-state value. A slightly better performance in terms of RoCoF from the SIC has been observed. However, the FFC performed better in terms of frequency nadir and steady-state value.

This investigation has shown that the high share of converter connected resources replacing conventional power plants reduces the system inertia and the primary frequency reserves. However, it was also shown that SIC and FFC can help support the system while increasing the share of RES. The performance of the two controllers could be summarized as follows: the SIC is characterized by slightly better performance in terms of RoCoF while FFC has a much better performance in terms of frequency nadir and steady-state value. Simultaneously, the response time plays a crucial

Table 3.5: Frequency characteristics

	RoCoF	Nadir	Steady-state
No additional control	0.128 Hz/s	49.953 Hz	49.98 Hz
SIC	0.111 Hz/s	49.965 Hz	49.98 Hz
FFC	0.1220 Hz/s	49.975 Hz	49.99 Hz

role in providing frequency support by any of the two controllers. However, response time has a much higher effect on SIC's performance by limiting its participation because in FFC positive effects would still be present on the steady state value given that it acts on Δf.

3.3 SIC and FFC employing single phase EVs

Essentially, EVs are energy storage devices and most of the time they are plugged into a charging spot. Therefore, a transmission system operator (TSO) can greatly benefit from EVs' participation in frequency services provision. In principle, EVs are capable of providing fast regulating power in both directions in case of Vehicle-to-Grid (V2G) or they can simply modulate the charging power [103]. The majority of EVs that are present in the market comply with the IEC 61851 and SAE J1772 standards [99], according to which, the EV charging current should be limited between the minimum charging current of 6 A and the maximum value, which is the electric vehicle supply equipment (EVSE)'s rated current (10 A, 16 A, 32 A, etc.) in discrete 1 A steps [115, 116]. These standards are valid for both single phase and three phase connections. For example, 16 A is equivalent to 3.6 kW and 11 kW for single phase and three phase connections, respectively. In this study, only unidirectional charging is possible.

This study aims to investigate the capabilities, benefits and drawbacks of single phase EVs in providing frequency services in terms of SIC and FFC. The implemented EV models are characterized by unidirectional charging and they comply with the IEC 61851 and SAE J1772 standards. Therefore, they are capable of modulating the charging current between 6 and 16 A in discrete 1 A steps [4].

3.3.1 Controller specifications

As in Section 3.2, two controllers are implemented in this study, namely: SIC and FFC. In recent experimental activities for frequency control by series produced EVs, the authors have noticed frequency oscillations under certain circumstances (e.g. steep droops, low-inertia, large response time, etc.), due mainly to the 1 A granularity of the EV's charging current foreseen by IEC 61851 [115] and SAE J1772 [116] standards. The reason for this is the calculated charging current, which, in case it falls near the exact middle of two consecutive set-points, will be continuously rounded up and down. For example, if the calculated current is 7.51 A, then the set-point will be 8 A, which is sent to an aggregated number of EVs. The difference between the required 7.51 A and the actual 8 A in all the EVs would cause a significant change in the power flow in terms of total absorbed active power. This will affect the frequency behaviour, resulting in a new calculated current of around 7.49 A, which is then rounded down to 7 A. This process will turn into a loop, which creates the 1 A-oscillations.

Various solutions have been suggested to overcome these oscillations. For example, by implementing an adaptive droop slope which is dependent on the specific grid parameters and the EV's

response time or by implementing an additional hysteresis characteristic [117]. Therefore, it has been decided in this study to integrate the two controllers, namely SIC and FFC, with a stabilizer algorithm. The modified version of the two controllers are further addressed as SIC_S and FFC_S, respectively.

3.3.1.1 SIC & SIC_S controllers

The controllers' participation is provided by a droop control. It represents how much the controllers are sensible to the RoCoF. In this study, the RoCoF is measured over a 100 ms window. The measuring window is inspired by the RoCoF relays' parameters. These parameters are used for islanding detection [106] in connection with the concern expressed by generators connected to the Irish transmission system, that the RoCoF level calculated over 100 ms period could be significantly higher than the 1 Hz/s calculated over 500 ms, as required by the grid code [118]. Similarly to the previous study, the gain of each controller is determined using the Ziegler-Nichols method. The following three droops have been considered: α (the RoCoF limits are $\pm$ 0.0625 Hz/s), β ($\pm$ 0.125 Hz/s), and γ ($\pm$ 0.1875 Hz/s). If the RoCoF exceeds the limits, then the current limit value (6 or 16 A) is set. The three droops are RoCoF-I droops and they are presented in Figure 3.8 by the dashed lines. The amount of regulated power from the three EVs is 3.4 kW. This represents around 17% of the generated power (3.4 kW/19.5 kW) and around 6% of the installed power (3.4 kW/58 kW).

To comply with the [115] and [116] standards, the calculated current values need to be rounded. This results in step functions, as shown by the solid lines in Figure 3.8. To ensure that there is room to increase and decrease the charging level equally ($\pm$5 A), the EVs' initial current set-point is set to 11 A, which is the central point.

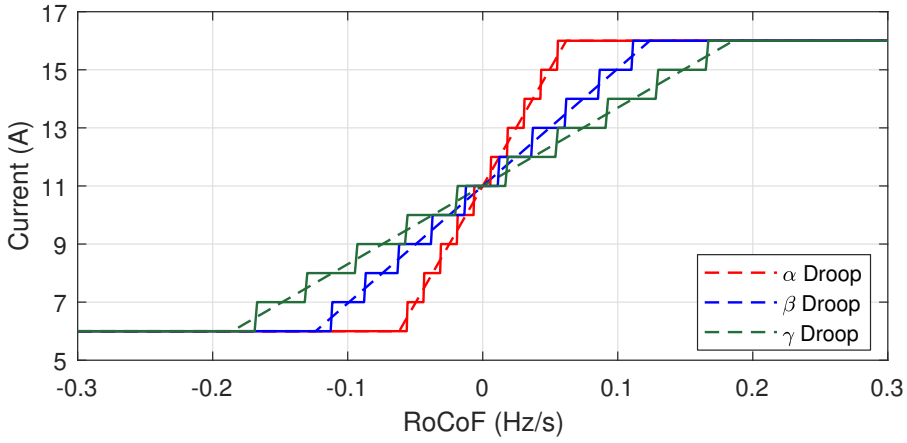

Figure 3.8: RoCoF-Current droops: ideal droop (dashed lines) and 1 A steps droop (solid lines).

The two controllers are implemented in DIgSILENT-PowerFactory and the block diagram is shown in Figure 3.9a. Basically, it is composed of three main blocks: the frequency measurement device, the control algorithm and the EV model. The control algorithm is presented in Figure 3.9b. This algorithm receives the frequency measurement, calculates the RoCoF, and provides the EV with a current set-point according to a particular RoCoF-I droop. The EVs and the control/communication dynamics are modelled by considering the appropriate response times and latencies for all of

the operational steps. The EV's response characteristics are based on the experimental finding described in [4]. The EV model is composed by:

- A time constant block, to imitate the EV's battery dynamics.
- A time delay block, to represent the delay due to internal EV's communication and activation of the inverter (T_EV = 1.5 s). The EV's activation time varies among models and year of production [99].
- A block that converts the current to a power signal. As for RMS simulations in PowerFactory, these loads need power inputs.
- A load block, which is the EV unit in the modelled grid.

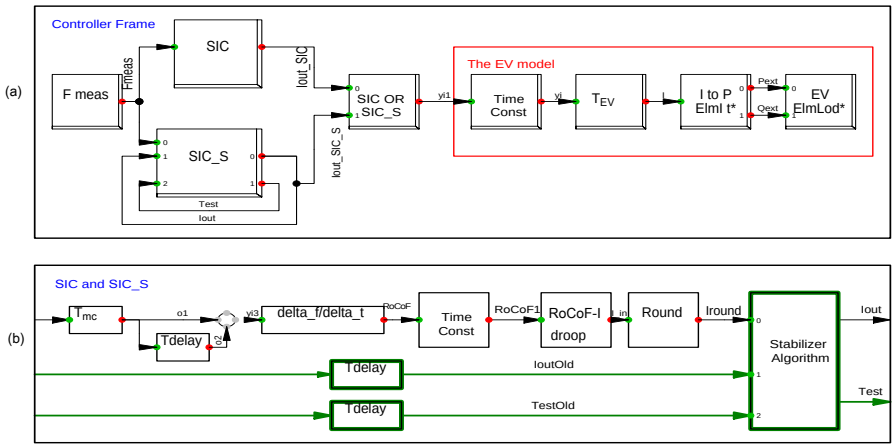

Figure 3.9: SIC and SIC_S block diagram. The highlights show the additional blocks for SIC_S. (a) shows the measurement block, a layout of SIC and SIC_S controllers and the EV model. (b) shows the SIC and SIC_S' control algorithm block diagram.

A more detailed description of the two control algorithms (i.e. SIC and SIC_S) follows.

1. **SIC controller**: The SIC is a RoCoF based controller. It calculates the RoCoF and, according to a predefined droop, it changes the EV's charging current set-point. The SIC control algorithm is composed by the following functions:
   - Delay function, representing the measurement and communications delays ($T_{mc} = 0.5$ s), due mainly to the DEIF MTR-3 device [119].
   - A RoCoF calculation block.
   - A low-pass filter.
   - A block with the RoCoF-I droop.
   - A round function to comply with the standards to recreate the 1 A steps.
2. **SIC_S controller**: The SIC_S is composed by the SIC controller that has been enhanced by a stabilizer algorithm, as highlighted in green in Figure 3.9. The stabilizer algorithm aims to avoid the 1 A current oscillations that were previously described. Practically, it prevents the 1 A current oscillations, while allowing larger and highly less probable 2 A or higher

oscillations. This will reduce the overall probability of current oscillations and, consequently, frequency oscillations. Basically, it freezes the current set-point if a 1 A oscillation is detected. The stabilizer algorithm's flow-chart is presented in Figure 3.10.

The controller calculates the current set-point (Iout) based on an algorithm that evaluates two conditions: the current set-point and an internal parameter (Test). The first condition is obtained by comparing the new calculated set-point (Iround) with the one from the previous time-step (IoutOld). The second condition is evaluated through a consideration of a memory status (TestOld), which is the Test from the previous time-step. Test indicates whether or not, and how, the current set-point is going to change compared to the value of the previous time-step. It will take values of -1, 0 or 1: where -1 indicates that in the previous time-step the current set-point has been reduced, 1 indicates it has been increased, while 0 initializes the controller. Because the aim of the controller is to avoid 1 A oscillations, the algorithm prevents 1 A steps from one time-step to the next one under certain conditions. To do so, the algorithm compares Iround with IoutOld, taking into account the value of TestOld. For instance, where Iround is greater than IoutOld by 1 A difference, and TestOld is -1, then Iout will be kept as IoutOld. In contrast, Iout will be changed only when the difference is at least 2 A. For example, if Iround is 9 A, IoutOld is 8 A and TestOld is -1, then the controller will prevent the current changing. Iout will take the same value of Ioutold and Test will be kept as TestOld. In case Iround increases to 10 A (or decrease to 7 A), then the current change will be allowed: Iout will be 10 A (or 7 A) and Test will be 1 (or -1).

3.3.1.2 FFC & FFC_S controllers

In this case, the controllers' participation is provided by a droop control. The control concept is similar to the conventional PFC [11], which is commonly provided by droop controllers applied to synchronous generators. As previously mentioned in Section 3.2, the droop constant represents how much the machine is sensible to frequency variation and it quantifies its contribution to primary frequency/power control. The relationship between active power and frequency variation is shown in (3.2) and reported here for convenience:

$$R = -\frac{\Delta f / f_{nom}}{\Delta P / P_{nom}} \tag{3.3}$$

where R is the so called speed regulation or droop constant, ΔP and P_{nom} are the generator's active power variation and nominal power, respectively. Similarly, Δf and f_{nom} are frequency variation and nominal frequency, respectively. Nevertheless, in this study, the regulation is provided by modulating the EVs's active power consumption, and according to [115] and [116], this could be achieved by modulating the charging current. Therefore, (3.3) can be rewritten as:

$$R = -\frac{\Delta f / f_{nom}}{\Delta I / I_{nom}} \tag{3.4}$$

where ΔI is the current variation and I_{nom} is the nominal current. Because the technical requirements delimit the EV's charging current between 6 and 16 A, this available range of the regulating current of 10 A has been assumed as the EV's I_{nom}.

Three different $f - I$ droops have been considered: 2% (frequency limits of 49.5-50.5 Hz), 4% (49-51 Hz) and 6% (48.5-51.5 Hz). If the frequency exceeds the limits, then the current limit value (6 or 16 A) is set. The three droops are shown in Figure 3.11 by the dashed lines.

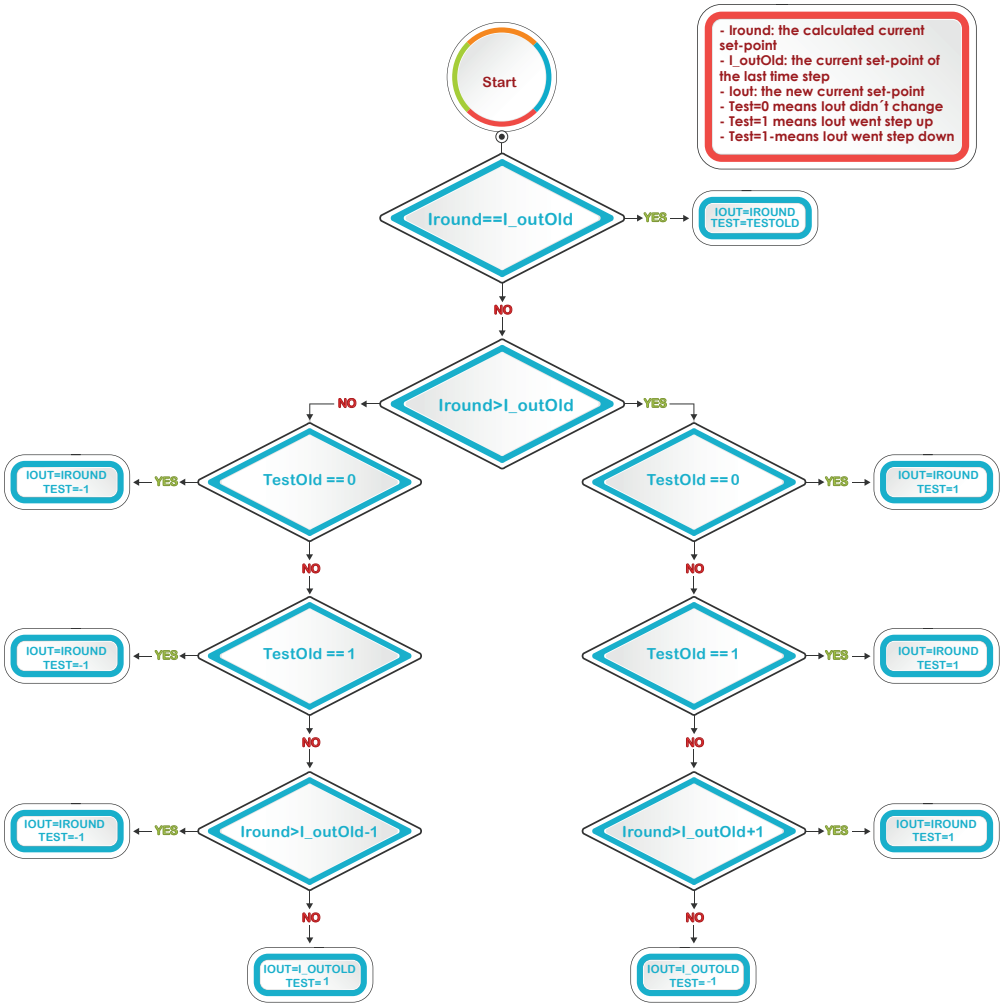

Figure 3.10: Stabilizer algorithm flow-chart.

To comply with the [115] and [116] standards, the calculated current values need to be rounded. This results in step functions, as shown by the solid lines in Figure 3.11. To ensure that there is room to increase and decrease the charging level equally (± 5 A), the EVs' initial current set-point is 11 A, which is the central point.

The two controllers, namely FFC and FFC_S, are implemented in DIgSILENT-PowerFactory and the block diagram is shown in Figure 3.12. Similarly to the SIC, this is composed of three main blocks: the frequency measurement device, the control algorithm, and the EV model. The same EV model that was used in SIC and which was previously presented is used. A more detailed description of the two control algorithms, namely FFC and FFC_S is presented in the following.

1. **FFC controller**: The FFC is a frequency deviation based control that measures the frequency and determines the EV's current set-point according to a certain droop. The FFC control algorithm is composed of the following functions:
   - Delay function, representing measurements and communications' delays ($T_{mc} = 0.5$ s).
   - A block with the f-I droop.
   - A round function block, to comply with the standards to recreate the 1 A steps.

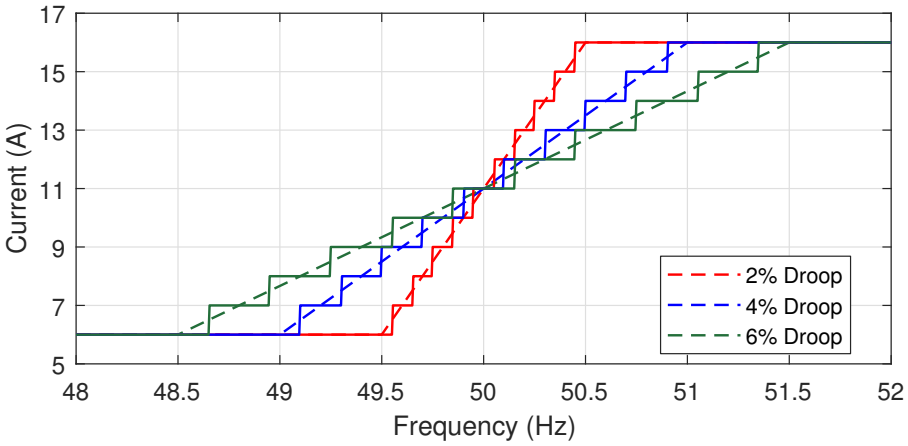

Figure 3.11: Freq-Current droops: ideal droop (dashed lines) and 1 A steps droop (solid lines).

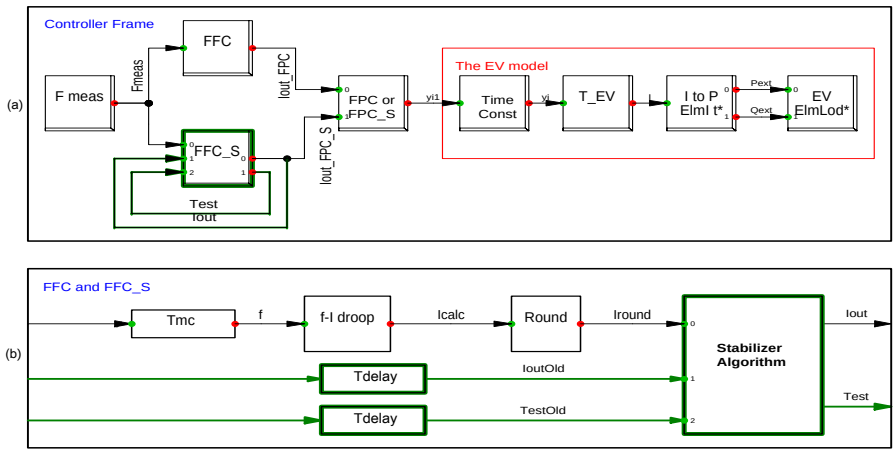

Figure 3.12: FFC and FFC_S' block diagram. The highlights show the additional blocks for FFC_S. (a) shows the measurement block, a layout of FFC and FFC_S controllers and the EV model. (b) shows the FFC and FFC_S' control algorithm block diagram.

2. **FFC_S controller**: The FFC_S controller is composed of the FFC controller that has been enhanced by a stabilizer algorithm. This employs the same stabilizer algorithm as the SIC_S, as previously presented and detailed.

3.3.2 Grid layout

As previously mentioned, the analysis has been carried out by means of the simulation software DIgSILENT-PowerFactory. The modelled power system, in which the analyses are carried out, is a reproduction of an islanded configuration of the experimental low voltage (LV) grid SYSLAB PowerLabDK infrastructure. SYSLAB is a research laboratory facility that is used to develop and test control and communication technology for active and distributed power systems, which is located at the Technical University of Denmark, Risø campus.

To allow future experimental validation in the SYSLAB infrastructure, the modelled grid is based on real available power system components. The following units are used for the proposed simulation studies:

- Three controllable EVs, each equipped with single-phase 16 A (230 V) charger and 24 kWh Lithium-ion battery. The chargers only allow unidirectional power flows; that is, V2G capability is not available. The charging current can be modulated between 6 and 16 A, with 1 A granularity. The EVs's initial current set-point is 11 A, which is the central point and which assures room to increase and decrease the charging level equally. The total amount of regulating power by the three EVs is 3.4 kW.
- A 60 kVA diesel synchronous generator, with active power provision up to 48 kW. This provides inertia to the islanded grid. The diesel's governor is activated to provide primary frequency support in case of SIC or SIC_S and deactivated in case of FFC or FFC_S. Inspired from [4], a diesel inertia of $2H = 50$ s is used.
- A controllable 45 kW resistive load unit with up to 15 kW per phase, adjustable with steps of 0.1 kW.
- A 10 kW Aircon wind turbine (nominal wind speed 11 m/s), equipped with full converter.

Figure 3.13 shows a single line diagram representation of the whole SYSLAB experimental facility.

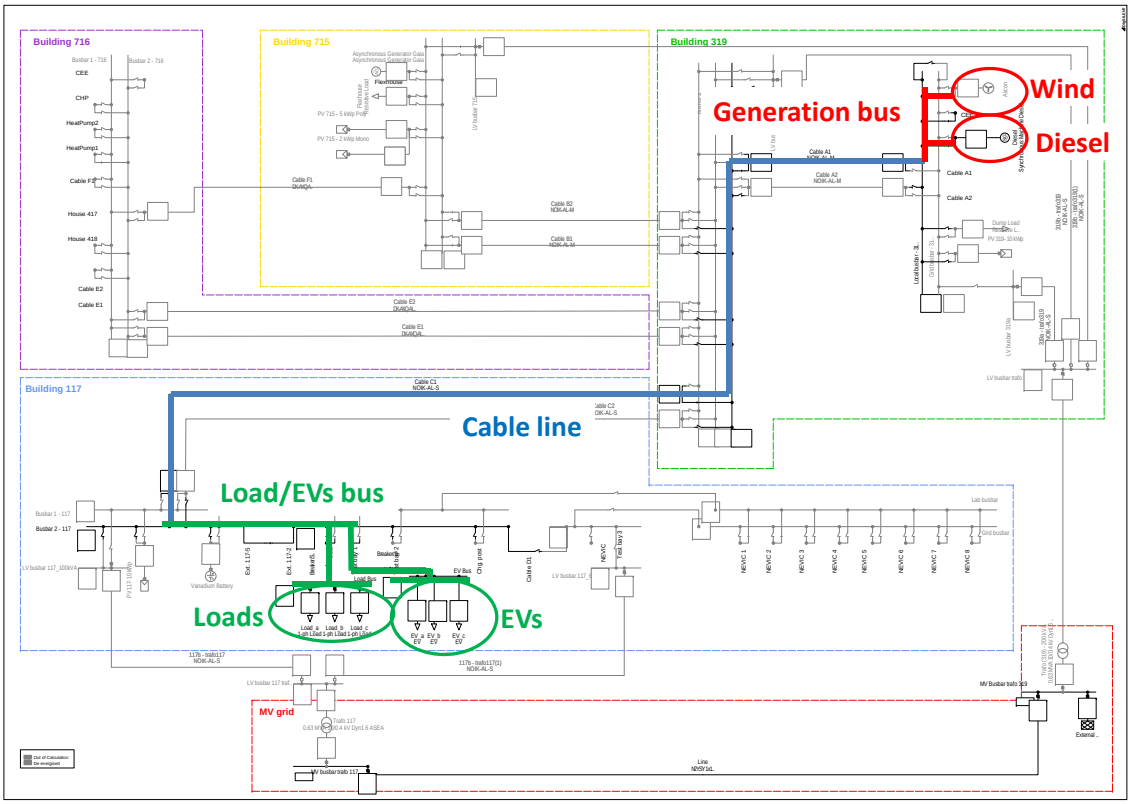

Figure 3.13: Single line diagram representation of the whole SYSLAB PowerLabDK experimental LV grid. The components that are used to compose the analyzed system are highlighted.

The highlights represent the various components that are used for the proposed simulations studies. As can be seen from the highlights, a 725 m Aluminium cable is used to connect the two bus-bars at which the units are connected. Both the synchronous and the wind turbine generators are connected to the same busbar, while the resistive load and the EVs are placed on the other

terminal of the line. The active power set-points of the different units for the two investigated scenarios are summarized in Table 3.6.

Table 3.6: Active power set-points

Device	Scenario 1	Scenario 2
Diesel	19.5 kW	$\sim$ 15.5 kW
Wind turbine	-	$\sim$ 4 kW
Resistive load	12 kW	12 kW
EVs	7.5 kW	7.5 kW

3.3.3 Simulation scenarios and results

Two scenarios have been considered to evaluate the various controllers' effectiveness under different operating conditions. To better investigate the EVs's ability to mitigate the frequency deviation, the automatic frequency controller of the diesel's governor has been disabled for the FFC and FFC_S. Because SIC and SIC_S are RoCoF based control and not capable to compensate for the active power imbalance, the diesel's governor frequency controller was enabled. Nevertheless, this study does not aim to compare FFC and SIC capabilities but aims instead to identify the benefits and drawbacks of EVs in providing ancillary services in terms of frequency support.

The first scenario aims to provide a general evaluation of the different controllers in case of contingencies taking place during stationary situations. The various controllers are investigated using the previously presented droops, namely 2%, 4% and 6% droops for FFC and FFC_S; and α, β and γ droops for SIC and SIC_S. This scenario aims to evaluate the various controllers' effectiveness on the frequency dynamics in terms of frequency nadir and RoCoF values (in case of SIC and SIC_S), including an evaluation of the stabilizer algorithm's ability to limit the EV's charging current set-point oscillation.

The second scenario aims to evaluate the effectiveness of the different controllers in a more realistic and challenging situation, where continuous power fluctuations are present and, therefore, continuous actions of the controllers are needed. Consequently, the Aircon wind turbine was connected and a 10 minutes registered wind production profile, in terms of active and reactive power, has been considered.

3.3.3.1 Scenario 1

As previously mentioned, the first scenario aims to evaluate the stabilizer algorithm's capabilities in limiting the EV's charging current set-point oscillations. The various controllers are evaluated by monitoring the frequency and EV's charging current, in addition to the RoCoF trends in case of SIC or SIC_S. Balanced load events have been used to destabilize the system's frequency.

For FFC and FFC_S, the governor frequency control is disabled. Therefore, the system frequency requires a larger time to stabilize compared to SIC or SIC_S. Consequently, the simulations have been carried out for 20 minutes, during which the events took place in 5 minute intervals. Meanwhile, only 3 minutes of simulation were needed to analyze the SIC and SIC_S controllers for the same number of events. The frequency was stabilized much more quickly thanks to the activated frequency control of the diesel governor. Table 3.7 presents the amplitude of each load event and the time at which it took place. The events' size amounts to $\pm$3 kW, which corresponds

Table 3.7: Load events to destabilize the frequency

Time (SIC)	Time (FFC)	Load event
10 s	10 s	+3 kW
50 s	310 s	-3 kW
90 s	610 s	-3 kW
130 s	910 s	+3 kW

to ±15.4% of the total generated power and to ±5% of the rated power of the diesel generator. Simulations have been carried out for each of the presented droops.

FFC and FFC_S: Figure 3.14 presents the system frequency. In the case of a 2% droop, the first and third load events led to undesired frequency fluctuations because of the previously mentioned 1 A oscillations. However, they are substantially reduced by the FFC_S controller, which reduces the number of switches from one set-point to the other, as shown in Figure 3.15 and Table 3.8. An enlargement of the frequency deviations appears because the controller's action is stopped until a larger frequency change is present. Although similar effects are noticeable after the first event in the case of 6% droop, now no larger fluctuation is caused. For the 4% droop, the two controllers are characterized by a similar performance in terms of frequency.

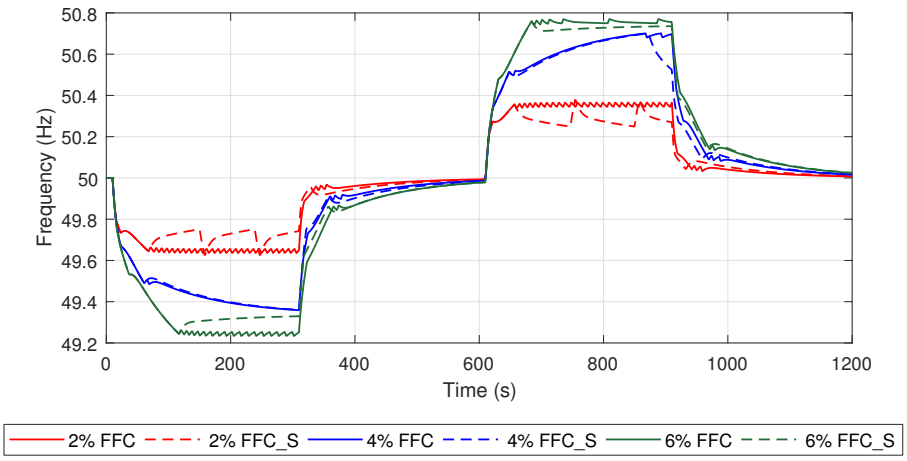

Figure 3.14: Frequency trends employing FFC and FFC_S.

In terms of frequency nadir and steady state values, the two controllers perform in a similar manner. Nevertheless, the FFC_S was able to reduce the number of EVs's charging current set-point switching, which can also be appreciated from the reduced frequency oscillations.

Table 3.8: Number of switchings

Droop	FFC Nr. switching	FFC_S Nr. switching
2%	128	22
4%	28	12
6%	62	10

SIC and SIC_S: Similarly, the same analysis are carried out. Figure 3.16 presents the system frequency and RoCoF for the 3 minute simulation.

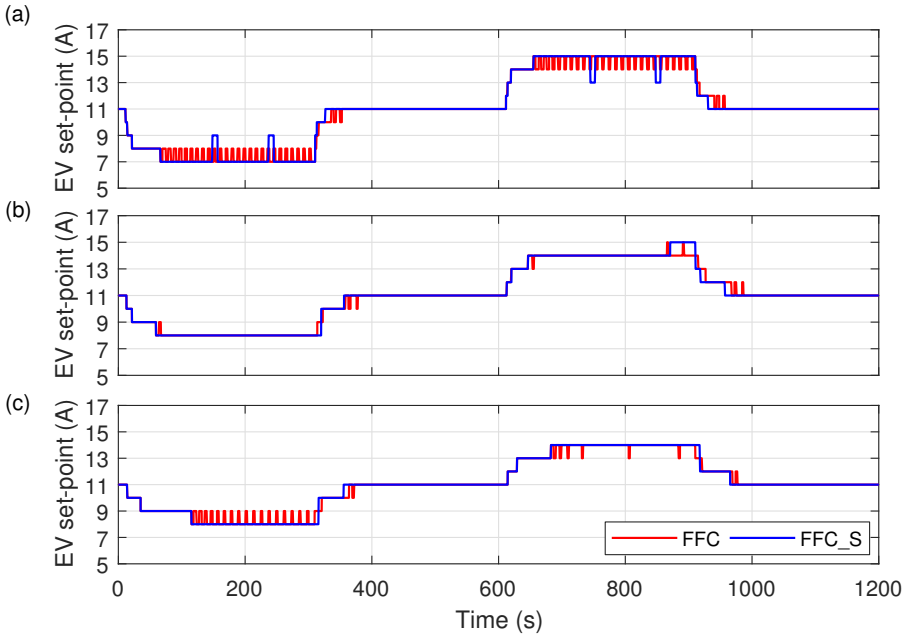

Figure 3.15: EV's current set-point signals employing FFC and FFC_S: (a) for 2% droop, (b) for 4% droop, and (c) for 6% droop.

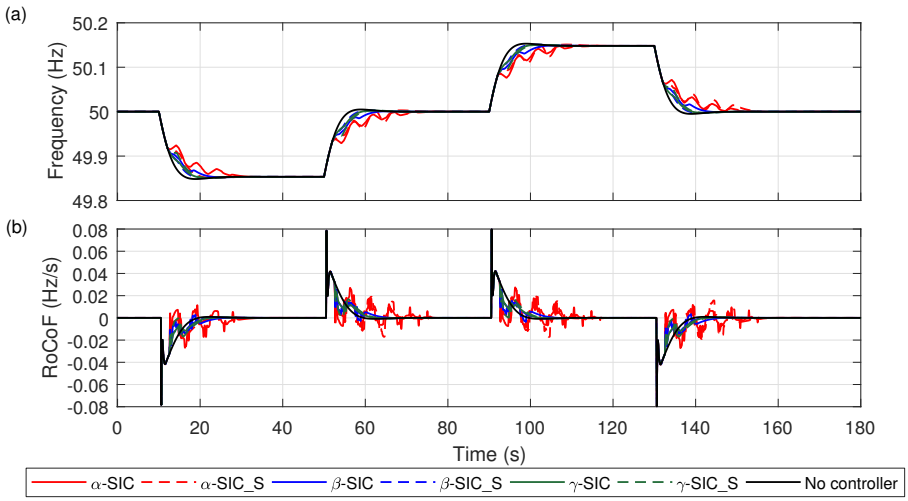

Figure 3.16: Frequency and RoCoF trends employing SIC and SIC_S: (a) the frequency trends, and (b) the RoCoF trends. The RoCoF is measured over a 100 ms measuring window.

Because of the large system inertia and the activated primary frequency control from the diesel's governor, Figure 3.16 does not give a very clear comprehension of the controllers' effects in terms of frequency and RoCoF. Therefore, it has been decided to concentrate only on the first 40 s of the simulations. The frequency and RoCoF trends are shown in Figure 3.17a and Figure 3.17b, respectively.

It is noticeable from Figure 3.17a that the system frequency oscillates when applying the α droop. This effect is due to the combination of having a steep droop and relatively large delay in terms of synthetic inertia control (i.e. 2 s). Frequency oscillations could also be noticed from the RoCoF behaviour presented in Figure 3.17b.

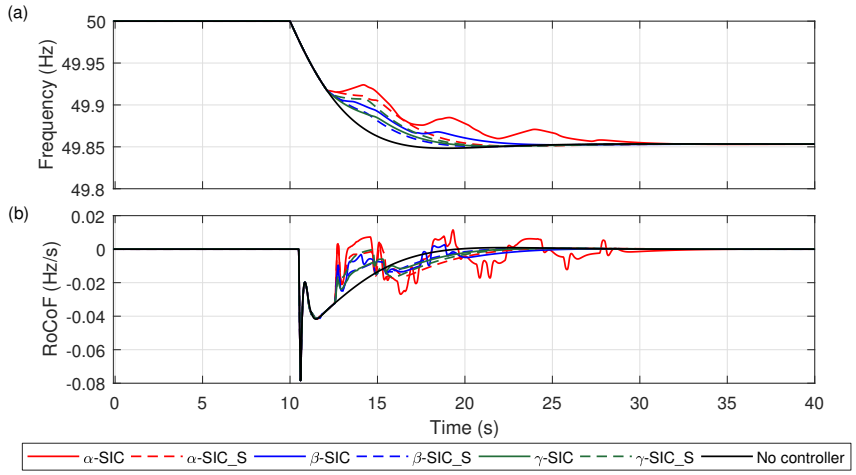

Figure 3.17: Frequency and RoCoF trends employing SIC and SIC_S for the first 40 s: (a) the frequency trends, and (b) the RoCoF trends. The RoCoF is measured over 100 ms measuring window.

The RoCoF takes positive values in the event of shortage of generation. However, due to the high inertia of the analyzed grid, the two controllers (i.e. SIC and SIC_S) have similar effects on the frequency behaviour. In contrast, Figure 3.18 and Table 3.9 show that SIC_S has substantially reduced the number of switchings of the EV's charging current set-point.

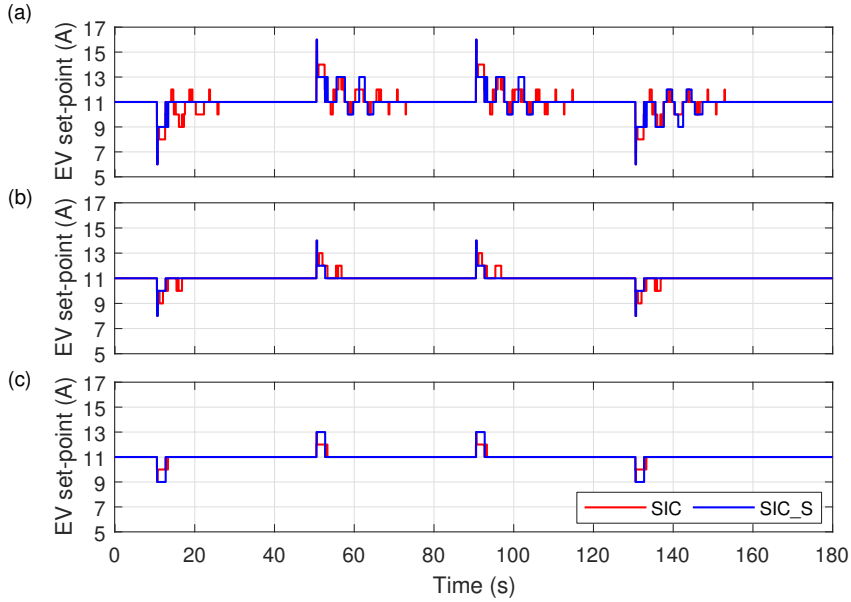

Figure 3.18: EV's current set-point employing SIC and SIC_S: (a) α droop, (b) β droop, (c) γ droop.

3.3.3.2 Scenario 2

This scenario considers 10 minutes wind production profile in terms of active and reactive power, as reported in Figure 3.19. This allows a better evaluation of the controllers' performance in a more realistic and challenging situation, where continuous actions are required to follow the continuous frequency variations.

Table 3.9: Number of switchings

Droop	SIC Nr. switching	SIC_S Nr. switching
α	184	70
β	52	19
γ	24	11

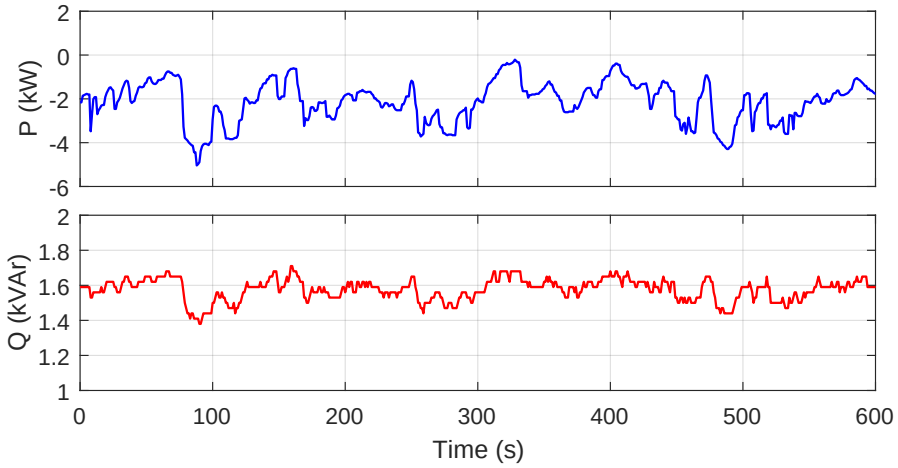

Figure 3.19: 10-minute active and reactive power wind generation profile.

FFC or FFC_S: Due to the continuous active power fluctuation from the wind turbine, no load events were required. The system frequency is shown in Figure 3.20. As in Scenario 1, Figure 3.20 shows that the two controllers have a very similar performance in terms of frequency containment. Meanwhile, the FFC_S provides absolute benefits in terms of the number of EVs current set-point adjustments, as deducible from Figure 3.21. As reported in Table 3.10, for the 2%, 4% and 6% droops, the switching operations have been reduced by 48% (from 166 to 87), 59% (from 106 to 43) and 67% (from 88 to 29), respectively. However, this limited effect in improving the frequency is due to the limited number of EVs.

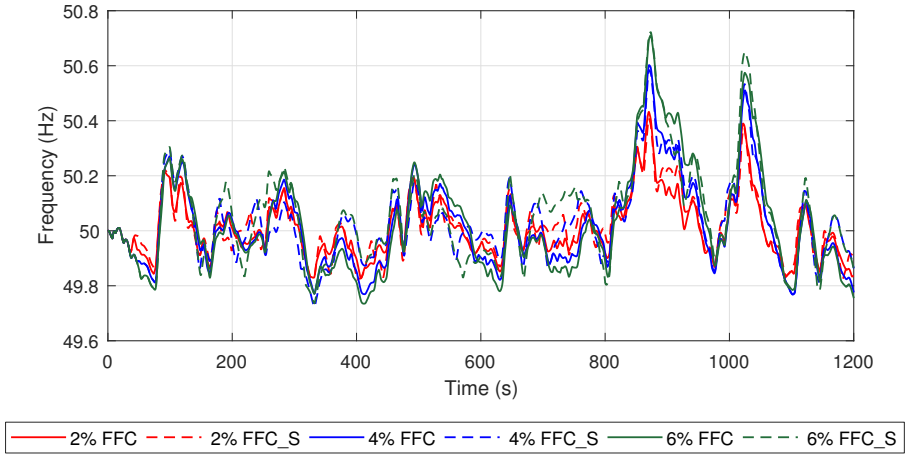

Figure 3.20: Frequency trends employing FFC and FFC_S when a wind profile is considered.

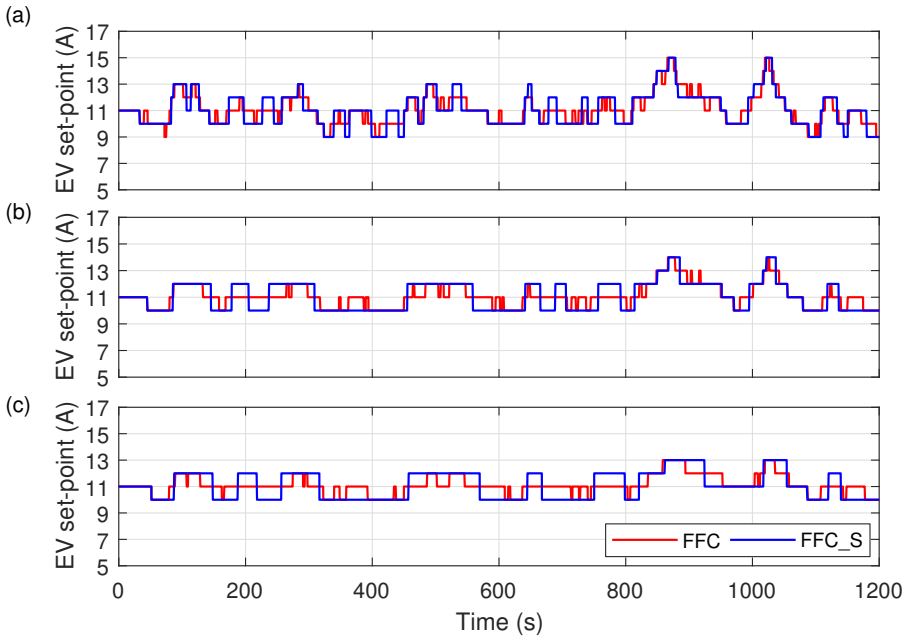

Figure 3.21: EV's current set-point signals employing FFC and FFC_S when a wind profile is considered: (a) 2% droop, (b) 4% droop, and (c) 6% droop.

Table 3.10: Number of switchings

Droop	FFC Nr. switching	FFC_S Nr. switching
2%	166	87
4%	106	43
6%	88	29

SIC and SIC_S: The wind profile that was reported in Figure 3.19 is applied in this scenario. However, due to the governor's automatic frequency controller and the high system inertia, load events were required to better appreciate the controllers' response. Four load events have been applied by changing the load consumption by 25% of its rated power as flows, by +25%, -25%, -25% and +25%, respectively at, 0 s, 180 s, 360 s and 540 s.

This analysis aims to present a comparative performance between SIC and SIC_S in terms of frequency dynamics and EV's current set-point oscillations. The system is analyzed by using the previously proposed droops in Figure 3.8. Frequency and RoCoF trends are shown in Figure 3.22a and Figure 3.22b, respectively.

Figure 3.22 shows the effectiveness of the two controllers in slightly improving the RoCoF compared to the non-controlled case. This limited improvement is due to the limited number of EVs participating in the control. Meanwhile, Table 3.11 and Figure 3.23 show the much better performance of SIC_S compared to SIC in terms of total number of switchings of the EV's current set-point.

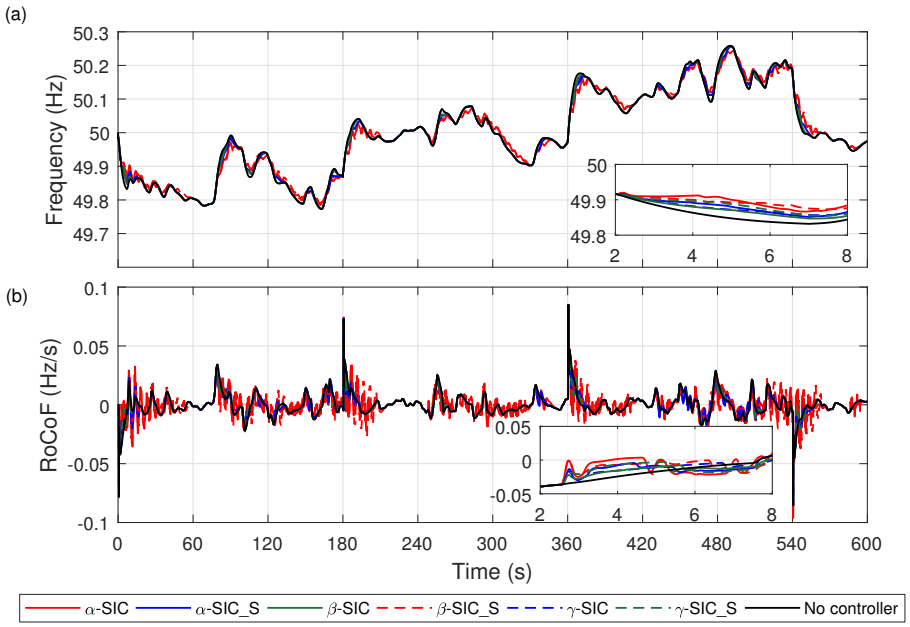

Figure 3.22: Frequency and RoCoF trends employing SIC and SIC_S when a wind profile is considered: (a) the frequency trends, and (b) the RoCoF trends. The RoCoF is measured over a 100 ms measuring window.

Table 3.11: Number of switchings

Droop	**SIC** **Nr. switching**	**SIC_S** **Nr. switching**
α	528	300
β	120	38
γ	36	14

The number of switchings has been reduced by 43%, 68% and 61% for the α, β and γ droop, respectively. This result is valuable from the perspective of integrating EVs for ancillary services (e.g. frequency support). Given that EVs will participate in the ancillary services during the whole charging process, this can help in providing the same frequency support performance with less degradation of the battery performance [120, 121].

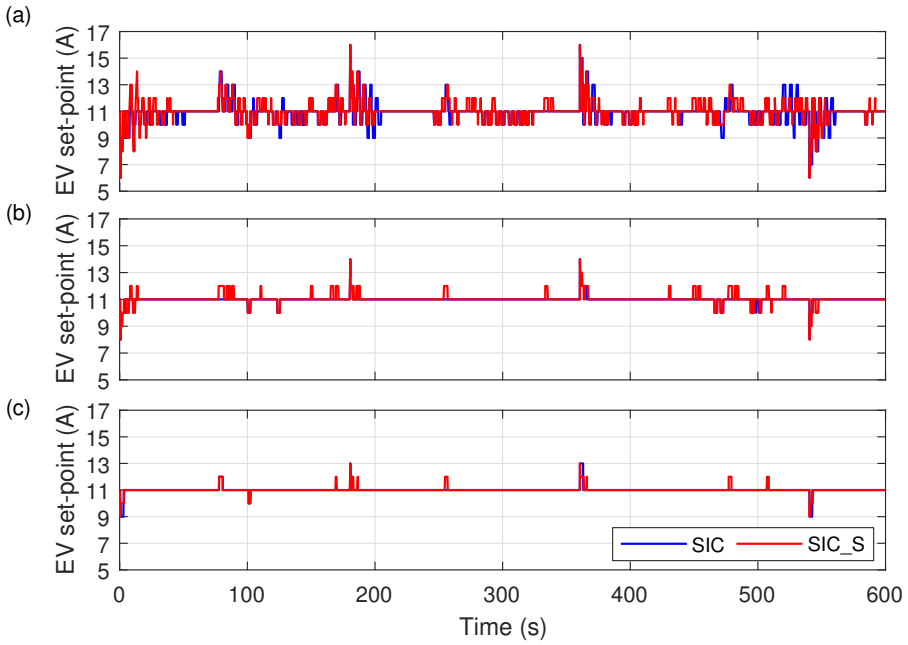

Figure 3.23: EV's current set-point signals employing SIC and SIC_S when a wind profile is considered: (a) α droop, (b) β droop, and (c) γ droop.

3.4 Summary

This chapter has presented the impacts of the high penetration of converter connected resources on frequency dynamics. Two control solutions were proposed and detailed, namely: SIC and FFC. First, this chapter began with a trade-off analysis between the two controllers employing energy storage. The benefits and drawbacks of each controller were then presented and discussed. It has been shown that SIC limits the RoCoF slightly more than FFC. Meanwhile, FFC presented a better performance in terms of frequency nadir and steady state values. However, the analysis showed that the response time plays a crucial role in providing these services, including its drawback in causing frequency oscillation. Consequently, it has been decided not to compensate for the primary frequency reserves eliminated by turning off the machines due to the high penetration of PV. This choice is made to highlight the future need for more reserves that can provide primary frequency support, which is experienced by the reduced frequency steady state values.

Second, because EVs are essentially energy storage devices and most of the time they are plugged into a charging spot, the EVs's ability to provide frequency support was investigated. The analysis aimed to investigate the technical feasibility, benefits, and drawbacks of single phase EVs to provide frequency services employing the SIC and FFC controllers. The simulation analysis was carried out in an islanded configuration of the experimental LV grid SYSLAB. To allow future experimental validation (i.e. further addressed in Chapter 4), the modeled grid as well as the EV model are based on real available power system components and standards. In this case, two controllers were tested, namely: SIC and FFC. This study has shown that EVs are generally able to provide frequency support. However, due to some technical requirements established by the [115, 116] standards, the EVs participation in frequency services might lead to frequency oscillations under certain circumstances. A stabilizer algorithm was proposed to overcome this issue. A modified version of the two controllers that was enhanced by the stabilizer algorithm was proposed and

tested. The modified version showed a much better performance in damping the oscillation while maintaining approximately the same frequency performance.

Nevertheless, the question remains: Are series produced EVs able to improve the overall system frequency in terms of RoCoF, frequency nadir and steady-state value? What are the technical limitations and the performance of each controller (SIC and FFC) when series produced EVs are used as flexibility resources. Chapter 4 will conduct a validation study and a trade-off analysis between the two controllers employing series produced EVs as flexibility resources.

CHAPTER 4

Experimental validation of EVs frequency support

The main results of Pub. [F] and Pub. [G] focus on validating the capability of series-produced electric vehicles (EVs) in providing frequency support services, which will be presented in this chapter. The focus of this chapter is twofold. First, it aims to describe and validate synthetic inertia control (SIC) and fast frequency control (FFC), while employing distributed energy resources (DER) units as flexibility resources. In this case, series produced single phase EVs are used. Second, it will make a comparison between SIC and FFC, and it will also outline the technical limitations of EVs in providing frequency support. The main results of experimental trials are given. This chapter will conclude with a discussion and a summary of the results and recommendations.

4.1 Motivation for experimental validation

As described in Chapter 2, and as recognized in Chapter 3 by simulation analysis, EVs can provide frequency support services by modulating their charging current. However, a distinction between the EV's current set-point and the actual EV charging current must be made. In principal, the EV charging current set-point can be allocated to each EV through a predefined control strategy. Nevertheless, the internal EV charging controller might choose not to follow the set-point due; for example, to battery-dependent constraints such as the temperature or state of charge (SOC). Most of the previous literature has focused on simulation-based studies, assuming an ideal EV response while neglecting the potential latencies and the response inaccuracies. However, these issues do have a crucial role when dealing with fast frequency services and synthetic inertia.

The authors in [122] present the limitations of employing classic simulations using simplified distributed generators (DG) models due to the complexity of the adequate modeling of power electronic interfaces. This study emphasizes the importance of the hardware-in-the-loop tests for evaluating the ancillary services provision of converter connected units. The results show that pure digital simulation approaches cannot reproduce the true system behaviour in all circumstances and, therefore, testing real hardware is of crucial importance. The same reasoning can be extended to the importance of testing the ability of series-produced EVs to provide frequency support. Simultaneously, experimental activities are required to examine the technical feasibility of the various control strategies with commercially available EVs. Moreover, further experimental studies are required to better evaluate and update the accuracy of existing models for further theoretical studies.

This chapter focuses on validating the use of SIC and FFC controllers to provide frequency support services with commercially available EVs. In particular, this chapter aims to identify any potential challenges that might arise when dealing with real components and also possible recommendations.

The majority of EVs that are present in the market comply with the IEC 61851 and SAE J1772 standards [99], according to which, the EV charging current should be limited between the minimum charging current of 6 A and the maximum current, which is the electric vehicle supply equipment (EVSE)' rated current (10 A, 16 A, 32 A, etc.) in discrete 1 A steps [115, 116]. To better investigate the effects of the 1 A granularity imposed by the aforementioned standards, a sensitivity analysis of the different granularity values is carried out in the simulation platform DIgSILENT PowerFactory. .

4.2 Smart charging controller, grid layout, and EV model

A universal smart charging controller is developed to validate the technical feasibility of commercially available EVs to provide frequency support, which is applicable to any EV that is compliant with the IEC 61851 and SAE J1772 standards [115, 116]. The developed controller can be used for centralized control architecture, such as sending set-point to a large number of EVs by the EV aggregator, or for a decentralized control architecture that is implemented directly in the EVSE.

4.2.1 Control logic

The implemented control logic for both FFC and SIC is based on conventional droop controls, which are commonly used in the power system. As shown in Chapter 3 and in various studies [123–125], EVs equipped with a droop control can provide frequency support in terms of FFC and SIC. Nevertheless, to define the EV droop characteristic, the following parameters are needed:

- The input signal to which the EV is responding (e.g. rate of change of frequency (RoCoF), frequency).
- The minimum and the maximum EV charging current, I_EV min and I_EV max, respectively.
- The minimum and maximum threshold for the provided service, $Threshold_{min}$ and $Threshold_{max}$, respectively. This defines the range within which the EV should provide support to the system.

Figure 4.1 shows an example of how the droop characteristic is calculated.

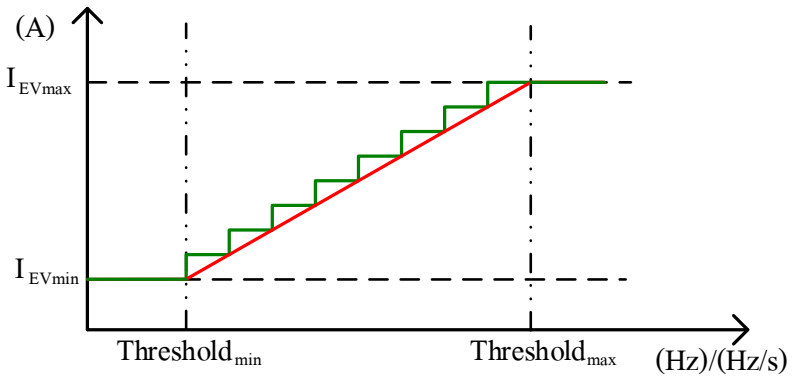

Figure 4.1: Schematic overview of the droop calculation, ideal droop (red lines) and 1 A steps droop (green lines).

As detailed in Section 3.3, due to the IEC 61851 and SAE J1772 standards, the EVs charging current must be limited to between 6 A and the maximum EVSE rated current in discrete 1 A steps. Therefore, the effective droop characteristic cannot be linear, as the ideal theoretical one, and this results in a step-wise droop. In this study the I_{EVmax} is set to 16 A as the EVSE rated current and the I_{EVmin} is set to 6 A, as established by the standards. Thus, the EV charging current, I_{EV}, is defined as follows:

$$I_{EVmin} \leq I_{EV} \leq I_{EVmax} \tag{4.1}$$

where I_{EV} is an integer number.

The thresholds are defined by the system operator as a function of the desired response. Generally, the thresholds can either be constant or they can dynamically change, based on the grid conditions or the desired power that the aggregator wants to offer. Given that this study will focus on assessing the FFC and the SIC controllers, and also the EVs technical parameters such as response time, the threshold has been set to constant values.

4.2.1.1 Fast frequency control

As explained in Section 3.3.1, the FFC is achieved by a joint action of FFC providing units and it is a frequency deviation based control. In this study, the frequency thresholds are chosen as 48 and 52 Hz, for $Threshold_{min}$ and $Threshold_{max}$, respectively.

The droop is presented in Figure 4.2a, where the dashed line represents the ideal droop and the solid line represents the real droop with 1 A granularity. To provide a bidirectional regulation capability of ± 5 A, the EVs' initial current set-point is set at 11 A. During the tuning process, due to the 1 A granularity and the established operating point, the EVs' current set-point oscillated between 11 and 12 A when the system frequency was oscillating around 50 Hz. To avoid this oscillation, the droop characteristic was shifted so that the frequency limits became 48.2 and 52.2 Hz. The control diagram for FFC is presented in Figure 4.3a. The frequency is also measured every 200 ms.

4.2.1.2 Synthetic inertia control

The SIC control is a RoCoF based control where the EV's charging current is calculated as a function of a RoCoF-current droop characteristic, as detailed in Section 3.3.1. The droop is implemented by defining the RoCoF thresholds, namely ± 2 Hz/s, with zero RoCoF corresponding to 11 A. The RoCoF is measured over 200 ms. The droop characteristic is shown in Figure 4.2b, where the dashed line represents the ideal droop and the solid line represents the 1 A granularity. Defining a deadband is a challenging task that depends on the grid characteristics (e.g. system inertia) and the desired output. To identify a suitable deadband value, a tuning process was carried out. This consisted of applying different deadband values (i.e. spanning from ± 0.2 to ± 0.8 Hz/s), and examining the performance of the system and the controller. For deadband values lower than ± 0.8 Hz/s, frequency oscillations were experienced due to the combination of low inertia, diesel's active power fluctuation, and the EVs' response time. Therefore, a deadband of ± 0.8 Hz/s has been chosen. However, this choice results in a very limited contribution from the EVs. The control diagram for the SIC is presented in Figure 4.3b.

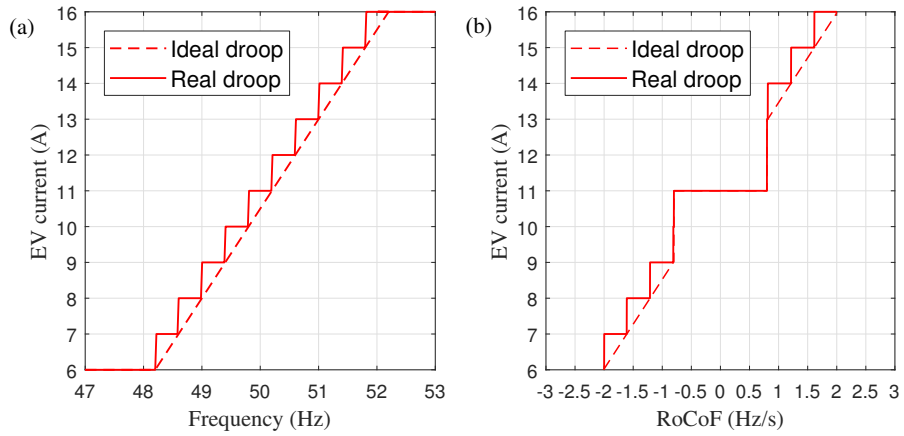

Figure 4.2: (a)FFC droop characteristic, (b) SIC droop characteristic

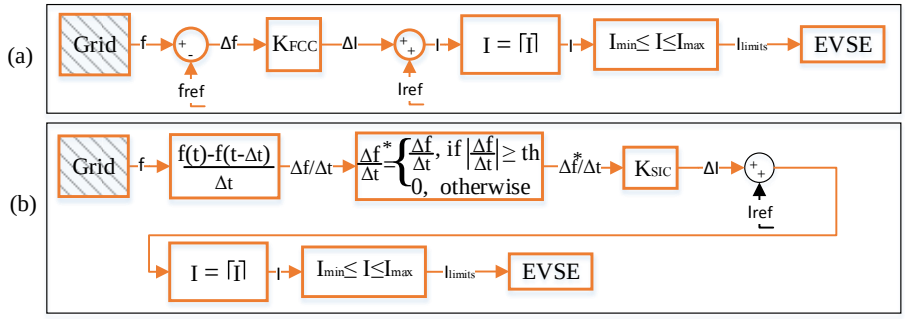

Figure 4.3: (a) FFC control diagram, (b) SIC control diagram

4.2.1.3 EV dynamic model

To successfully integrate EVs into power systems, it is necessary to correctly understand and characterize their dynamic behaviour. Therefore, a detailed model is derived by considering the battery charging and discharging characteristics, the battery dynamics (e.g. time response, ramping time, etc.), the 1 A granularity, and the control/communication delays.

The EV model is presented in Figure 4.4. Since this chapter aims at investigating and validating the EV's capabilities and limits in providing FFC and SIC, the battery state of charge is neglected. The EV model is presented in Figure 4.4.

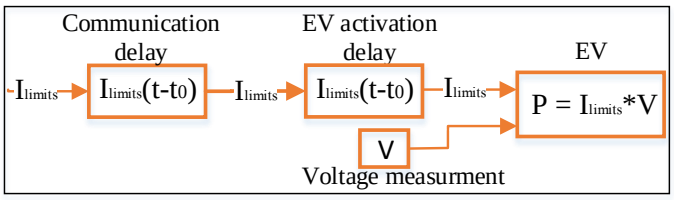

Figure 4.4: EV dynamic model

The EV dynamic model in this chapter is slightly different then that presented in Chapter 3, which focuses on energy storage dynamics in general. In this chapter the EV dynamic model is inspired by different studies where series produced EV were used [4, 99, 126]. From the dynamic point of

view, it is possible to identify two main latencies between the set and the actual current due to the communication delay and the EV activation delay, the sum of which varies between 150 ms and 2 s. The communication delay depends mainly on latencies in the IT infrastructure, which is in the range of tens of milliseconds. The EV activation delay varies among brands and it heavily depends on the embedded power electronics. The most recent models show a faster response time, as demonstrated during the experimental validation. The current standard IEC 61851 only requires the car to respond within 3 s. The total delay observed in the experimental trials ranges between 200 and 400 ms. Therefore, in the simulation study, the total delay is considered to be 250 ms. As a final note with respect to the voltage dependency, the EVs are modelled as constant current loads.

4.2.2 Experimental layout

The experiments are executed in the experimental infrastructure SYSLAB, which is part of the PowerLabDK platform [127]. SYSLAB represents a small scale, low voltage power system. This infrastructure consists of a number of real power components interconnected by a three-phase 400 V AC power grid, distributed over the Risø campus of the Technical University of Denmark [4]. SYSLAB is also characterized by its communication and control nodes, which allow a strong controllability over the grid and the ability to employ different control architectures. The different components that are used during the experiment are listed in Table 4.1. The system may be connected to the utility network or it can be islanded if desired. The experimental layout is shown in Figure 4.5.

Table 4.1: Properties of the devices used in the experiments

Device	Capability	Description	2H
Diesel genset	0 - 48 kW −20 - 30 kVAr	IVECO genset S = 60 kVA, 2 pole pairs	1 s
Aircon wind turbine	10 kW @ 11 ms	Wind turbine type 4	-
Battery	±15 kW ±12 kVA	Vanadium redox battery, 120 kWh	-
Dump-load	0 - 78 kW	Resistor load bank	-
EV1	6 - 16 A 1.4 - 3.7 kW	Nissan leaf 2016, 30 kWh lithium battery	-
EV2	6 - 16 A 1.4 - 3.7 kW	Nissan e-NV200 2014, 24 kWh lithium battery	-
EV3	6 - 16 A 1.4 - 3.7 kW	Nissan e-NV200 2015, 24 kWh lithium battery	-

The experimental setup is composed of two busbars that are connected by a 675 m underground cable. The vanadium redox battery (VRB) is connected to Busbar 2 and it is installed in Building 2, where the busbar is located. The other components are connected to Busbar 1 and they are installed in the same building as the busbar. The Aircon wind turbine is installed around 10 m from Busbar 1. The VRB, the Aircon wind turbine and the dump-load are controlled through a MATLAB/Java interface, while the EVs are controlled through a Python interface.

Given that all of the components are three-phase, except the EVs, it has been necessary to create an intermediate phase splitter. Each EV is supplied on a different phase via a standard Mennekes (IEC 62196 Type 2) connector, as shown in Figure 4.6. The three Mennekes plugs are controlled separately by three different EVSEs.

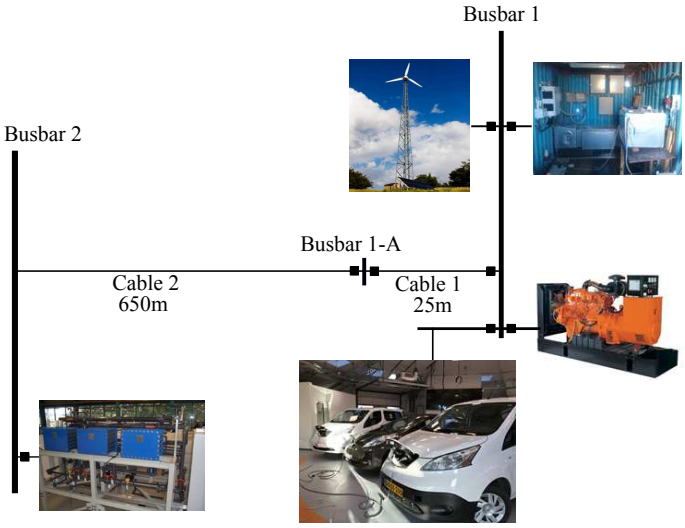

Figure 4.5: Experimental layout.

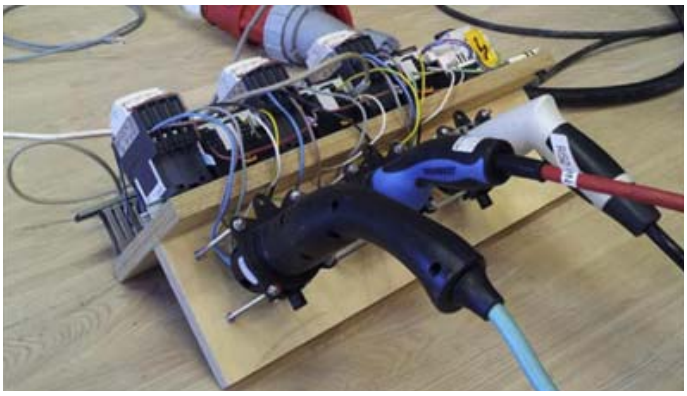

Figure 4.6: Three-phase splitter: three Mennekes plugs used to connect each EV to a separate phase. Used with permission from the author in [4].

The experiments are executed in an islanded configuration, where the diesel generator-set acts as the grid forming unit and is the only unit providing synchronous inertia (2 H=1 s). The diesel generator also compensates for the small amount of inductive reactive power drawn by each EV, corresponding to 200 VAr each.

4.2.3 Communication architecture

Each of the three single phase EVs are connected to a different phase of the grid by means of three EVSEs. The control and communication setup is shown in Figure 4.7.

This setup consists of the following components:

- The smart charging controller – which receives the measurements from the multi-instrument, calculates the response, and sends the control signals to the EVSE.
- DEIF MIC-2 – which is a multi-instrument measurement device that shows the voltage, current and power measurements with 0.5% accuracy. This device is only used for data logging.

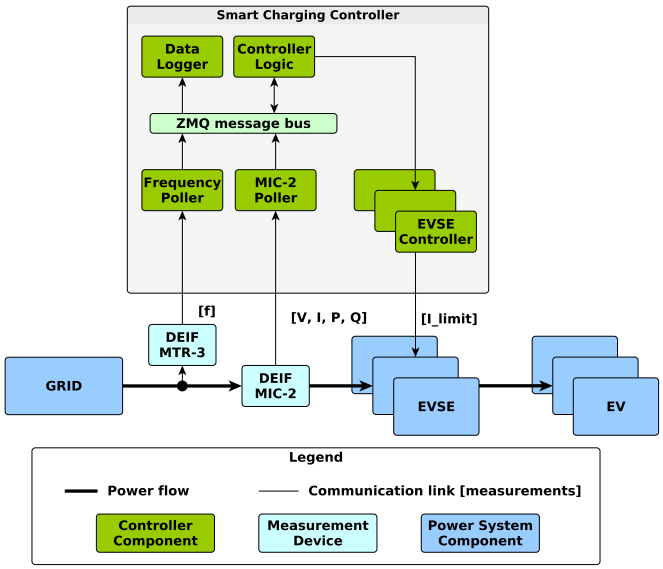

Figure 4.7: The communication architecture for the implemented smart charging controller.

- DEIF MTR-3 – which is a multi-instrument measurement device that is used here for fast frequency measurements, which are polled every 200ms.
- EVSE – which is rated for 16 A
- EV – which is the tested vehicle.
- Grid – which is the grid connection at the SYSLAB experimental facility.

The smart charging controller consists of the following sub-components:

- Controller logic – which reads the latest frequency measurements from the message bus and then calculates the $\Delta f/\Delta t$ and the Δf. The calculated set-points are directly sent to the EVSE controller.
- EVSE controller – which acts as an interface between the physical EVSE and the controller logic.
- Frequency poller – which acts as an interface to the frequency measurement device. In this case, the DEIF MTR-3 instrument is used for frequency sampling every 0.2 s with accuracy of ± 10 mHz.
- MIC-2 poller – which is a multi-instrument device interface.
- Data logger – which monitors the data exchange on the message bus and logs it to the database.
- ZMQ message bus – which is the message bus that is used to represent the data exchange between the previously mentioned controller components.

The timing of the response is crucial for the provision of fast frequency services in terms of FFC and SIC. Therefore, the timing of each component in the control loop is important, as follows: frequency and RoCoF are measured every 200 ms, the controllers' response is almost instantaneous and communication delay in the order of 10–20 ms. Each EV/EVSE pair is controlled independently. This uses multi-threading and each EVSE only receives a new control signal if the set-point has changed. Finally, the EV's reaction time is approximately 200–300 ms and, therefore, the whole control and actuator chain has an overall latency equal to 400–500 ms.

4.2.4 Simulation layout

The simulations are carried out by means of the simulation software DigSILENT PowerFactory. The modelled power system, in which the analysis is carried out, is a reproduction of the experimental facility at SYSLAB. The same components that were previously mentioned in Section 4.2.2 and summarized in Table 4.1 are used.

4.3 Simulation analysis

As previously mentioned, the simulation analysis is carried out in the simulation platform DigSILENT PowerFactory. This aims to investigate the effects of synthetic inertia control and fast frequency control, and to achieve preliminary results before experimentally validating the controllers. To explore the effects of the 1 A granularity that is imposed by the standard, a sensitivity analysis of different granularity values is also conducted. It should be noted that the simulation analyses in Chapter 3 were intended to investigate the capabilities and limitations of DER (including EVs) in providing frequency support services. In contrast, the simulation analysis in this chapter are intended to provide a more detailed investigation of series produced EVs with validated models from previous experimental studies and the controllers' performance before the experimental validation. To better replicate the same response between simulation and validation, the same active power set-points are used and the active power fluctuations due to the diesel' dynamics are emulated during the simulation analysis.

The same components and grid configurations that are presented in Figure 4.5 have been modelled here. A load event with amplitude of 2 kW (8.7% of the total consumption) is applied at $t = 10$ s. Three scenarios are investigated. In the first scenario, the EVs are treated as a constant load; that is, constant current set-point equal to 11 A (Base case scenario). In the second scenario, the EVs participate with SIC. In the third scenario, the EVs participate with FFC. The active power set-points of the various components are listed in Table 4.2.

Table 4.2: Device set-points used in the simulation

Device	**Active power set-point (kW)**
Diesel genset	24
Aircon wind turbine	-
Battery	9
Dump-load	7
EV1	2.5
EV2	2.5
EV3	2.5

To make this study as realistic as possible, an oscillatory frequency trend has been introduced in the system. This has been induced by fluctuating the active power absorbed by a three-phase resistive load as a function of a measurement file, which contains a 10 min SYSLAB frequency measurement. This has made it possible to emulate the realistic frequency oscillation that the real diesel synchronous generator would generate in such an islanded grid configuration. Both the SIC and FFC controllers are implemented according to the control diagrams in Figure 4.3, thus applying integer EV current set-points to assure standard-compliance. Figure 4.8 shows the grid frequency, the RoCoF, and the EVs' current set-point.

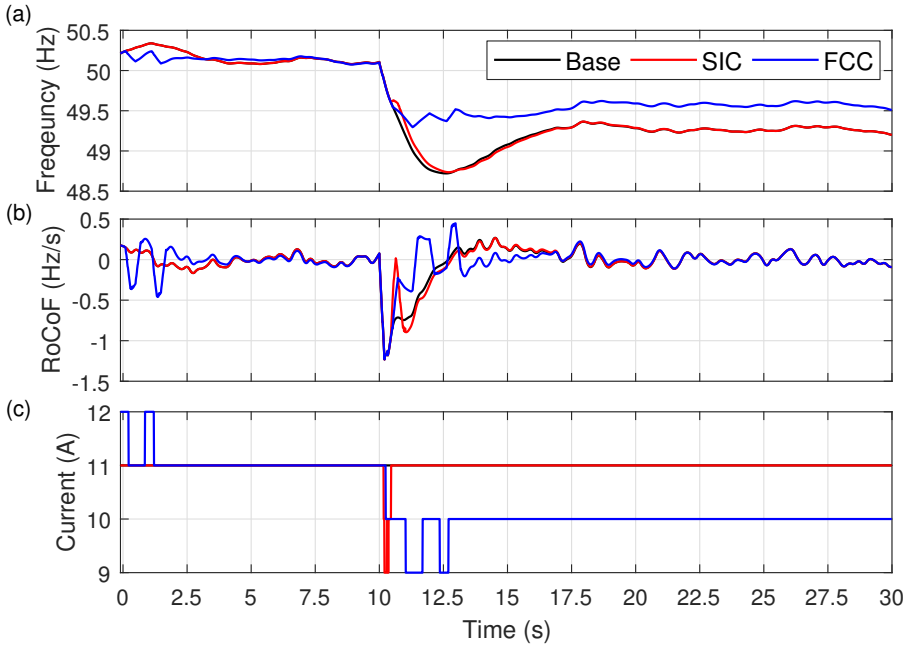

Figure 4.8: Simulation results obtained by applying ± 0.8 Hz/s deadband for SIC: (a) frequency, (b) RoCoF measured over 200 ms, and (c) EV current set-points for the three analysed scenarios, in case of granularity of 1 A.

As expected, Figure 4.8a shows that FFC improves the frequency behaviour in terms of frequency nadir and steady state value. It also shows that SIC ameliorates the frequency slope, which is a typical behaviour of introducing more synchronous and/or synthetic inertia into the system. In contrast, unexpectedly, Figure 4.8b shows that FFC has a relatively better performance in terms of RoCoF compared to SIC .

A steeper droop and/or smaller deadband for SIC would have led to better performance regarding the RoCoF and the frequency slope. To demonstrate this point, the same simulations were executed by changing the deadband of SIC to ± 0.5 Hz/s instead of ± 0.8 Hz/s. The results are presented in Figure 4.9.

Figure 4.9a shows an improvement regarding the frequency slope compared to the previous case. Figure 4.9b shows a marginal improvement regarding the RoCoF. However, it should be noted that the RoCoF depends mainly on the time window over which the RoCoF is measured. Compared to the previous scenario, Figure 4.9c shows that the EVs were participating more by changing the current set-point.

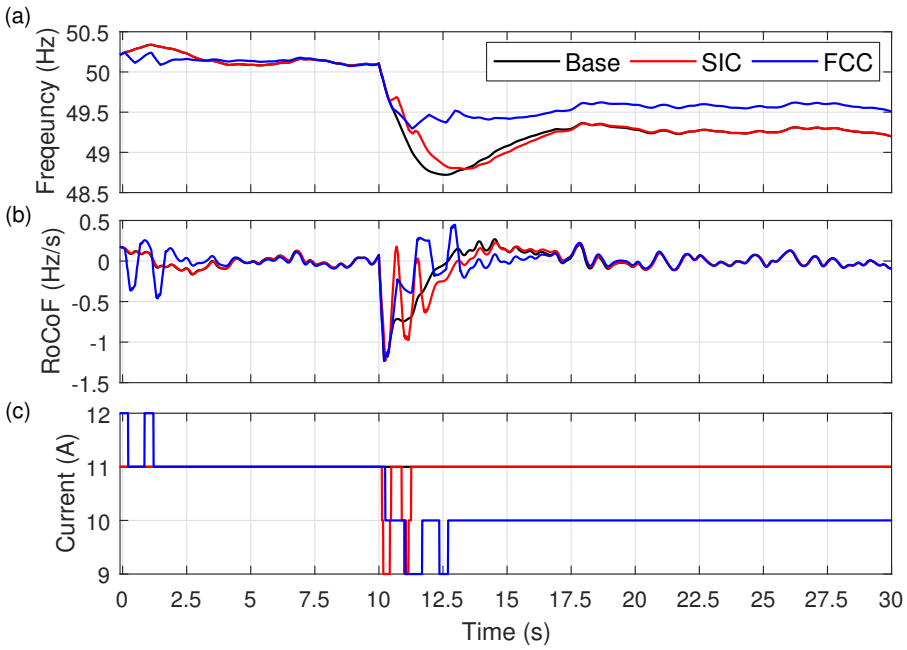

Figure 4.9: Simulation results obtained by applying ± 0.5 Hz/s deadband forSIC: (a) frequency, (b) RoCoF measured over 200 ms, and (c) EV current set-points for the three analyzed scenarios, in case of granularity of 1 A.

A sensitivity analysis is performed to better understand the effects of the 1 A granularity imposed by the standard IEC 61851 [115] on the performance of the two controllers in terms of system frequency. A series of simulations were carried out employing different load steps and different granularities. Frequency drops have been obtained by increasing the active power absorbed by the VRB by 20%, 40%, and 60%, which represent a load event of 8.7%, 15.7% and 23.5% of the total consumption, respectively. For the evaluation of the influence of the granularity, the following values of granularity have been applied, which are expressed as a fraction of the actual granularity of 1 A: $\frac{1}{4}$, $\frac{1}{2}$ and 1. Moreover, for the sake of completeness, the case of continuous regulation (no granularity) and the uncontrolled case have also been included in the analysis.

Figure 4.10 reports 3D bar plots of the results for all of the performed simulations. The results are reported by means of standard deviations (SD) for both frequency and RoCoF for FFC and SIC.

As expected, Figure 4.10 shows that, in all of the cases, the standard deviations depend on the size of the load step. On the one hand, they are mostly constant for the different considered granularities while, on the other hand, higher values are found in the uncontrolled cases. Moreover, it is noticeable that beneficial effects on the frequency are found in case of FFC. As presented in Figure 4.9, the EVs contribution makes the frequency rise to a higher steady-state value. It is of interest to highlight that the FFC shows an unexpected better contribution to the RoCoF limitation in comparison to the SIC. This is due to the limited number of control actions that took place in case of SIC, which is caused by the implemented RoCoF deadband (as shown in Figure 4.2b). Instead, when providing frequency support via FFC, no deadband is applied. This activates the controller more often, thus contributing more to the RoCoF containment.

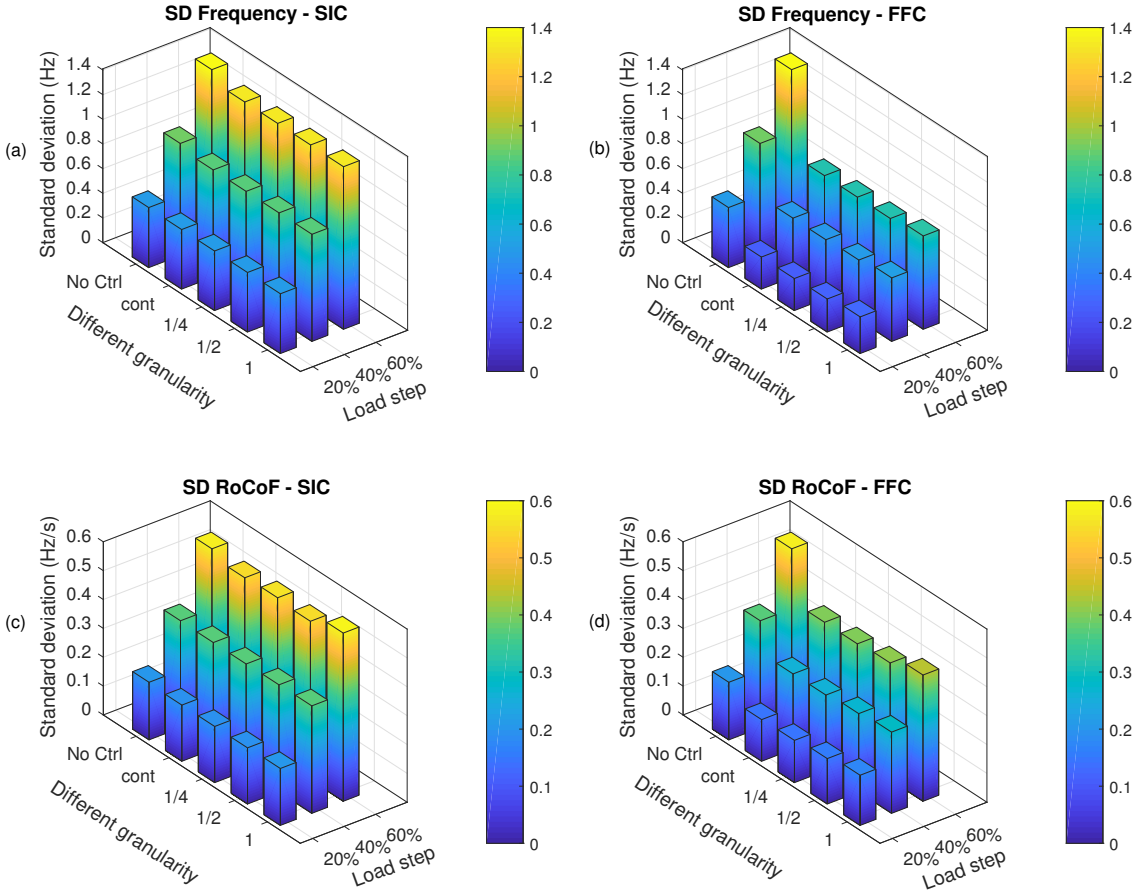

Figure 4.10: a) SD of the frequency applying SIC and b) SD of the frequency applying FFC, c) SD of the RoCoF applying SIC, and d) SD of the RoCoF applying FFC.

This sensitivity analysis shows that, in this islanded microgrid, the granularity does not influence the results. However, it should be noted that under a certain combination of system attributes (system inertia and stiffness of the power system) and control units parameters (amount of power involved in the regulation, droop and response time of the control actions), the granularity might lead to system instability or oscillation between two consequent set-points, as was experienced during the validation phase and discussed in Section 3.3.1.

4.4 Experimental validation

The experimental validation is executed in the islanded configuration that is shown in Figure 4.5, where the diesel generator is the grid forming unit. Two study cases are analyzed. In the first study case (SC1), the system includes a set of load steps. An alternate load-increase and load-decrease are applied, so that both over and under frequency dynamics can be analyzed. In the second study case (SC2), wind power generation is added to the system. This adds random power fluctuations over the tested period, which allows the possibility of investigating the behaviour of the two controllers and the EVs in a more realistic and challenging situation.

The two study cases are each composed of three scenarios. In the first scenario, the EVs are treated as constant loads; that is, constant current set-point equal to 11 A (Base case scenario). In the second scenario, the EVs participate with a synthetic inertia response. In the third scenario, the

EVs participate with a fast frequency response. The grid units and also the initial conditions are reported in Table 4.3.

Table 4.3: Device set-points used in the experimental validation

Device	**SC1** P_0 **(kW)**	**SC2** P_0 **(kW)**
Diesel genset	24	24
Aircon wind turbine	-	$\sim$4
Battery	9	-
Dump-load	7	21
EV1	2.5	2.5
EV2	2.5	2.5
EV3	2.5	2.5

4.4.1 Study Case 1

In the first study case, the frequency variation is triggered by several load steps. A set of load events from the VRB of the same amplitude is applied ($\approx \pm 2$ kW), namely: 8.7% of the initial installed load. To better investigate the controllers and also the frequency dynamics, an additional set of load events with a different amplitude is applied, specifically: ($\approx \pm 4$ kW), 17% of the initial installed load.

The three scenarios are characterized by the same initial conditions and load steps. The first scenario (S1) is a base case, in which the EVs receive a constant current set-point; that is 11 A, absorbing around 2.5 kW. In the second scenario (S2), the EVs are controlled by means of the synthetic inertia controller, which modulates the charging level between 6 and 16 A with steps of 1 A as a function of the RoCoF-current droop characteristic presented in Figure 4.2b. In the third scenario (S3), the EVs are controlled by means of a fast frequency controller. The controller modulates the EVs' charging level between 6 and 16 A with steps of 1 A as a function of the frequency-current droop characteristic presented in Figure 4.2a. The results of the experiments are presented in Figure 4.11.

Figure 4.11a shows the system frequency for the three scenarios. Figure 4.11b shows the RoCoF measured over 200 ms in grey and the filtered signal after applying the deadband in red (± 0.8 Hz/s deadband is considered). In Figure 4.11c the controllers' current set-point is plotted versus the EVs' absorbed current. Because the three EVs act similarly, only the current of EV1 is presented.

Figure 4.11c shows that the EVs change the absorbed current as desired by the different controllers. However, due to the 1 A granularity and the implemented droop, the 2 kW load event results in an operating condition in which the FFC implies the EV's current set-point to oscillate between 12 and 13 A, and between 9 and 10 A. To highlight the affects of the operating condition on the current set-point oscillation, a 6 kW load event was introduced for Scenario 3. In fact, Figure 4.11c shows that the EV's current did not oscillate for this load event (around t = 450 s). However, this oscillation can be reduced by implementing a hysteresis function.

Figure 4.11a shows that FFC limits the maximum frequency deviation compared to the base case, while the SIC does not effect it. In contrast, due to the oscillation between the different set-points in case of FFC, Figure 4.11b shows that the RoCoF was outside the deadband more frequently when compared to Scenarios 1 and 2.

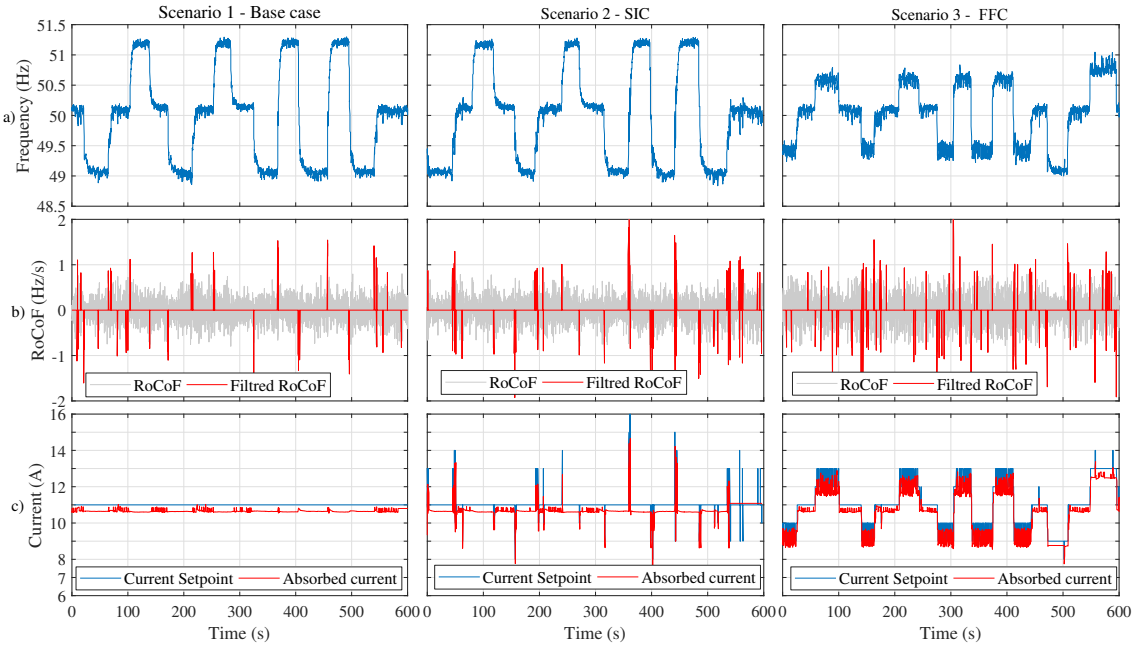

Figure 4.11: a) Frequency, b) RoCoF measured over 200 ms in grey and the filtered signal after applying the deadband in red (± 0.8 Hz/s deadband is considered), and c) EV1's set-point vs absorbed current.

Due to the response delay of the EVs and the dynamics of the diesel generator, which led to a continuous frequency oscillation, it is difficult to perceive a valuable improvement in terms of the RoCoF from SIC.

To better compare the performance of the two controllers in terms of RoCoF and frequency, the standard deviation and the energy contained in the signal (also addressed as normalized energy) is calculated and presented in Table 4.4. For a discrete signal $x(n)$, the normalized energy is calculated as $\frac{1}{N}\sum_{n=1}^{N} x(n)^2$, where N represents the number of samples taken for computation. This shows that the two controllers do not improve the RoCoF when compared to the base case.

Table 4.4: SC1—Standard deviation and normalized energy

	RoCoF		Frequency
	SD	Normalized energy	SD
Base	0.29	0.083	0.77
SIC	0.31	0.093	0.79
FCC	0.33	0.11	0.48

To understand the effects of the SIC on the frequency compared to the base case, Figure 4.12 shows a zoom of the frequency, the RoCoF, and the EV's absorbed current for the three scenarios. In Figure 4.12a, one can notice that the SIC has improved the frequency slope as expected and as experienced during the simulations. Due to the embedded deadband, the SIC contribution is very limited. However, since the three EVs are characterized by the same delay and granularity (i.e. acting simultaneously with steps), one can observe a sharp change in frequency. This will lead to worse RoCoF compared to the base case, as shown in Figure 4.12b. To overcome this issue, it might be of interest to study different delays and droops among the EVs. This might induce a

more smooth frequency change and, therefore, a better RoCoF. However, the potential unbalances due to the use of single phase EVs should be considered. It is of interest to notice from Table 4.4, where the SD is reported, and Figure 4.12b that the FFC has worsened the RoCoF when compared to the SIC and the base case.

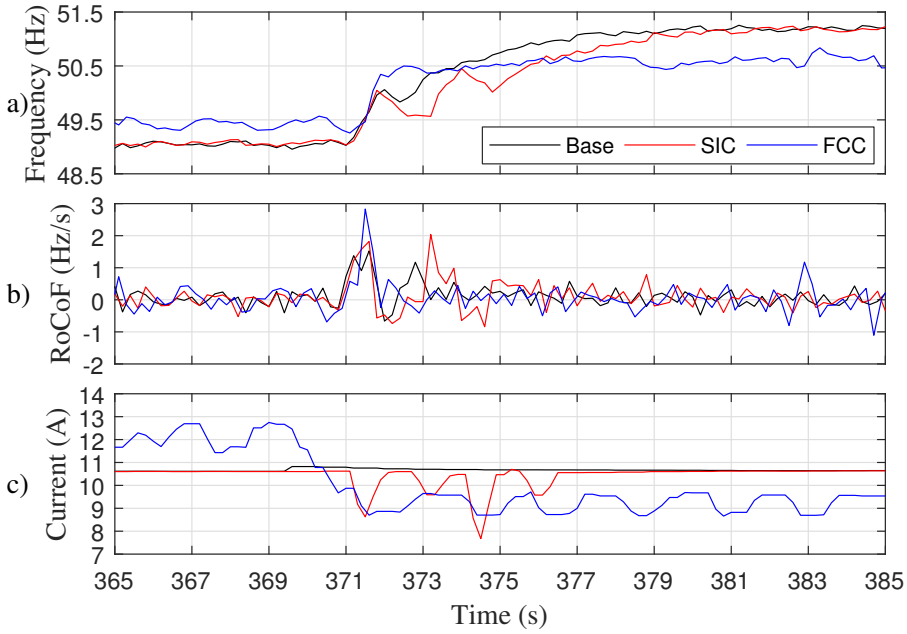

Figure 4.12: a) Frequency, b) RoCoF measure over 200 ms window, c) EV1's absorbed current.

4.4.2 Study Case 2

In the second study case, the two controllers are analyzed when the Aircon wind turbine is connected. The VRB is set to zero during this study case. The same scenarios and droop characteristic as the previous study case are applied. Due to the random stochasticity of the wind generation and the diesel generator's dynamics, the initial and boundary conditions are not exactly identical. Nevertheless, this study case aims to investigate the performance of each controller and the EVs in a more challenging and realistic configuration rather than comparing the different scenarios. The experimental results for SC2 are presented in Figure 4.13.

Figure 4.13a shows the grid frequency for the three scenarios. Figure 4.13b shows the RoCoF measured over 200 ms in grey and the filtered signal after applying the deadband in red. In Figure 4.13c, the controllers' current set-point is plotted versus the EVs' absorbed current. Given that the three EVs are acting similarly, only the current of EV1 is presented.

The three scenarios were executed over a total period of 30 minutes. The average wind production did not differ so much among the three scenarios and, therefore, the different scenarios are still comparable. Figure 4.13a shows that the FFC does have a remarkable effect in limiting the maximum frequency deviation. Figure 4.13b shows that by applying the SIC, the RoCoF is outside the deadband more frequently.

To better compare the three scenarios, the mean value and standard deviation of the wind production together with the standard deviation of the frequency and the RoCoF are calculated and presented in Table 4.5.

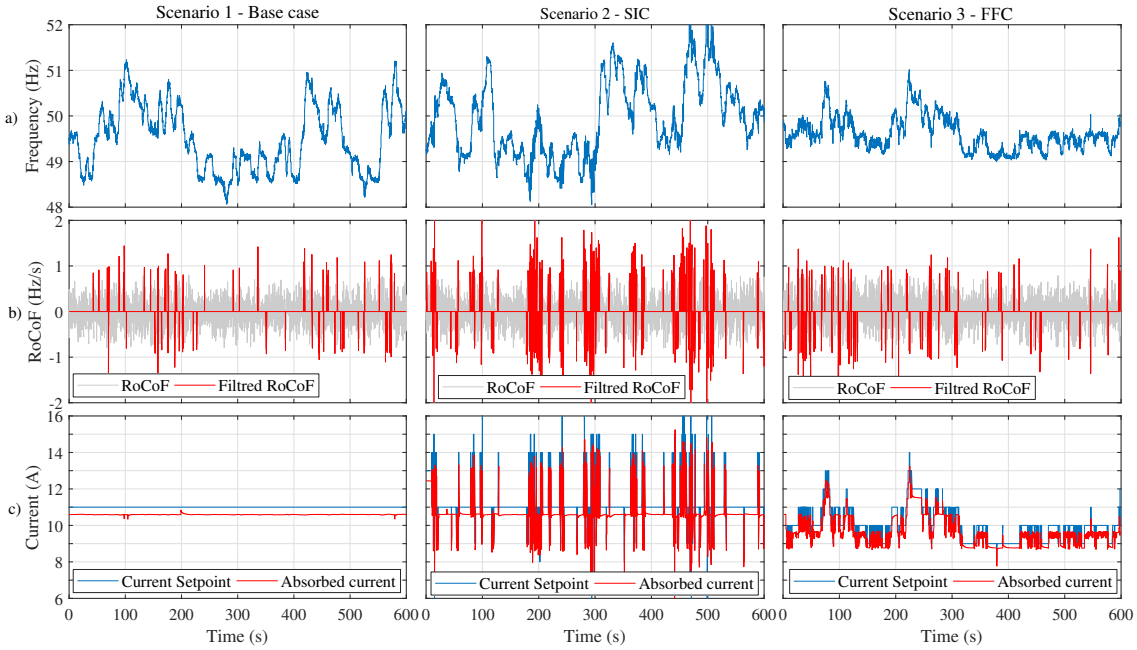

Figure 4.13: a) Frequency, b) RoCoF measured over 200 ms in grey and the filtered signal after applying the deadband in red (± 0.8 Hz/s deadband is considered), and c) EV1's set-point vs absorbed current.

Table 4.5: SC2—Standard deviation and normalized energy

	Wind generation		RoCoF		Frequency
	Mean	SD	SD	Normalized energy	SD
Base	3.5	1.4	0.31	0.098	0.71
SIC	4.6	1.68	0.45	0.2	0.83
FFC	3.1	1.28	0.34	0.11	0.36

As mentioned previously, due to the random wind production and the non-perfect replicability of the same conditions, the comparison among the different scenarios is not completely accurate, especially in terms of RoCoF due to the continuous variation of the wind profile.

However, the mean value of the wind production among the three scenarios does not differ excessively, which allows a comparison to be made of the standard deviation of the frequency among the scenarios. Table 4.5 and Figure 4.13a shows the remarkable positive effect of FFC on the frequency.

4.5 Summary

This chapter has investigated the technical ability of current series-produced EVs to provide frequency support by improving RoCoF, frequency nadir, and steady state value. A decentralized smart charging controller based on droop control has been developed and used by the FFC and SIC controllers. The experimental analysis focused on presenting the capabilities and limitations of the two controllers, and consequently of the EVs in providing these services when both load events and exogenous wind generation profiles are applied. To better investigate the effects of the

1 A granularity imposed by the standards, a sensitivity analysis was carried out in the simulation platform DIgSILENT PowerFactory.

Employing the FFC, the experimental validation the controller ability in limiting the maximum frequency deviation, both following a series of load events or considering wind power generation. Although in simulation the sensitivity analysis showed a very limited effect of the granularity, in the experimental phase, due to the 1 A granularity, the FFC caused the EV absorbed current to oscillate between two consecutive set points, which worsened the calculated RoCoF. It should be noted that this oscillation was due to the combination of 1 A granularity, the implemented droop, and the operating point. By changing the amplitude of the load event, the oscillation was eliminated.

Similarly for the SIC, the experiments were conducted by following a series of load events and then considering wind power generation. In terms of frequency nadir and steady state values, the SIC effects were negligible for both cases. When only load events were applied, even if the EVs were able to follow the desired set points, the SIC did not show a noticeable improvement in terms of RoCoF. Considering wind power generation, the SIC had negative effects in terms of RoCoF. It should be noted that this effect might have been limited by employing less steep droop parameters; however, this would have limited the EVs participation (i.e. flexibility margin).

All in all, it can be concluded that the actual series produced EVs are able to provide ancillary services in terms of fast frequency response and synthetic inertia by solely relying on unidirectional charging. In contrast, the experiments show that with the actual EV's response time, the system inertia and the diesel dynamics, a large deadband was needed for the SIC and this limited its contribution. To achieve better performance, new requirements in terms of the EV's response time need to be set.

CHAPTER 5

The quantitative relationship between converter connected reserves and synchronous inertia

The focus of this chapter is twofold. First, it aims to investigate the ability of fast frequency control (FFC) and synthetic inertia control (SIC) to mitigate the rate of change of frequency (RoCoF), using an equivalent model of the All Island Power System (AIPS) and simulated system dispatches provided by the transmission system operator of the Republic of Ireland. Second, it will analyze the quantitative relationship between the MW of converter connected reserves and the correspondent MWs of synchronous inertia that they will replace. This chapter includes results of the separate paper Pub. [H].

5.1 Overview

As previously discussed in Chapter 2, the increasing share of distributed and inertia-less resources requires balancing and system stabilization services. The reduction of system inertia has two implications for system frequency stability: the first is faster RoCoF, resulting in possible tripping of grid components, especially embedded renewable generation, conventional generation pole slipping and cascade tripping.; and the second is higher frequency deviations (nadirs/zeniths), which can potentially lead to load shedding and, in the worst cases, system collapse.

Various transmission system operators (TSOs) with limited AC interconnections have identified these issues to be of critical significance and they have initiated mitigation measures. To deal with the implications of the reduction of system inertia, TSOs are generally interested in investigating the capability of SIC and FFC in augmenting system inertia through fast acting reserves (FAR). They are also interested in evaluating the volume of FAR that can potentially compensate for the reduction in system inertia [26, 27, 37].

In this chapter, an equivalent model of the AIPS is used, which is the synchronized power system linking the Republic of Ireland and Northern Ireland. First, this chapter will examine the possibility of mitigating the RoCoF by using SIC and FFC. Second, this chapter will use 780 simulated dispatches to define a quantitative relationship between the MW of converter connected reserves and the MWs of synchronous inertia.

5.2 System model and methodology

Similarly to Chapter 3, SIC and FFC controllers are implemented and energy storage system (ESS) is used as a flexibility resource. However, this study is characterized by the use of an equivalent

power system model and generation units data of the AIPS. The data of the AIPS are provided by the TSO of the Republic of Ireland (EirGrid). This study will also assess the quantitative relationship between the MW of FAR and the MWs of synchronous inertia. A detailed description of the power system model and the proposed methodology is presented in the following section.

5.2.1 System model and generating units

A single busbar equivalent model of the AIPS, which is the synchronized power system linking the Republic of Ireland and Northern Ireland, has been considered as the study case system [128]. The AIPS is projected for the year 2020, has been developed as a single busbar dynamic model, and has been employed to assess system frequency stability. This model will be described as the single frequency model (SFM). The AIPS is an islanded system with two HVDC connections to Great Britain. An overview of the system installed capacity is represented in Table 5.1. The system has a total dispatchable power of 10064 MW [129].

Table 5.1: The AIPS installed capacity and load

Fuel Type	**Installed capacity**
Gas and/or distillate oil	6249 MW
Pumped storage hydro	292 MW
Milled peat and biomass	346 MW
Coal and/or heavy fuel oil	1961 MW
Hydro	216 MW
DC interconnector	1000 MW
All wind (partially/non-dispatchable)	5000 MW
Peak load	6900 MW

Specifically, the SFM is used to examine the frequency behaviour of the power system following the loss of the largest single infeed (LSI). The model had been previously developed on MATLAB/Simulink platform and more details can be found in [130]. The SFM employs a single busbar that concentrates on the energy imbalance of the power system, while ignoring any of the transmission characteristics. The SFM assumes a single busbar and it represents the dynamic interactions of turbines, governors, boilers and load. This model has been developed over many years for the power system of Ireland and Northern Ireland, and it has been validated based on the manufacturers' data and real event traces to provide accurate traces of the overall system frequency response in the first 30 s following significant generation/demand imbalance events [131, 132].

The SFM model includes all of the generators present in the AIPS fed by any desired dispatch. All generation units are assumed to be grid code compliant with droop settings of approximately 4%. The characteristics of individual plants, such as plant inertia, are based on data provided by the manufacturers. Fixed speed wind turbines and variable speed wind turbines are modelled separately to recognize the inertia contribution from the fixed speed turbines. A schematic layout of the single bus frequency model is shown Figure 5.1. The Plexos production cost modelling tool was used to simulate hourly dispatch schedules for the year 2020 [128]. The key assumptions of the Plexos 2020 model include installed wind generation of 5 GW and system peak load of 6900 MW. In this study, 780 dispatches that are representative of different operational scenarios, are used.

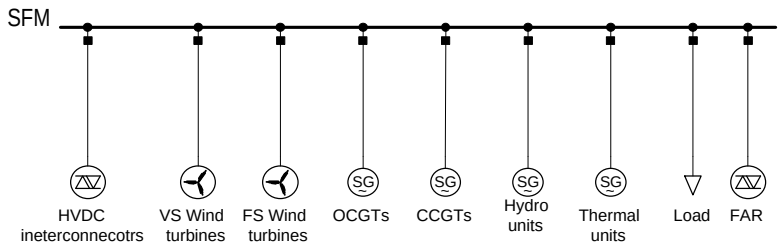

Figure 5.1: The single frequency model representation

5.2.2 Methodology

This study applies a bottom-up inductive approach for a quantitative evaluation of synchronous inertia, which can be potentially replaced by a specified magnitude of FAR. The inductive approach provides a systematic set of procedures for analyzing data that can produce reliable and valid findings. This study employs two different control mechanisms for FAR, namely SIC and FFC. The method begins by examining the RoCoF following the loss of the LSI and it then removes one conventional plant and its associated inertia, which is substituted with FAR. An equivalence is established when the RoCoF value from the pre-plant removal and post FAR addition equalizes. This process will be done over a large number of dispatches. It has been decided to calculate the RoCoF over a 500 ms moving window, similar to the RoCoF relay's requirements in the Irish grid code [37]. A flow chart of the applied method is presented in Figure 5.2 and the following procedure is used:

1. Apply a simulated system dispatch (e.g. dispatch A) to the SFM, and then evaluate the system frequency and RoCoF following the loss of the LSI.

2. Dispatch A is modified by removing a conventional plant and its associated inertia, and then re-dispatching the power of the removed plant over the remaining ones (dispatch A'). The LSI must remain the same as in dispatch A.

3. Add FAR reserves to the modified dispatch to compensate for the removed inertia. An equivalence between the MW of FAR and the MWs of synchronous inertia is established when the maximum average RoCoF from the pre-plant removal and post FAR addition equalizes.

The implemented control diagrams of the SIC and FFC are represented in Figure 5.3-a and Figure 5.3-b, respectively. The proportional control (K_{SIC} and K_{FFC}) are calculated through an iteration process to determine the required amount of reserves that are able to compensate for the reduced synchronous inertia, as previously explained in the methodology. As detailed in Section 3.2, FAR's dynamics can be represented through a transport delay and a first order system, as have been used in many studies [107–110]. The values of the two parameters are determined based on various studies and energy storage data-sheets [95, 96]. For example, Sodium Sulphur batteries (NaS) are characterized by their fast response time and, as claimed by certain manufacturers, the response time is within 1 ms [94] .

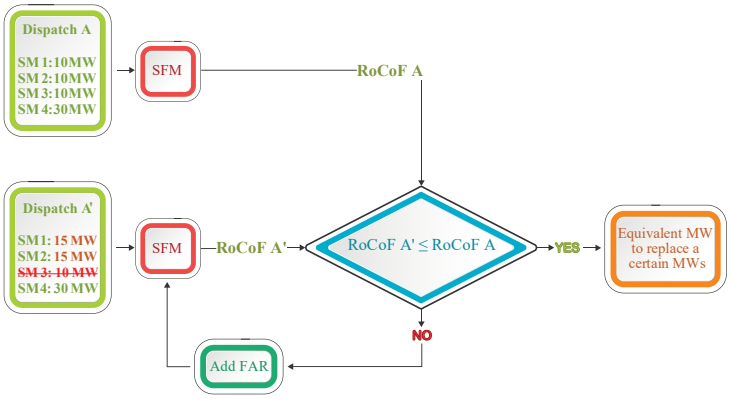

Figure 5.2: Applied methodology flow chart

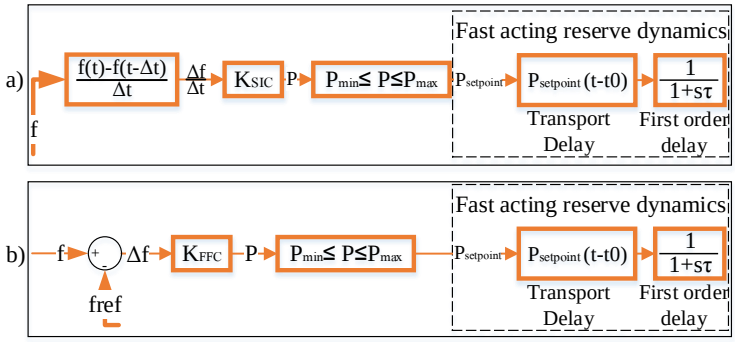

Figure 5.3: a)SIC control diagram, b)FFC control diagram

5.3 Results

Four different scenarios are analyzed. In all four scenarios, the system response is triggered by the loss of the LSI, which varies over the different dispatches. A brief description of different scenarios follows:

- Scenario 1: The first scenario investigates the ability of SIC and FFC in mitigating the RoCoF and their effects on the system stability. Applying the proposed methodology, this scenario presents the performance of the two control mechanisms when two different dispatches are applied: high inertia and low inertia dispatches.
- Scenario 2: This scenario uses 780 dispatches and applies the proposed methodology. The second scenario determines the relationship between MW of FAR and MWs of equivalent synchronous inertia.
- Scenario 3: The third scenario carries out a sensitivity analysis of the FAR's response time. It highlights the response time's effects on the system stability, and on the relationship between MW and MWs. Response times of 50 ms, 100 ms and 150 ms are used.
- Scenario 4: This scenario carries out a sensitivity analysis of the deadband applied on the control signal. The following values are used for FFC: 80 mHz, 120 mHz and 300 mHz. Similarly, for the SIC the following values are used: 80 mHz/s, 120 mHz/s and 300 mHz/s.

5.3.1 Scenario 1: FFC's and SIC's ability to mitigate the RoCoF

The first scenario analyzes the capability of FFC and SIC to limit the RoCoF and their effects on the system stability. The following deadbands are used: 80 mHz and 80 mHz/s for FFC and SIC, respectively, and 50 ms response time is applied. Using the system inertia as a metric, two different dispatches are investigated: high inertia case and low inertia case, respectively, 36855 MWs and 16649 MWs. It should be noted that although AIPS is currently not operated with such a low value of inertia, these values are considered low or high in relationship to the AIPS. It should be noted that the SFM does not consider the loads' inertia contribution and, therefore, the system inertia is composed only by the generations' inertia. The system frequency, RoCoF and energy storage's active power for the high inertia case are presented in Figure 5.4.

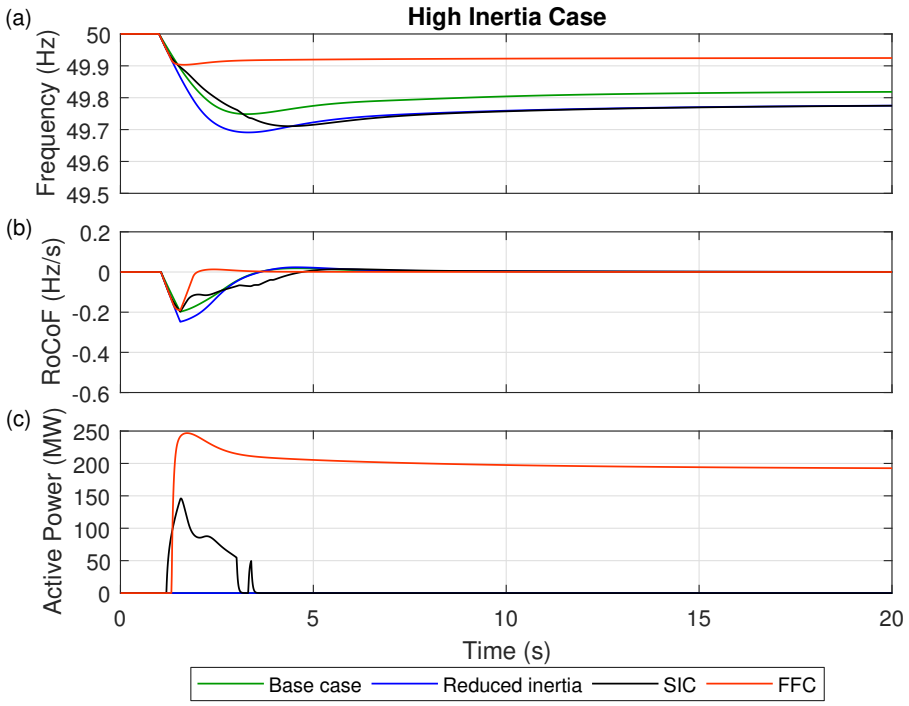

Figure 5.4: a) Frequency, b) RoCoF measured over 500 ms, c) Energy storage active power - high inertia.

Because of the different control approaches (i.e. FFC and SIC) and the applied deadbands, different amounts of MW were needed to replace the same amount of MWs of synchronous inertia. This point will be further addressed in Scenarios 2 and 3 by employing more dispatches. It can, however, be noted that the FFC required roughly the double amount of MW compared to SIC, which is due to the different deadbands. Employing 80 mHz deadband for a high inertia case where the frequency deviation is relatively small delays the FFC participation. Due to this effect, the FFC starts responding when the frequency deviation is larger compared to the start point of SIC and, therefore, it requires a larger amount of MW. Applying a 50 mHz deadband for the same study case, the FFC required only 63 MW of active power opposed to 108 MW with 80 mHz deadband.

Although this study does not aim to improve the system frequency (i.e. in terms of nadir and steady state value), the FFC has a better performance compared to the SIC. In other words, the employment of FFC to mitigate the RoCoF will implicitly support the system frequency, improving

the overall system stability. Figure 5.4 shows that FFC continues to deliver power, even after the mitigation of the RoCoF, because it is a frequency deviation based control.

In the case of low inertia (i.e. 16649 MWs), Figure 5.5 shows the ability of FFC and SIC to mitigate the maximum average RoCoF value by compensating for the reduced generation's inertia. Because of the system's low inertia, the frequency deviation was larger and steeper. This led to faster activation of the FFC compared to the high inertia case. However, the FFC still requires a larger amount of MW to compensate for the reduced generators' inertia compared to the SIC. In this case, the SIC was triggered before FFC due to the different deadband.

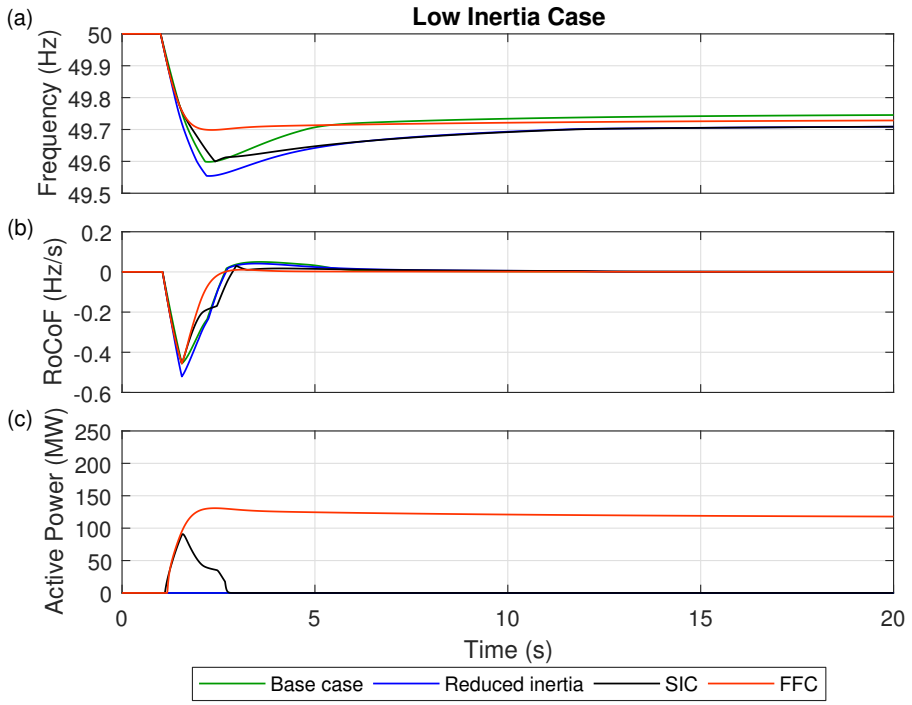

Figure 5.5: a) Frequency, b) RoCoF measured over 500 ms, c) Energy storage active power - low inertia.

5.3.2 Scenario 2: Relationship between MW of FAR and MWs of synchronous inertia

In the second scenario, 780 dispatches are used. This scenario aims to define the relationship between 1 MW of FFC (or SIC) and MWs of synchronous inertia. Applying the previously proposed methodology over the various dispatches, Figure 5.6 shows the relationship between MW to MWs and maximum average RoCoF (i.e. measured over 500 ms) for the FFC control approach. The Y axis represents the MWs that can be replaced by 1 MW of FFC while the X axis represents the maximum average RoCoF following the loss of the LSI. The blue dots represent the different dispatches. Although the relationship between MW to MWs is not constant over the different dispatches, one can see a clear trend between the MW to MWs and the system maximum average RoCoF. Using MATLAB's fitting algorithm, it was possible to determine the 3rd order polynomial regression among the different dispatches, which is represented by the following function: $y = -3.3e03x^3 - 3.8e03x^2 - 1.4e03x - 1.2e02$.

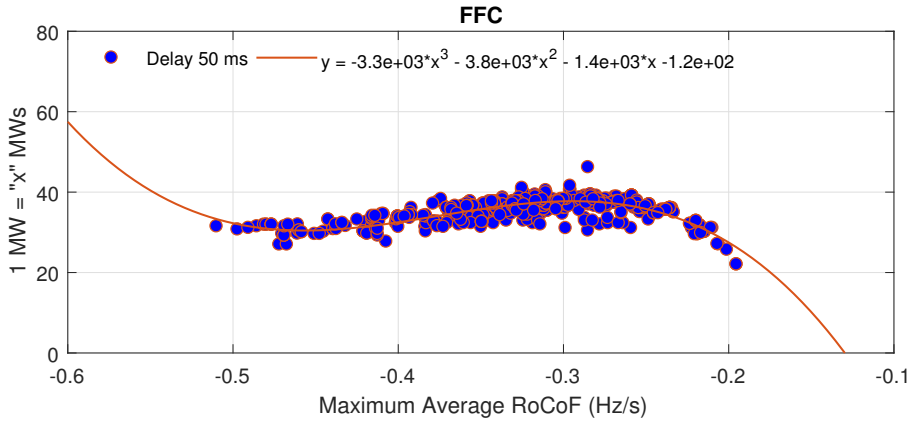

Figure 5.6: Relationship between MW/MWs and RoCoF - FFC

For low inertia cases and/or larger infeed loss (i.e. fast RoCoF), the equivalent MWs of inertia that can be substituted with 1 MW of FFC is falling. Meanwhile, due to the applied deadband as shown and explained in Scenario 1, for high inertia cases and/or small infeed loss, the equivalent MWs of inertia to 1 MW of FFC is also falling.

The same study is performed with the SIC controller. Figure 5.7 shows the relationship between MWs to MW and the system maximum RoCoF for the SIC control approach. The same dispatches are used. As in the FFC, for low inertia cases and/or larger infeed loss (i.e. fast RoCoF), the equivalent MWs of inertia that can be substituted with 1 MW of SIC are lower than for high inertia cases. In contrast, for high inertia cases, the equivalent MWs of inertia to 1 MW of SIC are not decreasing, as for FFC. This behaviour is mainly due to the different deadband between the two controllers. In other words, the 80 mHz/s deadband does not limit the SIC participation, as the 80 mHz does for FFC.

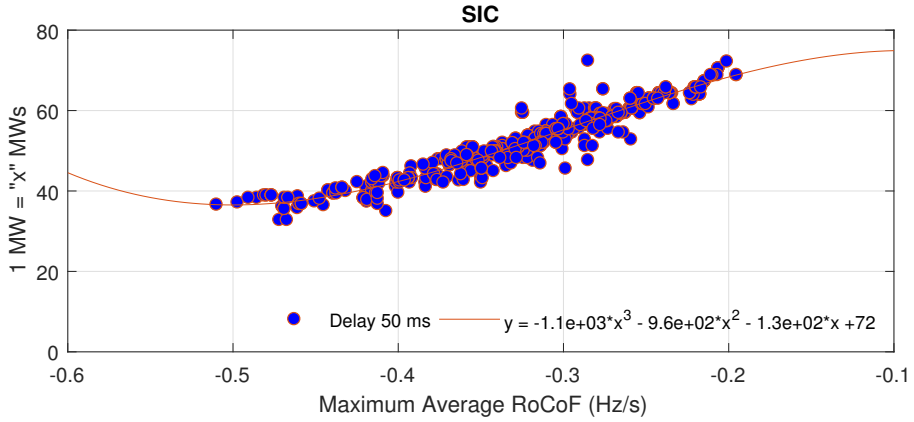

Figure 5.7: Relationship between MW/MWs and RoCoF - SIC

5.3.3 Scenario 3: Sensitivity analysis of the FAR's response time

A sensitivity analysis of the device's response time is carried out to better understand the effects of the fast acting reserves' time response on the relationship between MW and MWs, and on the overall system stability. The following time delays (i.e. response time) are applied: 50 ms,

100 ms and 150 ms. The chosen values are inspired from different energy storage manufacturers' data-sheets [94–96].

Figure 5.8 shows the time delay effect on the relationship between MW and MWs when FFC is applied. It can be noted that the larger response time reduced the FFC effects on mitigating the RoCoF, leading to the need of larger reserves. However, in some dispatches, the larger response time led to frequency oscillations and, therefore, no solution was found. Due to the delay, the controller is acting on system conditions that were occurring, for example, 150 ms in the past and not on the current conditions [133]. For dispatches with high inertia and/or small infeed loss, employing 150 ms delay with the 80 mHz deadband, the controller was unable to mitigate the maximum average RoCoF because it was occurring before the unit's response (i.e. which is represented by zero on the x axes). Figure 5.8 points out that the units' characteristics (e.g. response time, ramp rate etc.) will influence the 3rd order regression and, therefore, the method needs to be applied for each group of units of certain characteristics that are allowed to participate in this grid service.

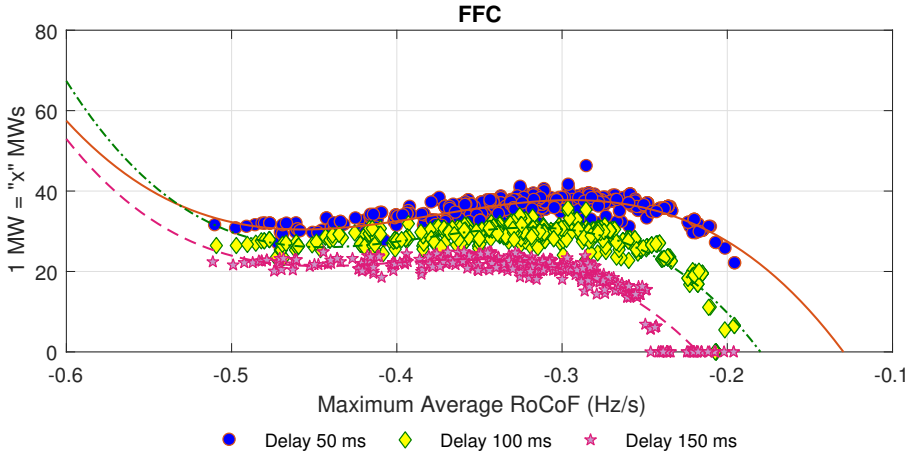

Figure 5.8: Response time sensitivity analysis - FFC

To emphasis the effects of the reserves' response time on the overall system stability, Figure 5.9 divides the dispatches into two groups: stable and unstable. This shows the number of dispatches in which the system frequency becomes unstable due to the FFC controller. Frequency oscillations cases were only present with response time of 150 ms.

Similarly to the FFC, Figure 5.10 shows the time delay effects when the SIC is applied. Also in this case, the larger response time reduced the effect of SIC in improving the RoCoF, which can be seen from the 3rd order polynomial regressions of the three utilized response times.

To highlight the effects of the reserves' response time on the overall system stability when the SIC is applied, Figure 5.11 presents the cases for which the system frequency became unstable. Compared to the FFC, Figure 5.11 shows the increased vulnerability of the system stability when a SIC control approach is applied.

Nevertheless, due to the different deadbands used by the two controllers, SIC was able to participate in mitigating the RoCoF for all of the tested dispatches. However, applying SIC, the system was more vulnerable to oscillation in a much higher number of dispatches compared to FFC and the larger response time has amplified the amplitude of the oscillation.

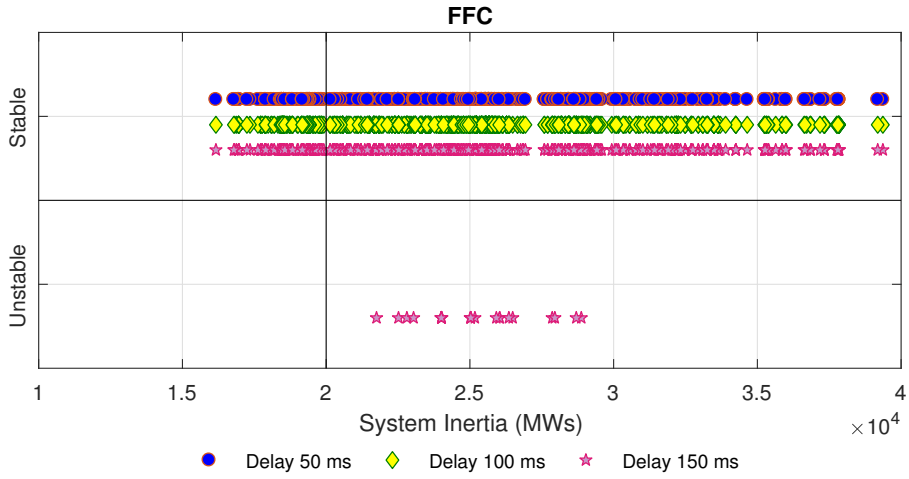

Figure 5.9: Response time effects on system stability - FFC

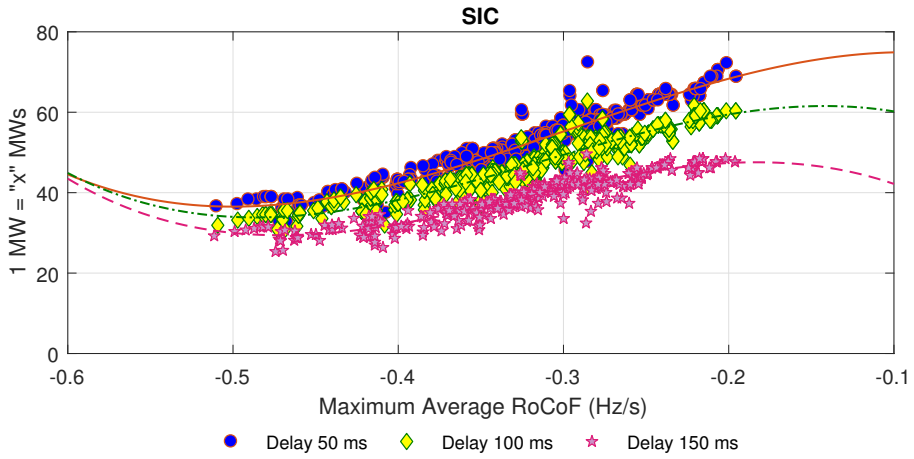

Figure 5.10: Response time sensitivity analysis - SIC

5.3.4 Scenario 4: Sensitivity analysis of the applied deadband

To better investigate the effects of the deadband used on the controllers' performance, and on the relationship between MW of converter connected reserves and MWs of synchronous inertia, this scenario carries out a sensitivity analysis of the deadband applied on the control signal. Given that this study assumes that this inertia service is a contingency based service, it has been decided to use deadband values relatively larger than the frequency deadband present on conventional generators and interconnectors established by the grid code [67]. For example, the Republic of Ireland's grid code requires that a frequency deadband of no greater than ± 15 mHz may be applied to the operation of the governor control system [59]. In this study, the following deadband values are used for FFC: 80 mHz, 120 mHz and 300 mHz. Similarly, for the SIC the following deadband values are used: 80 mHz/s, 120 mHz/s and 300 mHz/s.

Figure 5.12 shows that the larger deadband reduced the effects of FFC in mitigating the RoCoF. Employing 120 mHz deadband, for high inertia cases and/or small infeed loss, the controller was unable to influence the maximum average RoCoF because it was occurring within the applied deadband. Applying 300 mHz deadband, FFC was unable to participate in any of the dispatches

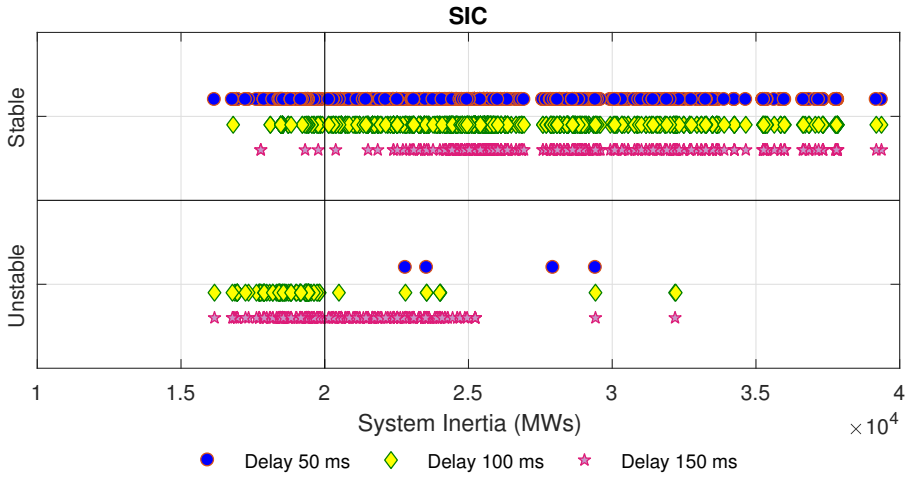

Figure 5.11: Response time effects on system stability - SIC

because all of the congestions were occurring within the deadband. On the one hand, employing a large deadband will limit the FFC participation to large congestion cases avoiding its activation following normal load change. On the other hand, Figure 5.12 points out that employing a large deadband will reduce the equivalent MWs that can be replaced by 1 MW of FFC as might also make the controller completely useless as the case with 300 mHz deadband.

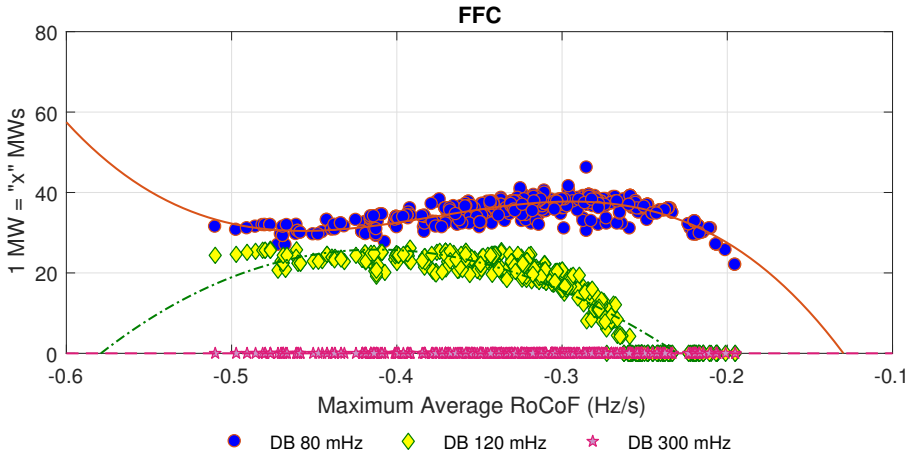

Figure 5.12: Deadband sensitivity analysis - FFC

Figure 5.13 shows that the larger deadband reduces the equivalent MWs that can be replaced by 1 MW of SIC. For low inertia cases and/or larger infeed loss (i.e. fast RoCoF), one can notice that when applying 120 mHz/s deadband the SIC performance did not differentiate so much from 80 mHz/s deadband. Employing 300 mHz/s deadband limited the SIC participation for the majority of dispatches and imposed oscillation for the remaining ones.

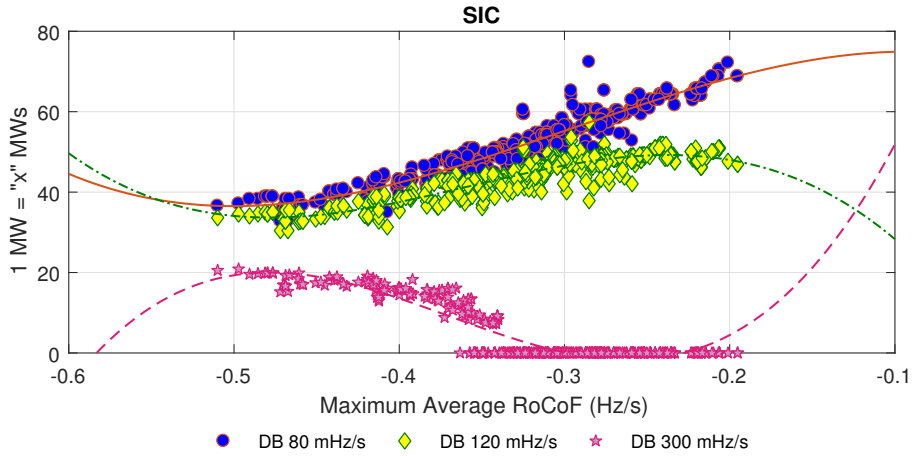

Figure 5.13: Deadband sensitivity analysis - SIC

5.4 Summary

This chapter investigated the ability of FFC and SIC to mitigate the RoCoF and compensate for the system inertia reduction. A technology neutral approach was applied to allow generic results and to guarantee the applicability of the methodology on any system and with any FAR unit. This allows any technology that is capable of providing this service to be eligible. For example, this service may be provided by technologies such as HVDC interconnectors, energy storage and other emerging technologies. Although the proposed methodology has been tested on an equivalent model of the Republic of Ireland and Northern Ireland power system, this does not limit its applicability on other systems because no direct connection between the equivalent model and the methodology is present.

The application of the presented methodology can assess the system operator in increasing the penetration of renewable energy by reducing the minimum synchronous inertia required while respecting the grid code constraint of maximum RoCoF. For example, during the dispatch phase, the system operator knows the maximum RoCoF by knowing the generation inertia and the LSI. Access to the 3rd order polynomial regression will enable the operator to find the relationship between MW and MWs, and, therefore, he or she will be able to replace the desired amount of MWs by FFC or SIC.

The analysis has shown that with the tested deadbands and response times, 1 MW of SIC was able to compensate for a higher amount of MWs compared to FFC. Meanwhile, it also showed that SIC has a higher probability in leading to system oscillation compared to FFC. It also showed that FFC was able to improve the frequency nadir and the steady state value improving the overall system stability. However, it should be noted that although FAR can replace inertia from conventional plant, they may still be needed for synchronous torque and short circuit contribution. FAR will need to be used in conjunction with other technologies (e.g. rotating condensers and FACTS devices) for large scale integration.

This work has shown the ability of FAR to mitigate the RoCoF when these reserves are controlled by frequency deviation based control or by RoCoF based control. By exploiting more than 700 simulated dispatches of the AIPS, it was possible to define an analytical relationship between MW of reserve and MWs of synchronous inertia for the two applied control mechanisms (i.e. FFC and SIC).

CHAPTER 6

Conclusion and future work

This thesis has focused on the challenges that are imposed by the high integration of converter connected resources and the consequent reduction in system inertia on the system frequency. The presented work covers in detail two solutions, namely fast frequency control (FFC) and synthetic inertia control (SIC) exploiting fast acting reserves (FAR) flexibility, such as energy storage system (ESS) and electric vehicles (EVs), which could actively help with the system's operation. In Section 1.4, four research questions have been outlined for the PhD project. In this chapter, the results are concluded.

[Q1] *What are the state-of-the-art control schemes and technologies that could potentially compensate for the effects of reduction in system inertia and assist in the transition toward a renewable energy sources (RES)-based power system?*

First, the impacts of high integration of converter connected resources on power system stability have been discussed in Chapter 2. The current transition toward a high share of RES, mainly converter connected, is altering the power system characteristics and imposing various challenges in maintaining and operating the power system in a secure state. Based on the literature review and on the simulations, it can be concluded that the reduced system inertia will mainly lead to faster rate of change of frequency (RoCoF) and lower frequency nadir values.

From the literature review and the simulations, it can be concluded that the reduced system inertia has two main implications with regards to system frequency stability: faster RoCoF, which increases the likelihood of tripping of grid components; and, higher frequency deviations (nadirs/zeniths), which can potentially lead to unintentional load shedding.

The literature review examined the most prominent control approaches and technologies suitable to compensate for reduction in system inertia, and it also presented and discussed the benefits and drawbacks of each solution. The various solutions were grouped under two main categories, namely: synchronous inertia and emulated inertia services. The emulated inertia services were divided into three groups control approaches: FFC, SIC and virtual synchronous machines (VSM), whose key features and weaknesses were discussed.

An overview of the most common methods to measure system frequency and the RoCoF, and the associated key challenges were presented. One of the most critical parameters in delivering SIC is the RoCoF measurement, which can vary significantly across the system under transient conditions. Generally, the electrical transients need to be removed and only the mechanical ones should be considered. Choosing the appropriate measuring window over which the RoCoF is calculated plays a fundamental role in eliminating these transients. However, the measuring window for SIC needs to be defined as a function of each system, where the system inertia and RoCoF protection relays play a fundamental role.

[Q2] *What are the properties of synthetic inertia and fast frequency control on the frequency dynamics?*

Due to the high integration of inertia-less resources, SIC and FFC are currently gaining interest among system operators. However, the employment of these controllers and their effects on the system's stability presents several challenges. A trade-off analysis between SIC and FFC employing converter connected resources was presented in Chapter 3. In particular, this thesis has investigated the capabilities and limitations of ESS and EVs in providing these services. First, the results showed that the high share of converter connected resources replacing conventional plants imposes an increase in the frequency gradient, leading to larger frequency variation. It also showed that the energy storage response time plays a crucial role in providing frequency support by any of the two controllers. Because SIC is a RoCoF based control, it was shown that the controller implementation was ineffective for a relatively large response time (i.e. 1 s). The controller was found to be incapable of limiting the frequency gradient, nadir or improving the steady-state value. However, given that FFC is a frequency deviation based control, the controller was capable of improving the frequency steady-state value for the same response time. For a smaller response time (e.g. 100 ms), the two controllers performed similarly in terms of RoCoF. Nevertheless, it was shown that the FFC had a much better performance in terms of frequency nadir and steady-state value.

A similar investigation was carried out but employing EVs as flexibility resources. It was shown that FFC was able to improve the overall performance of the system frequency dynamics in terms of frequency nadir and steady-state value. In contrast, SIC showed a limited improvement in terms of frequency nadir. Because of the IEC 61851 and SAE J1772 standards, according to which the EV charging current can change in discrete 1 A steps, frequency oscillation was experienced by employing any of the two controllers. Therefore, a stabilizer algorithm was implemented and integrated into the two controllers, which showed a better performance in damping the oscillations.

All in all, it was shown that, in principle, FFC and SIC can mitigate the RoCoF and limit the frequency nadir. However, the flexible resource response time and characteristics play a fundamental role in providing these services. It was also shown that SIC can easily lead to frequency oscillation, which in theory can be mitigated by employing a less steep droop characteristic but in practice leads to the reserve capabilities not being exploited (e.g. applying a very small gain value).

[Q3] *What are the capabilities and limitations of series-produced EVs in providing frequency services in terms of synthetic inertia and fast frequency control?*

Electric vehicles can represent an effective solution to enhance frequency stability thanks to their property of being quick-response units. In Chapter 4, three single-phase series produced EVs were used in an experimental validation by employing SIC and FFC. A simulation study was also carried out by employing EVs as flexibility resources. It should be noted that the simulation analysis in Chapter 4 differentiates from the analysis in Chapter 3 by employing EV dynamics model, which was validated in the laboratory facility by using series produced EVs.

The simulation analysis showed the better performance of FFC compared to SIC, mainly in terms frequency nadir and steady state value, while the two controllers were similar in terms RoCoF. However, for SIC, a deadband of ± 0.8 mHz/s was needed to avoid frequency oscillation, which limited the controller's participation. A sensitivity analysis was carried

out to better understand the effects of the 1 A granularity imposed by the IEC 61851 and SAE J1772 standards on the two controllers. It was shown that the granularity did not influence the results in the tested islanded microgrid. However, it should be noted that under a certain combination of system attributes (i.e. system inertia and stiffness of the power system) and control units parameters (i.e. amount of power involved in the regulation, droop and response time of the control actions), the granularity might lead to system instability or oscillation between two consequent set-points; as was experienced during the validation phase.

The experimental validation showed the ability of series produced EVs to participate in frequency services. It was shown that FFC had a very noticeable effect in improving the frequency dynamics in terms of frequency nadir and steady-state value. However, due to the 1 A granularity and certain combination of system attributes, the FFC implied that the EV's absorbed current to oscillate between two set-points, which led to a worse RoCoF compared to the base case. In contrast, SIC did not have any noticeable effect in terms of frequency nadir, steady-state value or RoCoF. It should be noted the the SIC had a negligible effect on the RoCoF due to the applied deadband, as was experienced in the simulation. To better investigate the two controllers and the EVs capability under more challenging circumstances, a wind turbine was connected by imposing a continuous power fluctuation. Similarly to the previous study case, the FFC did have a particularly noticeable effect in mitigating the frequency fluctuation. However, it did lead to slightly worse behaviour in terms of RoCoF. In contrast, the SIC did not show an improvement in terms of frequency performance and it had a noticeable negative effect in terms of RoCoF.

All in all, it should be noted that for such a small system with low inertia, the actual series produced EVs are capable of improving the frequency performance when FFC is applied. However, with the actual EV's response time, the FFC had only marginal effects in terms of RoCoF. With the actual EV's response time, a large deadband was needed for the SIC, which limited its contribution. Nevertheless, one should consider that, in principle, EVs were not intended to provide frequency services and, therefore, new requirements in terms of the EV's response time need to be set to achieve better performance.

[Q4] *How to asses the equivalent amount of synchronous inertia replaced by fast acting reserves (FAR)?*

As previously discussed in Chapter 3 and Chapter 4, FAR are seen as a possible solution to improve the frequency dynamics, in general, and to mitigate the RoCoF, in particular. There is, however, a lack of clarity regarding the volume of FAR that can potentially compensates for a reduction in system inertia.

By employing an equivalent and validated model of the All Island Power System (AIPS), which is the synchronized power system linking the Republic of Ireland and Northern Ireland, it was shown that the SIC and FFC are able to mitigate the RoCoF. However, as in the previous chapters, the FFC showed a much better performance in terms of frequency nadir and steady-state value.

A bottom-up inductive approach to quantitatively evaluate synchronous inertia, which can be potentially replaced by a specified magnitude of FAR, was applied. The proposed methodology was applied for SIC and FFC, separately. By employing 780 dispatches, which are representative of different operational scenarios, it was shown that it was not possible to establish a constant relationship between MW of FAR and MWs of synchronous inertia.

However, a clear relationship trend between MW and MWs as a function of the system RoCoF was found. By employing MATLAB's fitting algorithm, it was possible to determine the 3rd order polynomial regression, which represents the relationship between the MW of FAR and the MWs of synchronous inertia.

For the FFC, it was shown that for fast RoCoF (i.e. low inertia cases and/or larger infeed loss), the equivalent MWs of inertia that can be substituted with 1 MW of FFC was lower. Due to the applied deadband on the control signal, or high inertia cases and/or small infeed loss, the equivalent MWs of inertia to 1 MW of FFC were also lower. Similarly, the same methodology was applied for SIC. Likewise for the FFC, for low inertia cases and/or larger infeed loss (i.e. fast RoCoF), the equivalent MWs of inertia that can be substituted with 1 MW of SIC was lower than for high inertia cases. For high inertia cases, the equivalent MWs of inertia to 1 MW of SIC was not decreasing, as it was for FFC. This behaviour was mainly due to the different deadband between the two controllers.

A sensitivity analysis was carried out to better understand the effects of the units' time response on the relationship between MW of FAR and MWs of synchronous inertia. It was shown that the relationship between MW and MWs was reduced as a function of the time response for both controllers. However, it was noticeable that system stability was more vulnerable when the SIC approach was applied with larger response time.

6.1 Future work

The results obtained in this thesis have also uncovered several possible topics for further research, as follows:

- As seen in this thesis, many of the FARs providing frequency support are connected to the distribution system; however, the effects of these units on voltage stability remain an open research question. Due to the dominant resistive nature of the distribution grid, active power regulation heavily affects the voltage levels. Therefore, the classic approach of decoupling V/Q and f/P control loops is challenged.
- The effects of using a large aggregated number of single phase EVs characterized by different delays has not been investigated, which could help to define an aggregation scheme to prevent frequency oscillation.
- It should be noted that during the experimental validation using series-produced EVs, different response delays were experienced among EVs. Therefore, more experimental investigations are needed for other EVs models to test their ability to comply with the service requirements and to establish dynamic models of different EVs.

Bibliography

[1] D.E. Morales Bondy. *Demand response for a secure power system operation - Service specification, validation and verification in view of distributed energy systems*. PhD thesis, Technical University of Denmark, 2016.

[2] Venkatachalam Lakshmanan, Mattia Marinelli, Junjie Hu, and Henrik W. Bindner. Provision of secondary frequency control via demand response activation on thermostatically controlled loads: Solutions and experiences from Denmark. *Applied Energy*, 173:470–480, 2016.

[3] P. Mancarella, S. Puschel, H. Wang, M. Brear, T. Jones, M. Jeppesen, R. Batterham, R. Evans, and I. Mareels. Power system security assessment of the future National Electricity Market. Technical Report June, Melbourne Energy Institute, Melbourne, 2017.

[4] Mattia Marinelli, Sergejus Martinenas, Katarina Knezović, and Peter Bach Andersen. Validating a centralized approach to primary frequency control with series-produced electric vehicles. *Journal of Energy Storage*, 2016.

[5] N. H. Stern. Stern review: The Economics of Climate Change. Technical report, Cambridge University, 2006.

[6] European Commision. A policy framework for climate and energy in the period from 2020 to 2030. Technical report, EuropeanCommision, Brussels, 2014.

[7] Danish Energy Agency. Energy and Climate Policies beyond 2020 in Europe -Overall and selected countries. Technical report, Danish Energy Agency, 2015.

[8] Energinet. Ancillary services to be delivered in Denmark Tender conditions. Technical report, Energinet, Fredericia, 2012.

[9] P. Tielens and D. V. Hertem. The relevance of inertia in power systems. *Renewable and Sustainable Energy Reviews*, 55:999–1009, 2016.

[10] M. Beck and M. Scherer. Overview of ancillary services. Technical report, SwissGrid, 2010.

[11] Entso-E. Supporting Document for the Network Code on Load - Frequency Control and Reserves. Technical report, Entso-E, 2013.

[12] REN21. Renewables 2017: Global Status Report. Technical Report October 2016, REN21, 2017.

[13] National Institute of Standards and Technology. NIST framework and roadmap for smart grid interoperability standards, release 3.0. Technical report, National Coordinator for Smart Grid Interoperability, 2014.

[14] T. Ackermann. *Wind Power in Power Systems*. John Wiley, 2011.

[15] M. Rezkalla, M. Marinelli, H. Qazi, and J. O'Sullivan. Augmenting System Inertia Through Fast Acting Reserve - A Power System Case Study with High Penetration of Wind Power. In *PSCC Power Systems Computation Conference under review*, pages 1–7, Dublin, 2018.

[16] Y. Mu, J. Wu, N. Jenkins, H. Jia, and C. Wang. A Spatial-Temporal model for grid impact analysis of plug-in electric vehicles. *Applied Energy*, 114(February):456–465, 2014.

[17] J. R. Pillai and B. Bak-Jensen. Impacts of electric vehicle loads on power distribution systems. In *2010 IEEE Vehicle Power and Propulsion Conference*, pages 1–6, Sept 2010.

[18] ELECTRA IRP Project, www.electrairp.eu.

[19] Y. Gao, B. Zhang, and W. Wu. Functional requirements of next generation control center applications. In *International Conference on Advanced Power System Automation and Protection*, volume 1, pages 396–401, 2011.

[20] Mattia Marinelli, Kai Heussen, Thomas Strasser, Roman Schwalbe, Sandra Merino-Fernández, Julia Riaño, Alexander Maria Prostejovsky, Michael Pertl, Michel Rezkalla, Julian Croker, Berend Evenblij, Victoria Catterson, and Minjiang Chen. ELECTRA Deliverable 8.1: Future Control Room Functionality: Demonstration of visualisation techniques for the control room engineer in 2030. Technical report, the ELECTRA Consortium, 2017.

[21] Luciano Martini, Luca Radaelli, Helfried Brunner, Chris Caerts, Andrei Morch, Seppo Hänninen, and Carlo Tornelli. ELECTRA IRP Approach to Voltage and Frequency Control for Future Power Systems with High DER Penetration. In *23rd International Conference on Electricity Distribution (CIRED)*, 2015.

[22] Victoria Catterson, Stephen McArthur, Minjiang Chen, Michael Pertl, Tor Inge Reigstad, Roberto Ciavarella, Marialaura Di Somma, Sandra Riano, Mattia Marinelli, and Roberto Zuelli. ELECTRA Deliverable 8.2: Future Control Room Functionality: Demonstration of decision support for real time operation. Technical report, the ELECTRA Consortium, 2017.

[23] Ebrahim Vaahedi. *Practical Power System Operation*. John Wiley & Sons, 1st edition, 2014.

[24] Ariana Isabel Ramos Gutierrez, Enrique Rivero Puente, and Daan Six. D1.2: Evaluation of current market architectures and regulatory frameworks and the role of DSOs. Technical report, EvolvDSO, 2014.

[25] CEER. Status review on the transposition of unbundling requirements for DSOs and closed distribution system operators. Technical report, CEER, 2013.

[26] EirGrid and SONI. DS3 RoCoF Alternative Solutions Phase 1 Concluding Note. Technical report, EirGrid, 2015.

[27] National Grid. Fast Reserve Service Description. Technical Report April, National Grid, 2013.

[28] F.M Gonzalez-Longatt. Effects of the Synthetic Inertia from Wind Power on the Total System Inertia: Simulation Study. In *Environment Friendly Energies and Applications (EFEA), 2nd International Symposium*, pages 389 – 395, Newcastle upon Tyne, 2012. IEEE.

[29] E. Muljadi, V. Gevorgian, M. Singh, and S. Santoso. Understanding inertial and frequency response of wind power plants. *2012 IEEE Power Electronics and Machines in Wind Applications*, pages 1–8, 2012.

[30] Olivier Teller, Jean-Philippe Nicolai, Marcos Lafoz, Doerte Laing, Rainer Tamme, Allan Schroeder Pederson, Mattias Andersson, Christian Folke, Charles Bourdil, Mario Conte, Gianlucci Gigliucci, Irene Fastelli, Mario Vona, Milagros Rey Porto, Thomas Hackensellner, Robert Knapp, Hans Jürgen Seifert, Mathias Noe, Michael Sander, Jesus Lugaro, Michael Lippert, Peter Hall, Rainer Saliger, Atle Harby, Mikko Pihlatie, Noshin Omar, Jean-Michael Durand, and Patrick Clerens. European Energy Storage Technology Development Roadmap Towards 2030. Technical report, EERA EASE, 2013.

[31] M Marinelli, S Massucco, A Mansoldo, and M Norton. Analysis of Inertial Response and Primary Power-Frequency Control Provision by Doubly Fed Induction Generator Wind Turbines in a Small Power System. In *17th Power Systems Computation Conference*, pages 1–7, 2011.

[32] E. Muljadi, V. Gevorgian, M. Singh, and S. Santoso. Understanding inertial and frequency response of wind power plants. In *2012 IEEE Power Electronics and Machines in Wind Applications*, pages 1–8, July 2012.

[33] S. Sharma, S. H. Huang, and N. Sarma. System inertial frequency response estimation and impact of renewable resources in ERCOT interconnection. In *2011 IEEE Power and Energy Society General Meeting*, pages 1–6, July 2011.

[34] P. W. Christensen and G. T. Tarnowski. Inertia of wind power plants State of the art review. In *The 10th International Workshop on Large Scale of Wind Power, Aarhus, Denmark*, 2011.

[35] The Commission for Energy Regulation. Rate of Change of Frequency (RoCoF) Modification to the Grid Code. Technical report, CER, 2014.

[36] EirGrid-Group. Operational Constraints Update. Technical Report October, EirGrid-Group, 2015.

[37] DNV GL Energy Advisory. RoCoF Alternative Solutions Technology Assessment. Technical report, DNVGL, 2015.

[38] J. Brisebois and Noël Aubut. Wind Farm Inertia Emulation to Fulfill Hydro-Québec's Specific Need. In *Power and Energy Society General Meeting IEEE*, volume 7, pages 1–7, 2011.

[39] Jeff Palermo. International review of frequency control adaptation. Technical report, DGA, 2016.

[40] U. Tamrakar, D. Galipeau, R. Tonkoski, and I. Tamrakar. Improving Transient Stability of Photovoltaic- Hydro Microgrids Using Virtual Synchronous Machines. In *PowerTech, IEEE*, Eindhoven, 2015.

[41] U. Tamrakar, D. Shrestha, M. Maharjan, B. P Bhattarai, T. M. Hansen, and R. Tonkoski. applied sciences Virtual Inertia : Current Trends and Future Directions. *Applied Sciences*, pages 1–29, 2017.

[42] H.P. Beck and R. Hesse. Virtual Synchronous Machine. In *9th International Conference on Electrical Power Quality and Utilisation*, Barcelona, Spain, 2007.

[43] J. Machowski, J. W. Bialek, and J. R. Bumby. *Power System Dynamics and Stability*. Wiley, Chichester, UK, 1997.

[44] E. W. Kimbark. *Power System Stability Volume III Synchronous Machines,*. Wiley, New York, USA, 1956.

[45] M. P.N. Van Wesenbeeck, S. W.H. De Haan, P. Varela, and K. Visscher. Grid tied converter with virtual kinetic storage. In *IEEE Bucharest PowerTech: Innovative Ideas Toward the Electrical Grid of the Future*, 2009.

[46] J. Driesen and K. Visscher. Virtual Synchronous Generators. In *Power and Energy Society General Meeting*, pages 1–3, Pittsburgh, PA, USA, 2008.

[47] S. D'Arco and J. Suul. Virtual Synchronous Machines - Classification of Implementations and Analysis of Equivalence to Droop Controllers for Microgrids. In *PowerTech IEEE*, Grenoble, 2013.

[48] Y. Chen, R. Hesse, D. Turschner, and H.P. Beck. Comparison of methods for implementing virtual synchronous machine on inverters. In *International Conference on Renewable Energies and Power Quality*, pages 1–6, Santiago de Compostela, 2012.

[49] C. Pelczar. *Mobile Virtual Synchronous Machine for Vehicle-to-Grid Applications*. PhD thesis, Clausthal University of Technology, 2012.

[50] M. Rezkalla, A. Zecchino, S. Martinenas, A.M. Prostejovsky, and M. Marinelli. Comparison between synthetic inertia and fast frequency containment control based on single phase EVs in a microgrid. *Applied Energy*, 2017.

[51] Spark Xue, Bogdan Kasztenny, Ilia Voloh, and Dapo Oyenuga. Power System Frequency Measurement for Frequency Relaying. In *Western Protective Relay Conference, At Spokane, WA*, 2007.

[52] M. M. BegoviC, P. M. DjuriC, S. Dunlap, and A. G. Phadke. Frequency Tracking ih Power Networks in the Presence of Harmonics. *IEEE Transactions on Power Delivery*, 8(2):480–486, 1993.

[53] D. Hart, D. Novosel, Y. Hu, B. Smith, and M. Egolf. A new frequency tracking and phasor estimation algorithm for generator protection. *IEEE Transactions on Power Delivery*, 12(3):1064–1073, 1997.

[54] V. Eckhardt, P. Hippe, and G. Hosemann. Dynamic measuring of frequency and frequency oscillations in multiphase power systems. *IEEE Transactions on Power Delivery*, 1989.

[55] P K Dash, S K Panda, B Mishra, and D P Swain. Fast estimation of voltage and current phasors in power networks using an adaptive neural network. *IEEE Transactions on Power Systems*, 1997.

[56] Z. Salcic, Z. Li, U.D. Annakkage, and N. Pahalawaththa. A comparison of frequency measurement methods for underfrequency load shedding. *Electric Power Systems Research*, 1998.

[57] T S Sidhu. Accurate measurement of power system frequency using a digital signal processing technique. *IEEE Transactions on Instrumentation and Measurement*, 1999.

[58] K. Temtem, S.and Creighton. Summary of Studies on Rate of Change of Frequency events on the All-Island System. Technical Report August 2012, Entso-E, 2012.

[59] EirGrid. RoCoF Modification Proposal - TSOs Recommendations. Technical Report September, EirGrid, 2012.

[60] W. Xu, K. Mauch, and S. Martel. An Assessment of Distributed Generation Islanding Detection Methods and Issues for Canada. Technical report, CETC, Canada, 2004.

[61] X Ding, P A Crossley, and D J Morrow. Islanding Detection for Distributed Generation. *Journal of Electrical Engineering & TechnologyJournal of Electrical Engineering & Technology*, 2007.

[62] A. Beddoes, P. Thomas, and M. Gosden. Loss of mains protection relay performances when subjected to network disturbances / events. In *18th International Conference on Electricity Distribution CIRED*, pages 1–5, 2005.

[63] CHUI FEN TEN. *Loss of Mains Detection and Amelioration on Electrical Distribution Networks*. PhD thesis, University of Manchester, 2010.

[64] A.A.M. Hassan and Tarek A. Kandeel. Effectiveness of frequency relays on networks with multiple distributed generation. *Journal of Electrical Systems and Information Technology*, 2015.

[65] K. Knezović, M. Marinelli, A. Zecchino, P. B. Andersen, and C. Traeholt. Supporting involvement of electric vehicles in distribution grids: Lowering the barriers for a proactive integration. *Energy*, 134:458–468, 2017.

[66] L. Pereira, J. Undrill, D. Kosterev, D. Davies, and S. Patterson. A New Thermal Governor Modeling Approach in the WECC. *IEEE Transactions on Power Systems*, 18(2), 2003.

[67] N W Miller, M Shao, S Pajic, and R D Aquila. Eastern Frequency Response Study. Technical Report May, NREL, 2013.

[68] S. Nakamura, T Yamada, T Nomura, M. Iwamoto, Y. Shindo, S. Nose, H. Fujino, and A. Ishihara. 30 MVA superconducting synchronous condenser: Design and it's performance test results. *IEEE Transactions on Magnetics*, 21(2):783–790, 1985.

[69] J.A. Oliver, B J Ware, and R.C. Carruth. 345 MVA Fully Water-Cooled Synchronous Condenser for Dumont Station Part I. Application Considerations. *IEEE Transactions on Power Apparatus and Systems*, PAS-90(6):2758–2764, 1971.

[70] H. T. Nguyen, G. Yang, A. H. Nielsen, and P. H. Jensen. Frequency stability improvement of low inertia systems using synchronous condensers. In *2016 IEEE International Conference on Smart Grid Communications, SmartGridComm 2016*, 2016.

[71] J Kueck, B Kirby, T Rizy, F Li, and N Fall. Reactive Power from Distributed Energy. *The Electricity Journal*, 2006.

[72] M. Mohanpurkar, A. Ouroua, R. Hovsapian, Y. Luo, M. Singh, E. Muljadi, V. Gevorgian, and P. Donalek. Real-time co-simulation of adjustable-speed pumped storage hydro for transient stability analysis. *Electric Power Systems Research*, 154:276–286, 2018.

[73] E; Ela, B; Kirby, A; Botterud, C; Milostan, I; Krad, and V; Koritarov. Role of Pumped Storage Hydro Resources in Electricity Markets and System Operation. In *HydroVision International Denver, Colorado, July 23-26, 2013*, 2013.

[74] NHA Pumped storage council. Challenges and Opportunities For New Pumped Storage Development. Technical report, Pumped Storage Development Council, 2012.

[75] S. Rehman, L. M. Al-Hadhrami, and M. M. Alam. Pumped hydro energy storage system: A technological review. *Renewable and Sustainable Energy Reviews*, 2015.

[76] X. Luo, J. Wang, M. Dooner, and J. Clarke. Overview of current development in electrical energy storage technologies and the application potential in power system operation. *Appl. Energy*, 2015.

[77] A. E. Tønnesen, A. H. Pedersen, B. Elmegaard, J. Rasmussen, J. H. Vium, L. Reinholdt, and A. S. Pedersen. Electricity Storage Technologies for Short Term Power System Services at Transmission Level. Technical Report October, ForskEl Project, 2010.

[78] L. Chen, T. Zheng, S. Mei, X. Xue, B. Liu, and Q. Lu. Review and prospect of compressed air energy storage system. *Journal of Modern Power Systems and Clean Energy*, 4(4):529–541, 2016.

[79] Brian Elmegaard and Wiebke Brix Markussen. Efficiency of Compressed Air Energy Storage. In *The 24th International Conference on Efficiency, Cost, Optimization, Simulation and Environmental Impact of Energy Systems*, 2011.

[80] ENTSO-E. Frequency Stability Evaluation Criteria for the Synchronous Zone of Continental Europe. Technical report, ENTSOE, 2016.

[81] C. S. Schifreen and W. C. Marble. Charging current limitations in operation or high-voltage cable lines [includes discussion]. *Transactions of the American Institute of Electrical Engineers. Part III: Power Apparatus and Systems*, 75(3), Jan 1956.

[82] J. Macak. Evaluation of Gas Turbine Startup and Shutdown Emissions for New Source Permitting. Technical report, Mostardi Platt Environmental, Florida, 2014.

[83] M. Cheng and Y. Zhu. The state of the art of wind energy conversion systems and technologies : A review. *Energy Conversion and Management*, 88:332–347, 2014.

[84] E Muljadi and A. Ellis. Validation of Wind Power Plant Models. In *IEEE Power and Energy Society General Meeting*, pages 1–7, 2008.

[85] M. Singh and S. Santoso. Dynamic Models for Wind Turbines and Wind Power Plants Dynamic Models for Wind Turbines and Wind Power Plants. Technical Report May, NREL, 2011.

[86] Y C Zhang, V Gevorgian, and E Ela. Role of Wind Power in Primary Frequency Response of an Interconnection Preprint. In *International Workshop on Large-Scale Integration of Wind Power Into Power Systems as Well as on Transmission Networks for Offshore Wind Power Plants*, 2013.

[87] J. Morren, J. Pierik, and S. W H De Haana. Inertial response of variable speed wind turbines. *Electric Power Systems Research*, 2006.

[88] IRENA. Wind power - Technology Brief. Technical report, IRENA, 2016.

[89] G. Mazzanti and M. Marzinotto. Fundamentals of HVDC Cable Transmission. In *Extruded Cables for High-Voltage Direct-Current Transmission:Advances in Research and Development*, chapter 2. Wiley-IEEE Press, 2013.

[90] G J Georgantzis, N A Vovos, and G B Giannakopoulos. A suboptimal static controller for HVDC links supplying isolated AC networks. *Electrical Engineering*, 75(6):451–458, 1992.

[91] B Silva, C L Moreira, L Seca, Y Phulpin, and J. A. Peças Lopes. Provision of Inertial and Primary Frequency Control Services Using Offshore Multiterminal HVDC Networks. *IEEE TRANSACTIONS ON SUSTAINABLE ENERGY*, 3(4):800–808, 2012.

[92] M. Andreasson, R.r Wiget, D. V. Dimarogonas, K. H. Johansson, and G. Andersson. Distributed Primary Frequency Control through Multi-Terminal HVDC Transmission Systems. In *American Control Conference (ACC)*, pages 1–6, Chicago, IL, USA, 2015.

[93] C. Du, E. Agneholm, and G. Olsson. Comparison of different frequency controllers for a VSC-HVDC supplied system. *IEEE Transactions on Power Delivery*, 2008.

[94] NGK INSULATORS. Structure of NAS Energy Storage System Principle of NAS Battery. Technical report, NGK INSULATORS, 2008.

[95] International Electrotechnical Commission. Electrical Energy Storage. Technical report, IEC, 2015.

[96] US Department of Energy. Grid Energy Storage. Technical Report December, U.S. Department of Energy, 2013.

[97] M H Syed, P Crolla, G M Burt, and J. K. Kok. Ancillary Service Provision by Demand Side Management : A Real-Time Power Hardware-in-the- loop Co-simulation Demonstration. In *Smart Electric Distribution Systems and Technologies*, pages 1–7, 2015.

[98] EirGrid. DS3 Demand Side Management Workstream Plan. Technical Report May, EirGrid, 2016.

[99] K. Knezović. *Active integration of electric vehicles in the distribution network - theory , modelling and practice*. PhD thesis, Technical University of Denmark, 2017.

[100] N Lu, M R Weimar, Y V Makarov, F. J. Rudolph, S. N. Murthy, and J. Arseneaux. An Evaluation of the Flywheel Potential for Providing Regulation Service in California. In *Power and Energy Society General Meeting*, pages 1–6, 2010.

[101] Andreas Ulbig, Ts Borsche, and Göran Andersson. Impact of Low Rotational Inertia on Power System Stability and Operation. In *The 19th World Congress ofthe International Federation of Automatic Control (IFAC14*, pages 1–12, 2014.

[102] D. M. Greenwood, K. Y. Lim, C. Patsios, P. F. Lyons, Y. S. Lim, and P. C. Taylor. Frequency response services designed for energy storage. *Applied Energy*, 2017.

[103] Willett Kempton and Jasna Tomić. Vehicle-to-grid power implementation: From stabilizing the grid to supporting large-scale renewable energy. *Journal of Power Sources*, 144(1):280–294, 2005.

[104] The Hawaiian Electric Companies. Hawaiian Electric Companies' PSIP Update Report: Book 2 of 2. Technical report, Companies, The Hawaiian Electric, 2016.

[105] J. Neely, J. Johnson, J. Delhotal, S. Gonzalez, and M. Lave. Evaluation of PV frequency-watt function for fast frequency reserves. In *Conference Proceedings - IEEE Applied Power Electronics Conference and Exposition - APEC*, 2016.

[106] J.C.M. Vieira, W. Freitas, Z. Huang, W. Xu, and A. Morelato. Formulas for predicting the dynamic performance of ROCOF relays for embedded generation applications. *IEE Proceedings - Generation, Transmission and Distribution*, 2006.

[107] D. Kottick, M. Blau, and D. Edelstein. Battery Energy Storage for Frequency Regulation in an Island Power System. *IEEE Transactions on Energy Conversion*, 1993.

[108] Dulal Ch Das, A. K. Roy, and N. Sinha. GA based frequency controller for solar thermal-diesel-wind hybrid energy generation/energy storage system. *International Journal of Electrical Power and Energy Systems*, 2012.

[109] Dong Jing Lee and Li Wang. Small-signal stability analysis of an autonomous hybrid renewable energy power generation/energy storage system part I: Time-domain simulations. *IEEE Transactions on Energy Conversion*, 2008.

[110] Tamunosaki Douglas. Dynamic modelling and simulation of a solar-PV hybrid battery and hydrogen energy storage system. *Journal of Energy Storage*, 2016.

[111] P. Kundur. *Power System Stability and Control*. McGraw-Hill, 1994.

[112] DIgSILENT. Standard Models in PowerFactory. *User Manual - Appendix D*, pages 1097–1117, 2015.

[113] G. Mallesham, S. Mishra, and A. N. Jha. Ziegler-Nichols based controller parameters tuning for load frequency control in a microgrid. In *Proceedings - 2011 International Conference on Energy, Automation and Signal, ICEAS - 2011*, 2011.

[114] F. M. Gonzalez-longatt. Impact of emulated inertia from wind power on under-frequency protection schemes of future power systems. *Journal of Modern Power Systems and Clean Energy*, 4(2):211–218, 2016.

[115] IEC 61851-1:2010. Electric vehicle conductive charging system - Part 1: General requirements, 2010.

[116] SAE J1772:2010. Electric vehicle and plug in hybrid electric vehicle conductive charge coupler, 2010.

[117] E. M. Baerthlein, M. Hartung, and A. Panosyan. Variable voltage set point control of tap changers in distribution grids. In *IEEE PES Innovative Smart Grid Technologies Conference Europe*, 2015.

[118] PPA-Energy. Rate of Change of Frequency (RoCoF) Review of TSO and Generator Submissions. Technical report, PPA energy, 2013.

[119] Katarina Knezovic, Sergejus Martinenas, Peter Bach Andersen, Antonio Zecchino, and Mattia Marinelli. Enhancing the Role of Electric Vehicles in the Power Grid: Field Validation of Multiple Ancillary Services. *IEEE Transactions on Transportation Electrification*, 2017.

[120] Alan Millner. Modeling lithium ion battery degradation in electric vehicles. In *IEEE Conference on Innovative Technologies for an Efficient and Reliable Electricity Supply, CITRES*, 2010.

[121] Anderson Hoke, Alexander Brissette, Kandler Smith, Annabelle Pratt, and Dragan Maksimovic. Accounting for lithium-ion battery degradation in electric vehicle charging optimization. *IEEE Journal of Emerging and Selected Topics in Power Electronics*, 2014.

[122] Panos C. Kotsampopoulos, Felix Lehfuss, Georg F. Lauss, Benoit Bletterie, and Nikos D. Hatziargyriou. The limitations of digital simulation and the advantages of PHIL testing in studying distributed generation provision of ancillary services. *IEEE Transactions on Industrial Electronics*, 2015.

[123] P. M.Rocha Almeida, F. J. Soares, and J. A.Peças Lopes. Electric vehicles contribution for frequency control with inertial emulation. *Electric Power Systems Research*, 2015.

[124] Seyedmahdi Izadkhast, Pablo Garcia-Gonzalez, and Pablo Frias. An Aggregate Model of Plug-In Electric Vehicles for Primary Frequency Control. *IEEE Transactions on Power Systems*, 2014.

[125] Hui Liu, Zechun Hu, Yonghua Song, Jianhui Wang, and Xu Xie. Vehicle-to-Grid Control for Supplementary Frequency Regulation Considering Charging Demands. *IEEE Transactions on Power Systems*, 2015.

[126] Katarina Knezović, Mattia Marinelli, Antonio Zecchino, Peter Bach Andersen, and Chresten Traeholt. Supporting involvement of electric vehicles in distribution grids: Lowering the barriers for a proactive integration. *Energy*, 2017.

[127] SYSLAB-PowerLabDK.

[128] Hassan W Qazi, Zakir H Rather, and Damian Flynn. Impact of Large Scale Demand Side Response on System Frequency- A Case Study. In *PowerTech IEEE*, pages 1–6, Eindhoven, 2015.

[129] EirGrid and SONI. All-Island Generation Capacity Statement. Technical report, EirGrid, 2017.

[130] Jonathan O'Sullivan and M.J. O'Malley. Identification and Validation of Dynamic Global Load Model Parameters for Use in Power System Frequency Simulations. *IEEE Transactions on Power Systems*, 11(2):851–857, 1996.

[131] Jonathan O'Sullivan, Alan Rogers, and Alan Kennedy. Determining and implementing an approach to system frequency and inertial response in the Ireland and Northern Ireland power system. In *Power and Energy Society General Meeting IEEE*, pages 1–6, 2011.

[132] Jon O'Sullivan, Alan Rogers, Damian Flynn, Senior Member, Paul Smith, Alan Mullane, and Mark O'Malley. Studying the Maximum Instantaneous Non-Synchronous Generation in an Island System - Frequency Stability Challenges in Ireland. *IEEE Transactions on Power Systems*, 29(6):2943–2951, 2014.

[133] S. Donnelly, S. Mattix, D. Trundowski, and J Deagle. Autonomous Demand Response for Primary Frequency Regulation. Technical Report January, U.S Department of Energy, 2012.

Collection of relevant publications

[A] M. Rezkalla, M. Pertl and M. Marinelli, "Electric Power System Inertia: Requirements, Challenges and Solutions", in Springer Electrical Engineering, under review.

[B] M. Rezkalla, K. Heussen, M. Marinelli, J. Hu and H. W. Bindner, "Identification of Requirements for Distribution Management Systems in the Smart Grid Context", in *Power Engineering Conference (UPEC), International Universities.* Stoke on Trent, United Kingdom, Sep. 2015.

[C] M. Rezkalla, M. Marinelli, M. Pertl and K. Heussen, "Trade-off Analysis of Virtual Inertia and Fast Primary Frequency Control During Frequency Transients in a Converter Dominated Network", *in IEEE PES Innovative Smart Grid Technologies Conference Asia (ISGT).* Melbourne, Australia, 2016.

[D] M. Rezkalla, A. Zecchino, M. Pertl and M. Marinelli, "Grid Frequency Support by Single-Phase Electric Vehicles Employing an Innovative Virtual Inertia Controller", in *Power Engineering Conference (UPEC), International Universities.* Coimbra, Portugal, 2016.

[E] A. Zecchino, M. Rezkalla and M. Marinelli, "Grid Frequency Support by Single-Phase Electric Vehicles: Fast Primary Control Enhanced by a Stabilizer Algorithm", in *Power Engineering Conference (UPEC), International Universities.* Coimbra, Portugal, 2016.

[F] M. Rezkalla, A. Zecchino, S. Martinenas, A. M. Prostejovsky and M. Marinelli, "Comparison Between Synthetic Inertia and Fast Frequency Containment Control Based on Single Phase EVs in a Microgrid", in Applied Energy, vol. 210, pp. 764-775,2018.

[G] M. Rezkalla, S. Martinenas, A. Zecchino, M. Marinelli and E. Rikos, "Implementation and Validation of Synthetic Inertia Support Employing Series Produced Electric Vehicles", in CIRED - Open Access Proceedings Journal, vol. 2017, no. 1, pp. 1197-1201, 2017.

[H] M. Rezkalla, M. Marinelli, H. Qazi and J. O'Sullivan, "Augmenting System Inertia Through Fast Acting Reserve - A Power System Case Study with High Penetration of Wind Power", in *IEEE Transaction on Sustainable Energy*, under review.

[A] Electric Power System Inertia: Requirements, Challenges and Solutions

Electric Power System Inertia: Requirements, Challenges and Solutions

Michel Rezkalla* · **Michael Pertl** · **Mattia Marinelli**

Received: date / Accepted: date

Abstract The displacement of conventional generation by converter connected resources reduces the available rotational inertia in the power system, which leads to faster frequency dynamics and consequently a less stable frequency behaviour. This study aims at presenting the current requirements and challenges that transmission system operators are facing due to the high integration of inertia-less resources. The manuscript presents a review of the various solutions and technologies that could potentially compensates for reduction in system inertia. The solutions are categorised into two groups, namely synchronous inertia and emulated inertia employing fast acting reserves (FARs). Meanwhile, FAR are divided into three groups based on the applied control approach, namely virtual synchronous machines, synthetic inertia control and fast frequency control. The analytical interdependency between the applied control approaches and the frequency gradient is also presented. It highlights the key parameters that can influence the units' response and limit their ability in participating in such services. The manuscript presents also a trade-off analysis among the most prominent control approaches and technologies guiding the reader through benefits and drawbacks of each solution.

This work is supported by the EU FP7 project ELECTRA (grant: 609687; electrairp.eu) and the Danish Research Project ELECTRA Top-up (grant: 3594756936313).

* corresponding author

M. Rezkalla, M. Pertl, M. Marinelli,
Technical University of Denmark
Department of Electrical Engineering
Frederiksborgvej 399
4000 Roskilde, Denmark
Tel.: +45 93511293 (Michel Rezkalla)
E-mail: {mirez,mpertl,matm}@elektro.dtu.dk

Keywords Frequency Control, Synchronous inertia, Synthetic inertia · Virtual Synchronous Machine.

1 Introduction

Conventional power systems rely on electricity generation from large rotating synchronous generators (SGs). Due to the continuous exchange of energy between the rotating masses of the SGs and the grid, the dynamics of the grid frequency are limited and the frequency is maintained within an admissible range. Following a large disturbance, which causes the frequency to significantly deviate from its nominal value, the SGs inherently release the kinetic energy stored in their rotating masses as inertia response. Additionally, SGs participate in primary and secondary frequency control by increasing/decreasing their active power generation [1].

Traditionally, inertia response has not been considered an ancillary service, but rather a natural characteristic of the power system. Due to the high integration of converter connected resources, which replace SGs, several transmission system operators (TSOs) in different countries began to recognise the value of inertia response provided by wind power plants, synchronous condensers and synthetic inertia [2,3,4,5,6].

In order to better comprehend the role of system inertia, Fig 1 shows how the system frequency could change after a contingency event in high and low inertia cases. The key parameters involved are: 1) Rate of change of frequency (RoCoF), 2) Frequency nadir, and 3) Steady state frequency. Since the capacity of the primary frequency reserve (PFR) is the same in both inertia cases, the steady state frequency after the event settles at the same value. However, the lower inertia system experiences a lower frequency nadir and a higher

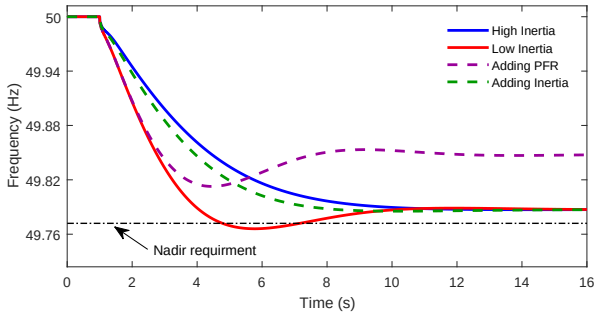

Fig. 1: Effects of lower inertia on system frequency performance

RoCoF. In order to maintain and operate the power system in secure state, the three aforementioned parameters that characterise the system frequency, should be constrained to avoid further implications such as load shedding, cascade tripping, and in worst case, system collapse.

The secure operation area for a given operating point can be represented by considering the system constraints. The authors in [7] represent the secure operation area by combining the PFR and inertia requirements as shown in Fig 2. The secure area is delimited by the maximum allowed RoCoF (vertical line), the steady state frequency requirement (horizontal line) and the frequency nadir (red curve). The frequency nadir constraint is determined through the swing equation presented in (2) which depends on the PFR and the system inertia.

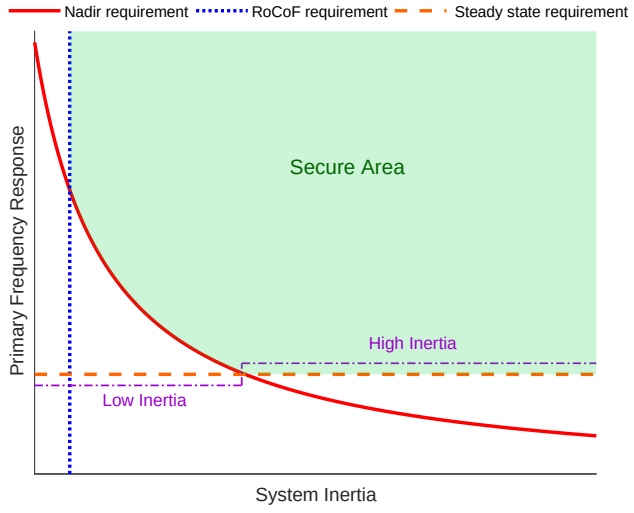

Fig. 2: Frequency response requirements [7]

Fig 2 shows that for high inertia cases the PFR requirement is prevalent on the frequency nadir. In fact, due to the high inertia and the PFR reserve required to satisfy the steady state limit, the frequency nadir constraint will be automatically respected as also shown by the blue curve in Fig 1, where the steady state frequency is lower than the frequency nadir. In other words, due to the high inertia, the steady state requirement is reached before the nadir constraint.

Nevertheless, moving towards low inertia system, the frequency nadir requirement start to dominate on the steady state requirement. This requirement can be achieved by acting on both PFR and/or system inertia as shown by the dashed curves in Fig 1. Indeed, the frequency nadir can be improved by adding PFR (purple dashed curve) and/or by augmenting system inertia (green dashed curve). The lower the system inertia, the faster the frequency will decline following an event (e.g. the loss of a generator). Hence, faster primary reserve response is needed. In contrast, in high inertia grids, slower-acting primary reserves are adequate to cope with the imbalance. Fig 2 also shows that for low inertia cases, the RoCoF requirement starts to dominate on the frequency nadir which is an indicator of how the grid requirements are evolving towards a new paradigm due to the high penetration of inertia-less resources.

TSOs with limited AC interconnection and high share of converter connected renewable energy sources (RES) have identified these issues to be of critical significance. For example, EirGrid, the Irish TSO has initiated the "Delivering a Secure Sustainable Electricity System (DS3)" programme to address those challenges [8]. From TSO perspective, the reduction of system inertia has mainly two implications with regards to system frequency stability:

1. Faster RoCoF possibly results in tripping of grid components. In particular embedded renewable generation and SGs due to reduced transient stability margins.
2. Higher frequency deviations (nadirs/zeniths) potentially leading to unintentional load shedding.

This manuscript presents the analytical background of frequency variations and the capability of emulated inertia control (EIC) in mitigating the RoCoF and improving the frequency response. Challenges and solutions regarding the large-scale integration of converter-based units are discussed. In addition, the state-of-the-art of possible solutions and devices to improve the frequency response are discussed.

This study is part of the EU project ELECTRA[1], in which novel frequency and voltage control concepts to

[1] The ELECTRA Integrated Research Programme on Smart Grids brings together the partners of the EERA Joint Programme on Smart Grids to reinforce and accelerate Europe's medium to long term research cooperation in this area and to drive a closer integration of the research programmes of

maintain and operate the power system in secure state are proposed. ELECTRA considers the grid inertia (i.e. synchronous and emulated inertia) as an active part of the frequency control process [9,10].

This paper is structured as follows: Section 2 presents the grid requirements and some of the grid code modifications to maintain and operate the power system in secure state. It also presents the background for frequency variations and the inter-dependency between EIC and RoCoF. Section 3 presents the Various control approaches to mitigate the RoCoF and the advantages and drawbacks of each. The key parameters and challenges of each control approach are presented in Section 4. Section 5 presents the suitable technologies that can reduce the frequency gradient as well as the characteristics of each technology. Lastly, Section 6 presents the conclusion.

2 Grid Requirements & Synchronous Inertia

2.1 Grid Requirements

The increasing share of distributed and inertia-less resources entails an upsurge in the requirements for balancing and system stabilisation services. Various TSOs have identified these issues to be of critical significance and have initiated mitigating measures and established new requirements. In the following, an overview of some of the new requirements and grid code modifications is presented.

EirGrid, the TSO of the Republic of Ireland has proposed a RoCoF modification in the grid code in order to facilitate the delivery of the 2020 renewables targets, whilst maintaining operational security on the power system. Generators are required to withstand a RoCoF event of 1 Hz/s over 500 ms instead of 0.5 Hz/s [11]. Within the DS3 program and the RoCoF alternative studies, EirGrid and SONI (TSO of Northern Ireland) investigate the deployment of synchronous and non-synchronous inertia to maintain the RoCoF at 0.5 Hz/s for a non-synchronous penetration up to 75 % [12]. EirGrid and SONI defined the minimum of rotational kinetic energy in the system as an operational constraint during the dispatch phase. The total rotational energy of the system is defined as the sum of each machine's rated power multiplied with the relative inertia constant as in (1), and generally referred to as system inertia floor [13].

$$E_{kin}^{sys} = \sum_{i=1}^{n} H_i S_{r,i} \tag{1}$$

the participating organisations and of the related national programmes.

H_i - inertia constant of the i-th generator (s)
$S_{r,i}$ - rated apparent power of the i-th generator (VA)
E_{kin}^{sys} - total rotational kinetic energy of the system (Ws)
n - number of generators

Due to the high share of inertia-less resources, UK's TSO, National Grid, procures fast reserves to provide the rapid delivery of active power through either increased output from a generator or the reduction of the demand to control frequency changes [14].

This control mechanism is a frequency deviation based control and is addressed in this manuscript as fast frequency control (FFC). The Hydro-Quebec Transenergie's (HQT) transmission connection requirement stipulates in detail that wind power plants must be equipped with an inertia emulation system. HQT is now in the process of procuring and validating manufacturers' models integrating inertia emulation features [15,16]. This control mechanism is a RoCoF based control and addressed further as synthetic inertia control (SIC).

This manuscript will demonstrate analytically the ability of FFC and SIC in limiting the frequency gradient and improving the frequency response. Advantages and drawbacks of each controller are also discussed.

2.2 Synchronous Inertia

Inertia is defined as the resistance of a physical object to a change in its state of motion including changes in speed and direction [17]. With reference to the power systems, the inertia refers to the rotating machines directly connected to the electrical grid without any power converter (e.g. SGs, induction generators and motors, etc.). The resistance to change in rotational speed is expressed by the moment of inertia of the rotating mass. Traditionally, the total inertia of a power system is determined by the large rotating masses of conventional power plants, i.e. the generator and turbine connected to the same shaft. Due to the synchronous coupling of the machines with the grid, their rotational speed (i.e. ω_m) is linked with the angular velocity of the electromagnetic field (i.e. ω_e). During a disturbance which causes an imbalance between the two opposing torques, the net torque on the rotor is different from zero leading to an acceleration or deceleration according to the electro-mechanical swing equation in (2).

$$J\frac{d\omega_m}{dt} = T_m - T_e = T_a \tag{2}$$

J - combined moment of inertia of the generator and the turbine (kg·m^2)
T_m - mechanical torque (N·m)
T_e - electrical torque (N·m)

T_a - acceleration/deceleration torque (N·m) (10)

SGs are characterised by their inertia constant H which is defined as the kinetic energy E_{kin}, stored in the rotating mass at rated speed, divided by the machine rating power S_r as shown in (3).

$$H = \frac{E_{kin}}{S_r} = \frac{J\omega_{m,0}^2}{2S_r} \tag{3}$$

$\omega_{m,0}$ - rated mechanical angular velocity (rad/s)

$\omega_e = p\omega_m$, where p is the number of pole pairs. Assuming p=1, equation (2) and (3) can be reformulated as:

$$P_m - P_e = \omega_m \frac{2HS_r}{\omega_{m,0}^2} \frac{\mathrm{d}\omega_m}{\mathrm{d}t} \tag{4}$$

P_m - mechanical power (W)
P_e - electrical power (W)
ω_e - angular velocity of the electromagnetic field (rad/s)

For limited angular velocity variation, one can assume $\omega_m = \omega_{m,0}$, thus (4) can be reformulated as:

$$P_m - P_e = \frac{2HS_r}{\omega_{m,0}} \frac{\mathrm{d}\omega_m}{\mathrm{d}t} \tag{5}$$

Assuming that P_m is constant and that the frequency regulation is only from the load side, then one can consider that P_e is composed by: frequency dependent loads (P_D), devices participating in FFC (P_{FFC}) and devices participating in SIC (P_{SIC}):

$$P_e = P_D + P_{FFC} + P_{SIC} \tag{6}$$

Where each is composed by a base value and frequency dependent value:

$$P_D = P_{D_0} + K_D(\omega_e - \omega_{m,0}) \tag{7}$$

$$P_{FFC} = P_{FFC_0} + K_{FFC}(\omega_e - \omega_{m,0}) \tag{8}$$

$$P_{SIC} = P_{SIC_0} + K_{SIC} \frac{\mathrm{d}\omega_e}{\mathrm{d}t} \tag{9}$$

P_{D_0}, P_{FFC_0} and P_{SIC_0} represent the base electric power in steady state and addressed further as $P_{e_0} = P_{D_0} + P_{FFC_0} + P_{SIC_0}$. K_D is a damping factor, it considers the electrical loads that change their active power consumption due to frequency changes. $K_{FCC} = K_{FCC}(t - t0)$ is the FCC proportional control coefficient. $K_{SIC} = K_{SIC}(t - t0)$ is the SIC proportional control coefficient. K_{FCC} and K_{SIC} are represented in function of the time to represent the time required from those devices to get activated (i.e. time delay). Therefore the electric power P_e can be expressed as:

$$P_e = P_{e_0} + (K_D + K_{FFC})(\omega_e - \omega_{m,0}) + K_{SIC} \frac{\mathrm{d}\omega_e}{\mathrm{d}t} + \Delta P_e$$

Where ΔP_e is the perturbation and in steady state the P_m is equal to P_{e_0}. The swing equation can be formulated as:

$$\frac{2H\frac{\mathrm{d}\omega_e}{\mathrm{d}t}}{\omega_{m,0}} = -(K_D + K_{FFC})(\omega_e - \omega_{m,0}) - K_{SIC}\frac{\mathrm{d}\omega_e}{\mathrm{d}t} - \Delta P_e \tag{11}$$

Solving the differential equation:

$$\omega(t) = \omega_{m,0} + \left(\frac{e^{-\frac{(K_D + K_{FFC})\omega_{m,0}}{K_{SIC}\omega_{m,0} + 2HS_r}t}}{K_D + K_{FFC}} - \frac{1}{K_D + K_{FFC}} \right) \Delta P_e \tag{12}$$

$$\frac{\mathrm{d}\omega(t)}{\mathrm{d}t} = -\omega_{m,0} \frac{e^{-\frac{(K_D + K_{FFC})\omega_{m,0}}{K_{SIC}\omega_{m,0} + 2HS_r}t} \Delta P_e}{k_{SIC}\omega_{m,0} + 2HS_r} \tag{13}$$

One can notice that both FFC and SIC affect the RoCoF variation during the transient. One can notice that due to the response time of FFC and SIC and the power ramp-rate limitations of the used resource (e.g. battery ramp-rate), it turns out to be a complex time-variant term. Nevertheless, the presented swing equation shows clearly that mitigating the impact of power imbalances in terms of RoCoF can be achieved by increasing the system rotational inertia H, employing fast reserves with RoCoF based control and/or with frequency deviation based control.

3 Various Solutions to for EIC

As analytically shown in (13), the system RoCoF can be mitigated by one of the following actions: increasing the system rotational inertia H and/or employing fast reserves with EIC approaches. EIC can be distinguished in three categories, namely virtual synchronous machines (VSM), SIC and FFC. Fig 3 presents an overview of the different solutions. In the following, a qualitative analysis of EIC approaches is presented.

For machines/units which are connected to the grid by means of power electronics, the electromagnetic coupling between grid and prime mover does not exist, e.g. Type 4 wind turbines [18]. Therefore, frequency changes will not induce a natural power change from the device and, in principle, they can only provide emulated inertia response.

Devices which are connected to the grid through power electronics could provide emulated inertia if the active power absorbed or generated is achieved through

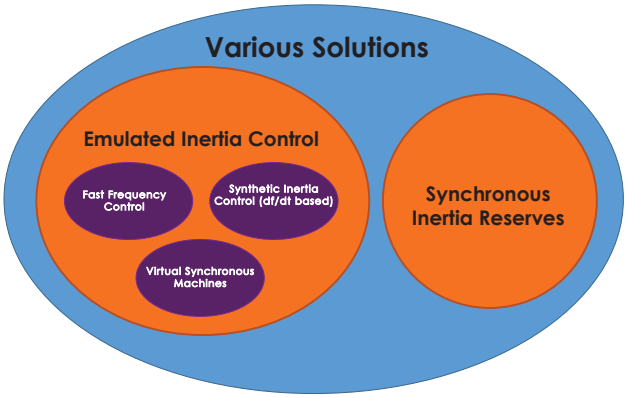

Fig. 3: Various Solutions

control strategy based on the frequency variation over time ($\frac{\Delta f}{\Delta t}$), emulating the synchronous inertia behaviour. Emulated inertia could also be achieved by extracting the kinetic energy stored in the rotating parts through dedicated control scheme as the case with wind turbines Type 3 and Type 4 [19,20].

Emulated inertia is a combination of control algorithms, renewable energy resources, energy storage systems and power electronics that emulate the inertia of a conventional power system [21]. The general concept of EIC is presented in Fig 4. The core of the system is the emulated inertia algorithm which varies among the different solutions, based on the application and the desired level of model sophistication [22]. Some typologies try to mimic the exact behaviour of the SG through a detailed mathematical model that represents the SG's dynamics, generally addressed as virtual synchronous machines (VSM). Other approaches try to simplify this by using just the swing equation, further indicated as SIC.

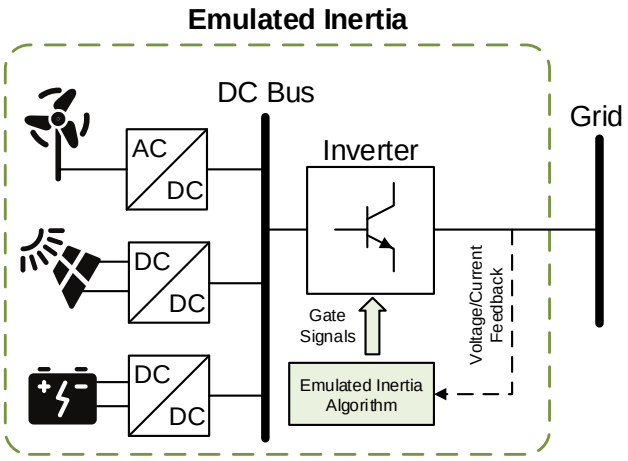

Fig. 4: Emulated inertia concept

3.1 Virtual Synchronous Machines

The first proposal of a VSM was published by Beck and Hesse in 2007 and labeled as VISMA [23]. The underlying idea behind the VSM concept is to emulate the essential behaviour of a real SG by controlling a power electronic converter. Thus, any VSM implementation contains more or less explicitly a mathematical model of a SG [24]. The inertia emulation is a common feature for every VSM implementation. Depending on the desired degree of complexity and accuracy in reproducing the SG dynamics, additional aspects can be included or neglected (e.g transient and sub-transient dynamics).

If the purpose of VSM is to accurately replicate the dynamic behaviour of a SG, a full order model of the SG has to be included in the converter control system. This includes a 5^{th} order electrical model with dq-representation of stator windings, damper windings and the field winding, together with a 2^{nd} order mechanical model resulting in a 7^{th} order model [25,26]. A VSM type is presented in Fig 5. This type is used by the European VSYNC research group [27,28] and has demonstrated the effectiveness of inertia emulation through real-time simulations [29] and field test [30].

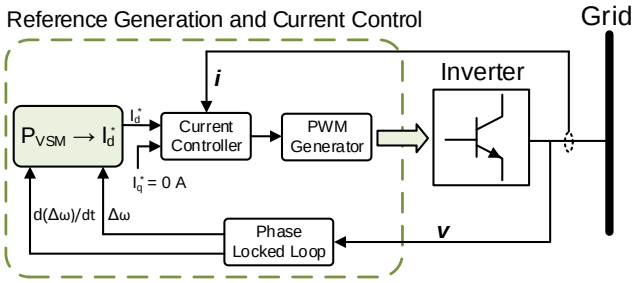

Fig. 5: **V**irtual **S**ynchronous **M**achine Type

Various control schemes for VSM, which represents the interface between the SG models and the power electronic converter, are presented and discussed in various studies [22,24]. The control schemes proposed in literature can be categorised into two main groups based on the nature of the output reference from the SG model, namely: Voltage Reference and Current Reference models.

1. **Voltage Reference**: This control scheme is configured to provide a voltage reference output [31]. If a reduced order model of the SG is applied, the power flow will be mainly related to the inertia emulation and the phase angle resulting from the swing equation. However, protections can be implemented at the hardware level or as parallel loops overriding the

references from the VSM, but their interaction with the inertia emulation and the resulting behaviour can be difficult to predict [24].

2. **Current Reference**: This control approach generates a current reference. This scheme allows the implementation of high order electrical models for the SG [23]. Nevertheless, in practical implementations this scheme can lead to numerical instability especially with high order SG models [32].

3.2 Synthetic Inertia Control

The inertia response can be also emulated by tracking the RoCoF and representing the SG only by the swing equation as shown in (9). This approach is only emulating the inertia effect with respect to the response to changes in the frequency gradient. The control structure is shown in Fig 6-a. A key parameter in this controller is the RoCoF measurement which is further addressed in Section 4.1. However, this control system does not have the inherent capability for black-start since it requires the system frequency as an input.

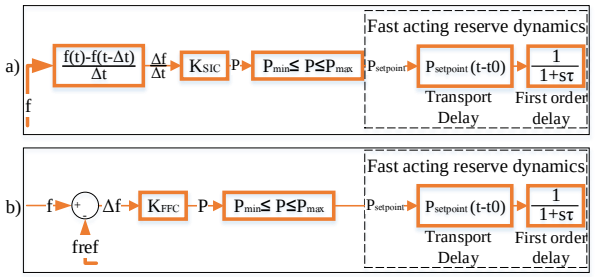

Fig. 6: SIC and FFC control diagram

3.3 Fast Frequency Control

FFC is a frequency deviation based control and is achieved by a joint action of FFC providing units within the synchronous area. FFC employs the same control mechanism as PFR which is generally achieved using droop controllers, so that governors operating in parallel can share the load variation according to their rated power. The droop constant represents the ratio of frequency deviation to change in power output [33]. The frequency variation, Δf (Hz), referred to the nominal frequency of the system is therefore given as a function of the relative power change ΔP (W) reported to the nominal machine power as shown in (14) and in Fig 7. However, governors' dynamics (e.g. time response and ramping rate) limit the PFR capability in improving the RoCoF. On the other hand, FFC is characterised by employing FAR, for example, energy storage and electric vehicles [34]. The FFC control diagram is presented in Fig 6-b.

$$\frac{-1}{K_{FFC}} = \frac{\Delta f / f_{nom}}{\Delta P / P_{nom}} \tag{14}$$

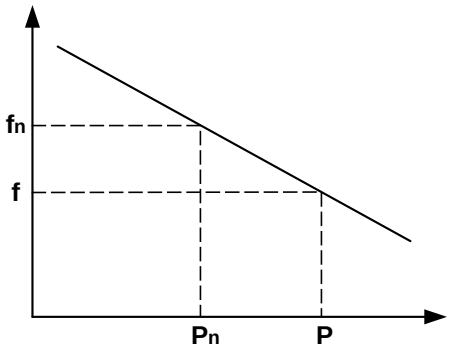

Fig. 7: Frequency control droop characteristic

The authors in [35] present a trade-off analysis of SIC and FFC. Fig 8 shows the system frequency and RoCoF following the loss of the largest single infeed. It shows the effects of the two controllers on the system frequency. One can notice that both controllers were able to improve the system RoCoF. Nevertheless, the FFC shows a much better performance in terms of frequency nadir and steady state value.

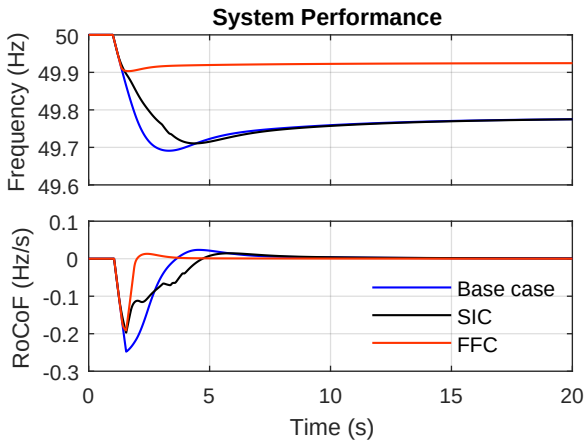

Fig. 8: System frequency and RoCoF performances

A summary which highlights the key features and weaknesses of the various inertia control schemes is presented in Table 1.

Table 1: Overview of the Various Control Schemes

Control Schemes	Key Features	Weaknesses
VSM	• Accurate representation of SG model • Frequency derivative not required • Black-start capability	• Can lead to numerical instability • Protections of the voltages and currents of the converter cannot be easily included
SIC	• Simple implementation compared to VSM	• Frequency derivative required • No black-start capability • System susceptible to noise
FFC	• Control type similar to conventional droop control in SGs • Local control (i.e. communication-less) • Stable performance	• Slow transient compared to the previous solutions • No black-start capability

4 Key Parameters & Challenges

The synthetic inertia and fast primary responses are characterised mainly by the controller and the device dynamics. Various parameters can radically change the controller and the device response and therefore their ability in delivering such services. The key parameters can be divided into four groups: 1) Signal measurement, 2) Response time, 3) Dead-band and 4) Device performance. Moreover, there is a lack of clarity regarding the volume of FAR that can potentially compensate for reduction in system inertia and the effects of the previously mentioned parameters on the required volume of FAR. In other words, the quantitative relationship between MW of reserve and the corresponding MWs of synchronous inertia that those will be able to replace. In the following an overview of the different key parameters are presented as well as the challenge of defining a quantitative relationship between MW of reserve and the corresponding MWs of inertia.

4.1 Signal Measurement and Processing

Traditionally, the common practice of utilities is to use the speed of SGs as proxy for the grid frequency because measuring the speed is easy and accurate. Generators' governors have been using deviations in rotor speed as measure for frequency deviation from the reference ever since. Nowadays, non synchronous resources delivering frequency support as well as protection relays (e.g. under-frequency and RoCoF relays) must measure the frequency directly from the grid. In the following, an overview of the most common methods to measure the system frequency and the RoCoF, and the associated key challenges are presented:

• **Frequency Measurement:**

The system frequency is an important operating parameter of an electrical power system which indicates the dynamic balance between power generation and consumption. The grid frequency is measured from voltage or current signals which are originated from the synchronous machines whose rotating speed are proportional to the frequency of the generated voltage. The system frequency and its rate of change are used directly in various protections and control schemes and low measurement accuracy (e.g. due to harmonics, random noise electromagnetic interference, etc.) can cause false operation leading to system instability.

In the past, a zero crossing algorithm which uses a pulse counting between zero crossings of the signal was the mostly adopted method [36]. Nowadays, with the technological progress in microprocessors and cheaper computational power, many numerical method for frequency measurement are applied and proposed:

- Modified Zero-crossing method [37,38,39]
- Digital Fourier Transformation [40,41,42]
- Phase locked loop [43,44,45]
- Orthogonal decomposition [46,47]
- Least square optimisation [48,49]
- Taylor approximation [50,51]
- Numerical analysis [52,53]
- Artificial intelligence [54,55,56]

To evaluate the performance of a frequency estimation method, the following three aspects should be considered: the accuracy, the estimation of latency and the robustness. The maximum error, the average error and the estimation delay could be used as the performance indexes for frequency measurements. The maximum error is the difference between the actual frequency and the estimated frequency. The average error is based on a number of data points in which the average values are taken for both, the actual and estimated frequency [36].

Most frequency estimation algorithms employs a window of data to derive the frequency, which causes estimation delay since the frequency is time-varying. Small window of data will reduce the estimation delay, on the other hand, it reduces the measurement accuracy due to the presence of noise and harmonics. One can see that frequency measurement is quite a challenging task and measurement errors or latency can lead to malfunction of protections or control schemes.

• **RoCoF Measurement:**

A key parameter in delivering synthetic inertia is the RoCoF measurement. The RoCoF is the time derivative of the power system frequency (df/dt) which varies in function of the chosen measurement window. This quantity was traditionally of minor relevance for systems with generation mainly based on SGs, because of the inertia of these generators, which inherently counteract to power imbalances and thus limiting the RoCoF.

A key issue in the measurement of RoCoF across the system is that the frequency measured at different points in the system can vary significantly under transient conditions. During transient events generator rotor speeds may also differ from each other due to local and inter-area interactions [57]. In order to obtain a consistent system wide measurement of RoCoF, the electrical transients need to be removed from the analysis and only the mechanical transients on the system should be considered [13]. Extending the measurement window the electrical transients can be removed from the RoCoF measurement allowing for a more consistent system RoCoF to be determined [58]. On the other hand, relatively large measurement window might also eliminate the mechanical transients leading to false RoCoF values. Fig 9 illustrate the effect of using different measuring windows on the RoCoF value. For example, employing a measuring window of 100 ms, the calculated RoCoF is 2.1 Hz/s versus 0.9 Hz/s for a 500 ms measuring window. Therefore, the chosen measuring window, over which the RoCoF is calculated, is just as important as the RoCoF value itself.

This issue is also concerning various TSOs since distributed energy resourcess (DERs) employ protection schemes for loss-of-mains. Generally these schemes utilise under- and over-frequency relays as well as RoCoF relays. These schemes aim to ensure that should a part of the distribution network become islanded from the rest of the distribution system, that there is no generation left operating on that local system, keeping it live [59]. From the TSO perspective, "false" RoCoF values influenced by the electrical transients might lead to unintended cascade tripping of distributed energy resources connected by means of RoCoF relays [60,61].

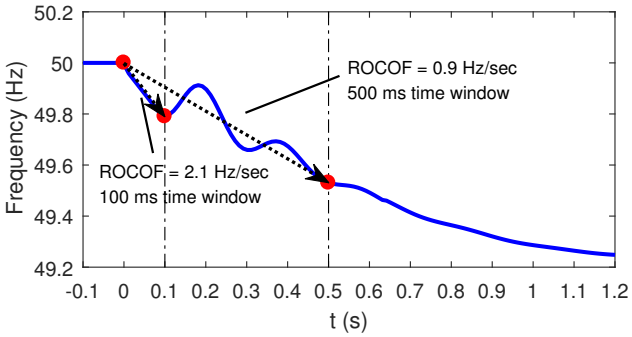

Fig. 9: Illustration of frequency change and the effect of using different measuring windows

Besides, different studies shows that commercially available RoCoF relays from different manufacturers respond rather differently to the same event, even when they are configured with the same settings [62,63,64]. This phenomenon is most likely due to the different measurements techniques employed by those relays. On the other hand, from the rotary electrical machine perspective, the use of a relatively large measurement window might lead to neglecting the mechanical transient and thus increasing the mechanical stress on the rotating machines [65,66].

RoCoF relays' characteristics (e.g. measurement window and threshold) are established by the grid code, which varies among countries. For example, the Irish grid code defines 1 Hz/s the RoCoF relays' threshold measured over 500 ms moving window. EirGrid determined that 1 Hz/s would be sufficient to cover for the loss of the current largest single infeed (i.e. East-West interconnector exporting 500 MW) [59]. In [35], the authors recommend that the RoCoF measurement window for the SIC should be the same as for the RoCoF relays' requirements present in the grid code. This choice is to guarantee the triggering of the reserves only for events which can threat the system stability by triggering RoCoF relays.

4.2 FAR Device Response Time

The response time is the total time that is needed for a FAR device to actively supply the grid with its service. For power electronic connected technologies, delivering synthetic inertia and/or fast frequency control, there is a delay between the event the device's response [67]. The response time is a combination of the following four different parameters:

– **Measurement time**, which is the time needed to detect and measure the RoCoF (or frequency in case of FFC)

- **Signal time**, which is the time required to get the activation signal from the measurement device to the FAR device.
- **Activation time**, which is the time required from the FAR device to deliver the initial power response once it received the activation signal.
- **Ramping time**, which is the time required from the FAR to ramp up to the required active power setpoint.

However, an adequate time response depends on the characteristics of the power system.

Generally, for low inertia system, the time response is of more importance than for high inertia systems. The authors in [68] present a sensitivity analysis of the response time and highlight its importance and impacts on the system stability.

4.3 Deadband

Deadbands are generally categorised into unintentional and intentional deadbands.

The unintentional deadband is used to describe the inherent effect of a unit, for example to describe the mechanical effect of a turbine-governor system, such as sticky valves, loose gears, and hydraulic system non linearity, which are unavoidable and unadjustable [69].

Intentional deadband is generally adopted in order to reduce excessive controller activities for normal power system frequency variations. For the governor control system, deadband values are established by the grid code [70]. For example, Republic of Ireland's grid code requires that a frequency deadband of no greater than ± 15 mHz maybe applied to the operation of the governor control system [59]. In the Continental Europe a frequency deadband of ± 20 mHz is permitted. On the other hand, some grid codes such as in the Nordic area, require that primary frequency support must be made without deadband [71]. However, one should differentiate between contingency based and regulation based service. In case of employing FAR for regulation based services, the controller should employ the same deadband established by the grid code for the governors control system. On the other hand, defining a deadband for contingency based services is less straight forward. In fact it depends on the system characteristics such as the system inertia. The authors in [35] present a sensitivity analysis of the deadband applied on the control signal for both FFC and SIC. The study shows that employing a large deadband will limit the FAR participation to large congestion cases avoiding its activation following normal load change. On the other hand, it shows that employing large deadband will reduce the FAR effects imposing the need of a higher number of reserves to limit the RoCoF.

4.4 Device performance

As previously mentioned, the FAR response is highly influenced by the controller as well as the device dynamics. In the following the key parameters that can influence the FAR response are presented:

- Response time: The time required by the device to react to frequency fluctuation.
- Active power ramp: The rate at which the active power will ramp after a frequency changes.
- Active power amplitude: The amount of active power delivered from the device in function of frequency changes.
- Active power duration: The time period for which the device will provide active power before its energy has been depleted. In case of employing FAR for synthetic inertia, this parameter can be neglected since it focuses on small time frame post event.

4.5 Quantitative relationship between MW and MWs

The high integration of converter connected resources is resulting in the reduction of the system inertia and consequently deterioration of frequency stability. FAR units controlled through SIC or/and FFC is seen as a possible solution and various control approaches have been previously proposed in different studies. Nevertheless, there is a lack of clarity regarding the volume of FAR in terms of MW that can potentially compensate for the reduction of a certain MWs of synchronous inertia.

In [35], the authors introduced this challenge and presented a methodology to determine the quantitative relationship between FAR and conventional inertia. The method was tested on an equivalent model of the Republic of Ireland and Northern Ireland power system using more than 700 simulated dispatches. The study shows that the equivalent MW of FAR to replace 1 MWs of inertia is influenced by the system characteristics and dispatches as well as the controller performance (e.g. response time, deadband and system inertia). For example, in function of the analysed system characteristics and dispatches, 1 MW of FFC is able to replace between $\{20 - 45\}$ MWs, while 1 MW of SIC is able to replace between $\{30 - 70\}$ MWs. To be noted, a higher number of system oscillation is seen employing the SIC. However, more investigation needs to be done in this area.

5 Suitable Technologies

This section provides a high level assessment of the different technologies that may be used to mitigate the RoCoF. The various technologies can be distinguished into two groups: synchronous inertia and emulated inertia employing fast acting reserves (FARs). The synchronous reserves are characterised by their inherent inertia response which does not require any measurement or control schemes. In the following, an overview of the different technologies including a high level assessment of each is presented. The assessment is based on the following criteria: 1) Geographic limitation, 2) Additional system services (e.g. voltage control and black start), 3) Type of the provided inertia service, 4) Inertia constant H (s) and the typical power capacity (MW) and 5) Capital cost.

1. **Synchronous Condensers**
   synchronous condenserss (SCs) are machines that are synchronised with the power system and operate as free spinning motors. SCs have been playing an important role for reactive power compensation and have been contributing to voltage stability in power systems for more than 50 years [72,73]. Currently, different TSO started to investigate their effect in mitigating the RoCoF and enhancing the frequency stability [74]. Nevertheless, SCs are characterised by a lower inertia compared to conventional plants since the prime mover's mass is missing. However, in some cases SCs can be equipped with additional masses to increase the inertia.
   - Geographic limitation
     Synchronous condensers are not influenced by the geographic location and in principle are flexible to install. Moreover, existing power plants can be converted to synchronous condensers.
   - Additional system services
     As previously mentioned, SCs have been used for many years for reactive power compensation to improve voltage stability.
   - Type of the inertia response
     Due to grid connection without power converters, they are able to provide an inherent inertia response without the need for measurements and controls.
   - Inertia constant and power capacity range
     Typical inertia constant $2H = \{2-3\}$ s and power capacity range of $\{50-250\}$ MVA [13].
   - Capital cost
     Large cost range because it depends on the installation of new SC or converting exiting power plants into SC. However, an average cost for SCs varies between $\{9-35\}$ EUR/kVAr [75].
2. **Pumped Storage Hydro**
   Utility-sized energy storage systems are a small percentage of the total generating capability of the power system, but are gaining more and more attention for their role in enabling higher penetrations of variable renewable resources into the grid [76]. Currently, the most common type of utility-scale storage is pumped hydroelectric storage (PHS) [77]. The authors of a 2012 white paper by the *National Hydropower Association's Pumped Storage Development Council* indicated that development of new PHS, particularly in areas with increased wind and solar capacity, would significantly improve system reliability while reducing the need to construct new fossil-fuel generation [78]. Simultaneously, the power range of pumped storage devices are suitable for delivering sufficient synchronous inertia although significantly lower than that of a gas or coal fired power plant [77]. However, this technology requires the construction of an upper and a lower basin which delimits its application in some countries due to geographical limitations.
   - Geographic limitation
     The geographical circumstance is a key requirement to be able to employ this technology. In fact, it requires the construction of an upper and a lower basin which delimits its application to areas which fulfil these requirements.
   - Additional system services
     Capability to provide various system services as conventional power plants. Additionally, pumped hydro power plants can also consume active power from the grid to pump water from the lower basin to the higher one.
   - Type of the inertia response
     Synchronous inertia response due to direct grid connection.
   - Inertia constant and power capacity range
     Inertia constant in the range of $2H = \{2-4\}$ s and power capacity of $\{1-3000\}$ MW [79,80].
   - Capital cost
     Capital costs for PHS differ very much. Reliable, experimentally confirmed numbers are only available for traditional geographically determined installations and reported to be in the range of $\{800-1000\}$ EUR/kW [81].
3. **Compressed Air Energy Storage**
   Energy storage systems are effective for supporting the integration of renewable energy and delivering system services. Compressed air energy storage

(CAES) is a promising energy storage technology due to its high efficiency, cleanness and long service life [82]. CAES makes use of underground caverns where air is compressed for storage and decompressed in order to release the stored energy. A CAES plant consists of a large volume that can store the compressed air (the battery) and what is in principle a gas turbine. The plant store the compressed air underground in caverns or rock formations [83].

- Geographic limitation
  One can notice that the geology plays a significant role for this technology since it requires an underground cavern limiting its applicability.
- Additional system services
  CAES is capable of providing multiple system services as frequency and voltage support.
- Type of the inertia response
  CAES is characterised by its synchronous inertia response.
- Inertia constant and power capacity range
  Inertia constant in the range of $2H = \{3-4\}$ s and power capacity that range between $\{15-600\}$ MW [79].
- Capital cost
  Based on the analysis on 2^{nd} generation CAES, estimated capital costs range between $\{750-1000\}$ EUR/kW [81].

4. **AC Interconnection**
An AC interconnection between two power systems, by means of overhead lines or cables, will lead to a single synchronous network. In case of loss of generation, the inertia of both power systems will start to supply the power imbalance, leading to lower RoCoF and better frequency performance [84, 13].
   - Geographic limitation
     Geographical flexibility and large distance play a significant role regarding AC interconnectors installation. For example, if an interconnector was to be built between the Island of Ireland and United Kingdom, the distance would be one of world's longest sub-marine AC cables which is likely to challenge current technology.
   - Additional system services
     The power system will be strengthened due to the connection of the two subsystems. However, due to the long high voltage cables, the charging current limits the power transfer capability [85].
   - Type of the inertia response
     Inherent inertia response improving the overall frequency performance.
   - Inertia constant and power capacity range
     For AC inerterconnectors, the inertia constant depends on the inertia of the two interconnected systems. The power capacity depends on the interconnecting link.
   - Capital cost
     AC interconnection depends on the distance of the two connected systems as well as the geography which determines the possibility of using overhead lines or cables.
5. **Power Plant Technical Minimum Reduction**
One possible solution for maintaining the same inertia level while allowing greater headroom for non-synchronous generation is by operating SGs at low power setpoints. Most conventional power plants are designed to run in the upper capacity range closer to the rated power with a minimum low power setpoint. Reducing the minimum setpoint value is another option with the same benefits. However, the power plant type plays a fundamental role for the provision of this service. For example, thermal power plants operating in the lower output range are characterised by high CO_2 emissions [86].
   - Geographic limitation
     No location restrictions since it concerns existing power plants.
   - Additional system services
     The same system services of a conventional plant operating in normal conditions but reduced down-regulation reserves.
   - Type of the inertia response
     Synchronous inertia response.
   - Inertia constant and power capacity range
     The inertia time constant is not alterated and it is the same as for conventional plants which is in the range of $2H = \{2-9\}$ s and power capacity of $\{0.1-1\}$ GW [79].
   - Capital cost
     It depends on the type of plant and if a refurbishment is needed.
6. **Wind Turbines**
Wind Turbines are generally classified into Type 1, Type 2, Type 3 and Type 4 [18, 87]. Early wind turbines of Type 1 and Type 2 were used with a constant speed asynchronous generator, directly connected to the power system and thus, capable of providing synchronous inertia. Modern wind turbines (i.e. Type 3 and Type 4) are designed to operate at a wider range of rotor speeds. Their rotor speed varies with the wind speed or other system variables, based on the design employed. Additional speed and power controls allow variable-speed turbines to extract more energy from a wind regime than fixed-speed turbines.

Nevertheless, for Type 3 and Type 4 turbines, power converters are needed to interface the wind turbine with the grid and thus do not provide any inherent inertia response [88]. However, several wind turbines manufactures offer synthetic inertia response control for the Type 3 and Type 4 wind turbines (e.g. ENERCON inertia emulation control and General Electric WindINERTIA) [89,90].

- Geographic limitation
  The location plays a significant role for the presence of the wind turbine itself. However, for existing wind turbines the geographic location should not present any limitation for providing such services.
- Additional system services
  Wind turbines of Type 3 and Type 4 are capable of providing a wide range of system services due to their controllability. Nevertheless, they can only provide system services only if sufficient wind is present.
- Type of the inertia response
  Wind turbines of Type 1 and Type 2 provide inherent inertia response while Type 3 and Type 4 in principal can only provide emulated inertia.
- Inertia constant and power capacity range
  Wind turbines of Type 1 and Type 2 with rated power more than 1 MW have values of inertia constant in the range of $2H = \{3-5\}$ s [91]. On the other hand, in Type 3 and Type 4 the mechanical inertia is decoupled from the grid. The machine power capacity spans between $\{1-10\}$ MW [79].
- Capital cost
  Wind turbines capital cost varies among technologies. However, for onshore installation capital cost varies between $\{1100-1950\}$ EUR/kW while for offshore wind turbines, the capital cost varies between $\{2300-4300\}$ EUR/kW [92].

7. **HVDC Interconnectors**
High-voltage DC (HVDC) transmission links provide a means of non-synchronously connecting two (or more) AC power systems whilst maintaining control of the power flow over the HVDC-link. HVDC-link is an economical way of transferring electrical power over long distances [93]. Due to the asynchronous interconnection between the interconnected power systems, no inherent inertia response is available since the DC connection fully decouples the two areas. Nevertheless, various studies have investigated the ability of HVDC in providing frequency control services, including inertia emulation and primary frequency control [94,95,96]. Frequency control can be achieved by including frequency control loop either in the active power controller or the DC voltage controller [97].
   - Geographic limitation
     The location of the HVDC interconectors plays a fundamental role in its applicability. Generally, the main challenge is related to the long distance and high costs.
   - Additional system services
     HVDC interconectors are capable of providing a large number of system services depending on the employed converter technology.
   - Type of the inertia response
     Due to the decoupling between the two subsystems, only emulated inertia can be provided.
   - Inertia constant and power capacity range
     HVDC interconnectors do not provide an inherent inertia response. HVDC power capacity depends from the employed technology. The current installed HVDC links are characterised by a power capacity in the range of $\{3-8000\}$ MW [79].
   - Capital cost
     HVDC capital cost depends on the applied technology and the distance over which the two areas are connected.
8. **Various Batteries Technologies**
Batteries are energy storage units that store electrical energy and operate at direct current, thus, power electronic converters are needed to interface the batteries with the grid. Batteries can provide multiple benefits to the power system in terms of ancillary services and RoCoF enhancement. Nevertheless, the battery's technology plays a fundamental role in deciding the suitability in providing such services. For example, Sodium-Sulfur batteries (NaS) are characterised by their fast response time and as claimed by certain manufactures, the response time is within 1 ms [98] allowing the provision of synthetic inertia services and/or fast frequency control services. On the other hand, hydrogen storage system and synthetic natural gas do have a relatively slow response time (i.e. in the range of seconds) which limits their capabilities for synthetic inertia services [99,100].
   - Geographic limitation
     Generally, batteries technologies do not have locational restrictions and are flexible to install. However, some minor exceptions might occur for flow batteries due to the additional space required for the auxiliary services and for the more complex technology.

- Additional system services
  Due to their controllability batteries are able to offer multiple system services.
- Type of the inertia response
  In principal, they can provide only emulated inertia.
- Inertia constant and power capacity range
  Batteries do not have any inherent inertia response. Batteries' power capacity depends on the applied technology, however, typical power capacity is generally up to several MW.
- Capital cost
  Batteries' capital cost vary among the applied technologies. However, it can range between $\{250 - 2600\}$ EUR/kW [80].

9. **Demand Side Management**
In theory, demand and generation can participate in frequency control. In the current control schemes, adopted by the majority of TSOs, demand is used to restore severe power imbalance that cannot be alleviated by fast acting generators (i.e. load shedding). Nevertheless, demand capability to contribute to frequency control has been underestimated in the past due to the complexity involved in the real-time monitoring and control of aggregated loads [101]. On the other side, with the advancements in measuring and monitoring techniques, demand side management (DSM) starts to gain more consideration and application from various TSOs in managing the power system efficiently and in accommodating a higher share of renewable energy generation [102]. Simultaneously, different projects and studies are investigating DSM technology in providing additional system services as fast primary frequency control and SIC from aggregated loads. Various studies are analysing through simulations and field tests the capability of electric vehicles in delivering frequency support and system services [34,67].
   - Geographic limitation
     Location plays a crucial role to allow the aggregation of a number of loads to provide adequate response power.
   - Additional system services
     DSM is able to provide multiple system services such as frequency and voltage control. However, it depends from the nature and capability of the aggregated units.
   - Type of the inertia response
     DSM is able to provide regulating power in terms of emulated inertia.
   - Inertia constant and power capacity range
     DSM does not provide inherent inertia response and therefore an inertia constant can not be provided. Similarly, a power capacity range can not be provided because it depends on the number of the aggregated electrical loads.
   - Capital cost
     A large range of cost depending on the applied technology and infrastructure
10. **Flywheel**
Flywheels store kinetic energy in the rotation of a wheel. The moving mass is accelerated and decelerated by a motor/generator and therefore charging or discharging the system [13]. High speed flywheels are interfaced with the grid through power electronics, thus, are only capable of delivering synthetic inertia. Flywheels energy storage systems are characterised by its fast ramping capability and long-term durability. Due to their fast response time (i.e. in order of milliseconds), flywheels can provide ancillary services including synthetic inertia and frequency response to power grids [103].
   - Geographic limitation
     Flywheels do not have a locational restrictions and can be easily installed.
   - Additional system services
     Flywheels are capable of providing frequency support in terms of regulating power.
   - Type of the inertia response
     Due to the connection to the grid through power electronics, flywheels are capable of providing only emulated inertia.
   - Inertia constant and power capacity range
     Flywheels are not characterised by an inertia constant due to the connection to the grid through power electronics. Typical power capacity range between $\{0.1 - 20\}$ MW [79,80].
   - Capital cost
     Flywheels have a capital cost that range between $\{210 - 300\}$ EUR/kW [80].

6 Conclusion

The paper presented an overview of the various challenges which TSOs and distribution system operators (DSOs) are facing due to the increasing share of inertia-less resources. It focuses generally on the frequency performance and in particular on the RoCoF. The effects of the system inertia and the primary frequency response on the RoCoF, frequency nadir and steady state value are presented graphically and analytically. The study presented also the various methods that can

Table 2: Overview of the various technologies

Technology	Synch. / EIC	Inertia (2H)	Power capacity	Geography limitations	Additional services			Capital cost
					Voltage Support	Energy Supply	Black start	
Synchronous Condensers	Synch.	{2 - 3} s	{50 - 250} MVA	Low	YES	NO	NO	{9- 35} EUR/kVAR
Pumped Storage Hydro	Synch.	{2 - 4} s	{1 - 3000} MW	High	YES	Limited	YES	{800-1000} EUR/kW
Compressed Air Energy Storage	Synch.	{3 - 4} s	{15 - 600} MW	High	YES	Limited	YES	{750-1000} EUR/kW
AC Interconnection	Synch.	Depends on the interconnected systems	Depends on the line rating	Medium	Limited	YES	Limited	-
Parking or Reduction of the minimum MW generation	Synch.	{2- 9} s	Plant dependent	Low	YES	YES	Limited	-
Wind Turbines (Type 1 & 2)	Synch. & EIC	{3 - 5} s	0.5 -2	Medium	Limited	YES	NO	Onshore: {1100 - 1950} EUR/kW
Wind Turbines (Type 3 & 4)	Synch. & EIC	-	0.5 -2	Medium	YES	YES	NO	Offshore: {2300 - 4300} EUR/kW
HVDC interconnectors (VSC based)	EIC	-	{100 - 1000} MW	Average	YES	YES	YES	
Electrochemical and Chemical Batteries	EIC	-	0.1 - 100 MW	Low	YES	Limited	YES	{250 - 2600} EUR/kW
Demand Side Management	EIC	-	Depends on the aggregated units	Low	Limited	NO	NO	-
Flywheels	EIC	-	{0.1 - 20} MW	Low	YES	NO	NO	{210 - 300} EUR/kW

be employed to improve the frequency gradient, categorised into two groups, namely synchronous inertia and emulated inertia. The emulated inertia methods are divided into three groups, based on the applied control scheme, namely VSM, SIC and FFC.

The manuscript presented the key features and weaknesses of each control schemes detailing also the key parameters and challenges in applying those methods. However, more attention was given to SIC and FFC, showing that both schemes are able to mitigate the RoCoF with a better performance in terms of frequency nadir and steady state frequency when the FFC is applied. The quantitative relationship between MW of reserves (applying SIC or FFC) and MWs of synchronous inertia was also discussed, highlighting the effects of the controllers' performance.

Moreover, a qualitative investigation of the most prominent technologies that can be used to mitigate the RoCoF is presented. Each technology is assessed based on five criteria, namely, 1) Geographic limitation, 2) Additional system services (e.g. voltage control and black start), 3) Type of the provided inertia service, 4) Inertia constant H (s) and the typical power capacity (MW) and 5) Capital cost. The assessment showed that the adequate solution will depend mainly from the system requirement and the geographic restriction which can limit the applicability of certain technologies.

References

1. T. Ackermann. *Wind Power in Power Systems*. John Wiley, 2011.
2. M Marinelli, S Massucco, A Mansoldo, and M Norton. Analysis of Inertial Response and Primary Power-Frequency Control Provision by Doubly Fed Induction Generator Wind Turbines in a Small Power System. In *17th Power Systems Computation Conference*, pages 1–7.
3. P. W. Christensen and G. T. Tarnowski. Inertia of wind power plants State-of-the-art review. In *The 10th*

International Workshop on Large-Scale of Wind Power, Aarhus, Denmark, 2011.
4. E. Muljadi, V. Gevorgian, M. Singh, and S. Santoso. Understanding inertial and frequency response of wind power plants. In *2012 IEEE Power Electronics and Machines in Wind Applications*, pages 1–8, July 2012.
5. S. Sharma, S. H. Huang, and N. Sarma. System inertial frequency response estimation and impact of renewable resources in ERCOT interconnection. In *2011 IEEE Power and Energy Society General Meeting*, pages 1–6, July 2011.
6. M. Pertl, T. Weckesser, M. Rezkalla, and M. Marinelli. Transient stability improvement: a review and comparison of conventional and renewable based techniques for preventive and emergency control. *Springer Electrical Engineering*, 2017.
7. P. Mancarella, S. Puschel, H. Wang, M. Brear, T. Jones, M. Jeppesen, R. Batterham, R. Evans, and I. Mareels. Power system security assessment of the future National Electricity Market. Technical Report June, Melbourne Energy Institute, Melbourne, 2017.
8. EIRGRID and SONI. RoCoF Alternative & Complementary Solutions Project. Technical Report March, 2016.
9. L. Martini, A. Morch, L. Radaelli, C. Caerts, C. Tornelli, S. Hänninen, and H. Brunner. Electra IRP approch to voltage and frequency control for future power systems with high DER penetration. In *23rd International Conference on Electricity Distribution CIRED*, number June, pages 1–5, 2015.
10. M. Rezkalla, K. Heussen, M. Marinelli, J. Hu, and H. W. Bindner. Identification of requirements for distribution management systems in the smart grid context. In *Power Engineering Conference (UPEC), 2015 50th International Universities*, pages 1–6, Sept 2015.
11. The Commission for Energy Regulation. Rate of Change of Frequency (RoCoF) Modification to the Grid Code. Technical report, 2014.
12. EirGrid and SONI. DS3 RoCoF Alternative Solutions Phase 1 Concluding Note. Technical report, 2015.
13. DNV GL Energy Advisory. RoCoF Alternative Solutions Technology Assessment. Technical report, 2015.
14. National Grid. Fast Reserve Service Description. Technical Report April, 2013.
15. J. Brisebois and Noël Aubut. Wind Farm Inertia Emulation to Fulfill Hydro-Québec's Specific Need. In *Power and Energy Society General Meeting IEEE*, volume 7, pages 1–7, 2011.
16. Jeff Palermo. International review of frequency control adaptation. Technical report, 2016.
17. R Serway, R Beichner, and J. Jewett. *Physics for Scientists and Engineers*. Holt Rinehart & Winston, Philadelphia, 5th edition, 2000.
18. M. Cheng and Y. Zhu. The state of the art of wind energy conversion systems and technologies : A review. *Energy Conversion and Management*, 88:332–347, 2014.
19. J. Licari, J. Ekanayake, and I. Moore. Inertia response from full-power converter-based permanent magnet wind generators. *Journal of Modern Power Systems and Clean Energy*, 1:26–33, 2013.
20. F. M. Gonzalez-longatt. Impact of emulated inertia from wind power on under-frequency protection schemes of future power systems. *Journal of Modern Power Systems and Clean Energy*, 4(2):211–218, 2016.
21. U. Tamrakar, D. Galipeau, R. Tonkoski, and I. Tamrakar. Improving Transient Stability of Photovoltaic- Hydro Microgrids Using Virtual Synchronous Machines. In *PowerTech, IEEE*, Eindhoven, 2015.
22. U. Tamrakar, D. Shrestha, M. Maharjan, B. P Bhattarai, T. M. Hansen, and R. Tonkoski. applied sciences Virtual Inertia : Current Trends and Future Directions. *Applied Sciences*, pages 1–29, 2017.
23. H.P. Beck and R. Hesse. Virtual Synchronous Machine. In *9th International Conference on Electrical Power Quality and Utilisation*, Barcelona, Spain, 2007.
24. S. D'Arco and J. Suul. Virtual Synchronous Machines Classification of Implementations and Analysis of Equivalence to Droop Controllers for Microgrids. In *PowerTech IEEE*, Grenoble, 2013.
25. J. Machowski, J. W. Bialek, and J. R. Bumby. *Power System Dynamics and Stability*. Wiley, Chichester, UK, 1997.
26. E. W. Kimbark. *Power System Stability Volume III Synchronous Machines,*. New York, USA, 1956.
27. M P N Van Wesenbeeck, S W H De Haan, P Varela, and K Visscher. Grid Tied Converter with Virtual Kinetic Storage. In *PowerTech IEEE*, number 1, pages 1–7, Bucharest, 2009.
28. J. Driesen and K. Visscher. Virtual Synchronous Generators. In *Power and Energy Society General Meeting*, pages 1–3, Pittsburgh, PA, USA, 2008.
29. V. Karapanos, S. Haan, and K. Zwetsloot. Real Time Simulation of a Power System with VSG Hardware in the Loop. In *IECON - 37th Annual Conference on IEEE Industrial Electronics Society*, pages 1–7, Melbourne, VIC, Australia, 2011.
30. V. Thong, A. Woyte, M. Albu, M. Hest, J. Bozelie, J. Diaz, T. Loix, D. Stanculescu, and K. Visscher. Virtual Synchronous Generator : Laboratory Scale Results and Field Demonstration. In *PowerTech IEEE*, pages 1–6, Bucharest, 2009.
31. Y. Chen, R. Hesse, D. Turschner, and H.P. Beck. Comparison of methods for implementing virtual synchronous machine on inverters. In *International Conference on Renewable Energies and Power Quality*, pages 1–6, Santiago de Compostela, 2012.
32. C. Pelczar. *Mobile Virtual Synchronous Machine for Vehicle-to-Grid Applications*. PhD thesis, Clausthal University of Technology, 2012.
33. M. Marinelli, S. Martinenas, K. Knezovi, and P. B. Andersen. Validating a centralized approach to primary frequency control with series-produced electric vehicles. *Journal of Energy Storage*, 7:63 – 73, 2016.
34. M. Rezkalla, A. Zecchino, S. Martinenas, A.M. Prostejovsky, and M. Marinelli. Comparison between synthetic inertia and fast frequency containment control based on single phase EVs in a microgrid. *Applied Energy*, 2017.
35. M. Rezkalla, M. Marinelli, H. Qazi, and J. O'Sullivan. Augmenting System Inertia Through Fast Acting Reserve A Power System Case Study with High Penetration of Wind Power. Manuscript submitted for publication. 2018.
36. S. Xue, B. Kasztenny, I. Voloh, and D. Oyenuga. Power System Frequency Measurement for Frequency Relaying. Technical Report 2.
37. M. M. BegoviC, P. M. DjuriC, S. Dunlap, and A. G. Phadke. Frequency Tracking ih Power Networks in the Presence of Harmonics. *IEEE Transactions on Power Delivery*, 8(2):480–486, 1993.
38. L. Asnin, V. Backmutsky, M. Gankin, J Blashka, and M Sedlachek. DSP methods for dynamic estimation of frequency and magnitude parameters in power system transients. In *IEEE Power Tech Conference*, pages 1–6, Porto, 2001.

39. C.T. Nguyen and K. Srinivasan. A New Technique for Rapid Tracking of Frequency Deviations Based on Level Crossings. *IEEE Transactions on Power Apparatus and Systems*, (8):2230–2236, 1984.
40. D. Hart, D. Novosel, Y. Hu, B. Smith, and M. Egolf. A new frequency tracking and phasor estimation algorithm for generator protection. *IEEE Transactions on Power Delivery*, 12(3):1064–1073, 1997.
41. B. Kasztenny and E. Rosolowski. Two New Measuring Algorithms for Generator and Transformer Relaying. *IEEE Transactions on Power Delivery*, 13(4):1053–1059, 1998.
42. M. Wang and Y. Sun. A Practical, Precise Method for Frequency Tracking and Phasor Estimation. *IEEE Transactions on power delivery,*, 19(4):1547–1552, 2004.
43. V. Eckhardt, P. Hippe, and G. Hosemann. Dynamic measuring of frequency and frequency oscillations in multiphase power systems. *IEEE Transactions on Power Delivery*, 1989.
44. M Karimi-Ghartemani and M.R Iravani. Wide-range, fast and robust estimation of power system frequency. *Electric Power Systems Research*, 2003.
45. H. Karimi, M. Karimi-Ghartemani, and M.R. Iravani. Estimation of Frequency and its Rate of Change for Applications in Power Systems. *IEEE Transactions on Power Delivery*, 2004.
46. P.J. Moore, R.D. Carranza, and A.T. Johns. A new numeric technique for high-speed evaluation of power system frequency. *IEE Proceedings - Generation, Transmission and Distribution*, 1994.
47. T S Sidhu. Accurate measurement of power system frequency using a digital signal processing technique. *IEEE Transactions on Instrumentation and Measurement*, 1999.
48. P. K. Dash, G. Panda, A. K. Pradhan, A. Routray, and B. Duttagupta. An extended complex Kalman filter for frequency measurement of distorted signals. In *2000 IEEE Power Engineering Society, Conference Proceedings*, 2000.
49. H.C. Lin. Fast tracking of time-varying power system frequency and harmonics using iterative-loop approaching algorithm. *IEEE Transactions on Industrial Electronics*, 2007.
50. Z. Salcic, Z. Li, U.D. Annakkage, and N. Pahalawaththa. A comparison of frequency measurement methods for underfrequency load shedding. *Electric Power Systems Research*, 1998.
51. J P Patra and P. K. Dash. Fast frequency and harmonic estimation in power systems using a new optimized adaptive filter. *Electrical Engineering*, pages 171–184, 2012.
52. J. Wu, J. Long, and J. Wang. High-accuracy, wide-range frequency estimation methods for power system signals under nonsinusoidal conditions. *IEEE Transactions on Power Delivery*, 2005.
53. M. B. Duric, V V Terzija, and I A Skokljev. Power system frequency estimation utilizing the Newton-Raphson method. *Electrical Engineering*, 77:221–226, 1994.
54. P K Dash, S K Panda, B Mishra, and D P Swain. Fast estimation of voltage and current phasors in power networks using an adaptive neural network. *IEEE Transactions on Power Systems*, 1997.
55. Khaled M. El-Naggar and Hosam K.M. Youssef. Genetic based algorithm for frequency-relaying applications. *Electric Power Systems Research*, 2000.
56. P. Kostyla, T. Lobos, and Z. Waclawek. Neural networks for real-time estimation of signal parameters. *Proceedings of IEEE International Symposium on Industrial Electronics*, 1996.
57. P. Kundur, J. Paserba, V. Ajjarapu, G. Andersson, A. Bose, C. Canizares, N. Hatziargyriou, D. Hill, A. Stankovic, C. Taylor, T. Van Cutsem, and V. Vittal. Definition and Classification of Power System Stability. *IEEE Transactions on Power Systems*, 21(3):1387–1401, 2004.
58. K. Temtem, S.and Creighton. Summary of Studies on Rate of Change of Frequency events on the All-Island System August 2012. Technical Report August 2012.
59. EirGrid. RoCoF Modification Proposal TSOs ' Recommendations. Technical Report September, 2012.
60. W. Xu, K. Mauch, and S. Martel. An Assessment of Distributed Generation Islanding Detection Methods and Issues for Canada. Technical report, Canada, 2004.
61. X Ding, P A Crossley, and D J Morrow. Islanding Detection for Distributed Generation. *Journal of Electrical Engineering & TechnologyJournal of Electrical Engineering & Technology*, 2007.
62. A. Beddoes, P. Thomas, and M. Gosden. Loss of mains protection relay performances when subjected to network disturbances / events. In *18th International Conference on Electricity Distribution CIRED*, pages 1–5, 2005.
63. C. F. TEN. *Loss of Mains Detection and Amelioration on Electrical Distribution Networks*. PhD thesis, 2010.
64. A.A.M. Hassan and Tarek A. Kandeel. Effectiveness of frequency relays on networks with multiple distributed generation. *Journal of Electrical Systems and Information Technology*, 2015.
65. W. Uijlings. An independent analysis on the ability of Generators to ride through Rate of Change of Frequency values up to 2Hz / s . Technical report, 2013.
66. Tom Mccartan. Rate of Change of Frequency (RoCoF) project Six Monthly Report for November 2016. Technical Report November, 2016.
67. K. Knezović, M. Marinelli, A. Zecchino, P. B. Andersen, and C. Traeholt. Supporting involvement of electric vehicles in distribution grids: Lowering the barriers for a proactive integration. *Energy*, 134:458–468, 2017.
68. M. Rezkalla, M. Marinelli, M. Pertl, and K. Heussen. Trade-off Analysis of Virtual Inertia and Fast Primary Frequency Control during Frequency Transients in a Converter Dominated Network. In *Innovative Smart Grid Technologies - Asia (ISGT-Asia), IEEE*, pages 1–6, Melbourne, VIC, Australia, 2016.
69. L. Pereira, J. Undrill, D. Kosterev, D. Davies, and S. Patterson. A New Thermal Governor Modeling Approach in the WECC. *IEEE Transactions on Power Systems*, 18(2), 2003.
70. N W Miller, M Shao, S Pajic, and R D Aquila. Eastern Frequency Response Study. Technical Report May, 2013.
71. Energinet.dk. Ancillary services to be delivered in Denmark Tender conditions. Technical report, Fredericia, 2012.
72. S. Nakamura, T Yamada, T Nomura, M. Iwamoto, Y. Shindo, S. Nose, H. Fujino, and A. Ishihara. 30 MVA superconducting synchronous condenser: Design and it's performance test results. *IEEE Transactions on Magnetics*, 21(2):783–790, 1985.
73. J.A. Oliver, B J Ware, and R.C. Carruth. 345 MVA Fully Water-Cooled Synchronous Condenser for Dumont Station Part I. Application Considerations. *IEEE Transactions on Power Apparatus and Systems*, PAS-90(6):2758–2764, 1971.
74. H. T. Nguyen, G. Yang, A. H. Nielsen, and P. H. Jensen. Frequency stability improvement of low inertia systems using synchronous condensers. In *2016 IEEE International Conference on Smart Grid Communications, SmartGridComm 2016*, 2016.

75. J Kueck, B Kirby, T Rizy, F Li, and N Fall. Reactive Power from Distributed Energy. *The Electricity Journal*, 2006.
76. M. Mohanpurkar, A. Ouroua, R. Hovsapian, Y. Luo, M. Singh, E. Muljadi, V. Gevorgian, and P. Donalek. Real-time co-simulation of adjustable-speed pumped storage hydro for transient stability analysis. *Electric Power Systems Research*, 154:276–286, 2018.
77. E Ela, B Kirby, A. Botterud, C. Milostan, I. Krad, and V. Koritarov. The Role of Pumped Storage Hydro Resources in Electricity Markets and System Operation Preprint. In *HydroVision International*, number July, Denver, Colorado, 2013.
78. NHA Pumped storage council. Challenges and Opportunities For New Pumped Storage Development. Technical report, 2012.
79. S. Rehman, L. M. Al-Hadhrami, and M. M. Alam. Pumped hydro energy storage system: A technological review. *Renewable and Sustainable Energy Reviews*, 2015.
80. X. Luo, J. Wang, M. Dooner, and J. Clarke. Overview of current development in electrical energy storage technologies and the application potential in power system operation. *Appl. Energy*, 2015.
81. A. E. Tønnesen, A. H. Pedersen, B. Elmegaard, J. Rasmussen, J. H. Vium, L. Reinholdt, and A. S. Pedersen. Electricity Storage Technologies for Short Term Power System Services at Transmission Level. Technical Report October, 2010.
82. L. Chen, T. Zheng, S. Mei, X. Xue, B. Liu, and Q. Lu. Review and prospect of compressed air energy storage system. *Journal of Modern Power Systems and Clean Energy*, 4(4):529–541, 2016.
83. Brian Elmegaard and Wiebke Brix Markussen. Efficiency of Compressed Air Energy Storage. In *The 24th International Conference on Efficiency, Cost, Optimization, Simulation and Environmental Impact of Energy Systems*, 2011.
84. ENTSO-E. Frequency Stability Evaluation Criteria for the Synchronous Zone of Continental Europe. Technical report, ENTSOE, 2016.
85. C. S. Schifreen and W. C. Marble. Charging current limitations in operation or high-voltage cable lines [includes discussion]. *Transactions of the American Institute of Electrical Engineers. Part III: Power Apparatus and Systems*, 75(3), Jan 1956.
86. J. Macak. Evaluation of Gas Turbine Startup and Shutdown Emissions for New Source Permitting. Technical report, Florida, 2014.
87. E Muljadi and A. Ellis. Validation of Wind Power Plant Models. In *IEEE Power and Energy Society General Meeting*, pages 1–7, 2008.
88. M. Singh and S. Santoso. Dynamic Models for Wind Turbines and Wind Power Plants Dynamic Models for Wind Turbines and Wind Power Plants. Technical Report May, NREL, 2011.
89. Y C Zhang, V Gevorgian, and E Ela. Role of Wind Power in Primary Frequency Response of an Interconnection Preprint. In *International Workshop on Large-Scale Integration of Wind Power Into Power Systems as Well as on Transmission Networks for Offshore Wind Power Plants*, 2013.
90. E. Muljadi, V. Gevorgian, M. Singh, and S. Santoso. Understanding inertial and frequency response of wind power plants. *2012 IEEE Power Electronics and Machines in Wind Applications*, pages 1–8, 2012.
91. J. Morren, J. Pierik, and S. W H De Haana. Inertial response of variable speed wind turbines. *Electric Power Systems Research*, 2006.
92. IRENA. Wind power - Technology Brief. Technical report, 2016.
93. G. Mazzanti and M. Marzinotto. Fundamentals of HVDC Cable Transmission. In *Extruded Cables for High-Voltage Direct-Current Transmission:Advances in Research and Development*, chapter 2. Wiley-IEEE Press, 2013.
94. G J Georgantzis, N A Vovos, and G B Giannakopoulos. A suboptimal static controller for HVDC links supplying isolated AC networks. *Electrical Engineering*, 75(6):451–458, 1992.
95. B Silva, C L Moreira, L Seca, Y Phulpin, and J. A. Peças Lopes. Provision of Inertial and Primary Frequency Control Services Using Offshore Multiterminal HVDC Networks. *IEEE TRANSACTIONS ON SUSTAINABLE ENERGY*, 3(4):800–808, 2012.
96. M. Andreasson, R.r Wiget, D. V. Dimarogonas, K. H. Johansson, and G. Andersson. Distributed Primary Frequency Control through Multi-Terminal HVDC Transmission Systems. In *American Control Conference (ACC)*, pages 1–6, Chicago, IL, USA, 2015.
97. C. Du, E. Agneholm, and G. Olsson. Comparison of different frequency controllers for a VSC-HVDC supplied system. *IEEE Transactions on Power Delivery*, 2008.
98. NGK INSULATORS. Structure of NAS Energy Storage System Principle of NAS Battery. Technical report.
99. International Electrotechnical Commission. Electrical Energy Storage. Technical report.
100. US Department of Energy. Grid Energy Storage. Technical Report December, 2013.
101. M H Syed, P Crolla, G M Burt, and J. K. Kok. Ancillary Service Provision by Demand Side Management : A Real-Time Power Hardware-in-the- loop Co-simulation Demonstration. In *Smart Electric Distribution Systems and Technologies*, pages 1–7, 2015.
102. EirGrid. DS3 Demand Side Management Workstream Plan. Technical Report May, 2016.
103. N Lu, M R Weimar, Y V Makarov, F. J. Rudolph, S. N. Murthy, and J. Arseneaux. An Evaluation of the Flywheel Potential for Providing Regulation Service in California. In *Power and Energy Society General Meeting*, pages 1–6, 2010.

[B] Identification of Requirements for Distribution Management Systems in the Smart Grid Context

Identification of Requirements for Distribution Management Systems in the Smart Grid Context

Michel Rezkalla, Kai Heussen, Mattia Marinelli, Junjie Hu, Henrik W. Bindner
Department of Electrical Engineering (Center for Electric Power and Energy), DTU – Technical University of Denmark
Contact Person: Michel Rezkalla, mirez@elektro.dtu.dk

***Abstract*-The integration of significant volumes of distributed and renewable energy resources directly connected to the distribution network raises new requirement to maintain and operate the power system in secure state. Thus the Distribution Management System (DMS) needs to be updated and integrated with new functionality to provide effective support for the operators. The DMS is a control center solution that provides the needed functionality for the management of medium and low voltage distribution networks. This paper aims to provide an overview of the main functions present in today´s DMS platforms and to identify the new requirements to better serve in a smart grid context.**

***Index Terms*—active distribution networks, distribution management system, frequency control, smart grid, synthetic inertia.**

I. INTRODUCTION

To ensure the integration of significant volumes of distributed energy resources (DER) connected to different voltage levels, adequate observability of the system operating state is a requirement for a reliable and secure supply of electricity. From a control system perspective, transmission system operators (TSOs) are able to keep the system stable and balanced because they can observe the transmission grid and control a significant share of the total generation. TSOs control and maintain the system in secure state using energy management system platform (EMS). Energy system management and distribution system management (DMS) have different control objectives. Since the majority of generation resources are connected to the transmission grid, the EMS has an energy focus and provides different functionality compared to the DMS.

The high integration of renewable energy sources (RES) and distributed generation (DG) directly connected to the distribution grid (e.g. wind plants, photovoltaic plants, and active consumers such as electric vehicles) and the deployment of demand response technique transforms the distribution grid from passive grid to active grid. However, the majority of the power flow will be managed by the distribution system operators (DSOs) instead of TSOs.

A great challenge is to control many small and distributed generation units instead of controlling few large generation units. The system could be kept stable and balanced using a centralized control action as it is today (from TSO). In this case we need advanced information communication technology (ICT) infrastructure with huge amount of data to be transmitted to the TSO. Alternative solution is the transition to distributed control action where distributed units could be locally or remotely controlled from the operator. In this case the operator control area is much smaller than TSO´s area. Therefor DSO needs to address the challenges since the majority of generation units are connected to the distribution grid which is not sufficiently observed. Implementing a distributed architecture, DSOs will be responsible for local balancing and voltage control replacing some of TSO´s role. Therefore, the distribution management system should be updated to better serve the new requirements.

The DMS has a control room focus in assisting the operator to maintain and operate the system in secure state, minimizing losses and optimizing the lines power flow capacity. DMS coordinates real-time functions within the distribution network with the non-real-time (manually operated devices) information needed to properly control and manage the network on a regular basis. The key to a DMS is the organization of the distribution network model database, access to all supporting ICT infrastructure and applications necessary to populate the model and support the other daily operating tasks. DMS functionality can be divided into three categories:

1) *System monitoring*
2) *Decision support*
3) *Control actions*

Moreover, different vendors describe DMS using the combination of two different terms or products, supervisory control and data acquisition (SCADA) and human machine interface (HMI). The major function of SCADA is acquiring data from remote devices such as transmitters and providing an overall control remotely from a SCADA host software platform. The HMI provides a user interface with a graphics-based visualization to monitor and control the system.

This analysis of DMS functionality is conducted as a part of EU FP7 project ELECTRA IRP[1]. ELECTRA aims to develop new control schemes for the real time operation of the 2030 power system to ensure dynamic balance and stability in a future power system with a high share of decentralized generation. The future power system envisaged in the ELECTRA project will consist in web of cells, defined as a network area with distributed energy resources and loads in a delimited geographical area. Each cell managed by a single operator who takes responsibility of frequency and voltage control. An inter-cell coordination control layer will support system-wide optimized reserves activation if the cell state and system state allows, which imply advanced

communication infrastructure and new functionality to be integrated into the DMS.

This paper is divided into five sections: in section II we present state of the art of the DMS defining the main functions present in different DMS platforms. In section III we present the future DMS platform requirements to maintain and operate the system in secure state. In section IV conclusion and future work are reported.

II. STATE OF THE ART

DMS functionality can be divided into three categories as shown in Fig. 1.

1) *System monitoring*
2) *Control actions*
3) *Decision support*

The system monitoring provides an accurate state of the system using a significant number of real time and near real time information about the current status. The real-time information would include data from remote terminal units (RTU) in substations and feeders. The "near real time" information would include measurement equipment (e.g. distribution substation transformers, load tap changers and distributed generating resources).

The control action is able to control power system apparatus located at distribution substations and field locations. The DMS platform makes available different control actions such as direct control and operator control. The direct control action is realized directly by the DMS without any operator intervention, for example opening a switch breaker to interrupt a fault. The operator control can be divided into two categories, the remote control and the manual control. The remote control is when the operator able to control remotely the apparatus using the SCADA system. The manual control is when the operator needs to call the field crew to open or close a switch which is not remotely controlled [2].

The decision support provides the operator with a set of solutions to enhance the system reliability and efficiency. It provides a decision support solutions as well as appropriate control actions.

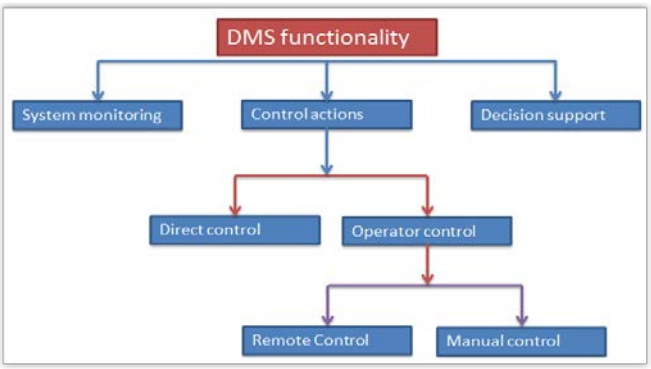

Fig. 1 DMS functionality

The DMS platform is provided by various vendors with different functions. The common and main functions can be summarized as:

1) *State estimation*
2) *Power flow*
3) *Volt / Var control*
4) *Fault management and system restoration*
5) *Short circuit analysis*
6) *Load management*

Following the DMS functionality classification as described in the beginning of this section, the above mentioned functions can be regrouped into the three different categories.

1) *System monitoring*
   - *State estimation*
   - *Power flow*
2) *Control actions*
   - *Volt / Var control*
3) *Decision support*
   - *Fault management and system restoration*
   - *Short circuit analysis*
   - *Load management*

The three categories interact with each other and the operator in order to maintain the system in secure state and optimize the system operation. The different functions are linked to each other even if they belong to a different group. For example, the state estimation belongs to the system monitoring category but at the same time the state estimation evaluation is used in the Volt / Var tool. In Fig. 2 we represented the interaction between the three functionality categories.

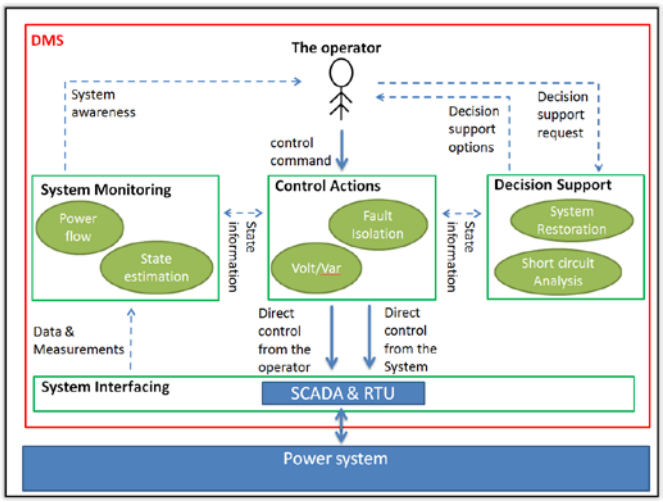

Fig. 2 Interaction between the different DMS functionality categories; solid arrow means control actions, dotted arrow means data and measurements

A. State estimation

The state estimation has a fundamental role in monitoring and controlling the system and is a key functionality in the EMS, being responsible for estimating the state of the power system. As the distribution grid is becoming active due

mainly to the integration of distributed renewable generators directly connected to the low and medium voltage grid, the state estimation started to be a key function in the DMS. The state estimation recreates values for different distribution system variables using the available data present in the SCADA system[3].

B. *Power flow*

The power flow function is a numerical analysis of the power flow in an interconnected system. These calculations are initiated on periodic basis or in case of any significant change in the network. The operator can also initiate the calculation if needed. This tool use different visualization technique, for example a single line diagram to provide the operator with the electrical conditions as well as the power distribution on the different lines, assisting the operator to understand the system state and abnormal conditions e.g. overload in line sections [2].

C. *Volt / Var control*

Volt / Var control determines the best control action to maintain the voltage profile within a desired range and minimizing system losses controlling the reactive power flow in the distribution system [4]. This function provides the operator with the best actions and recommendations to maintain the high quality voltage profile minimizing the losses and the reactive power demands. During this operation different resources can be used such as Tap Changer, Facts devices and capacitor banks.

D. *Fault management and system restoration*

This is a restoration functionality which improves reliability and power quality reducing the number of customer affected by the fault and the outage time duration. The tool detects and isolates the faulted section, then restores the service using a new configuration of the network. In the following paragraph is presented a use case with three loads and a fault between Load 1 and Load 2 as shown in Fig. 3.

The logical intelligent devices identify the fault location and decide the best action to isolate the fault and restore the service to the unaffected customers. The programmed logic based on the RTU will isolate the fault by opening Breaker 2 to interrupt the power flow to Load 2 and Load 3, as shown in Fig. 4. Afterwards the normally open Breaker 4 will be closed to restore the service to Load 3 minimizing the number of customers affected by the fault, as it is shown in Fig. 5[5].

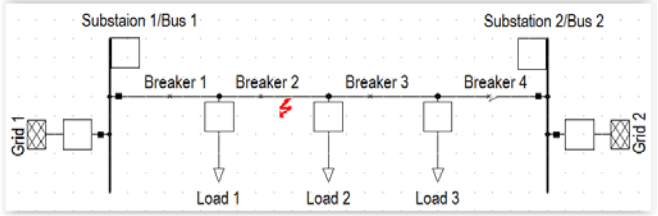

Fig. 3 Load 1, Load 2 and Load 3 are connected to substation 1

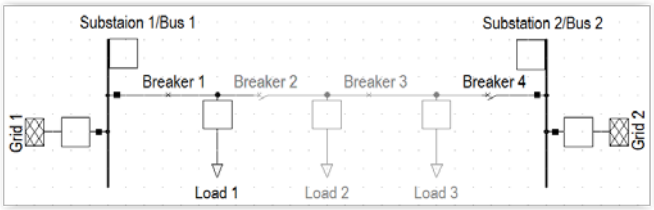

Fig. 4 The fault management tool will isolate the fault opening Breaker 2 and isolating Load 2 and Load 3

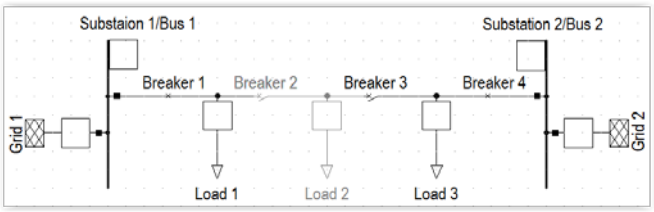

Fig. 5 The fault management tool will restore the service to Load 3opening Breaker 3 and closing Breaker 4

E. *Short circuit analysis*

Short circuit analysis allows the operator to calculate the current after an estimated fault condition in the system, providing him the estimated value to be compared with the switchgear breaking capabilities and limits. This function assists the operator during the network reconfiguration.

F. *Load management*

Since base load peak load ratio can be very high in distribution network which cause a stress on both lines and feeders, the load management must reconfigure the network to handle this situation achieving high efficiency in the system operation. Fig. 6 shows a normal configuration of the network where all the three loads are connected to Grid A. Assuming an overloading on the connection line between Grid A and the others loads, the DMS will propose a different switching configuration to optimize the grid operation as shown in Fig. 7.

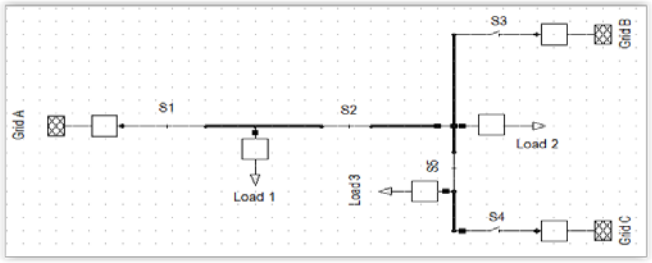

Fig. 6 Load 1, Load 2. and Load 3 are connected to Grid A

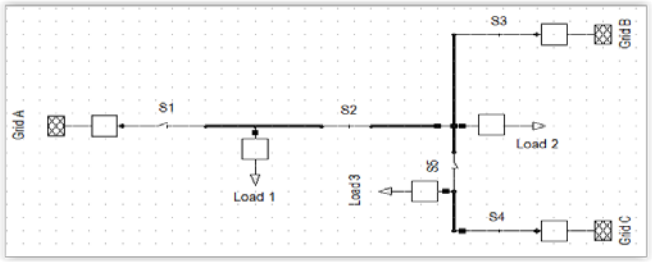

Fig. 7 Load 1and Load 2. are connected to Grid B while Load 3 is connected to Grid C

III. FUTURE REQUIREMENTS

Based on different EU projects, it is expected that by 2030 between 52% and 89% of electricity production will be generated by renewable energy resources mainly connected to the distribution grid [6], [7]. The integration of distributed generators and renewable resources into the grid raises new needs to control and maintain the system in secure state. To provide solutions for the different challenges that DSOs are facing today (addressed in the first section), advanced DMS applications are needed. The authors foresee new needs to operate and control the system and consequently new functions to be integrated into the DMS. Fig. 8 presents an overview of the DMS platform new requirements.

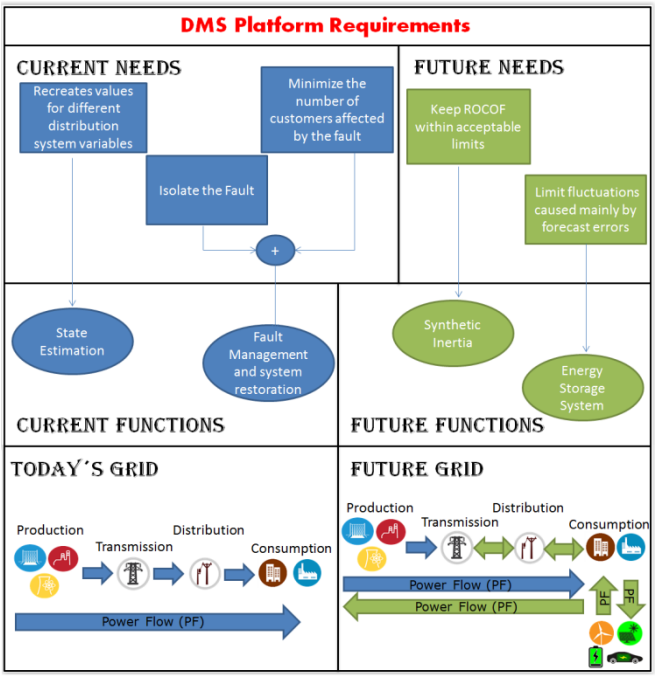

Fig. 8 DMS presentation with the actual and future needs

On the left side of Fig. 8 we have the current functions related to the current needs while on the right side we have new needs and the related functions. This section defines different uses cases taking into account the smart grid context and the ELECTRA project.

A. *Load Estimation*

Since the distribution system was mainly passive there was no need to measure and monitor the different bus loads. Nowadays with the integration of active consumers such as electric vehicles (EV) and residential photovoltaic (PV) systems, the load estimation and forecasting become complicate but more fundamental for operational planning and real time control of the grid. One of the solutions to overcome the lack of measurement in the distribution grid is the use of intelligent devices (IED) that can be programmed to perform certain automated tasks. IED can replace the traditional electromechanical relays providing additional functionality such as measurement of instantaneous volts, amp and power improving the load estimation reliability [5]. One of the challenges is to collect and communicate in real time those values to the DMS database updating the load estimation algorithm. Thus advanced communication technologies and new measurement devices need to be integrated between the DMS and the field to support the load estimation function. For example, different RTU devices are integrated with Modbus/TCP/IP/ fiber optic ports to improve the communication between field devices and RTU.

B. *Load Geographical Information System (GIS)*

Following the distributed control architecture and the transition of the power production from few large generation units to many small generation units, raise new needs for the system operator. The system operator could be a cell operator referred to the ELECTRA project or the DSO referred to the current architecture. The system operator need to control voltage deviation and power flow imbalances using resources located as close as possible to the occurring problem to minimize the reactive power flow distance and consequently the losses. Therefore the operator needs to be aware of the resources position. The geographical Information System should be integrated into the network model providing the operator with a geographical representation of the network, as it is shown in Fig. 9.

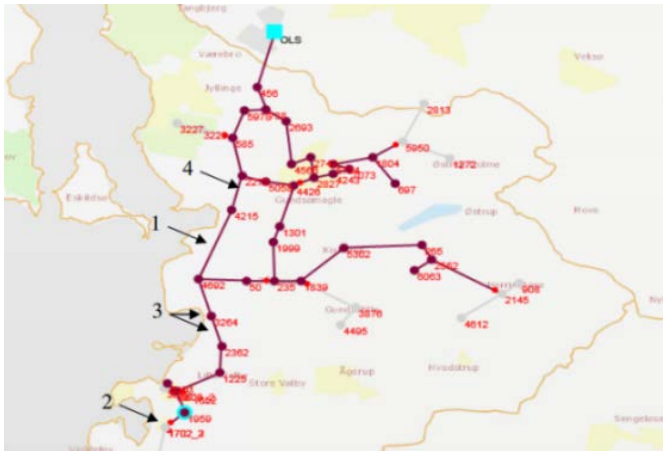

Fig. 9 A portion of the LV network operated by DONG-Denmark [8]

Different Distribution System Operators (DSO) started to upgrade the DMS to achieve better real time visualization. For example, Dong Energy in collaboration with Schneider Electric started to integrate a new DMS system. The new DMS can represent the network as a schematic representation as well as a geographical representation. Thus the operator will have a better overview of the system and will be also able to guide more efficiently the field crew [8].

C. *Synthetic inertia*

The system inertia in the power system smooths both small and large frequency variations after a disturbance, keeping the rate of change of the frequency (ROCOF) within acceptable limits. In today´s power system the ROCOF is limited mainly by the kinetic energy in the rotating generators. The variation in the rotor speed implies a

variation in the kinetic energy transformed into electric power to be changed with the grid. This dynamic is described by the equation of motion[9]:

$$T_m - T_e = J \frac{d\omega_m}{dt} \quad (1)$$

The rotational rate of change $\frac{d\omega_m}{dt}$ of the machine is proportional to the difference between the mechanical input torque to the machine T_m and the electrical load on the machine T_e. The rotational rate of change is scaled by the moment of inertia J.

In the future power system we are facing a new challenge due to the integration of static generators (converters) replacing the rotating machines. Thus the direct coupled inertia provided by direct-coupled machines decreases [10]. For example PV systems and wind turbines connected to the grid with full converter. A solution could be the synthetic inertia response which is a facility able to replicate the inertia response of rotating machines. For example some wind turbine manufactures such as General Electric and ENERCON have started to integrate controllers on modern wind turbine generators in order to provide synthetic inertia [11], [12]. Synthetic inertia can also be provided using energy storage connected to converter coupled generators.

As envisioned in the ELECTRA architecture, also the inertia needs to be properly handled by the DMS [10]. Therefore the DMS should include a new function to provide the operator in real time the total available amount of inertia response within the cell, the available amount that could be delivered to neighbor cells and the available amount that could be received from neighbor cells.

D. Energy storage monitoring

According to the recommendations for the European Energy Storage Technology Development Roadmap [13] , electrical storage prices are projected to drop. Therefore storage will be a cost effective solution for offering ancillary service. Electrical storage could deal with the fluctuations caused mainly by forecast errors and renewable resources intermittency. The storage technology started to be tested in different EU projects such as Grid4EU. The DMS should provide the operator with the battery schedules, location and the related energy prices in such a way to enable the operator to use energy storage systems available within the cell as well as energy storage systems from neighbor cells.

E. Vehicles to grid

Electric Vehicles have become quite popular in some countries due to climate change concerns and different advantages such as cheaper fuel and more silent operation. For example, in Norway are present more than 13.000 EVs [14]. Through smart grid, EVs can offer a unique benefit called vehicle to grid (V2G) technology. Electric vehicles with V2G capabilities can be considered as controllable loads responding to frequency fluctuations [15]. The operator needs to take advantage of the connected EVs to the grid and the relative percentage of power that could participate in the primary frequency control [16], [17]. Therefore the DMS needs to integrate new algorithms to allow the participation of EVs in the primary frequency control.

F. Scaling DMS for supervisory control

The increasing penetration of distributed generation units into distribution grids implies new requirement to control the system from TSOs and DSOs level. The deployment of DER units increases the responsibility of DSOs. Increasingly TSO and DSO are required to communicate to maintain the system in secure state. We observe a development to more active distribution grids, which we can classify into four stages:

1) *Increased observability*
2) *Active network management*
3) *Transfer of (control) responsibility to DSOs*
4) *Self-responsible distribution system operation*

Stage 1: In the near future DSOs need to increase the distribution grid observability due to the high integration of DER units and renewable resources which are weather dependent[18]. For example in Germany PV are monitored and support frequency by local control. According to the German VDE AR-N 4105 guidelines for the low and medium voltage grid, frequencies over 50.2 Hz lead to smooth power reduction of PV systems according to a predefined characteristic curve [19].

Stage 2: Active power management of DER units is becoming increasingly important for solving congestions in both transmission and distribution grid. For example, German feed-in tariff law has required owners of PV systems with active power less than 30 kWp to either limit the reactive power output to 70% of the installed capacity or install a remote control interface to receive temporal power reduction signals from the DSO, if necessary. Units with more than 30 kWp must be controllable remotely[19].

Stage 3: We foresee that DSO in the feature will support more actively TSO in controlling the system, transferring some of TSO´s responsibility to DSO. For example, reactive power management could be handled by the DSO. In line with that, Swissgrid, the Swiss TSO, developed a concept for the coordinated voltage control of the 220/380 kV transmission system that enables, along with transmission connected power plants, the active participation of underlying distribution grids[20].

Stage 4: Following the ELECTRA web of cells concept, the DSO will be completely responsible of the voltage and frequency control of his own cell. For example, active and reactive power management.

It can be observed that stages 1 and 2 already led to more TSO-DSO interaction. For example TSOs having access to online measurement of DER units connected to the MV grid which belong to the DSO´s grid; and able to curtail those units in case of necessity by an official communication to the DSO (e.g. phone call).

To analyze how the supervisory control supported by the DMS, we distinguish three types of control approaches: *local*, *centralized* and *distributed* control.

The *local* control of Stage 1 does not require communication with the DMS since the DER units react to specific situations according to predefined parameters. For example, disconnection of PV inverters at over frequency values predefined from DSOs. Here, no supervisory control, but only increased observability is needed.

The *central* control technique is a communication based approach where the distribution system operator able to control remotely and individually each DER unit. For example, remotely curtail the active power of a wind plant to resolve congestion issues [19]. Supervisory control for centralized control systems is straightforward, due to a clear command hierarchy.

The *distributed* control techniques are communication based control strategy. For example, different DER units clustered into different cells with integrated autonomous control to support grid stability and optimize the economic efficiency. Practical application is implemented in the PV systems. Different PV units are clustered together and controlled from a micro DMS in the substation and monitored by the DSO. Supervising such is more complex, as it requires observation of both the internal state and goals of the distributed controller as well as the of the detailed network state.

In a realistic distribution grid, the need for supervision and control will depend on the actually deployed resources. Therefore a flexible, layered or modular DMS architecture will be required.

IV. Conclusion and Future Work

The introduction of distributed energy resources into the power system requires new control schemes and coordination between different actors. This paper presented the state of the art of the distribution management system related to the current needs and detailing some of the functions present in different platform. This paper also presented the new requirement of the system operator to maintain and operate the system in secure state and identify the related new function to be integrated in the DMS. Supervisory control of the DMS, new roles of DSOs and the interaction between TSOs and DSOs have been presented.

Future work will deal with the definition of analytics for power systems supervisory controls and with the investigation of new control architecture and DMS system architecture.

Acknowledgements

Michel Rezkalla is Ph.D. student at the Technical University of Denmark (DTU) and is supported by the EU FP7 project ELECTRA (grant: 609687) and the Danish Research Project "ELECTRA Top-up" (grant: 3594756936313). More information at www.electrairp.eu

References

[1] L. Martini, A. Morch, L. Radaelli, C. Caerts, C. Tornelli, S. Hänninen, and H. Brunner, "Electra IRP approch to voltage and frequency control for future power systems with high DER penetration," in *23rd International Conference on Electricity Distribution CIRED*, 2015, no. June, pp. 1–5.

[2] E. Vaahedi, *Practical Power System Operation*, 1st ed. John Wiley & Sons, 2014.

[3] A. Jain and N. R. Shivakumar, "Power system tracking and dynamic state estimation," *Conf. Expo. 2009. PSCE '09. IEEE/PES, pp.1,8, 15-18 March 2009*.

[4] S. Rahimi, M. Marinelli, and F. Silvestro, "Evaluation of requirements for Volt/Var control and optimization function in distribution management systems," *2012 IEEE Int. Energy Conf. Exhib. ENERGYCON 2012*, pp. 331–336, 2012.

[5] K. M. Muttaqi, J. Aghaei, V. Ganapathy, and A. E. Nezhad, "Technical challenges for electric power industries with implementation of distribution system automation in smart grids," *Renew. Sustain. Energy Rev.*, vol. 46, pp. 129–142, Jun. 2015.

[6] D. Six, A. Ramos, and E. R. Puente, "D1.2: Evaluation of current market architectures and regulatory frameworks and the role of DSOs," 2014.

[7] "Status review on the transposition of unbundling requirements for DSOs and closed distribution system operators," 2013.

[8] M. Møller, R. Larsen, I. Stefani, and D. Djapic, "On the Implementation of an Advanced Distribution Management System," in *NORDAC 2014*, 2014.

[9] P. Kundur, *Power System Stability and Control*. McGraw-Hill, 1994.

[10] C. Caerts, R. D'hulst, S. De Breucker, E. Rikos, D. Kolodziej, J. M. Fernandez, E. Rodríguez, and K. Heussen, "ELECTRA Deliverable D3.1 Specification of Smart Grids high level functional architecture for frequency and voltage control," vol. 3. http://www.electrairp.eu, pp. 1–100, 2014.

[11] F. . Gonzalez-Longatt, "Effects of the Synthetic Inertia from Wind Power on the Total System Inertia: Simulation Study," in *Environment Friendly Energies and Applications (EFEA), 2012 2nd International Symposium on*, pp. 389 – 395.

[12] E. Muljadi, V. Gevorgian, and M. Singh, "Understanding Inertial and Frequency Response of Wind Power Plants," in *IEEE Symposium on Power Electronics and Machines in Wind Applications*, 2012, no. July.

[13] O. Teller, J.-P. Nicolai, M. Lafoz, D. Laing, R. Tamme, A. Schroeder Pederson, M. Andersson, C. Folke, C. Bourdil, M. Conte, G. Gigliucci, I. Fastelli, M. Vona, M. Rey Porto, T. Hackensellner, R. Knapp, H. J. Seifert, M. Noe, M. Sander, J. Lugaro, M. Lippert, P. Hall, R. Saliger, A. Harby, M. Pihlatie, N. Omar, J.-M. Durand, and P. Clerens, "Joint EASE / EERA recommendations for a European Energy Storage Technology Development Roadmap towards 2030," 2013.

[14] T. E. Nørbech, "Incentives and infrastructure – crucial elements in the build-up of Norway's EV fleet," in *EVS 27 Barcelona, Spain*, 2013, pp. 17–20.

[15] A. Zarogiannis, M. Marinelli, C. Træholt, K. Knezovi, and P. B. Andersen, "A Dynamic Behaviour Analysis on the Frequency Control Capability of Electric Vehicles," in *Power Engineering Conference (UPEC)*, 2014, pp. 1–6.

[16] S. Martinenas, M. Marinelli, P. B. Andersen, and C. Træholt, "Implementation and demonstration of grid frequency support by V2G enabled electric vehicle," in *Proceedings of the 49th International Universities Power Engineering Conference (UPEC) IEEE*, 2014, pp. 1–6.

[17] J. R. Pillai, B. Bak-Jensen, and P. Thogersen, "Electric vehicles to support large wind power penetration in future Danish power systems," *IEEE Veh. Power Propuls. Conf. VPPC*, no. 09–12 Oct, pp. 1475–1479, 2012.

[18] C. Bovo, V. Ilea, M. Subasic, F. Zanellini, C. Arigoni, and R. Bonera, "Improvement of Observability in Poorly Measured Distribution Networks," in *18th Power Systems Computation Conference*, 2014, pp. 1–7.

[19] J. von Appen, M. Braun, T. Stetz, K. Diwold, and D. Geibel, "The Challenge of High PV Penetration in the German Electric Grid," *IEEE Power Energy Mag.*, no. February, pp. 55–64, 2013.

[20] M. Zerva and M. Geidl, "Contribution of active distribution grids to the coordinated voltage control of the Swiss transmission system," in *18th Power Systems Computation Conference*, 2014, pp. 1–8.

[C] Trade-off Analysis of Virtual Inertia and Fast Primary Frequency Control During Frequency Transients in a Converter Dominated Network

Trade-off Analysis of Virtual Inertia and Fast Primary Frequency Control during Frequency Transients in a Converter Dominated Network

Michel Rezkalla, Mattia Marinelli, Michael Pertl, Kai Heussen
Center for Electric Power and Energy, Department of Electrical Engineering
Technical University of Denmark (DTU)
Email: mirez@elektro.dtu.dk

***Abstract*—Traditionally the electricity generation is based on rotating synchronous machines which provide inertia to the power system.The increasing share of converter connected energy sources reduces the available rotational inertia in the power system leading to faster frequency dynamics, which may cause more critical frequency excursions. Both, virtual inertia and fast primary control could serve as a solution to improve frequency stability, however, their respective impacts on the system have different consequences, so that the trade-off is not straightforward.**

This study presents a comparative analysis of virtual inertia and a fast primary control algorithms with respect to ROCOF, frequency nadir and steady state value considering the effect of the dead time which is carried out by a sensitivity analysis. The investigation shows that the virtual inertia controller is effective in reducing the ROCOF compared to fast primary control. However, it is worsening frequency nadir and steady state value. Moreover, the sensitivity analysis shows the very limited effect of the two controllers on the voltage magnitude.

I. Introduction

In traditional power system operation with a reduced amount of renewable sources converter driven (such as PV and wind turbines type 3 and 4) [1], the amount of inertia is assumed to be constant. The power supply is mainly provided by conventional generators such as hydro plants, thermal power plants or nuclear power plants involving synchronous machines. Through their rotating masses they add rotational inertia to the power system which has an important implication on frequency dynamics and system stability [2]. Due to the electro-mechanical coupling between the machine and the grid, the generators rotating mass continuously exchanges kinetic energy with the grid in case of power imbalances between generation and consumption. Following a relevant load/generation event, the system frequency starts to deviate from its nominal value. This initial frequency dynamic is dominated by the inertial response of the rotating machines connected to the grid. The provided kinetic energy released or absorbed by the generators reduces the initial rate of change of frequency (ROCOF) and increases the available response time allowing governor actions to contribute to frequency stabilization [3]. The large scale deployment of converter based generation displacing conventional generators will have a large impact on the system frequency stability. In [4], different impacts on the primary frequency control due to the increased penetration of variable renewable generation have been identified. The lower system inertia is identified as one of those impacts that would increase the requirements for primary frequency control reserves in order to arrest frequency at the same nadir (i.e. lowest frequency reached) following the sudden loss of generation. Also the reduced number of primary frequency control (PFC) reserves has been mentioned in [4] since conventional generators providing PFC are displaced by renewable generation which currently does not provide PFC. As a consequence the ROCOF increases and the nadir decreases [5].

In this study, two different techniques have been implemented and investigated to enhance the frequency dynamics after a power imbalance [6], [7]. Both Virtual Inertia Control (VIC) [8] and Fast Primary Control (FPC) [9] have been implemented and analyzed using the power system simulation software PowerFactory.

The study aims also at highlighting the constraints of the two controllers on a power system with high penetration of converter connected resources and the time delay effect on the proposed droop and consequently on the frequency stability.

The system is studied with different levels of converter driven generation such as photovoltaic (PV): 0%, 27% and 55% of the total load. In the following study the impact of high integration of converter connected resources on the frequency behavior is illustrated and discussed, highlighting the reduced grid inertia impact as well as the reduced primary frequency reserve impact. A sensitivity study for the two controllers considering different time delays is carried out. A comparison between the two controllers effect on the frequency dynamics is also presented.

This paper is divided into five sections: Section II presents the mathematical background and the frequency variation. Section III presents the controllers specifications and the study cases setup. Section IV presents the results of the different scenarios and comparison between VIC and FPC. In section V conclusion and future work are reported.

II. Assessing the frequency variations

Active power imbalance between generation and consumption is reflected instantaneously as a change in the electrical torque output of the generator. This creates a mismatch between

the electrical and mechanical torque resulting in acceleration or deceleration as described by the swing equation in (1) [10]:

$$J\frac{d\omega_m}{dt} = T_a = T_m - T_e \tag{1}$$

T_a is the accelerating torque [Nm],
T_m is the mechanical torque[Nm],
T_e is the electrical torque[Nm].
J is the combined moment of inertia of the generator and the turbine $[kgm^2]$,
ω_m is the angular velocity of the rotor $[rad/s]$.

The combined inertia of the generator and prime mover is accelerated by the imbalance of the applied torques. As a consequence of a frequency deviation, the kinetic energy stored in the rotating mass of the generator will be released. The kinetic energy is expressed as $E_{kin} = \frac{1}{2}J(2\pi f_m)^2$ where f_m is the rotating frequency of the machine. f_m is equal to the electrical frequency f_e for a 2 poles machine (i.e. $f_m = \frac{f_e}{P}$ where P is the pair number of poles).

Rotating generators are characterized by an inertia constant H measured in seconds ($H = \frac{E_{kin}}{S_B}$ where S_B is the rated power of the generator [VA]). It denotes the time duration during which the machine can supply its rated power solely with its stored kinetic energy. Typical values for H are in the range of 2-10 seconds. Following a frequency deviation, kinetic energy stored in the rotating masses of the generator is released, determining slower frequency dynamics and hence, increasing the available response time to take counteractions to an event [3].

Following a power imbalance, the change in the frequency f_e can be described reformulating the swing equation:

$$\dot{E_{kin}} = \frac{2HS_B}{f_e}\dot{f_e} = P_m - P_e \tag{2}$$

P_m is the mechanical power supplied to the generator [W],
P_e is the electric power demand [W].

Since the frequency excursions are usually small deviations around the reference value, it is possible to assume that $f_e = f_0$ where f_0 is the reference frequency.

$$\dot{f_e} = \frac{f_0}{2HS_B}(P_m - P_e) \tag{3}$$

To complete the classical swing equation it is possible to add the frequency-dependent load damping, a self-stabilizing property of the power system due to the presence of frequency dependent loads such as electric motors.

$$\dot{f_e} = -\frac{f_0}{2HS_BD_{load}}f_e + \frac{f_0}{2HS_B}(P_m - P_e) \tag{4}$$

$\dot{f_e}$ is the frequency deviation,
D_{load} is the frequency dependent load damping [p.u.].

Modelling an interconnected power system with n generators, j loads and l lines leads to the aggregated swing equation:

$$\dot{f} = -\frac{f_0}{2HS_BD_{load}}f + \frac{f_0}{2HS_B}(P_m - P_{load} - P_{loss}) \tag{5}$$

$$f = \frac{\sum_{i=1}^{n} H_iS_{Bi}f_i}{\sum_{i=1}^{n} H_iS_{Bi}} \tag{6}$$

$$S_B = \sum_{i=1}^{n} S_{Bi} \tag{7}$$

$$H = \frac{\sum_{i=1}^{n} H_iS_{Bi}}{\sum_{i=1}^{n} S_{Bi}} \tag{8}$$

Where $P_m = \sum_{i=1}^{n} P_{mi}$, $P_{load} = \sum_{i=1}^{j} P_{loadi}$ and $P_{loss} = \sum_{i=1}^{l} P_{lossi}$.

The term f is the center of inertia (COI) grid frequency and can be considered as a definition of "system frequency" [3].
H is the aggregated inertia constant of n generators [s],
S_B is the total rated power of the generators [VA],
P_m is the total mechanical power of the generators [W],
P_{load} is the total system load of the grid [W],
P_{loss} the total transmission losses of l lines which identify the grid topology [W].

The above section has been included to point out the power system aspects influencing the frequency dynamics.

III. Controller Specification and Study Cases

A. Virtual Inertia Controller

In case the active power generation exceeds the active power consumption, the system frequency will rise, resulting in a deviation from the nominal frequency (vice versa in case of an opposite event). The gradient of frequency deviation depends on both, the load/gen step amplitude and the amount of kinetic energy stored and released by the synchronously connected rotating masses after a disturbance. The developed controller attempts to emulate the same effect in connection with an energy storage system. The controller is sensitive to df/dt.

The controller has been implemented in PowerFactory and its block diagram is shown in Fig. 1.

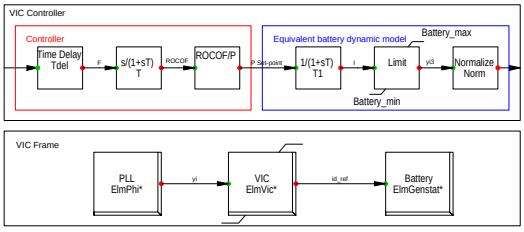

Fig. 1. Virtual Inertia Controller Block Diagram

The controller consists of three main blocks: The phase-locked loop (PLL), the control algorithm and the energy storage. The PLL measures the frequency and the control algorithm calculate the ROCOF and the energy storage active power

set-point. If a variation is detected, the controller sends the power set point according to a particular droop to the energy storage system.
As shown in Fig. 1 the controller is composed by two big rectangles, the red one represents the controller while the blue one represents the battery dynamic model. The controller is composed by:

- A time delay block to represent the digital time delay (e.g. communication delay).
- ROCOF calculation block.
- ROCOF-Power droop represented by a look-up table.

The battery dynamic model is composed by:

- Time constant block.
- Limiter to represent the energy storage limits.
- Normalization block.

The same dead time has been considered for the two controllers (i.e. VIC and FPC).

B. Fast Primary Controller

The primary control reserve aims at containing the frequency fluctuation after a relevant load/generation event within a pre-defined range. The activation is done locally and independently employing a droop control in every participating unit.
The relation between frequency and active power variation can be written as:

$$\Delta P = -R\Delta f \tag{9}$$

R is the system frequency regulation constant, also called frequency droop, given in MW/Hz.

Due to the slow dynamics of prime movers of the generators, the PFC can not contribute with a faster response on the frequency behaviour. A solution could be achieved by using a fast primary control (FPC) employing energy resources without a mechanical delay (e.g. energy storage systems, electric vehicles) [8], [11].

The controller has been implemented in PowerFactory and its block-diagram is shown in Fig. 2. The FPC is composed by the three main blocks as in the VIC. As shown in Fig. 2 the FPC is also composed by two big rectangles, the red one represent the controller while the blue one represent the battery dynamic model which is exactly the same as in the VIC. The controller is composed by:

- A time delay block to represent the digital time delay (e.g. communication delay).
- Frequency-Power droop represented by a look-up table.

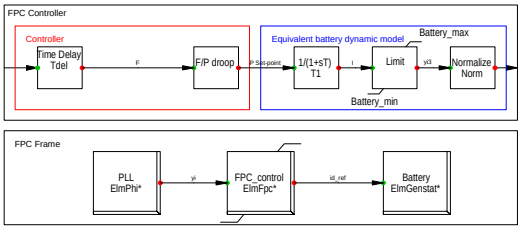

Fig. 2. Fast Primary Controller Block Diagram

C. Network model

The modeled power system is shown in Fig. 3. It contains a constant power load equal to 180 MW and is divided into 60% of asynchronous machines and 40% of static loads as recommended in [10]. Thirteen transformers with rated power 120 MVA and $220/33$ kV rated voltage. Twentyfour transformers with rated power 7 MVA and $33/6.6$ kV rated voltage. Six generators with rated voltage of 33 kV. Table I summarizes the generation units rated power with their relative inertia values. All connected generators operate in Power-Voltage mode where the net active power and the voltage magnitude are specified. PV farm with a rated power of 100 MW is installed. The energy storage system used by the two controllers has a rated power of 1 MW.

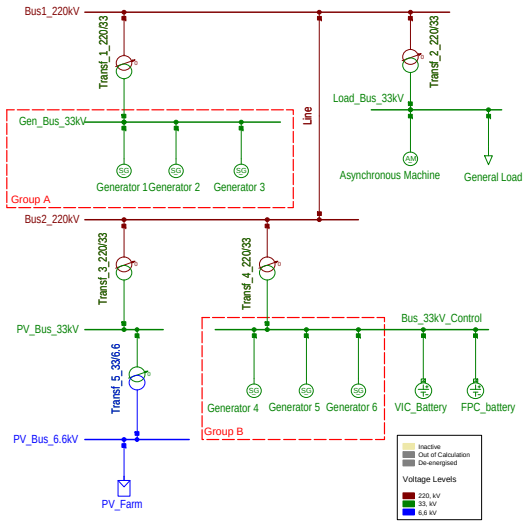

Fig. 3. Power system network

TABLE I
GENERATION DATA

Generation	Rated power	Inertia 2 H(s)
Generator 1	120 MVA	4 s
Generator 2	60 MVA	2 s
Generator 3	60 MVA	2 s
Generator 4	30 MVA	2 s
Generator 5	30 MVA	2 s
Generator 6	3 MVA	2 s
PV	100 MW	-

The system is studied with different levels of PV penetration:

- 0% PV generation of the total load (0 MW).
- 27% PV generation of the total load (50 MW).
- 55% PV generation of the total load (100 MW).

Table II shows the generators set points for the three levels of PV generation. It is assumed that all conventional generators are equipped with IEEE standard models [12]:

- Governor: gov_TGOV2, steam turbine gov. with fast valving.

- Excitation System: avr_IEEET1, 1968 IEEE type 1 excitation system.

Generator 1 is equipped also with a power system stabiliser

- Stabilizer Model: pss_PSS2A, 1992 IEEE type PSS2A dual input signal stabiliser.

TABLE II
GENERATORS SET POINTS

Generation	**0%PV**	**27%PV**	**55%PV**
Generator 1	50 MW	50 MW	50 MW
Generator 2	50 MW	50 MW	disconnected
Generator 3	50 MW	disconnected	disconnected
Generator 4	15 MW	15 MW	15 MW
Generator 5	15 MW	15 MW	15 MW
Generator 6	1.8 MW	1.8 MW	1.8 MW
PV	-	50 MW	100 MW

D. Scenarios

Three different scenarios are analysed. In the three scenarios the system response is triggered by the loss of one of the synchronous generators of group B (i.e. Generator 6) determining around 1% loss of the production related to the total consumption. The loss of 1% of generation is inspired by the ENTSO_E network guidelines [13].

In the following an overview of the three scenarios is presented:

- The first scenario highlights the impact of converter connected resources on frequency dynamics (i.e. ROCOF, frequency nadir and steady state value). The first analysis aims at highlighting the importance of the inertial response as well as the primary frequency reserve provided by conventional machines versus the converter connected resource contribution.
- The second scenario carries out a sensitivity analysis of the dead time for both, VIC and FPC. In this case the PV penetration level is set to 55% of the total load. The considered dead times are 10 ms, 100 ms, 1 s and 2 s.
- The third scenario presents a performance analysis of the FPC versus the VIC on the frequency behaviour. It higlits the effect of the two controllers on the ROCOF, the nadir and the steady state value.

IV. RESULTS

This section is composed by three subsections which present the results of the three scenarios presented and detailed in section III. Subsection IV-A presents the effect of replacement of rotating generators by converter connected resources on the frequency behaviour. Subsection IV-B presents the time delay effect of the two controller on the frequency behaviour in case of high penetration of converter connected resources (i.e. low inertia). And finally, considered the same time delay and the same level level of PV penetration, subsection IV-C presents a performance analysis of FPC and VIC.

A. Scenario 1: Frequency dynamics

The first scenario investigates the frequency behaviour after the loss of a conventional generation unit (i.e. generator 6) with different levels of PV generation replacing conventional generators. The conventional generator is tripped at 0 seconds of the simulation. Three sub-scenarios have been implemented corresponding to the three levels of PV penetration. The frequency behaviour of the three sub-scenarios is shown in Fig. 4. It illustrates how the system frequency behaves after a sudden event when the amount of kinetic energy in the system varies. As already explained in (4), the ROCOF increases due to the lower inertia in the system, determining a larger variation in the frequency (i.e. green curve versus red curve). Due to the lower amount of primary frequency reserves, frequency nadir and steady state values are lower (i.e. green curve versus red curve).

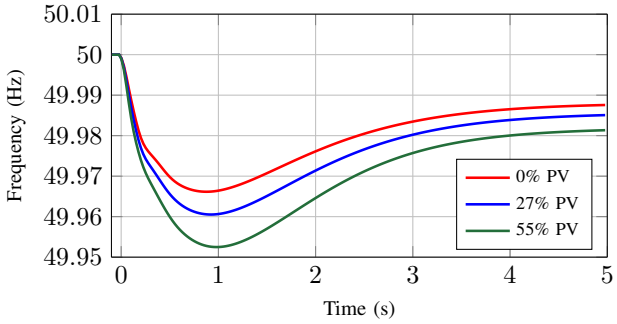

Fig. 4. Frequency behaviour with different levels of PV penetration

B. Scenario 2: Sensitivity analysis of the dead time

This scenario aims to highlight the dead time importance and impact on the two controllers in case of high penetration of converter connected resources. The dead time implemented in this study is a digital time delay which represent the communication delay as well as the required time to activate the energy resource participating in the control (e.g. activation of electric vehicles). The different dead times are 10 ms, 100 ms, 1 s and 2 s. It has been used a different droop for each time delay and each controller. Each droop is chosen as the steepest allowed droop (i.e. less steep droop from the chosen one will imply a lower contribution from the energy storage and steeper droop will create a frequency instability). The simulation results are shown in Fig. 5.

Since the VIC is activated when df/dt $\neq$ 0 reducing the ROCOF, its implementation with relatively large dead time would make it useless. Namely because it does not influence the steady state value and has a limited influence on the frequency nadir. The large dead time reduces also the FPC efficiency but in contrast the FPC is able to increase the steady state value.

Since large voltage variations could influence and distort the analysis, the voltage course during the different simulation is shown in Fig. 6.

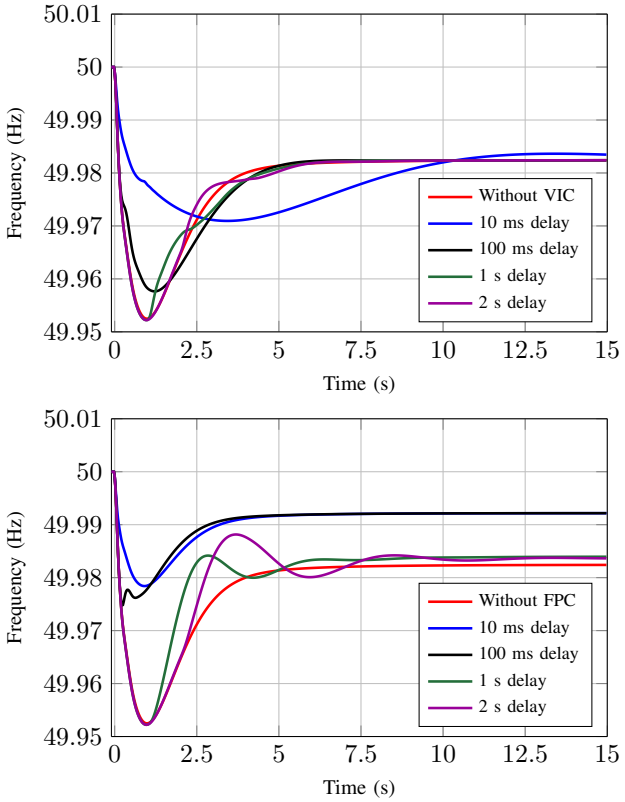

Fig. 5. Frequency behaviour employing VIC and FPC, the curves refer to different dead time

It shows the voltage magnitude employing VIC or FPC at the bus "Bus_33kV_Control", represented respectively by dashed lines and solid lines. It can be seen clearly that the voltage variation during the different simulations is marginal due to the effective control of the automatic voltage regulator (AVR).

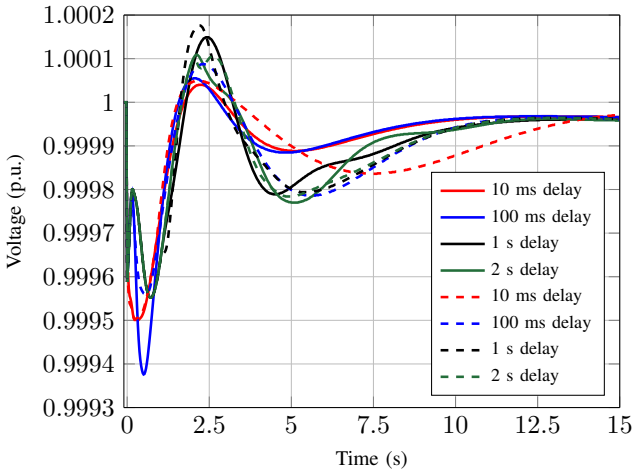

Fig. 6. Voltage behaviour during both VIC and FPC

C. Scenario 3: Performance analysis of FPC and VIC

In the last scenario the same triggering event as the previous cases has been used. A dead time of 100 ms has been considered. The main objective is to compare the two controllers impacts on the system frequency after the loss of a conventional generation unit corresponding to 1% of the total load. The frequency trend and the produced active power from the energy storage are shown in Fig. 7.

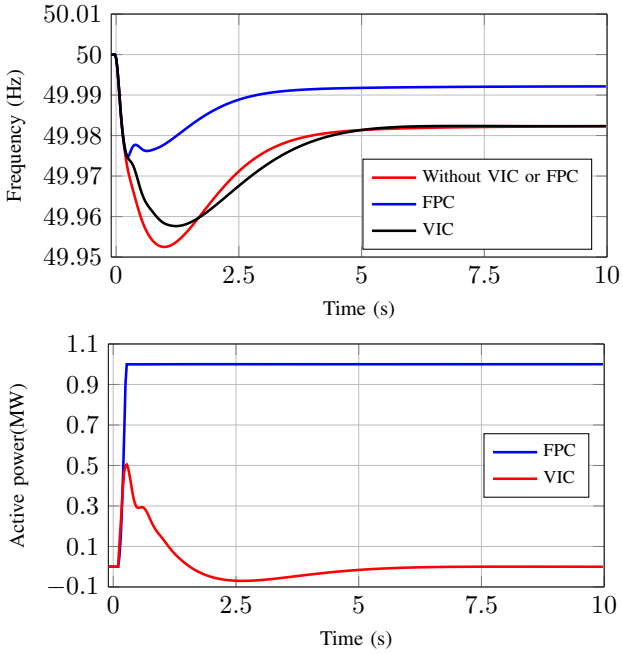

Fig. 7. Frequency behaviour and active power output from the battery during both VIC and FPC

As it can be notice from the active power behaviour of the energy storage, the VIC is participating slightly faster than the FPC during the first 200 ms following the event. Afterwards the FPC limits the frequency fluctuations more than the VIC providing constant power. The provided active power from the VIC has the same behaviour as the kinetic energy produced by synchronous machines. This behaviour could be explained as following: once the maximum instantaneous frequency deviation has been reached, synchronously connected rotating machines begin to accelerate and inertial response changes from positive to negative. The frequency stabilises once mechanical power from the turbine equals to the electrical power from the generator. At that point the inertial response is zero.

Table III shows the average ROCOF during the first 200 ms, the frequency nadir and the steady state value. The overall performance of the two controllers could be summarized as: On one hand VIC has a slower ROCOF compared to FPC and on the other hand lower nadir and steady state values.

As in the second scenario, Fig. 8 shows the voltage magnitude to guaranty the limited voltage deviation between the two controllers.

TABLE III
FREQUENCY CHARACTERISTICS

	ROCOF	Nadir	Steady state
No additional control	0.128 Hz/s	49.953 Hz	49.98 Hz
VIC	0.111 Hz/s	49.965 Hz	49.98 Hz
FPC	0.1220 Hz/s	49.975 Hz	49.99 Hz

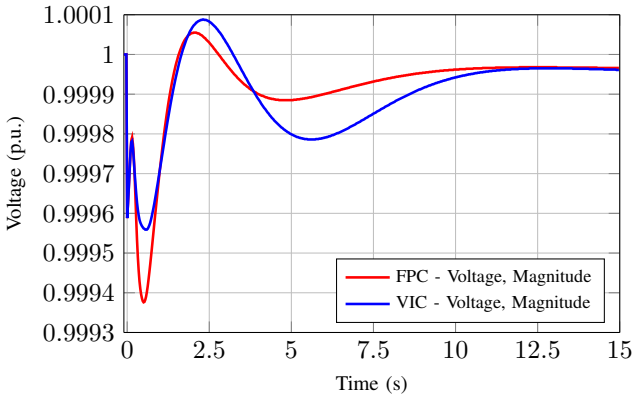

Fig. 8. Voltage behaviour during both VIC and FPC

The simulation results of the three subsections can be summarized as: The replacement of rotating generators with converter connected resources has two main effects on the frequency behaviour, it increases the ROCOF due to the lower inertia in the system and decreases the frequency nadir and steady state value due to the replacement of generators participating in the primary frequency control. Moreover, the sensitivity analysis shows the advantages of FPC compered to VIC and how the controllers parameters influence the frequency stability. In fact the time delay represent a constraint to the droop slope for the two controllers with much higher effect on the VIC.

V. Conclusion and Future work

The analysis showed that the high share of converter connected resources replacing conventional synchronous machines significantly influences the frequency behaviour due to the reduced system inertia and primary frequency reserves. It was shown that the implementation of a VIC or FPC employing an energy resource can enhance the frequency behaviour of the power system. It has been shown that on one hand the VIC limits the ROCOF slightly more than the FPC. On the other hand the FPC has a better performance on the nadir and the steady state values. The study reported the effect of the time delay on the controllers behaviour and frequency stability. The time delay has a worse effect on the VIC compared to the FPC. Therefore, the VIC needs a less sensitive droop in order to avoid instability problems, leading however to minor effectiveness. Further analysis will be carried out to implement a fast primary controller using EVs taking into account the state of charge of the battery which has been neglected in this study. Future work will also consider the implementation of a distributed controller architecture employing smaller units such as electric vehicles for providing either inertia or fast primary control using randomly different time delays. Finally, aggregated response from multiple single-phase units will be assessed in order to evaluate, on standard three-phase systems, consequences on voltage phase unbalances.

Acknowledgment

Michel Rezkalla is Ph.D. student at the Technical University of Denmark (DTU) and is supported by the EU FP7 project ELECTRA (grant: 609687) and the Danish Research Project ELECTRA Top-up (grant: 3594756936313). More information at www.electrairp.eu

References

[1] M. Cheng and Y. Zhu, "The state of the art of wind energy conversion systems and technologies: A review," *Energy Conversion and Management*, vol. 88, pp. 332–347, 2014.

[2] K. Prabha, J. Paserba, V. Ajjarapu, G. Anderson, A. Bose, C. Canizares, N. Hatziargyriou, D. Hill, A. Stankovic, C. Taylor, T. Van Vutsem, and V. Vittal, "Definition and Classification of Power System Stability," *IEEE Transactions on Power Systems*, vol. 21, no. 3, pp. 1387–1401, 2004.

[3] A. Ulbig, T. Borsche, and G. Andersson, *Impact of Low Rotational Inertia on Power System Stability and Operation*. The 19th World Congress of the International Federation of Automatic Control (IFAC14), Cape Town, South Africa, Aug. 2014.

[4] J. H. Eto, "Use of Frequency Response Metrics to Assess the Planning and Operating Requirements for Reliable Integration of Variable Renewable Generation," tech. rep., Lawrence Berkeley National Laboratory, 2011.

[5] P. Tielens and D. van Hertem, "Grid Inertia and Frequency Control in Power Systems with High Penetration of Renewables," in *Young Researchers Symposium in Electrical Power Engineering*, (Delft, The Netherlands), pp. 1–6, 2012.

[6] J. Conroy and R. Watson, "Frequency response capability of full converter wind turbine generators in comparison to conventional generation," *Power Systems, IEEE Transactions on*, vol. 23, pp. 649–656, May 2008.

[7] M. Marinelli, S. Massucco, A. Mansoldo, and M. Norton, "Analysis of inertial response and primary power-frequency control provision by doubly fed induction generator wind turbines in a small power system," in *Proceedings of the 17th Power Systems Computation Conference*, pp. 1–7, August 2011.

[8] G. Delille, B. Francois, and G. Malarange, "Dynamic frequency control support by energy storage to reduce the impact of wind and solar generation on isolated power system's inertia," *Sustainable Energy, IEEE Transactions on*, vol. 3, pp. 931–939, Oct 2012.

[9] E. Vrettos, C. Ziras, and G. Andersson, "Integrating large shares of heterogeneous thermal loads in power system frequency control," in *PowerTech, 2015 IEEE Eindhoven*, pp. 1–6, June 2015.

[10] P. Kundur, *Power System Stability and Control*. McGraw-Hill, 1994.

[11] S. Martinenas, M. Marinelli, P. Andersen, and C. Traholt, "Implementation and demonstration of grid frequency support by v2g enabled electric vehicle," in *Power Engineering Conference (UPEC), 2014 49th International Universities*, pp. 1–6, Sept 2014.

[12] DIgSILENT, "Standard Models in PowerFactory," *User Manual - Appendix D*, pp. 1097–1117, 2015.

[13] Entso-E, "Supporting Document for the Network Code on Load - Frequency Control and Reserves," tech. rep., 2013.

[D] Grid Frequency Support by Single-Phase Electric Vehicles Employing an Innovative Virtual Inertia Controller

Grid Frequency Support by Single-Phase Electric Vehicles Employing an Innovative Virtual Inertia Controller

Michel Rezkalla, Antonio Zecchino, Michael Pertl, Mattia Marinelli
Center for Electric Power and Energy, Department of Electrical Engineering, DTU - Technical University of Denmark
Contact person: Michel Rezkalla (mirez@elektro.dtu.dk)

***Abstract*—The displacement of conventional generation by converter connected resources reduces the available rotational inertia in the power system, which leads to faster frequency dynamics and consequently a less stable frequency behavior. Virtual inertia, employing energy storage systems, could be used to limit the rate of change of frequency of power systems, thus, improving frequency dynamics. Electric vehicles (EVs) can represent a reliable solution to enhance frequency stability due to their fast response and capability to provide a large amount of aggregated power. On one hand, EVs are capable of adjusting the battery charging process (i.e., power flow) according to pre-defined algorithms. On the other hand, in case of islanded operation (i.e., low inertia), some of the EV's technical constraints might cause oscillations. This study presents two control algorithms which show that the EVs are capable of providing virtual inertia support. The first controller employs a traditional droop control, while the second one is equipped with an innovative control algorithm to eliminate likely oscillations. It is shown that, the proposed innovative control algorithm compared to the traditional droop control, assures same effects in terms of frequency but reducing significantly the number of variation of the EV's current set-point.**

***Index Terms*—Electric Vehicle, Virtual Inertia, Grid Inertia, Time Domain Simulation, Converter Connected Resources**

I. Introduction

In conventional power systems, the electricity generation is based on rotating synchronous machines. The grid frequency is maintained within an admissible range all the time to guarantee a secure and stable operation. Following a large disturbance that causes the frequency to significantly deviate from its nominal value, the synchronous generators (SGs) inherently release the kinetic energy stored in their rotating masses, and the SGs that have operating reserve increase their active power via primary and secondary controls [1].

Traditionally, inertial response has not been considered as an ancillary service, but rather as a natural characteristic of the power system. Due to the high integration of converter connected resources, replacing conventional generation, several transmission system operators in different countries began to recognize the value of inertial response by wind power plants [2]–[5].

Different impacts on the primary frequency control due to the increased penetration of renewable energy are presented in [6]. The lower system inertia is one of those impacts that would increase the requirements for primary frequency control reserves in order to arrest frequency at the same nadir (i.e., lowest frequency reached) following the sudden loss of generation.

The growing number of Electric Vehicles (EVs) is typically seen as an additional load on the grid from system operators perspective [7], [8]. However, EVs are also one of the imminent candidates for providing grid regulation services (i.e., frequency and voltage control), since most of the time they are plugged into a charging spost. In principle, they are able to provide fast-regulating power in both directions in case of Vehicle-to-Grid (V2G), or just to modulate the charging power [9]. Nevertheless, EV's technical characteristics arise different challenges such as: the limited energy capacity of each EV, the requested activation time (i.e., the time of full transition response of the active power from the moment of activation of the controller) [10]. The EV's limited energy capacity could be solved by aggregating a large number of EVs, while the time delay issue could be solved employing high quality measurement devices to reduce measurement time and therefore reducing the overall response time.

In this study, the modeled EVs are not equipped with V2G capability. To comply with the IEC 61851 standard, they are capable of modulating the charging current between 6 and 16 A with 1-A steps [11], [12]. This technical constraint might cause the EV's current to oscillate.

This study presents the EV's capability of providing frequency support by employing a virtual inertia controller. Two different controllers are implemented and investigated, virtual inertia controller and virtual inertia controller integrated with a stabilizer algorithm. A comparative analysis between the two controller is conducted. Moreover, a sensitivity analysis is carried out, to emphasise the EV's time delay effect on the frequency stability.

In order to test the EVs capability of providing virtual inertia, an islanded microgrid is modeled. The modeled grid is a reproduction of an islanded configuration of the experimental low voltage grid SYSLAB PowerLabDK research infrastructure, which is located at the DTU Risø campus. Both, controllers and the analysed grid are implemented in the power system

simulation software PowerFactory DIgSILENT.

This paper is divided into four sections: Section II presents the specifications of the two controllers and the analysed scenarios. Section III presents the results of the comparison between the controllers and the time delay influence on the virtual inertia controller. In section IV conclusion and future work are reported.

II. Controller Specification and Study Cases

Virtual inertia in the power system could be emulated if the active power delivered (or absorbed) through the converter of an energy storage system is controlled in inverse proportion to the derivative of the grid frequency (df/dt).

This section presents the specifications of the two controllers, the network model and the different scenarios.

A. Controllers specifications

In this study, two controllers are implemented and investigated, namely virtual inertia controller (VIC) and virtual inertia controller integrated with a stabilizer algorithm (VIC_S). Both controllers use single-phase electric vehicles as an energy source, taking advantages of the installed batteries, by modulating the charging current.

The controllers' participation is provided by a droop control, which represents how much the controllers are sensible to the rate of change of frequency (ROCOF). In this study three different droops have been considered: α (the ROCOF limits are $\pm$ 0.0625 Hz/s), β ($\pm$ 0.125 Hz/s) and γ ($\pm$ 0.1875 Hz/s). The three droops are ROCOF-Current droops and are presented in Fig. 1. The solid lines represent the 1-A steps function required by the IEC 61851 standard [11].

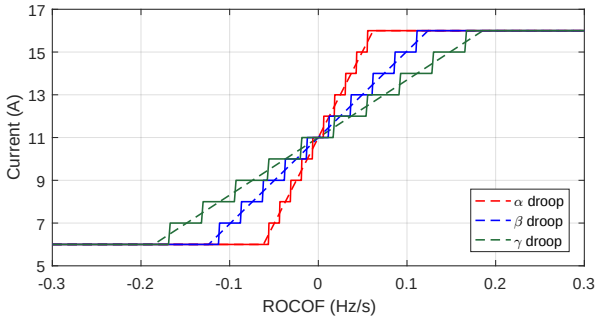

Fig. 1. α, β and γ ROCOF-Current droops: ideal functions (solid lines) and step functions (dashed lines).

The two controllers are implemented in PowerFactory and the block diagram is shown in Fig. 2. It consists of three main blocks as shown in Fig. 2_A: The frequency measurement device, the control algorithm and the EV model. The control algorithm block diagram is presented in Fig. 2_B. The green blocks and arrows are not needed in case of VIC.

1) Virtual Inertia Controller (VIC): The VIC is based on a traditional droop control sensitive to the ROCOF, and no dead-band has been considered. It calculates the ROCOF, and according to a predefined droop, it changes the EV's current set-point.

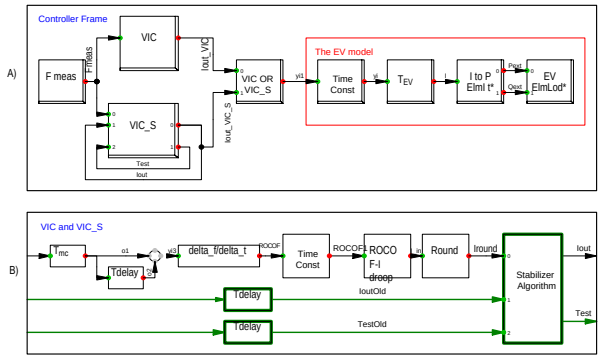

Fig. 2. Controller block diagram. The highlights show the parts added for VIC_S. (A) shows the measurement block, the control algorithm (VIC or VIC_S) and the EV model. (B) shows the control algorithm block diagram.

The VIC controller is composed by:

- A time delay block to represent the digital time delay due to measurement and communication, called T_{mc}.
- A ROCOF calculation block.
- A time constant block as low-pass filter.
- A block with the ROCOF-Current droop.
- A round function block to recreate steps of 1 A.

The EV model used by the two controllers is composed by:

- A time constant block to model the EV battery dynamics.
- A time delay block to represent the delay due to internal EV communication and activation of the inverter, called T_{EV}.
- A block that converts the current to a power signal.
- A load block representing the EV.

2) Virtual Inertia Controller Stabilizer (VIC_S): The VIC_S controller is composed mainly by the VIC integrated with a stabilizing algorithm. The controller block diagram is shown in Fig. 2_B.

As mentioned before, the modeled EVs respect the technical constraint of changing the current set-point only in 1-A steps. To comply with the mentioned limitation, the round block rounds the current set-point calculated as function of the ROCOF. This might cause 1-A oscillations, especially in presence of steep droops, low inertia grid, large response times and high share of EV's power employed as reserve . The reason is, if the calculated current set-point is close to the midpoint between two consecutive set-points, it may be continuously rounded up and down.

For example, if the calculated current is 7.51 A, then the set-point will be 8 A. The same set-point signal is sent to an aggregated number of EVs. The difference between the required 7.51 A and the actual 8 A in all the EVs would cause a significant change in the power flow in terms of total absorbed active power. This will affect the frequency trend, resulting in a new calculated current around 7.49 A, rounded down to 7 A. This process will turn in a loop that determines the 1 A-oscillations.

The aim of the stabilizer algorithm is to avoid 1-A oscillations while allowing larger but less-probable ones (e.g., 2-A

oscillations). This will reduce the overall probability of current oscillations.
The stabilizer algorithm flow-chart is presented in Fig. 3.

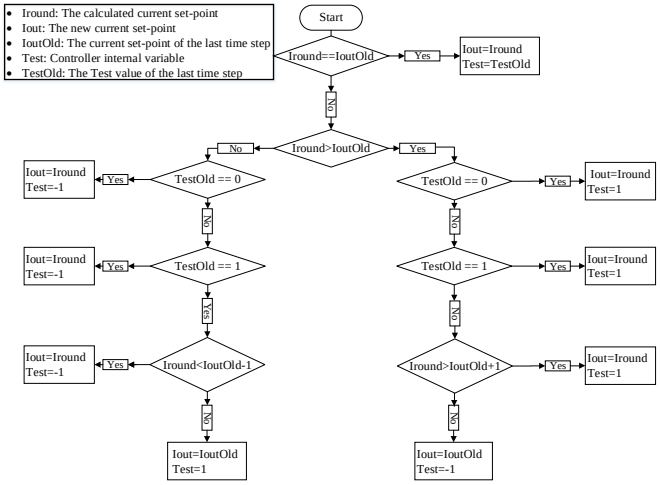

Fig. 3. Stabilizer Algorithm Flow-Chart of the VIC_S

The controller calculates the current set-point *Iout* based on the stabilizer algorithm which evaluates two conditions: The current set-point *Iout* and an internal parameter *Test*.

The first condition is obtained by comparing the new calculated current set-point *Iround* with the one from the previous time step *IoutOld*. The second condition is evaluated through a consideration of a memory status *TestOld*, which is the *Test* from the previous time step. *Test* indicates whether or not, and how, the current set-point is going to change compared to the value of previous time step. It will take the values of -1, 0 or 1. The -1 indicates that, the current set-point has been reduced in the previous time step, 1 that it has been increased, while 0 is utilized for the initialization of the controller.

Since the aim of the controller is to avoid 1-A oscillations, the algorithm prevents 1-A step from one time step to the next one under certain conditions. To do this, the algorithm compares *Iround* with *IoutOld* taking into account the value of *TestOld*. For instance, in case *Iround* is greater than *IoutOld* by 1 A difference, and TestOld is -1 then *Iout* will be kept as *IoutOld*. *Iout* will be changed only when the difference is at least 2 A up or 1 A down.

To give a practical example, if *Iround* is 9 A, *IoutOld* is 8 A and *TestOld* is -1 then the controller prevents the current change. In fact *Iout* will take the same value of *IoutOld* and Test will be kept as *TestOld*. In case *Iround* will increase to 10 A (or decrease to 7 A), then the set-point change will be allowed: *Iout* will be 10 A (or 7 A) and Test will be 1 (or -1).

B. Network model

This study has been carried out by means of root-mean-square (RMS) simulations activities in DIgSILENT PowerFactory software environment.

In order to allow a future practical experimental validation study, the modelled microgrid, has been built considering real available power system components. Specifically, the following devices have been considered for the proposed simulation studies:

- Three controllable EVs, each equipped with single-phase 16 A (230 V) charger and 24 kWh Lithium-ion battery. The charging current can be modulated between 6 and 16 A with steps of 1 A to comply with the technical constraints imposed by the IEC 61851 standard [11]. The EVs initial current set-point is 11 A, the central point, which assures room to increase and decrease the charging level equally.
- A 60 kVA diesel synchronous generator, with active power provision up to 48 kW. It provides inertia to the microgrid. Since designed for operating in microgrid contexts, the inertia of the unit is relatively high, i.e., 2H= 50 s. The diesel's governor is activated to provide primary frequency control.
- A controllable 45 kW (i.e., 15 kW per phase, adjustable with steps of 0.1 kW) resistive load unit.
- A 10 kW Aircon wind turbine equipped with full converter and active stall power control.

The modelled microgrid is composed by two bus-bars connected by a 725 m cable. The diesel generator and the wind turbine are connected at the first bus-bar, while the three EVs and the load are connected at the second one.

C. Scenarios

In order to test the EVs capability of providing virtual inertia support and to evaluate the effectiveness of the two controllers, three scenarios have been analyzed. In the three scenarios, the system response was triggered by changing the load consumption. The total absorbed active power is 19.5 kW, split into 12 kW from the load unit and 7.5 kW from the three EVs (3*2.5 kW). In the first two scenarios, the total absorbed active power is delivered only by the diesel generator. In the third scenario the active power is delivered also by the Aircon wind turbine.

The purpose of the first scenario is to emphasize the time delay effect on the VIC. The load event takes place at zero seconds of the RMS simulation by a 25 % (3 kW) increase of the load consumption. It represents around 15% increase of the total generated active power and around 5% of the diesel rated power. The choice of this large load step has been done to compensate the large inertia. The system has been analysed employing the β droop and applying the following time delays: 2, 3.5 and 5.5 s. The considered time delay represents the total response time of the vehicle and the controllers to the detected frequency deviation (i.e., T_{EV}+T_{mc}).
The 5.5 s is chosen as maximum acceptable time delay in accordance with the experimental results presented in [10]. In [12], the authors claim that most of the times the total time delay is between 2 to 3 s. For this reason, in the following analysis, 2 s is assumed to be the lowest time delay. The 3.5 s is chosen as intermediate value.

The second scenario aims at providing a general evaluation and comparison between VIC and VIC_S in case of contingen-

cies. To better evaluate the two controllers, the system response is analysed employing the three different droops, namely α, β and γ, adapting as time delay 2 s. The same load event was initiated to evaluate the behavior of the controller.

In the third scenario, the Aircon wind turbine is connected to the analysed microgrid. It originates continuous fluctuations of power generation and consequently less stable frequency behaviour. This made it possible to evaluate the efficiency of the two controllers in a more realistic situation, where frequency is always fluctuating. A 10 minutes wind production profile, in terms of active and reactive power, has been considered and reported in Fig. 4.

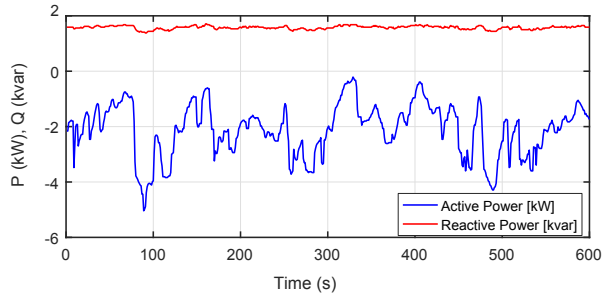

Fig. 4. 10-minutes active and reactive power wind generation profile.

In this case, the load events include load-increase and load-decrease, so that both over and under frequency dynamics can be analysed. Four load events have been applied, by changing the load consumption by 25% of it's rated power as flows, by +25%, -25%, -25% and +25%, respectively at, 0 s, 180 s, 360 s and 540 s.

The third scenario is divided into two study cases, the first study case reports a comparison between the two controllers employing the three droops. The second one reports the improvements and advantages of applying a combined droop in case of VIC_S, specifically combining the α and β droops.

III. Results

This section is composed by three subsections, which present the results of the three scenarios.

A. Scenario 1: Sensitivity analysis of the time delay

The first scenario presents the time delay effect on the controller and consequently on the frequency behaviour. The frequency and the ROCOF trends (signal "ROCOF1" in Fig. 2_B) are presented in Fig. 5_A and Fig. 5_B, respectively.

Fig. 5 shows that the frequency starts to have undesired behaviour by adapting 5.5 s time delay. In fact, Fig. 5_A shows that the frequency has a fast ramping at t=5.5 s, which is an index of likely oscillations. The described behavior might be more perceptible from the ROCOF trend present in Fig. 5_B. It can be seen that the ROCOF arrives to have positive values in case of shortage of generation, in contrary with what described by the swing equation [13], [14] .

One can note that, large time delays lead to a less stable frequency behaviour. An explanation is that the controller

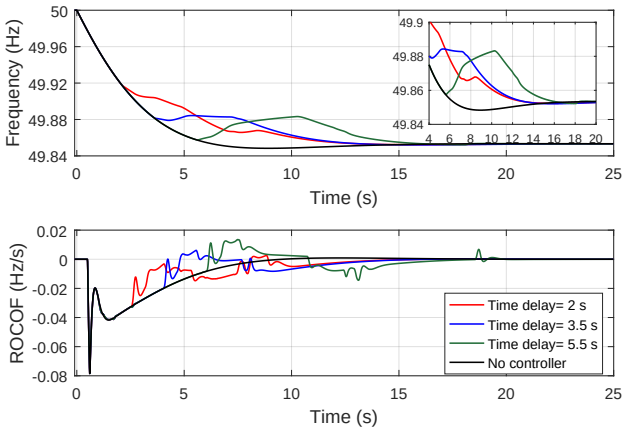

Fig. 5. Sensitivity Analysis, Fig. 5_A reports the frequency trends and Fig. 5_B reports the ROCOF trends.

performance is dependent from three parameters: System inertia, time delay and droop characteristic. The three parameters are strongly connected to each other. In fact, a high grid inertia allows the implementation of a steep droop, and employing a steep droop imposes the use of small time delay.

Since virtual inertia services must be delivered as fast as possible, and considering the results in this scenario, it has been decided to employ time delay of 2 s for Scenario 2 and Scenario 3.

B. Scenario 2: Comparative analysis between VIC and VIC_S

This scenario aims at evaluating the VIC and VIC_S effectiveness on the frequency dynamics, and at comparing the EV's current set-point. The frequency and ROCOF trends are shown in Fig. 6_A and Fig. 6_B, respectively. The VIC is represented with solid lines while VIC_S is represented with dashed lines.

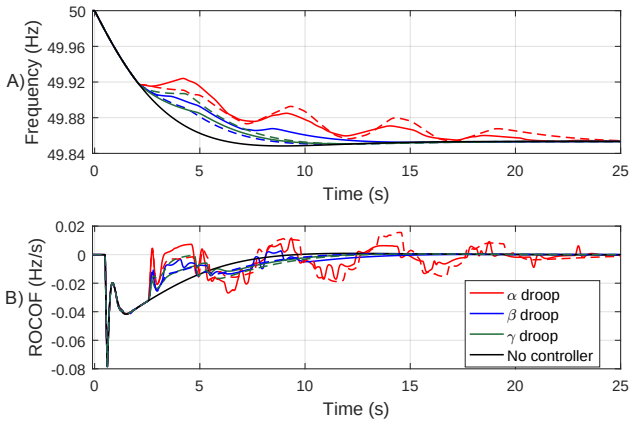

Fig. 6. Frequency and ROCOF trends employing VIC and VIC_S, Fig. 6_A reports the frequency trends and Fig. 6_B reports the ROCOF trends.

As shown in Fig. 6_A, the system frequency oscillates applying the α droop, and that is due to the combination of having a steep droop and relatively long time delay in terms of virtual inertia control (i.e., 2 s). The frequency oscillations

could also be noticed from the ROCOF behavior presented in Fig. 6_B. In fact, also in this case the ROCOF begun to have positive values in the event of shortage of generation.

Due to the high inertia of the analysed grid, the two controllers, namely VIC and VIC_S have a similar effects on the frequency behaviour. On the other hand, from Table I, one can note that the number of switching between the EV's current set-point is substantially reduced by the VIC_S.

TABLE I
NUMBER OF SWITCHINGS

Droop	VIC Nr. Switchings	VIC_S Nr. Switchings
α	48	22
β	14	5
γ	6	3

C. Scenario 3: Performance analysis of VIC and VIC_S

This scenario is composed by two study cases, the first one presents a comparative performance analysis between the two controllers in terms of frequency dynamics and EV's current oscillation. The second study case shows the advantages of applying a combined droop in case of VIC_S. Contrary to the previous scenario, the frequency is fluctuating around 50 Hz due to the wind generation. In the two study cases the system response is triggered by four load events as mentioned in section II-C.

1) Study case 1:) The system is studied by using the three droops. The frequency and the ROCOF trends are presented in Fig. 7_A and Fig. 7_B, respectively. The VIC is represented with solid lines while VIC_S with dashed lines.

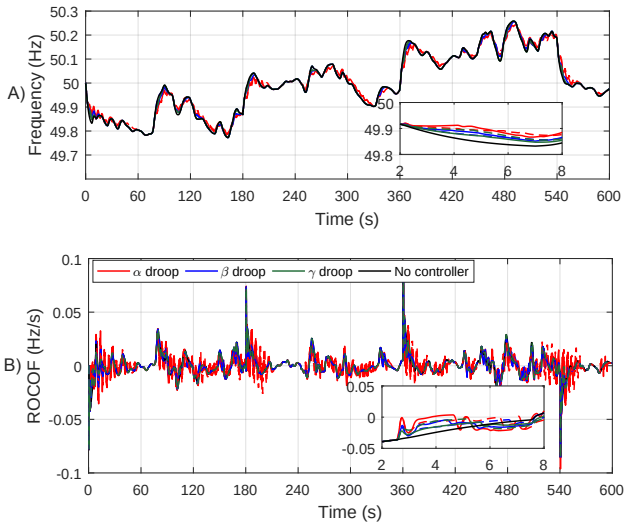

Fig. 7. Frequency and ROCOF trends employing VIC and VIC_S, Fig. 7_A reports the frequency trends and Fig. 7_B reports the ROCOF trends.

Fig. 7 shows the effectiveness of the VIC as well as VIC_S in reducing slightly the ROCOF compared to the non controlled case. It needs to be taken into account that this limited improvement is due the limited number of EVs participating in the control (i.e., three EVs). As explained in scenario 2, due to the high inertia of the modeled microgrid, the two controllers have a similar effects on the frequency behaviour. On the other hand, to highlight the higher performance of VIC_S compared to VIC on the EV's current set-point, the total number of switchings from one set-point to the other is reported in Table II.

TABLE II
NUMBER OF SWITCHINGS

Droop	VIC Nr. Switchings	VIC_S Nr. Switchings
α	528	300
β	120	38
γ	36	14

As deducible from Table II, the VIC_S has reduced significantly the number of switchings operations for the different droops. The number of switchings has been reduced by 43%, 68% and 61% for the α, β and γ droop, respectively. This result is very valuable in the future perspective of integrating EVs for ancillary services (e.g., virtual inertia and frequency support). Since EVs will participate in the ancillary services during the whole charging process, they might be able to provide the same support performance with less degradation of the battery performances.

2) Study case 2: Generally speaking, the controller participation is proportional to the droop steepness. On one hand the controller should always participate with all the available power reserve to reduce the ROCOF. On the other hand, continuous regulation will result in reducing the reserves availability (i.e., the state of charge of the battery will be reduced).

To overcome this issue, it has been decided to impose a combined droop with a deadband. The idea is to avoid the controller participation in case of very small ROCOF by imposing a deadband (i.e., ± 0.01 Hz/s). Exceeded the deadband, to avoid the full participation of the controller, it has been applied a droop with the same slope as the β droop, with a threshold at ± 0.035 Hz/s. To allow a higher participation of the controller in case of large events, exceeded the threshold, a droop with the same slope as the α droop will be applied, the ROCOF limits are ± 0.079 Hz/s. The implemented droop and the frequency behaviour are presented in Fig. 8 and Fig. 9, respectively.

Contrary to the previous scenarios, the results show the very limited participation of the controller. This response presents an advantage in terms of EVs. In fact, since EVs are not dedicated to provide ancillary services, they can not be handled as the traditional reserves. On one hand, they must guarantee a certain state of charge for the end user. On the other hand, they must assure the reserve availability in case of large events. Fig. 9 shows that the controller participates in the regulation very few times, mainly in case of contingencies and thats due to the preselected droop. The desired participation rate could be achieved by combining different droops and/or different deadbands.

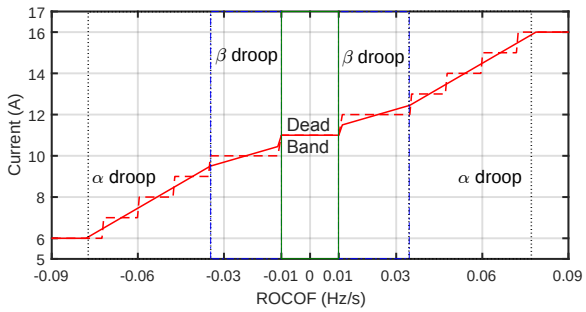

Fig. 8. Combined droop, composed by a deadband and the combination of α and β droop.

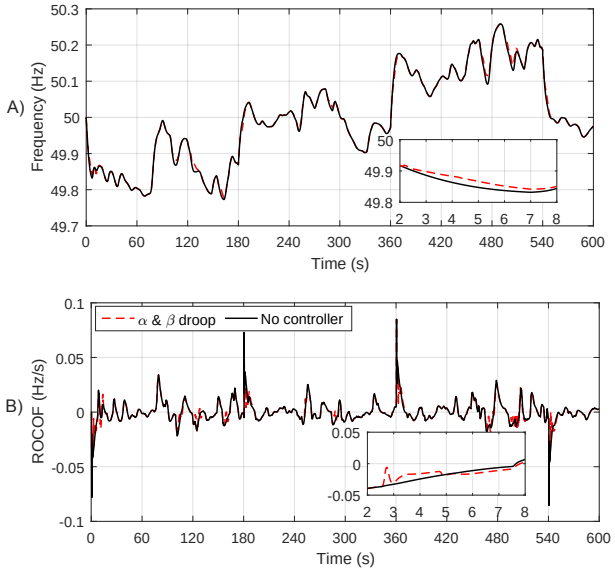

Fig. 9. Frequency and ROCOF trends employing VIC_S with a combined droop, Fig. 9_A reports the frequency trends and Fig. 9_B reports the ROCOF trends.

IV. Conclusion and Future Work

The analysis showed the EVs capability of providing virtual inertia services and the time delay effect on the controller response and consequently on the frequency aspect. It was shown that the implementation of VIC employing EV might causes oscillations on the EVs current set-point. But It has also been demonstrated that the presented stabilizer algorithm was able to reduce the oscillations significantly.

It has been shown, that the controller can be applied, respecting the technical constraints imposed by the IEC 61851 standard, in a realistic situation with continuous frequency fluctuations due to wind generation.

Moreover, a combined droop has been applied in case of VIC_S to limit the controller participation in case of small ROCOF and allow a higher participation in case of large events.

Further analysis will be carried out to test the VIC and VIC_S developed controllers in the experimental facilities SYSLAB-PowerLABDK. Future work will take into account the state of charge of the battery (SOC) in the developed controller to guaranty a certain SOC for the end user. Future work will also focus on modelling the battery considering the combination of the SOC and the implemented droop to represent the possible equivalent inertia of the battery.

Acknowledgment

Michel Rezkalla is Ph.D. student at the Technical University of Denmark (DTU) and is supported by the EU FP7 project ELECTRA (grant: 609687) and the Danish Research Project ELECTRA Top-up (grant: 3594756936313). More information at www.electrairp.eu

References

[1] T. Ackermann, *Wind Power in Power Systems*. John Wiley, 2011.

[2] M. Marinelli, S. Massucco, A. Mansoldo, and M. Norton, "Analysis of Inertial Response and Primary Power-Frequency Control Provision by Doubly Fed Induction Generator Wind Turbines in a Small Power System," in *17th Power Systems Computation Conference*, pp. 1–7, Aug 2011.

[3] P. W. Christensen and G. T. Tarnowski, "Inertia of wind power plants State-of-the-art review," in *The 10th International Workshop on Large-Scale of Wind Power, Aarhus, Denmark*, 2011.

[4] E. Muljadi, V. Gevorgian, and M. Singh, "Understanding Inertial and Frequency Response of Wind Power Plants," in *IEEE Symposium on Power Electronics and Machines in Wind Applications*, pp. 1–8, IEEE Symposium on Power Electronics and Machines in Wind Applications, 2012.

[5] S. Sharma, S. H. Huang, and N. D. R. Sarma, "System inertial frequency response estimation and impact of renewable resources in ERCOT interconnection," *IEEE Power and Energy Society General Meeting*, pp. 1–6, 2011.

[6] J. H. Eto, "Use of Frequency Response Metrics to Assess the Planning and Operating Requirements for Reliable Integration of Variable Renewable Generation," tech. rep., Lawrence Berkeley National Laboratory, 2011.

[7] K. Clement-Nyns, E. Haesen, and J. Driesen, "The impact of charging plug-in hybrid electric vehicles on a residential distribution grid," *IEEE Transactions on Power Systems*, vol. 25, pp. 371–380, Feb 2010.

[8] M. Rezkalla, K. Heussen, M. Marinelli, J. Hu, and H. W. Bindner, "Identification of requirements for distribution management systems in the smart grid context," in *Power Engineering Conference (UPEC), 2015 50th International Universities*, pp. 1–6, Sept 2015.

[9] W. Kempton and J. Tomic, "Vehicle-to-grid power implementation: From stabilizing the grid to supporting large-scale renewable energy," *Journal of Power Sources, J. Power Sources, J Power Sou, J Power Sources*, vol. 144, no. 1, pp. 280–294, 2005.

[10] S. Martinenas, M. Marinelli, P. Andersen, and C. Traholt, "Implementation and demonstration of grid frequency support by v2g enabled electric vehicle," in *Power Engineering Conference (UPEC), 2014 49th International Universities*, pp. 1–6, Sept 2014.

[11] IEC 61851-1:2010, "Electric vehicle conductive charging system Part 1: General requirements," 2010.

[12] M. Marinelli, S. Martinenas, K. Knezović, and P. B. Andersen, "Validating a centralized approach to primary frequency control with series-produced electric vehicles," *J. of Energy Storage*, vol. 7, pp. 63–73, Aug. 2016.

[13] P. Kundur, *Power System Stability and Control*. McGraw-Hill, 1994.

[14] A. Ulbig, T. Borsche, and G. Andersson, *Impact of Low Rotational Inertia on Power System Stability and Operation*. The 19th World Congress of the International Federation of Automatic Control (IFAC14), Cape Town, South Africa, Aug. 2014.

[E] Grid Frequency Support by Single-Phase Electric Vehicles: Fast Primary Control Enhanced by a Stabilizer Algorithm

Grid Frequency Support by Single-Phase Electric Vehicles: Fast Primary Control Enhanced by a Stabilizer Algorithm

Antonio Zecchino, Michel Rezkalla, Mattia Marinelli

Center for Electric Power and Energy, Department of Electrical Engineering, DTU – Technical University of Denmark
Contact person: Antonio Zecchino (antozec@elektro.dtu.dk)

***Abstract*—Electric vehicles are growing in popularity as a zero emission and efficient mode of transport against traditional internal combustion engine-based vehicles. Considerable as flexible distributed energy storage systems, by adjusting the battery charging process they can potentially provide different ancillary services for supporting the power grid. This paper presents modeling and analysis of the benefits of primary frequency regulation by electric vehicles in a microgrid. An innovative control logic algorithm is introduced, with the purpose of curtailing the number of current set-point variations that the battery needs to perform during the regulation process. It is shown that, compared to traditional droop-control approaches, the proposed solution assures same effects in terms of frequency containment, by employing a considerably lower number of variations of battery current set-point. The modeled low voltage microgrid is built to reproduce a real configuration of the experimental facility SYSLAB-PowerLabDK. Root-mean-square simulation studies have been carried out in DIgSILENT PowerFactory environment for the validation of the controller.**

***Index Terms*-- Distributed Energy Resources, Electric Vehicle, Fast Primary Control, Frequency Support.**

I. INTRODUCTION

Traditionally, frequency stability is assured relying on ancillary services provided by conventional large power plants, which nowadays are being replaced by renewable energy sources. This leads to the need of providing such services relying more and more on small aggregated units mostly connected to LV grids. Therefore, aiming at deferring grid reinforcement investments, system-wide ancillary services from distributed energy resources (DERs) need to be provided without violating distribution grids constraints.

Electric vehicles (EVs) can represent a reliable source of such services, since they can boast technical properties suitable for offering flexibility to the grid operators. In fact, they can be considered as distributed energy storage systems with large potential for network regulation [1], [2], and are almost continuously plugged into a LV charging post [3]. Furthermore, they are capable of adjusting the battery charging process according to pre-defined algorithms [4]–[8].

In [9]–[11] it is shown that EVs with or without vehicle-to-grid (V2G) capability can be effective in primary frequency regulation, both in isolated microgrids and larger systems. However, an ideal EV response to the control signals was assumed, in terms of response time and power, while communication and control latencies were neglected. These simplifications may greatly impact the results.

To fill this gap, in the here-presented paper both the EVs and the control/communication procedure are modelled considering appropriate response times and latencies for all the operational steps. EV response characteristics are based on the experimental finding described in [12]. Modeling and analysis of the effects of primary frequency regulation by single-phase EVs without V2G capability in an islanded LV microgrid are presented. Specifically, the work proposes an original controller to reduce the number of EV current set-point variations. The controller prevents undesired unstable situations due to frequency oscillations caused by the 1-Amp granularity for the setting of the charging current, foreseen by IEC61851 [13] and J1772 [14] standards.

For the characterization of the proposed controller, different droop functions are set, and, with the purpose of reproducing the real different behaviors that EVs may have, different response times are considered. In this way, situations of load unbalance among the three phases are introduced. These considerations allowed a further validation of the proposed controller. The implemented control algorithm complies with contemporary standards for limiting the EV charging rate. This means that it can be applied with all currently available EVs complying with [13] and [14]. For the validation of the controller, root-mean-square (RMS) simulations are carried out in DIgSILENT PowerFactory software environment. Both load events to destabilize the system frequency, and a realistic wind generation profile to create continuous frequency deviations are considered. To allow a future practical experimental validation study, the modelled microgrid, is built to reproduce a real configuration of the experimental facility SYSLAB-PowerLabDK.

The paper is structured as follows. Section II presents the modelled microgrid. Primary frequency regulation control by EVs is reported in Section III, together with a detailed description of the proposed innovative controller. Section IV presents the simulation studies: three scenarios are defined, and results are presented and discussed. Conclusions are reported in Section V.

II. MICROGRID LAYOUT

The study has been carried out by means of RMS simulation activities in DIgSILENT PowerFactory software environment. The modelled grid is a reproduction of an islanded configuration of the experimental LV grid SYSLAB-PowerLabDK. SYSLAB-PowerLabDK is a research laboratory facility for development and test of control and communication technology for active and distributed power systems, located at the DTU Risø campus.

In order to allow a future practical experimental validation study, the modelled microgrid, was built considering real available power system components. Specifically, the following units were considered for the proposed simulation studies:

- 3 controllable EVs, each equipped with single-phase 16 A (230 V) charger and 24 kWh Lithium-ion battery. The chargers allow only unidirectional power flows, i.e., not any V2G capability is utilized. The charging current can, however, be modulated between 6 and 16 A with granularity of 1 A [13], [14].
- A 60 kVA diesel synchronous generator, with active power provision up to 48 kW. Since designed for operating in microgrid contexts, the inertia of the unit is rather high (2H = 50 s). To allow the analysis of primary frequency regulation by EVs, the automatic frequency control of the governor of the diesel generator has been disabled.
- A 45 kW (up to 15 kW per phase) resistive load unit with active power independently settable on each phase.
- A 10 kW Aircon wind turbine (nominal wind speed: 11 m/s) with full converter and active stall power control.

As deducible from the highlights in the single line diagram representation of the whole mentioned experimental facility in Fig. 1, a 725 m Aluminum cable line is utilized to connect the two buses which the components are connected to (AC-Resistance at 20 °C and Reactance are respectively 0.313 and 0.077 Ohm/km). Both the synchronous and the wind generators are connected to the same bus, while the resistive load and the EVs are placed on the other terminal of the line.

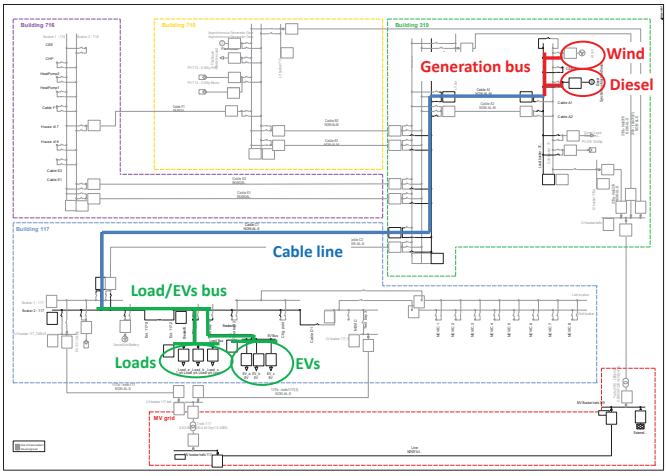

Fig. 1. Single line diagram representation of the whole SYSLAB-PowerLabDK experimental LV grid. Highlighted are the components utilized to compose the microgrid.

III. CONTROLLERS

This Section introduces a first possible approach for primary frequency regulation by EVs. Secondly, it describes the problem of undesired current oscillations. Finally, it presents the innovative logic algorithm to enhance the performances of the controller by preventing the oscillations.

A. FPC controller

By exploiting the high ramping times and precision that EVs can assure for primary frequency regulation [12], the regulation service here presented will be called Fast Primary Control (FPC).

Commonly, primary frequency control is provided by droop controllers, which modulate the synchronous machines' generation according to the power rating. The droop constant k_{droop} represents how much the machine is sensible to frequency changes, and quantifies its contribution to primary frequency/power regulation. The contribution in terms of active power variation ΔP [kW] referred to its nominal power P_n [kW] is correlated to the frequency variation Δf [Hz] referred to the nominal value f_n (50 Hz) by k_{droop}, as in (1).

$$\Delta f/f_n = k_{droop} \cdot \Delta P/P_n \quad (1)$$

In our application, the regulation is provided by EVs (loads), by modulating their power consumption. According to [13] and [14], the charging process is modulated by setting the charging current. Therefore, Equation (1) can be rewritten as in (2), where, for a defined droop, ΔI [A] is the current variation that the EV will assure in case of a certain Δf.

$$\Delta f/f_n = k_{droop} \cdot \Delta I/I_n \quad (2)$$

It is clear that, in order to define the droop value, the nominal current I_n – the correspondent of P_n in (1) – needs to be set. So, as the technical requirements delimit EV's charging current between 6 and 16 A, this available range of regulating current of 10 A has been assumed as the EV's I_n.

For this study, three different proportional f-I droops have been considered: 2% (frequency limits of 49.5 – 50.5 Hz), 4% (49–51 Hz), and 6% (48.5–51.5 Hz). If the frequency exceeds the limits, then the current limit value (6 or 16 A) is set. The three droops are showed in Fig. 2 by the dashed lines.

In order to comply with the aforementioned [13] and [14] standards, the calculated current values need to be rounded. This results in step functions, showed by the solid lines in Fig. 2. To assure room to increase and decrease the charging level equally (±5 A), the EVs' initial current set-point is 11 A, the central point.

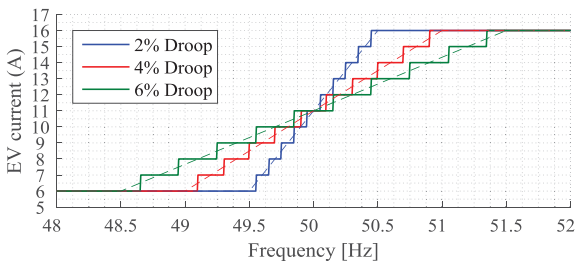

Fig. 2. 2%, 4% and 6% f-I droops: ideal and step functions.

Technically, EVs are largely capable of satisfying the requirements in terms of activation time for participating in the Danish market for primary frequency reserve in both the synchronous regions DK1 and DK2 [12]. In fact, DK1 requires the supply of the first half of the activated reserve within 15 s and the rest within 30 s, while DK2 requires the activation of the full reserve within 150 s. In practice, the participation in the Danish market is hindered by the minimum bid of 0.3 MW. This would correspond to a minimum number of EVs of about 260, considering a ±5 A flexibility per vehicle. Therefore, it is clear that an aggregator is needed to manage such a large number of units.

In this context, with the aim of reproducing a realistic scenario in which more EVs are managed by one single aggregator, the charging process of the three EVs is here managed by the same controller, which relies on a unique frequency measurement device. So, the EVs' inverters receive the same current set-point signal. It is clear that, in an ideal case of perfectly equal response time and inverter performance, the cars would charge exactly in the same way.

The controller's block diagram is shown in Fig 3-a. Basically, it is composed by three main blocks: the frequency measurement device, the control algorithm and the EV model. As explained, the control algorithm in Fig. 3-b receives the frequency measurement and provides the EV current set-point according to a particular f-I droop. To comply with the standards, the 'Round' block rounds the calculated current value. To represent the digital time delay due to measurement and communication, a time delay block is inserted inside the control algorithm block (T_{mc} = 0.5 s). The rounded current signal is sent to the EV model, which is composed by:

- A time constant block to imitate the EV battery dynamics.
- A time delay block to represent the delay due to internal EV communication and activation of the inverter (T_{EV} = 1.5 s).
- A block that converts the current to a power signal, as for RMS simulations in PowerFactory loads need power inputs.
- A load block, i.e., the EV unit in the modelled grid.

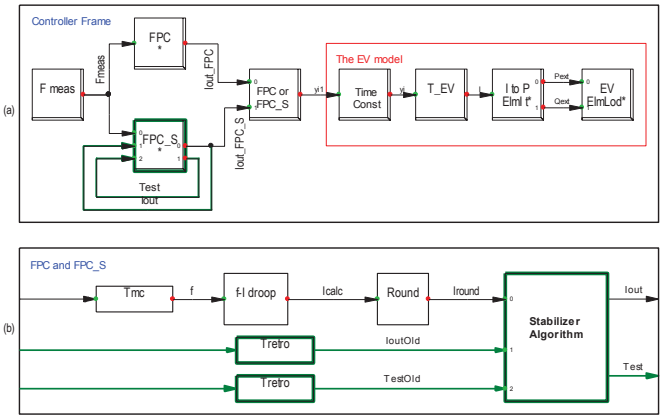

Fig. 3. Controller block diagram. The highlights show the parts added for FPC_S. (a) shows the measurement block, the control algorithm (FPC or FPC_S) and the EV model. (b) shows the control algorithm block diagram.

B. Current oscillations

In occasion of recent frequency regulation experimental and simulation activities in a microgrid using FPC by EVs, the authors have experienced some frequency oscillations [12]. The oscillations are due mainly to the technical requirement of 1-Amp granularity for the setting of the changing current. In fact, the rounding provided by the 'Round' block can cause 1-Amp oscillations, especially in presence of steep droops, low-inertia grid, large response times and high share of EVs power employed as reserve. The reason is the calculated current, which, in case it falls near the exact middle of two consecutive set-points, will be continuously rounded up and down.

For example, if the calculated current is 7.51 A, then the set-point will be 8 A. The same set-point signal is sent to an aggregated number of EVs. The difference between the 7.51 A and the 8 A in all the EVs would cause a significant change in the power flow in terms of total absorbed active power. This will affect the frequency, resulting in a new calculated current of 7.49 A, rounded down to 7 A. This process will turn in a loop that determines the 1-Amp oscillations.

C. Addition of a Stabilizer Algorithm: FPC_S controller

With the aim to avoid the mentioned 1-Amp current oscillations, an innovative controller called FPC_S is implemented. The proposed controller prevents 1-Amp current oscillations, while allows larger and highly less-probable 2-Amp or higher ones. This will reduce the overall probability of current oscillations.

To build the FPC_S controller, in addition to the presented FPC controller, the 'Stabilizer Algorithm' block is inserted. It, as the retroaction arrows, is highlighted in the block diagrams in Fig. 3. Basically, the Stabilizer Algorithm freezes the current set-point if a 1-Amp oscillation is detected. The Stabilizer Algorithm's flow-chart is presented in Fig 4. The controller calculates the current set-point (*Iout*) based on an algorithm which evaluates two conditions: the current set-point and an internal parameter (*Test*). The first condition is obtained by comparing the new calculated set-point (*Iround*) with the one from the previous time step (*IoutOld*). The second condition is evaluated through a consideration of a memory status (*TestOld*), which is the *Test* from the previous time step. *Test* indicates whether or not, and how, the current set-point is going to change compared to the value of the

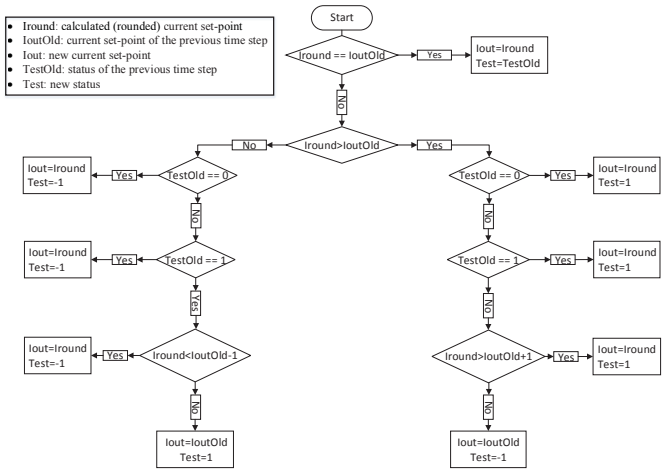

Fig. 4. Stabilizer Algorithm Flow-Chart of the FPC_S.

previous time step. It will take the values of -1, 0 or 1: the -1 indicates that in the previous time step the current set-point has been reduced, the 1 that it has been increased, while 0 is utilized for the initialization of the controller.

Since the aim of the controller is to avoid 1-Amp oscillations, the algorithm prevents 1-Amp steps from one time step to the next one under certain conditions. To do this, the algorithm compares *Iround* with *IoutOld* taking into account the value of *TestOld*. For instance, in case *Iround* is greater than *IoutOld* by 1-A difference, and *TestOld* is -1 then Iout will be kept as *IoutOld*. On the other hand, *Iout* will be changed only when the difference is at least 2 A.

To give a practical example, if *Iround* is 9 A, *IoutOld* is 8 A and *TestOld* is -1 then the controller prevents the current change. In fact *Iout* will take the same value of *Ioutold* and *Test* will be kept as *TestOld*. In case *Iround* will increase to 10 A, then the current change will be allowed: *Iout* will be 10 A and *Test* will be 1.

IV. SIMULATIONS: SCENARIOS' DEFINITION AND RESULTS

In order to evaluate the controller's effectiveness under different operating conditions, three scenarios have been considered and straightaway introduced. The purpose of the first scenario is to provide a general evaluation of the innovative FPC_S controller in case of contingencies taking place during stationary situations. On the other hand, the other two scenarios are characterized by continuous fluctuations of generation from the wind turbine, which now has been considered connected. This made it possible to evaluate the effectiveness of the controllers in a more realistic case, i.e., when continuous actions of the controllers are needed to follow continuous frequency deviations.

For Scenario #1, in the initial situation, the diesel power generation amounts to 19.5 kW, which corresponds to 12 kW of the resistive load (i.e., 4 kW per phase) plus 7.5 kW of the three EVs (i.e., 2.5 kW each, which corresponds to the mentioned initial condition of 11 A). For Scenarios #2 and #3, both load and EVs are kept as in #1, while, instead, the wind turbine is now considered connected.

A. *Scenario #1*

The first scenario aims at evaluating the FPC_S controller, by monitoring the frequency trends in case of balanced load events. The events have been used to destabilize the microgrid frequency, whose deviations will be contained by the FPC_S. The simulations have been carried out for a time slot of 20 minutes, during which, with intervals of 5 minutes, the events took place, as in Table I. The events' size amounts to ±3 kW, which corresponds to ±15.4% of the total generated power and to ±5 % of the rated power of the diesel generator.

TABLE I
LOAD EVENTS FOR DESTABILIZING THE FREQUENCY

Time	Load event
10 s	+ 3 kW
310 s	- 3 kW
610 s	- 3 kW
910 s	+ 3 kW

Comparisons of results with and without the Stabilizer Algorithm have been repeated for each one of the three droops presented in Section III-A, namely 2%, 4% and 6%. In this way, the effectiveness of the proposed controllers in case of different frequency limitations and slopes of the proportional controller has been tested.

Results from Fig. 5 show that, in case of 2% droop, the first and third load events led to undesired frequency fluctuations, due to the mentioned 1-Amp oscillations. It is possible to notice that they are substantially reduced by the FPC_S controller, which drastically reduces the number of switches from one set-point to the other (Fig. 6-a and Table II). An enlargement of the frequency deviations appears since it imposes to wait until the frequency change is big enough to make the set-point change by 2 A at the time. Similar effects are noticeable after the first event in case of 6% droop, with the difference that now not any larger fluctuation is caused.

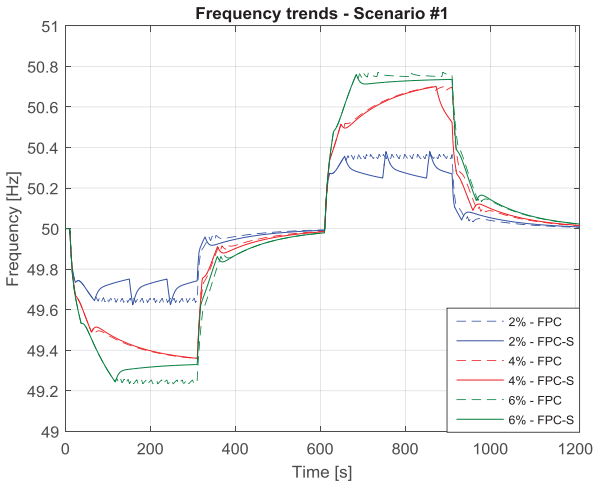

Fig. 5. Frequency trends employing FPC and FPC_S in Scenario #1.

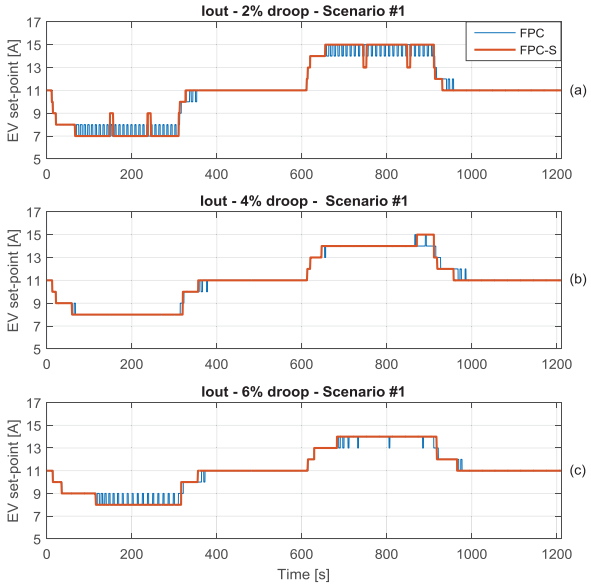

Fig. 6. EV current set-point signals employing FPC and FPC_S in Scenario #1. For 2% droop (a), for 4% droop (b), for 6% droop (c).

As general result for the three cases, it can be concluded that the primary frequency regulation effects are basically the same and potential oscillation conditions are avoided, with an absolute minor number of EV current set-point switching, as deducible from Fig. 6 and Table II.

TABLE II
RESULTS' OVERVIEW FOR SCENARIO #1

Droop	FPC				FPC_S			
	Nr. switchings	f_{max}	f_{min}	f_{mean}	Nr. switchings	f_{max}	f_{min}	f_{mean}
2%	128	50.37	49.64	50.00	22	50.38	49.63	50.00
4%	28	50.70	49.36	50.02	12	50.70	49.36	50.01
6%	62	50.77	49.23	50.01	10	50.76	49.24	50.02

B. *Scenario #2*

Scenario #2 considers a 30-minute wind production profile, in terms of active and reactive power, reported in Fig. 7. This allows an evaluation of the controllers in case of a realistic case, i.e., when continuous actions of the controllers are needed to follow continuous frequency variations.

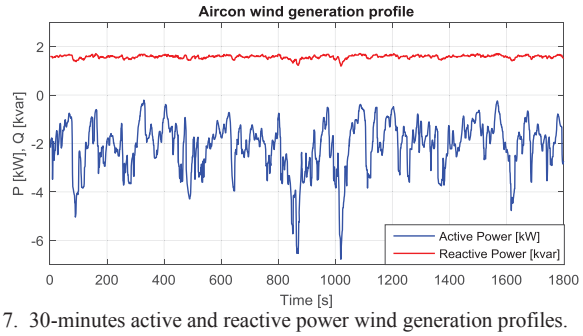

Fig. 7. 30-minutes active and reactive power wind generation profiles.

Fig. 8 shows that, as it was for Scenario #1, for all the considered droops the overall primary frequency containment benefits are not so influenced by the use of the additional Stabilizer Algorithm. A confirmation of this is provided by the numerical results in Table III, in terms of maximum, minimum and mean frequency values. Table III reports also frequency information in case of totally uncontrolled situation, the case presented by the black line in Fig. 11.

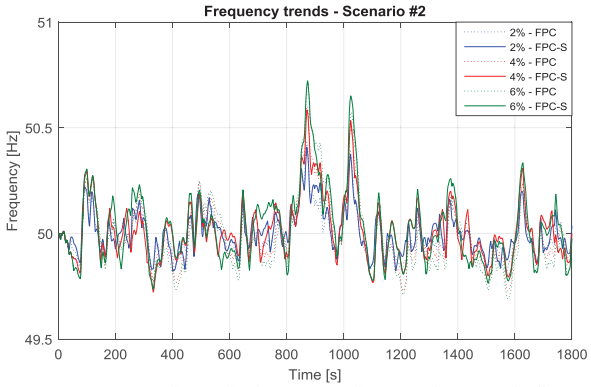

Fig. 8. Frequency trends employing FPC and FPC_S in Scenario #2.

On the other hand, the FPC_S controller provides absolute benefits in terms of EV current set-point adjustments number, as deducible from Fig. 9. In fact, as reported in Table III, for the 2%, 4% and 6% droops, the switch operations have been

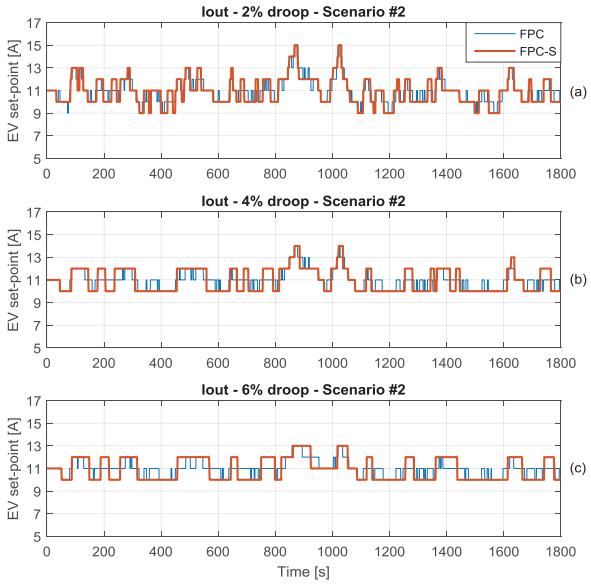

Fig. 9. EV current set-point signals employing FPC and FPC_S in Scenario #2. For 2% droop (a), for 4% droop (b), for 6% droop (c).

reduced by 48% (from 166 to 87), 59% (from 106 to 43) and 67% (from 88 to 29), respectively.

This result is very significant, especially if considered in a future scenario with EVs providing frequency regulation for the whole duration of the charging process. In fact, the FPC_S solution, allows significantly less degradation of the EV battery, assuring same performances in terms of frequency regulation.

Also the phase-neutral voltages at the EVs' connection point are monitored. It has been verified that the FPC_S controller does not influence them significantly.

TABLE III
RESULTS' OVERVIEW FOR SCENARIO #2

Droop	FPC				FPC_S			
	Nr. switchings	f_{max}	f_{min}	f_{mean}	Nr. switchings	f_{max}	f_{min}	f_{mean}
2%	166	50.43	49.82	49.99	87	50.41	49.82	50.00
4%	106	50.60	49.73	49.99	43	50.58	49.72	50.02
6%	88	50.71	49.69	49.99	29	50.72	49.74	50.03
No Contr.	-	51.11	49.34	49.99	-	-	-	-

C. *Scenario #3*

The main purpose of Scenario #3 is analyzing a situation characterized by different response times of the three EVs. In this way it is possible to reproduce the real different behaviors that EVs may have, although simultaneously receiving the same signal. As EVs are connected to different phases, controllers are tested in case of random unbalanced conditions, caused by the unsynchronized set-point variations.

Scenario #3 considers the same 30-minute wind production profile utilized for Scenario #2. However, only the 4% droop is considered. With the purpose of obtaining different EV response times, with reference to the block scheme representation of the EV model (in Fig. 3-a), it has been decided to modify the digital delay-time T_{EV}. For each time-

step of the RMS simulation, T_{EV} has been randomly changed for each EV, with values of 1.5 s, 2 s, 2.5 s or 3 s.

Fig. 10 reports a zoom-in capture of the switching events of the three EVs. It is possible to notice how the three EV set-points are changed in a non-synchronous way. The trends for the whole 30-minutes simulation is not reported, since it appears exactly as in Fig. 9-b (orange line).

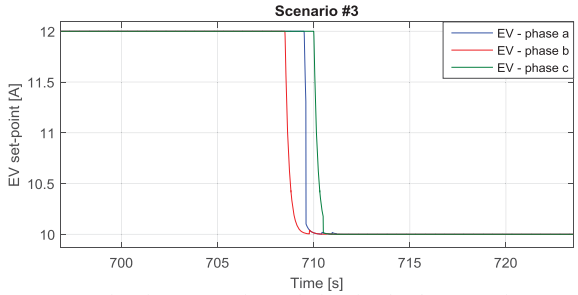

Fig. 10. Zoom-in of one set-point variation for the three EVs in Scenario #3.

As deducible from Fig. 11, the microgrid frequency is not subject to any kind of oscillations. This leads to the conclusion that, although the frequency is regulated by units with different response times that introduce unbalance conditions to the system, the proposed FPC_S controller does not cause any kind of system instability. Results also show that the Voltage Unbalance Factor ($VUF_{\%}$, defined in [15]) is contained below 0.18%. It would increase up to 0.3% in case the diesel generator would have only half of its apparent power or one tenth of its inertia. In any case, the unbalance introduced by the EVs in the microgrid is rather small, considering that the maximum acceptable limit is 2%.

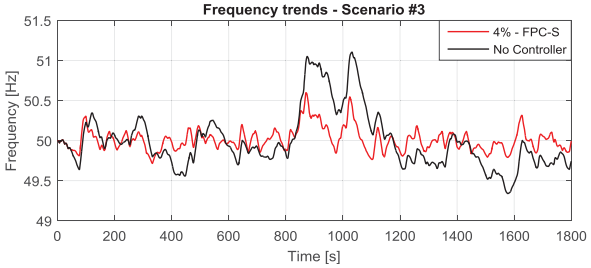

Fig. 11. Frequency trends for Scenario #3 and for uncontrolled case.

V. Conclusions and Future Works

This work presented modeling and analysis of frequency regulation provided by single-phase EVs connected to an islanded LV microgrid. By exploiting the high ramping times and precision that EVs can assure, the analyzed grid service was named Fast Primary Frequency Control (FPC).

The paper proposed an original solution to reduce the number of EV current set-point adjustment actions, which in a microgrid might become extremely high in case of standard droop-based primary frequency regulators. Specifically, the implemented logic prevented the undesired 1-Amp oscillations that the authors had experienced in occasion of previous frequency regulation experimental and simulation activities in a microgrid using FPC by EVs. Therefore, the paper presented a practical solution to the problem that appeared due to the 1-Amp granularity foreseen by the IEC 61851 and SAE J1772 technical standards.

Results showed that the addition of a Stabilizer Algorithm to the controller (now called FPC_S) certainly provided benefits in terms of EV current set-point switchings number, assuring same performances in terms of primary frequency regulation. The FPC_S controller has been further validated: it assured system stability in case of unbalances induced by the unsynchronized responses of the 3 single-phase EVs.

As future works, the innovative controller will be implemented in a real EV charging station at the experimental facility SYSLAB-PowerLabDK. The FPC_S controller will be validated in the same microgrid that has been utilized for the here-presented simulation studies.

References

[1] K. Knezović, M. Marinelli, P. Codani, and Y. Perez, "Distribution Grid Services and Flexibility Provision by Electric Vehicles: a Review of Options," *Proceedings of the 50th International Universities Power Engineering Conference (UPEC) IEEE*. Staffordshire, England, pp. 1–6, 2015.

[2] K. Clement-Nyns, E. Haesen, and J. Driesen, "The impact of vehicle-to-grid on the distribution grid," *Electric Power Systems Research*, vol. 81, no. 1, pp. 185–192, 2011.

[3] N. S. Pearre, W. Kempton, R. L. Guensler, and V. V Elango, "Electric vehicles : How much range is required for a day ' s driving?," *Transportation Research Part C*, vol. 19, no. 6, pp. 1171–1184, 2011.

[4] M. Esmaili and M. Rajabi, "Optimal charging of plug-in electric vehicles observing power grid constraints," *IET Generation, Transmission & Distribution*, vol. 8, no. 4, pp. 583–590, 2014.

[5] C. Gouveia, C. L. Moreira, J. Abel, P. Lopes, and D. Varajão, "Microgrid Service Restoration," *IEEE Industrial Electronics Magazine*, vol. 7, no. 4, pp. 26–41, 2013.

[6] J. Hu, S. Member, S. You, M. Lind, J. Østergaard, and S. Member, "Coordinated Charging of Electric Vehicles for Congestion Prevention in the Distribution Grid," *IEEE Transactions on Smart Grid*, vol. 5, no. 2, pp. 703–711, 2014.

[7] K. Knezović, M. Marinelli, R. J. Møller, P. B. Andersen, C. Træholt, and F. Sossan, "Analysis of Voltage Support by Electric Vehicles and Photovoltaic in a Real Danish Low Voltage Network," *Proceedings of the 49th International Universities Power Engineering Conference (UPEC) IEEE*. Cluj-Napoca, Romania, pp. 1–6, 2014.

[8] A. S. Masoum, S. Deilami, P. S. Moses, M. A. S. Masoum, and A. Abu-Siada, "Smart load management of plug-in electric vehicles in distribution and residential networks with charging stations for peak shaving and loss minimisation considering voltage regulation," *IET Generation, Transmission & Distribution*, vol. 5, no. 8, pp. 877–888, 2011.

[9] P. M. R. Almeida, F. J. Soares, and J. A. P. Lopes, "Electric vehicles contribution for frequency control with inertial emulation," *Electric Power Systems Research*, vol. 127, pp. 141–150, 2015.

[10] S. Izadkhast, P. Garcia-Gonzalez, and P. Frias, "An Aggregate Model of Plug-In Electric Vehicles for Primary Frequency Control," *IEEE Transactions on Power Systems*, vol. 30, no. 3, pp. 1475–1482, 2015.

[11] J. Meng, Y. Mu, H. Jia, J. Wu, X. Yu, and B. Qu, "Dynamic frequency response from electric vehicles considering travelling behavior in the Great Britain power system," *Applied Energy*, vol. 162, pp. 966–979, 2016.

[12] M. Marinelli, S. Martinenas, K. Knezović, and P. B. Andersen, "Validating a centralized approach to primary frequency control with series-produced electric vehicles," *Journal of Energy Storage*, vol. 7, pp. 63-73, 2016.

[13] IEC 61851-1:2010, "Electric vehicle conductive charging system – Part 1: General requirements." 2010.

[14] SAE J1772:2010, "Electric vehicle and plug in hybrid electric vehicle conductive charge coupler." 2010.

[15] P. Pillay and M. Manyage, "Definitions of voltage unbalance," *IEEE Power Engineering Review*, vol. 22, no. 11, pp. 49–50, 2002.

[F] Comparison Between Synthetic Inertia and Fast Frequency Containment Control Based on Single Phase EVs in a Microgrid

Comparison between Synthetic Inertia and Fast Frequency Containment Control Based on Single Phase EVs in a Microgrid

Michel Rezkalla[a], Antonio Zecchino[a], Sergejus Martinenas[a], Alexander M. Prostejovsky[a], Mattia Marinelli[a,*]

[a] *Center for Electric Power and Energy, Department of Electrical Engineering, Technical University of Denmark*

Abstract

The increasing share of distributed and inertia-less resources entails an upsurge in balancing and system stabilisation services. In particular, the displacement of conventional generation reduces the available rotational inertia in the power system, leading to high interest in synthetic inertia solutions. The objective of this paper is twofold: firstly, it aims at implementing and validating fast frequency control and synthetic (virtual) inertia control, employing single phase electric vehicles as flexibility resources. Secondly, it proposes a trade-off analysis between the two controllers. The interdependency between frequency containment and synthetic inertia control on the transient frequency variation is analytically showed. Capabilities and limits of series produced EVs in providing such services are investigated, first on a simulation based approach and subsequently by using real hardware. Results show that fast frequency control can improve the transient frequency behaviour. However, both on simulation and experimental level the implementation of synthetic inertia control is more challenging. In fact, due its derivative nature and the system dynamics, its performance is limited. Furthermore, the crucial importance of the EVs' response time for both controllers is highlighted.

Keywords: Electric vehicles, Experimental validation, Frequency containment control, Frequency stability, Synthetic inertia.

*Corresponding author
Email address: matm@elektro.dtu.dk (Mattia Marinelli)

Nomenclature

$\bar{T}_D$	Frequency dependent loads
$\bar{T}_{FCC}$	Electric torque of devices participating in FCC
$\bar{T}_{SIC}$	Electric torque of devices participating in SIC
δ	Electrical rotor angle
δ_0	Rotor angle at t=0
ω_e	Angular velocity of the electrical rotor
ω_m	angular velocity
ω_{0m}	Rated angular velocity
f	Frequency
H	Kinetic energy in Watt-per-seconds at rated speed
I	EV absorbed Current
J	Moment of inertia
K_D	Load damping factor
K_{FCC}	FCC proportional control coefficient
K_{SIC}	SIC proportional control coefficient
P	EV absorbed active power
p	Number of pole pairs
S_b	Generator's rated power

t	time
T_a	Acceleration or deceleration torque
T_e	Electrical torque
T_m	Mechanical torque

1. Introduction

The rising share of inverter-coupled distributed energy resources (DER) raises new challenges in maintaining stable grid operation. One of the main issues is the reduction of the system inertia due to the replacement of rotating generators by converter-connected resources as well as the expansion of high-voltage direct current (HVDC) connections, decoupling the inertial response between the interconnected areas [1]. Thus, the system's ability to withstand frequency changes by releasing or absorbing the energy stored in the rotating masses is notably reduced, leading to faster frequency dynamics [2]. Moreover, high volatility of renewable energy sources (RES) contributes to the frequency stability issue by changing the grid inertia over the time and increasing the need for better planning due to the higher uncertainty.

The inertia is the parameter that represents the capability of rotating machines (including loads, when applicable) to store and inject their kinetic energy to the system [3]. The amount of inertia influences the frequency gradient, generally addressed as rate of change of frequency (RoCoF), and the transient frequency values during a system incident. The RoCoF and the transient frequency values have a fundamental role in maintaining and operating the power system in secure state. A large RoCoF and/or transient frequency deviations can lead to automatic trip of conventional generators and DER units [4], since those are connected to the grid by means of RoCoF or frequency relays [3]. The RoCoF relay limit is established by the grid code, which varies among countries.

Several transmission system operators (TSOs) started to address the challenge, recognising the potential value of the inertial response of wind power plants, synchronous condensers, and synthetic inertia [5, 6]. One of the main concerns of TSOs is the RoCoF, which might lead to a cascade tripping of conventional and DER units connected by means of RoCoF relays [4, 7]. According to [8], an RoCoF relay has a typical delay in the range of 50 ms to 500 ms.

Further, the growing number of electric vehicles (EVs) concerns distribution system operators (DSOs). The uncertainty of EV driving patterns, high penetration levels and charging in the distribution network could result in new system peaks and negative distribution system impacts, exceeding the load capacities of distribution lines and transformers [9, 10].

The effects of EVs on future power systems are investigated in several studies as in [11, 12]. In [11], the negative effects of uncoordinated charging of EVs on the power system was addressed. The authors presented the impacts that EV charging can have in an actual working wholesale electricity market. In [12] it was analysed how a large scale implementation of plug-in hybrid electric vehicles and full electric vehicles would influence the power system. It shows that smart management of EVs bidirectional charging can alleviate peak power demand.

On the other hand, unscheduled high penetration of EVs may have detrimental effects on power system performance. Reliability and stability are the most aspects of grid that face challenges when EVs used widely. As a result there is an exigent need to predict the EVs' customers in order to avoid irreparable effects, especially for the distribution network. Different studies investigate those challenges as in [13, 14]. In [13] the authors propose a simultaneous approach for allocation of EV parking lots and DRRs in power distribution network to achieve a more reliable supply of the load demand. In [14] a probabilistic modelling of EVs' charging demand is presented.

A noticeable amount of research is focusing on the transition from the traditional system, where frequency is controlled by a small set of large generating units, to the future one where it is controlled by a vast amount of small distributed resources [15, 16].

As EVs are essentially battery storages with a seconds-range response time, the TSO

can greatly benefit from EV participation in frequency service provision. As analysed in [17] EV participation in the ancillary service market appears to be one of the most promising applications as it can offer substantial earnings to EV aggregators and EV owners. Ref. [18] concluded that V2G capable EVs can provide great benefits to the ancillary service market, but battery degradation may represent a challenge for the viability [19, 20].

EVs are able to provide fast regulating power bidirectionally using Vehicle-to-Grid or just to modulate the charging power unidirectionally [21, 22]. In this context EVs can play a fundamental role in the future ancillary service market. In [23] the potential benefits of exploiting the V2G capability for ancillary services was introduced but the study did not investigate the uni-direction EVs charging in providing such services.

Due to the reduced system inertia, various studies show the techno-economic benefits and challenges of primary frequency provision from EVs as in [24–26]. In [24] the authors present the impact of declining system inertia on the primary frequency control (PFC) and future requirements. It also presents the impact of PFC provision from EVs on the system frequency performance. In [25] the authors present the general ability of EV fleets to utilize fluctuating renewable energy sources for charging and their effects on the power system. The authors in [26] summarise the challenges to control a system with low inertia. In the actual study, unlike in [11, 12, 23], EVs have been controlled by only modulating the charging current between 6 and 16A with steps of 1 A to comply with the technical constraints imposed by the IEC 61851 standard [27, 28].

Simultaneously, very few literature investigated the EVs ability in providing synthetic inertia services. In [29] the authors presented a single-phase virtual synchronous machine (VSM) and its possible application for providing V2G services from EVs' batteries, the work was supported by experimental setup based on the Opal-RT platform. On the contrary, this paper presents a different approach in providing synthetic inertia services supported by an experimental investigation using series produced EVs.

The scope of this study is twofold: Firstly, the EVs capabilities as flexibility resources are investigated. In particular, the study looks at synthetic inertia control (SIC) and frequency containment control (FCC) as exemplary services. Secondly, it analyses and evaluates the

pros and cons of SIC and FCC on the frequency dynamics (e.g. RoCoF and frequency nadir and zenith). The general objective is to determine if SIC and FCC delivered by converter connected resources, which are relatively fast compared to conventional units, can replace or at least reduce the need for conventional inertial response.

Ultimately, the research question the study is tackling is: *given the trend of decreasing system inertia, can fast frequency containment compensate or replace the need for synthetic inertia?*

The method and the results presented in this study are part of the EU-funded project ELECTRA IRP, which proposes novel frequency and voltage control concepts to maintain and operate the power system in a secure state [30]. It considers the grid inertia (i.e. the synchronous and synthetic inertia) as an active part of the frequency control process and addressed as inertia response power control (IRPC). In this study the synthetic inertia is considered an active part of the IRPC process.

This paper is divided into 5 sections: Section 2 presents the frequency control in Europe and the analytical interdependency between frequency containment and synthetic inertia. Section 3 presents the frequency containment and the synthetic inertia controllers, along with the experimental layout. Simulations and experimental results are shown and discussed in section 4. Lastly, section 5 presents the conclusions and outlines future research points.

2. Frequency Control in Europe and Analytical Formulation

This section presents a summary of the current framework for frequency control in Europe and an overview of synthetic inertia and frequency assessment.

2.1. Framework for Frequency Control in Europe

Based on the network code defined by the European Network of Transmission System Operators for Electricity (ENTSO-E), frequency control is divided into three phases: (i)Primary frequency control, (ii)Secondary power-frequency control and (iii)Tertiary control. ENTSO-E refers to the reserves for frequency control as operating reserves, and specifically, indicates

the above mentioned controls respectively as: (i)Frequency Containment Reserves (FCR), (ii)Frequency Restoration Reserves (FRR) and (iii)Replacement Reserves (RR).

The Frequency containment stabilises the frequency, after a disturbance, at a steady-state value within the permissible maximum steady-state frequency deviation. That is done by a joint action of FCR within the synchronous area [31]. The frequency restoration process controls the frequency towards its set-point value by activation of FRR and replaces the activated FCR. The reserve replacement process replaces the activated FRR and/or supports the FRR activation by activation of RR. One can notice that the inertial response is considered as natural characteristic of the power system.

2.2. Analytical Interdependency Between Frequency Containment and Synthetic Inertia

According to IEEE/CIGRE task force, frequency stability is the ability of the power system to maintain steady state frequency, following a severe system upset, resulting in a significant imbalance between generation and load [32]. Frequency stability depends on the system ability to restore the equilibrium between generation and load demand.

During any disturbance causing imbalance between the torques acting on the rotor (i.e. active power imbalance between generation and consumption), the net torque causing acceleration or deceleration is $T_a = T_m - T_e$, where T_m is the mechanical torque applied on the rotor, T_e is the electrical torque on the rotor. The simplest model of electro-mechanical swings in a power system is based on the so called swing equation:

$$T_a = T_m - T_e = J\frac{d\omega_m}{dt} \tag{1}$$

J is the combined moment of inertia of the generator and the turbine (kgm^2), and ω_m is the angular velocity of the rotor (rad/s).

Following an imbalance between the torques (i.e. imbalance between generation and demand), the kinetic energy stored in the rotating masses of the generator and the prime mover is released. The kinetic energy at rated speed is expressed as $E_{kin} = \frac{1}{2}J\omega_{0m}^2$, where ω_{0m} is the rated angular velocity [33]. Normalising the previous equation in terms of the rated power of the generator S_b, the inertia constant H can be defined as the kinetic energy

in Watt-per-seconds at rated speed:

$$H = \frac{J\omega_{0m}^2}{2S_b} \qquad \Longrightarrow \qquad J = \frac{2HS_b}{\omega_{0m}^2} \tag{2}$$

Equation (1) can be reformulated as:

$$\frac{T_m - T_e}{S_b/\omega_{0m}} = 2H\frac{\mathrm{d}}{\mathrm{d}t}(\frac{\omega_m}{\omega_{0m}}) \tag{3}$$

Since S_B/ω_{0m} is the base torque T_{base}, the (3) can be expressed in p.u. as:

$$\bar{T}_m - \bar{T}_e = 2H\frac{\mathrm{d}\bar{\omega}_r}{\mathrm{d}t} \tag{4}$$

$$\bar{\omega}_r = \frac{\omega_m}{\omega_{0m}} = \frac{\omega_e/p}{\omega_0/p} = \frac{\omega_e}{\omega_0} \tag{5}$$

Where ω_e is the angular velocity of the electrical rotor, ω_0 is the rated one and p is the number of pole pairs.

The previous equations can be reformulated in terms of the electrical rotor angle. Assuming δ as the electrical rotor angle with respect to a synchronously rotating reference and δ_0 is the rotor angle at t=0, δ can be formulated as:

$$\delta = \omega_e t - \omega_0 t + \delta_0 \tag{6}$$

Therefore, the first and second derivative of (6) are:

$$\frac{\mathrm{d}\delta}{\mathrm{d}t} = \omega_e - \omega_0 = \Delta\omega_e \tag{7}$$

$$\frac{\mathrm{d}^2\delta}{\mathrm{d}t^2} = \frac{\mathrm{d}\omega_e}{\mathrm{d}t} = \omega_0\frac{\mathrm{d}\bar{\omega}_r}{\mathrm{d}t} \tag{8}$$

Equation(1) can be reformulated in terms of the rotor angle:

$$\bar{T}_m - \bar{T}_e = \frac{2H}{\omega_0}\frac{\mathrm{d}^2\delta}{\mathrm{d}t^2} \tag{9}$$

Reformulating (9) in terms of $\bar{\omega}_e$:

$$\bar{T}_m - \bar{T}_e = 2H\frac{\mathrm{d}\bar{\omega}_e}{\mathrm{d}t} \tag{10}$$

Assuming $\bar{T}_m$ is constant and that the frequency regulation is only from the load side, one can assume $\bar{T}_e$ composed by: The frequency dependent loads ($\bar{T}_D$), devices participating in FCC ($\bar{T}_{FCC}$) and devices participating in SIC ($\bar{T}_{SIC}$):

$$\bar{T}_e = \bar{T}_D + \bar{T}_{FCC} + \bar{T}_{SIC} \tag{11}$$

Where each is composed by a base value and frequency dependent value:

$$\bar{T}_D = \bar{T}_{D_0} + K_D \Delta\bar{\omega}_e \tag{12}$$

$$\bar{T}_{FCC} = \bar{T}_{FCC_0} + K_{FCC} \Delta\bar{\omega}_e \tag{13}$$

$$\bar{T}_{SIC} = \bar{T}_{SIC_0} + K_{SIC} \frac{\mathrm{d}\bar{\omega}_e}{\mathrm{d}t} \tag{14}$$

$\bar{T}_{D_0}$, $\bar{T}_{FCC_0}$ and $\bar{T}_{SIC_0}$ represent the base electric torques in steady state and addressed further as $\bar{T}_{e_0} = \bar{T}_{D_0} + \bar{T}_{FCC_0} + \bar{T}_{SIC_0}$. K_D is a damping factor in pu, it considers the electrical loads which change the active power consumption due to frequency changes. $K_{FCC} = K_{FCC}(t-t0)$ is the FCC proportional control coefficient. $K_{SIC} = K_{SIC}(t - t0)$ is the SIC proportional control coefficient. K_{FCC} and K_{SIC} are represented in function of the time to represent the time required from those devices to get activated (i.e. time delay). Therefore, the swing equation can be formulated as:

$$\bar{T}_m - \bar{T}_{e_0} = (2H + K_{SIC}) \frac{\mathrm{d}\bar{\omega}_e}{\mathrm{d}t} + (K_D + K_{FCC}) \Delta\bar{\omega}_e \tag{15}$$

Equation (15) can be expressed in function of $\frac{\mathrm{d}\bar{\omega}_e}{\mathrm{d}t}$ and $\Delta\bar{\omega}_e$:

$$\frac{\mathrm{d}\bar{\omega}_e}{\mathrm{d}t} = \frac{\bar{T}_m - \bar{T}_{e_0} - (K_D + K_{FCC}) \Delta\bar{\omega}_e}{2H + K_{SIC}} \tag{16}$$

$$\Delta\bar{\omega}_e = \frac{\bar{T}_m - \bar{T}_{e_0} - (2H + K_{SIC}) \frac{\mathrm{d}\bar{\omega}_e}{\mathrm{d}t}}{K_D + K_{FCC}} \tag{17}$$

From (16) one can notice that FCC and SIC can affect the RoCoF variation during transient. While (17) shows that the frequency deviation from steady state can be affected by introducing SIC and FCC. In this regard, the following investigation aims at assessing the effects of the two controllers on frequency and RoCoF, by means of simulations and experimental validation.

3. Methodology

In this section the mathematical formulation and characteristic of the implemented controllers as well as the experimental layout is presented.

3.1. Frequency Containment Control

The frequency containment control (FCC) is achieved by a joint action of FCC providing units within the whole synchronous area with respect to the frequency deviation. Generally, it is achieved using droop controllers, so that governors operating in parallel can share the load variation according to their rated power. The droop of the generator represents the ratio of frequency deviation to change in power output. The frequency variation, Δf, referred to the nominal frequency of the system is given as a function of the relative power change ΔP or current change ΔI reported to the nominal machine power or current respectively.

$$\text{a)}\frac{1}{K_{FCC}} = \frac{\Delta f/f_{nom}}{\Delta P/P_{nom}}; \quad \text{b)}\frac{1}{K_{FCC}} = \frac{\Delta f/f_{nom}}{\Delta I/I_{nom}} \tag{18}$$

For example, a 5% droop ($\frac{1}{K_{FCC}}$) means that a 5% frequency deviation causes 100% change in valve position or power output.

In this study the EVs are used to provide frequency support in terms of FCC by modulating the EVs' charging current. Defining a droop value for loads may not be straightforward since the nominal power can not be always determined unequivocally. To comply with the IEC 61851 standard, the EVs' charging current can be modulated with granularity of 1 A and in this case between 6 and 16 A. This available range of regulating current of 10 A has been assumed as the EV's I_{nom} [34]. The EVs charging is controlled by charging controller with a 8% frequency-current droop with frequency limits of $48 - 52$ Hz.

The droop is presented in Figure 1-a, where the dash line represents the ideal droop and the solid line represents the real droop with 1 A granularity. In order to have an up and down regulation capability of ± 5 A, the EVs' initial current set-point is set at 11 A. Due to the 1 A granularity and the established operating point, the EVs' current set-point was oscillating between 11 and 12 A. To avoid this oscillation the droop characteristic was shifted, so that the frequency limits became $48.2 - 52.2$ Hz. The control diagram for FCC is

presented in Figure 2-a. Following various experiments, it was noticed that the EVs' current were under-shooting. To compensate for this phenomena, it has been used the ceil function for the different controllers instead of the rounding.

3.2. Synthetic inertia control

Although no direct coupling from converter connected generators to the grid is made, a large amount of kinetic energy is stored in these units, (e.g. kinetic energy stored in wind turbines' blades and gearbox), together with different forms of energy storage in other units, can be used to deliver synthetic inertia. They could mimic synchronous generators by delivering active power response proportional to the RoCoF [35, 36].

In this study a Synthetic Inertia Controller (SIC) is implemented and the control diagram is presented in Figure 2-b. The RoCoF is measured over 200 ms. It controls the EVs' charging current in function of a RoCoF-current droop characteristic. The droop is shown in Figure 1-b, the dash line represents the ideal droop and the solid line represents the 1 A granularity. The droop is implemented by defining the RoCoF's low and high limits with zero RoCoF corresponding to 11 A. The deadband of ±0.8 Hz/s was introduced during the tuning phase where smaller deadband values have led to frequency oscillation. Therefore, it results in a very limited contribution from the EVs.

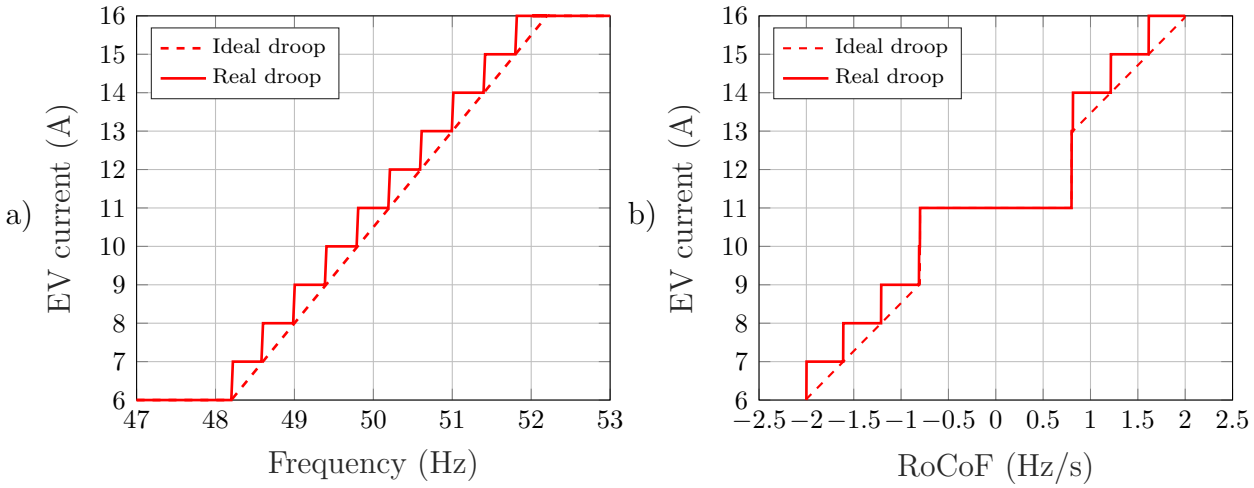

Figure 1: a)FCC droop characteristic, b) SIC droop characteristic

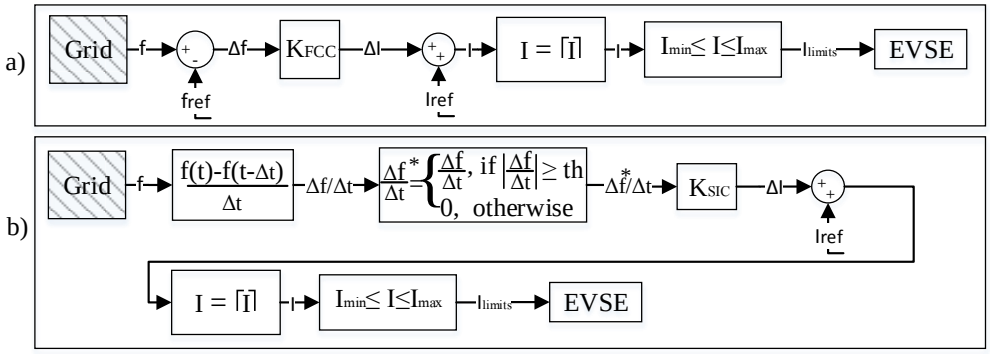

Figure 2: a) FCC control diagram, b) SIC control diagram

3.3. EV dynamic model

In order to successfully integrate EVs into power systems, it is necessary to correctly understand and characterize their dynamic behavior. A detailed model is therefore derived considering the EV users' driving requirements, the battery charging and discharging characteristics, the battery dynamics (e.g. time response, ramping time, etc..) and the control/communication delays. Since this study aims at investigating the EVs' capabilities and limits in providing fast primary control and synthetic inertia control, the battery state of charge was neglected. The EV model is presented in Figure 3. From the dynamic point of view it is possible to identify two main latencies between the set and the actual current. Specifically a communication delay and the EV activation delay, the sum of which varies between 150ms and 2s. The communication delay depends mainly on latencies in the IT infrastructure which is in the range of tens of milliseconds. The EV activation delay is varying among brand and heavily depends on the embedded power electronics. The most recent models show faster response time. In any case the current standard IEC61850 solely requires the car to respond within 3s. The total delay observed in the experimental trials range between 200 and 400ms. Therefore, in the simulation study the total delay is considered to be 250ms. As final note, with respect to the voltage dependency, the EVs are modelled as constant current loads.

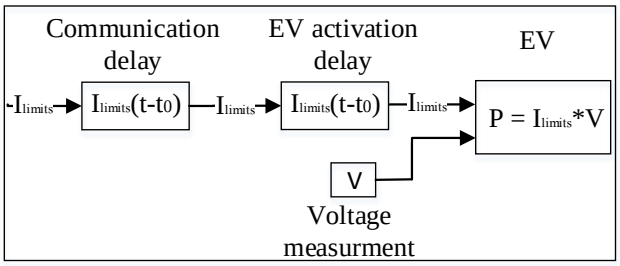

Figure 3: EV dynamic model

3.4. Experimental Layout and Power Components

The experiments are executed in the experimental infrastructure SYSLAB which is part of the PowerLabDK platform. SYSLAB represents a small scale low voltage power system. It consists of a number of real power components interconnected by a three-phase 400 V AC power grid, distributed over the Risø campus of the Technical University of Denmark [28]. SYSLAB is also characterised by its communication and control nodes allowing a strong controlability over the grid. The system may be connected to the utility or can be islanded if desired. The experimental layout is shown in Figure 4.

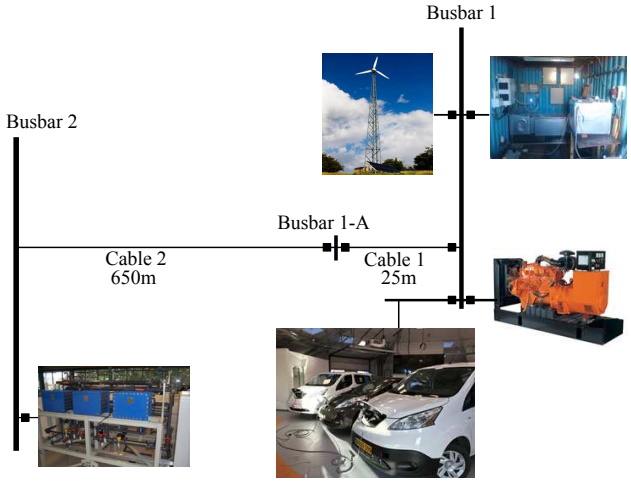

Figure 4: Experimental layout

The experimental setup is composed by two busbars connected by 675 m underground cable. The VRB is connected to busbar 2 and installed in building 2 where the busbar is located. The rest of the components are connected to busbar 1 and installed in the same

building as the busbar. The Aircon wind turbine is installed around 10 m from building 1. The VRB, the Aircon and the Dump load are controlled through a Matlab/Java interface while the EVs are controlled through a python interface. Since all the components are 3-phase except the EVs, it has been necessary to create an intermediate phase splitter as shown in Each EV is supplied on a different phase via a standard Mennekes (IEC 62196 Type 2) connector. The three Mennekes plugs are controlled separately by three different EVSE.

The experiments are executed in an islanded configuration where the diesel gen-set acts as the grid forming unit and is the only synchronous inertia device. It also compensates the small amount of reactive power drawn by each EV, corresponding to 200 VAr each.

The different components used during the experiment are listed in Table 1 where $P0$ is the base operating point. SC1 and SC2 refer to study case 1 and study case 2 respectively.

Table 1: Properties of Devices used in the Experiments

Device	Capability	P0 (kW) SC1	P0 (kW) SC2	Description
Diesel	0 - 48 kW -20 - 30 kVAr	24	24	IVECO genset S = 60 kVA, 2 pole pairs
Aircon	10 kW @ 11ms	-	∼4	Wind turbine type 4
Battery	±15 kW ±12 kVA	9	-	Vanadium redox battery, 120 kWh
Dumpload	0 - 78 kW	7	21	Resistor load bank
EV1	6 - 16 A (1.4 - 3.7 kW)	2.5	2.5	Nissan leaf 2016, 30 kWh lithium battery
EV2	6 - 16 A (1.4 - 3.7 kW)	2.5	2.5	Nissan e-NV200 2014, 24 kWh lithium battery
EV3	6 - 16 A (1.4 - 3.7 kW)	2.5	2.5	Nissan e-NV200 2015, 24 kWh lithium battery

3.5. EV Charging Controller and Communication Architecture

Each of the 3 single phase EVs is connected to a different phase of the grid by means of 3 electric vehicle supply equipment (EVSE). The control and communication setup is shown

in Figure 5.

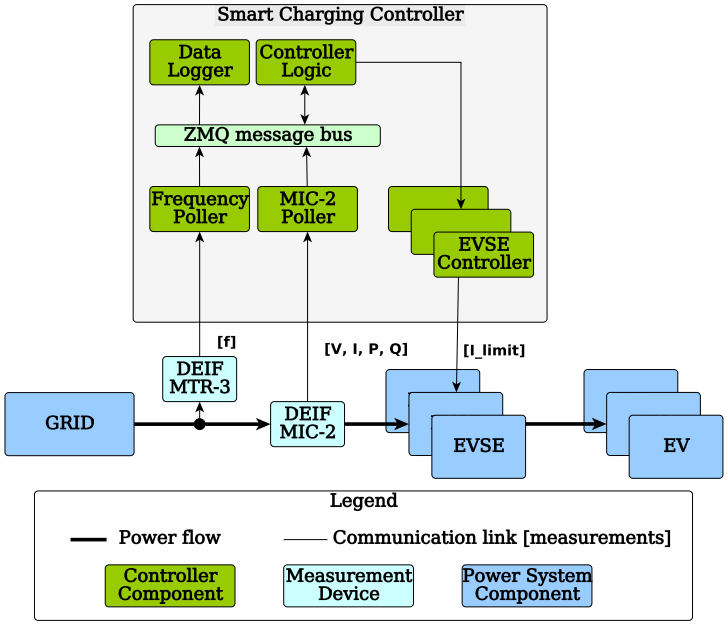

Figure 5: The communication architecture for the implemented smart charging controller

It consists of the following components:

- Smart Charging Controller – receives the measurements from the multi instrument, calculates the response and sends control signals to the EVSE.
- DEIF MIC-2 – multi instrument measurement device showing the voltage, current and power measurements with 0.5% accuracy. The device is only used for data logging.
- DEIF MTR-3 – multi instrument measurement device used here for fast frequency measurements, polled every 200ms.
- EVSE – Electric Vehicle Supply Equipment rated for 16A
- EV – the 3 tested electric vehicles.
- Grid – grid connection at the SYSLAB experimental facility.

The smart charging controller consists of many sub-components as described here:

- Controller logic − reads the latest frequency measurements from the message bus and calculates the $\Delta f/\Delta t$ and the Δf. Calculated set-points are directly sent to the EVSE controller.
- EVSE controller − acts as an interface between the physical EVSE and the controller logic.
- Frequency poller − acts as an interface to the frequency measurement device. In this case DEIF MTR-3 instrument used for frequency sampling every 0.2 seconds with accuracy of 10 mHz.
- MIC-2 poller − multi instrument device interface.
- Data logger − monitors the data exchange on the message bus and logs it to the database.
- ZMQ message bus − message bus used for representing the data exchange between the above mentioned controller components.

The timing of the response is crucial for the provision of synthetic inertia. Therefore, timing of each component in the control loop is important: frequency and RoCoF are measured every 200 ms, controllers' response is almost instantaneous and communication delay (10-20 ms) to each EV/EVSE pair is optimised by controlling them independently. It uses multi-threading and each EVSE receives a new control signal only if the set-point has changed. Finally, the EVs' reaction time is approximately 200-300 ms, therefore the whole control and actuator chain has an overall latency equal to 400-500 ms. According to this number, it is expected that the device could influence positively the whole frequency dynamic.

4. Results and Discussion

This section is composed by two subsections, in which simulations and experimental validation are presented. Two study cases are analysed. In the first study case (SC1), the

system is studied involving a set of load steps. An alternate load-increase and load-decrease are applied, so, both over and under frequency dynamics can be analysed.

In the second study case (SC2), wind power generation is added to the system. It adds random power fluctuations over the tested period and allows the possibility of investigating the behaviour of the two controllers and the EVs in a more realistic and challenging situation.

The two study cases are composed each by three scenarios, in the first scenario the EVs are treated as constant load, i.e. constant current set-point equal to 11 A (Base scenario). In the second scenario the EVs are participating with a synthetic inertia response, i.e. SIC. In the third scenario, the EVs are participating with a fast frequency response, i.e. FCC. The overview of the different scenarios is summarised in Table 2. During the simulation only study case 1 was analysed.

Table 2: Study cases overview

	Study Case 1	Study Case 2
Scenario 1	Base case	Base case + Wind
Scenario 2	SIC	SIC + Wind
Scenario 3	FCC	FCC + Wind

4.1. Simulations

In this section a simulation study in DigSilent PowerFactory is carried out. It aims at investigating the effects of synthetic inertia control and frequency containment control and achieving a preliminary results before validating experimentally the controllers. To explore the effects of the 1 A granularity imposed by the standard, a sensitivity analysis of different granularity values is conducted.

The same components and grid configuration presented in Figure 4 have been modelled, with the operating conditions of study case 1 (SC1), shown in Table 1.

To make this study as realistic as possible, an oscillatory frequency has been induced in the system by means of a fictitious zero-mean variable load, by means of fluctuating active power absorbed by the three-phase resistive load. In this way it has been possible to emulate

the realistic frequency oscillation that the real diesel synchronous generator would generate in such an islanded grid configuration.

First, a load event with amplitude of 2 kW (8.7% of the total consumption) was applied at $t = 10$ s and three scenarios were analysed. The first scenario is considered as base case where the EVs are treated as a constant load, i.e. constant current set-point equal to 11 A. In the second scenario the EVs are participating with a synthetic inertia response (SIC). In the third scenario the EVs are equipped with the FCC controller. Both the SIC and FCC controllers are implemented according to the control diagrams in Figure 2, thus applying integer EV current set-points to assure standard-compliance. Figure 6 shows the grid frequency, the RoCoF and the EVs' current set-point. As expected, Figure 6-a shows

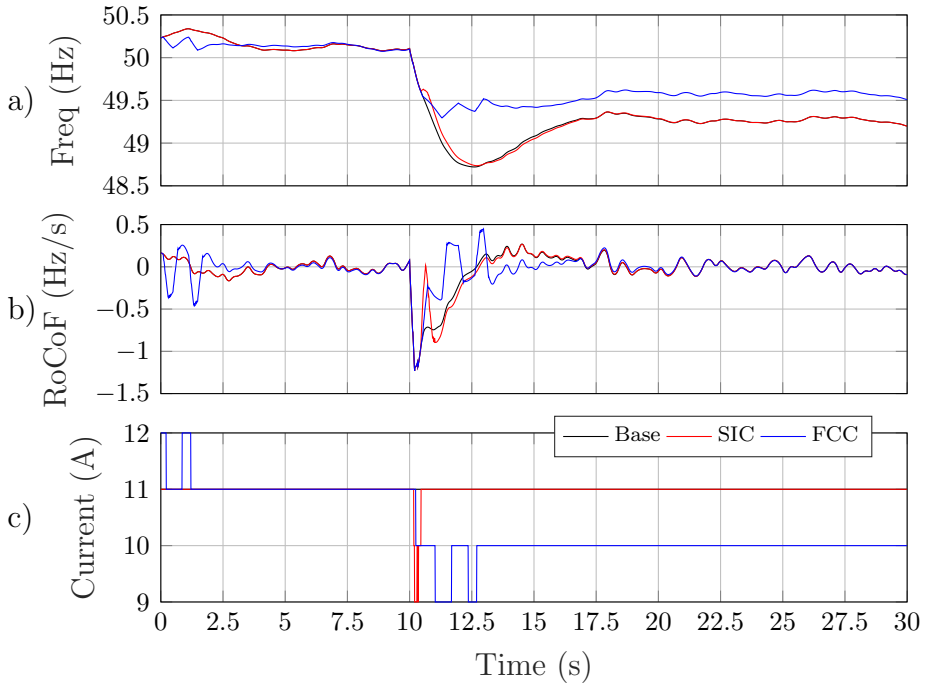

Figure 6: Simulation's results obtained by applying ±0.8 Hz/s deadband for SIC: a) frequency, b) RoCoF and c) EV current set-points for the three analysed scenarios, in case of granularity of 1 A.

that FCC improve the frequency behaviour in terms of frequency nadir and steady state value. It shows also that SIC ameliorates the frequency slope which is a typical behaviour of introducing more synchronous and/or synthetic inertia into the system. On the other hand,

unexpectedly, Figure 6-b shows that FCC has a better performance in terms of RoCoF compared to SIC.

However, a steeper droop and/or smaller deadband for SIC would have led to better performance regarding the RoCoF and the frequency slope. To demonstrate so, the same simulations were executed changing the deadband of SIC to ±0.5 Hz instead of ±0.8 Hz. The results are presented in Figure 7.

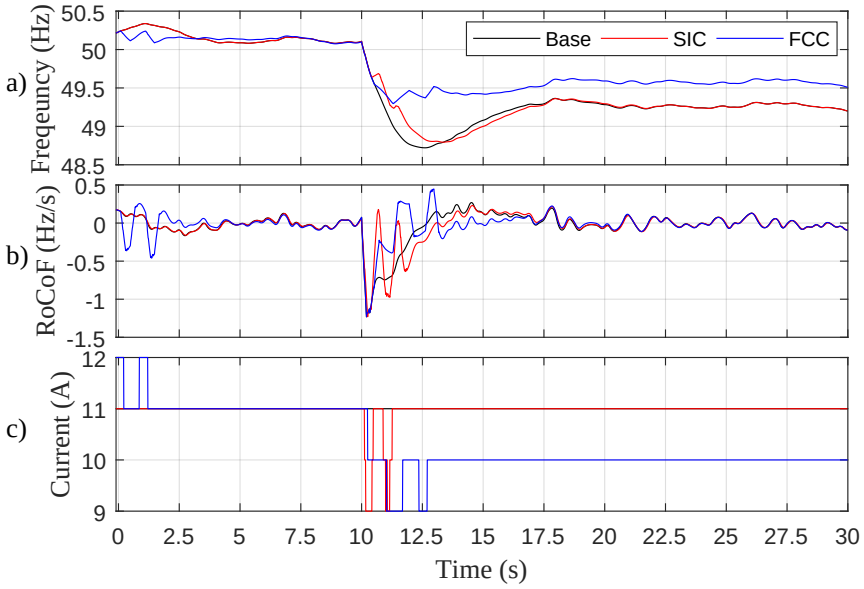

Figure 7: Simulation's results by obtained applying ±0.5 Hz/s deadband for SIC: a) frequency, b) RoCoF and c) EV current set-points for the three analysed scenarios, in case of granularity of 1 A.

Figure 7-a shows an improvement regarding the frequency slope compared to the previous case. On the other hand, Figure 7-b shows a marginal improvement regarding the RoCoF. One can notice from Figure 7-c that the EVs were participating more by changing the current set-point.

To better understand the effects of the 1 A granularity imposed by the standard IEC 61851 [27] on the performance of the two controllers, a sensitivity analysis was performed. A series of simulation was carried out employing different load steps and different granularity. Frequency drops have been obtained by increasing the active power absorbed by the VRB

by 20%, 40%, and 60%. They represent a load event of 8.7%, 15.7% and 23.5% of the total consumption, respectively. For the evaluation of the influence of the granularity, the following values of granularity have been applied, which are expressed as fraction of the actual granularity of 1 Ampere: $\frac{1}{4}$, $\frac{1}{2}$ and 1. Moreover, for the sake of completeness, also the case of continuous regulation (no granularity) and the uncontrolled case have been included in the analysis.

Figure 8 reports 3D bar plots of the results for all the performed simulations. Results are reported by means of standard deviations (SD) for both Frequency and RoCoF for FCC and SIC. As expected, Figure 8 shows that in all the cases the standard deviations depend

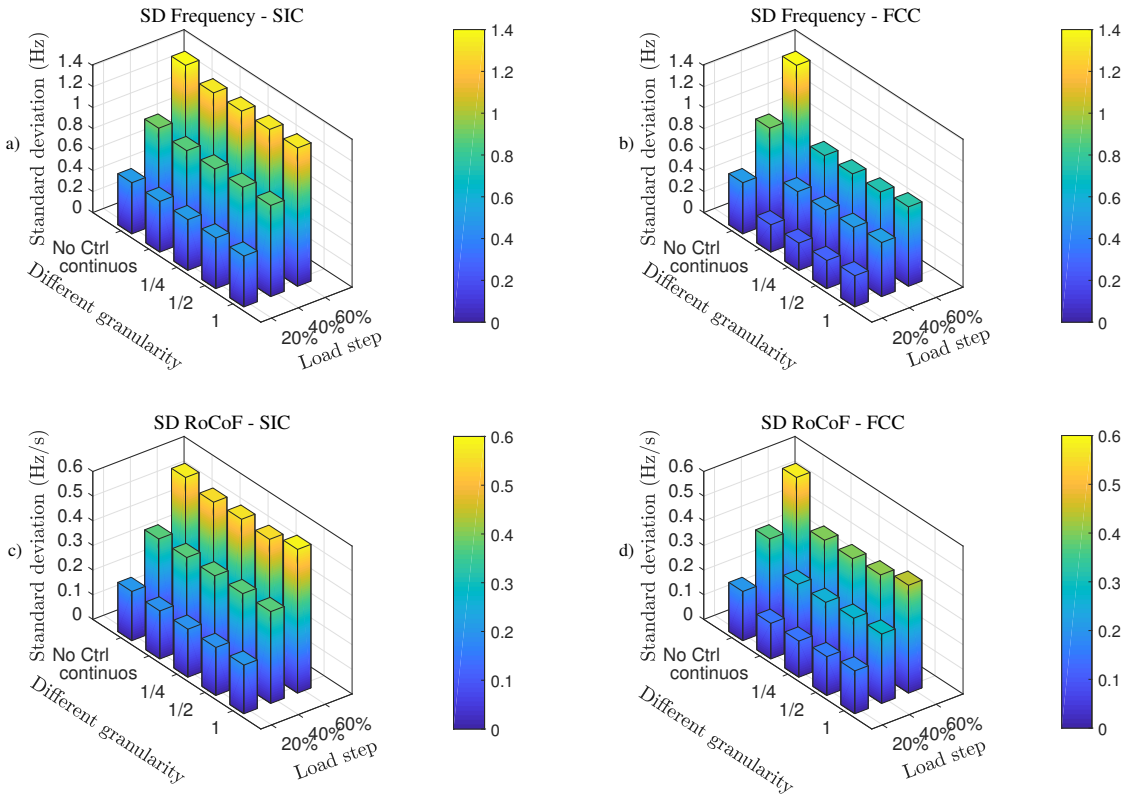

Figure 8: a)SD of the frequency applying SIC and b)SD of the frequency applying FCC, c)SD of the RoCoF applying SIC, d) SD of the RoCoF applying FCC

on the size of the load step.

On one hand, they are mostly constant for the different considered granularity, on the other hand higher values are found in the uncontrolled cases. Moreover, it is noticeable that

beneficial effects on the frequency are found in case of FCC. Since, as presented in Figure 6, the EVs' effect makes the frequency rise to a higher steady-state value. Meanwhile, the SIC controller has an embedded reset logic, which makes the EV set-point go back to 11 A right after the event. It is of interest to highlight that the FCC shows an unexpected better contribution to the RoCoF limitation in comparison to the SIC. This is due to the limited number of control actions that took place in case of SIC, due to the implemented RoCoF deadband (Figure 1-b). Instead, when providing primary regulation via FCC, no deadband is applied, making the controller activated more often, thus contributing more to the RoCoF containment.

Such a sensitivity analysis shows that, in this islanded microgrid, the granularity does not influence the results. However, one should note that under certain combination of system attributes (system inertia and stiffness of the power system) and control units (amount of power involved in the regulation, droop, response/ramp time and granularity of the control actions), the granularity might lead to system instability or oscillation between two consequent set-points as was experienced during the validation phase.

4.2. Experimental Validation

Following the results obtained during the simulations, the authors long for investigating the EVs capability in providing synthetic inertia and frequency containment control in an islanded grid in real circumstances. The experiments are executed in the islanded configuration shown in Figure 4, where the diesel is the grid forming unit.

4.3. Study case 1

In the first study case the frequency variation is triggered by several load steps. A set of load events from the VRB of the same amplitude is applied ($\approx \pm 2$ kW), namely, 8.7% of the initial installed load. To better investigate the controllers as well as the frequency dynamics, an additional set of load events with a different amplitude is applied, specifically ($\approx \pm 4$ kW), 17% of the initial installed load. The grid units as well as the initial conditions are reported in Table 1.

The three scenarios are characterised by the same initial conditions and load steps. The first scenario (S1) is a base case, in which the EVs are receiving a constant current set-point, i.e. 11 A absorbing around 2.5 kW. In the second scenario (S2) the EVs are controlled by the synthetic inertia controller which modulate the charging level between 6 and 16 A with steps of 1 A in function of the RoCoF-current droop characteristic presented in Figure 1-b. In the third scenario (S3) the EVs are controlled by the frequency containment controller. The controller modulates the EVs' charging level between 6 and 16 A with steps of 1 A in function of the frequency-current droop characteristic presented in Figure 1-a.

The results of the experiments are presented in Figure 9. Figure 9-a shows the system

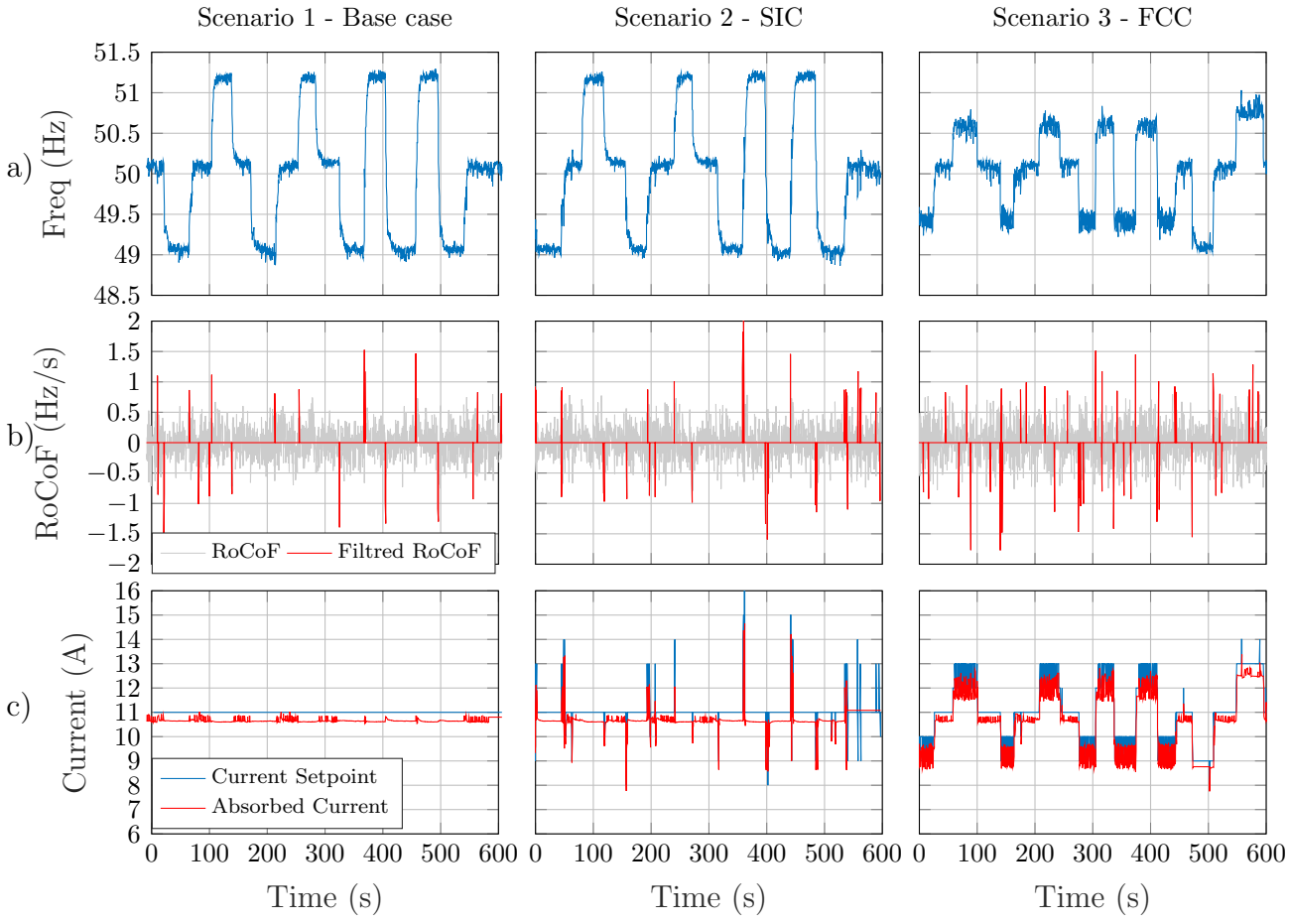

Figure 9: a)The grid frequency, b) The RoCoF, C)EV1's set-point vs absorbed current

frequency for the three scenarios. Figure 9-b shows the RoCoF measured over 200 ms in

grey and the filtered signal after applying the deadband in red (±0.8 Hz/s deadband is considered). In Figure 9-c the controllers' current setpoint is plotted versus EVs' absorbed current. Since the three EVs are acting similarly, the current of only EV1 is presented.

Figure 9-c shows that the EVs are changing the absorbed current as desired by the different controllers. However, due to the 1 A granularity, the implemented droop and the operating point, the 2 kW load event implies the FCC to oscillate between 12 and 13 A and between 9 and 10 A. A 6 kW load event is introduced only for Scenario 3, at which a stable operating point was found. In fact, Figure 9-c shows that the EV's current was not oscillating for this load event (around t=450s). However, this oscillation can be reduced by implementing a hysteresis function.

Figure 9-a shows that FCC limits the maximum frequency deviation compared to the base case, while the SIC does not have an effect on it. On the other hand, due to the oscillation between the different set-points in case of FCC, Figure 9-b shows that the RoCoF was outside the deadband more frequently compared to scenario 1 and 2.

Due to the response delay of the EVs and the dynamics of the diesel, which led to a continuous frequency oscillation, it is hard to perceive a valuable improvement in terms of the RoCoF from SIC. To better compare the performance of the two controllers in terms of RoCoF and frequency, the standard deviation and the energy contained in the signal (also addressed as normalised energy) is calculated and presented in Table 3. For a discrete signal $x(n)$, the normalised energy is calculated as $\frac{1}{N}\sum_{n=1}^{N} x(n)^2$, where N is the number of samples taken for computation. It shows that the two controllers are not improving the RoCoF compared to the base case.

Table 3: SC1 - Standard deviation and normalised energy

	RoCoF		Frequency
	SD	Normalised Energy	SD
Base	0.29	0.083	0.77
SIC	0.31	0.093	0.79
FCC	0.33	0.11	0.48

To better understand the effects of the SIC on the frequency compared to the base case, Figure 10 shows a zoom of the frequency, the RoCoF and the EV's absorbed current for the three scenarios.

In Figure 10-a on can notice that the SIC has improved the frequency slope as expected and as experienced during the simulations. Due to the embedded deadband, this contribution is very limited. However, since the three EVs are characterised by the same delay and granularity (i.e. acting simultaneously with steps), one can observe the sharp change in frequency which will lead to worse RoCoF compared to the base case as shown in Figure 10-b. To overcome this issue it might be of interest to study different delays and droops among the EVs. That might induce a more smooth frequency change and therefore a better RoCoF. It is of interest to notice from Table 3, where the SD is reported, and Figure 10-b that the FCC has worsen the RoCoF compared to the SIC and the base case.

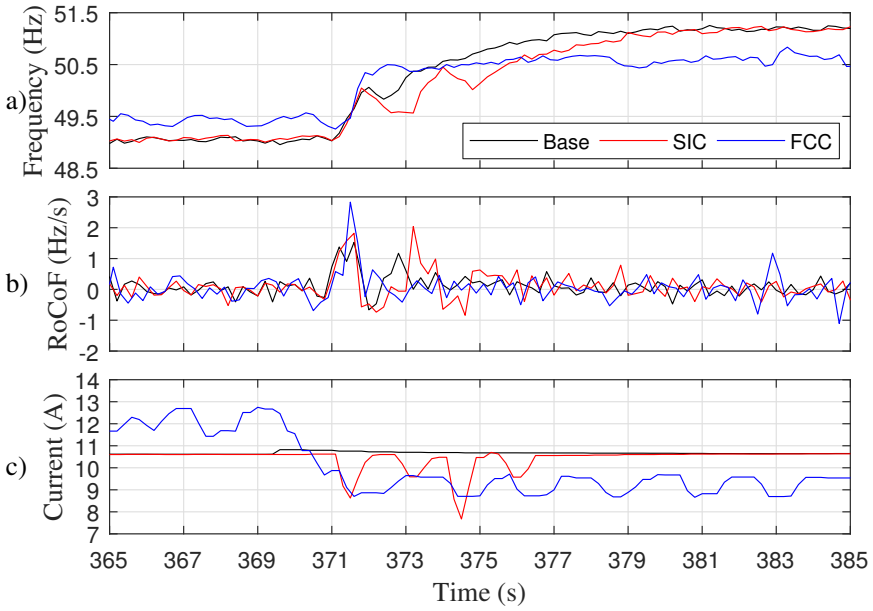

Figure 10: a) The grid frequency, b) The RoCoF, C) EV1's absorbed current

4.4. Study case 2

In the second study case, the two controllers are analysed during a wind power production. The VRB set-point is set to zero during this study case. The same scenarios and droop

characteristic as the previous study case are applied. Due to the random stochasticity of the wind generation and the diesel dynamics, the initial and boundary conditions are not exactly identical. Nevertheless, this study case aims at investigating the performance of each controller and the EVs in a more challenging and realistic configuration rather than comparing the different scenarios. The results for study case 2 are presented in Figure 11.

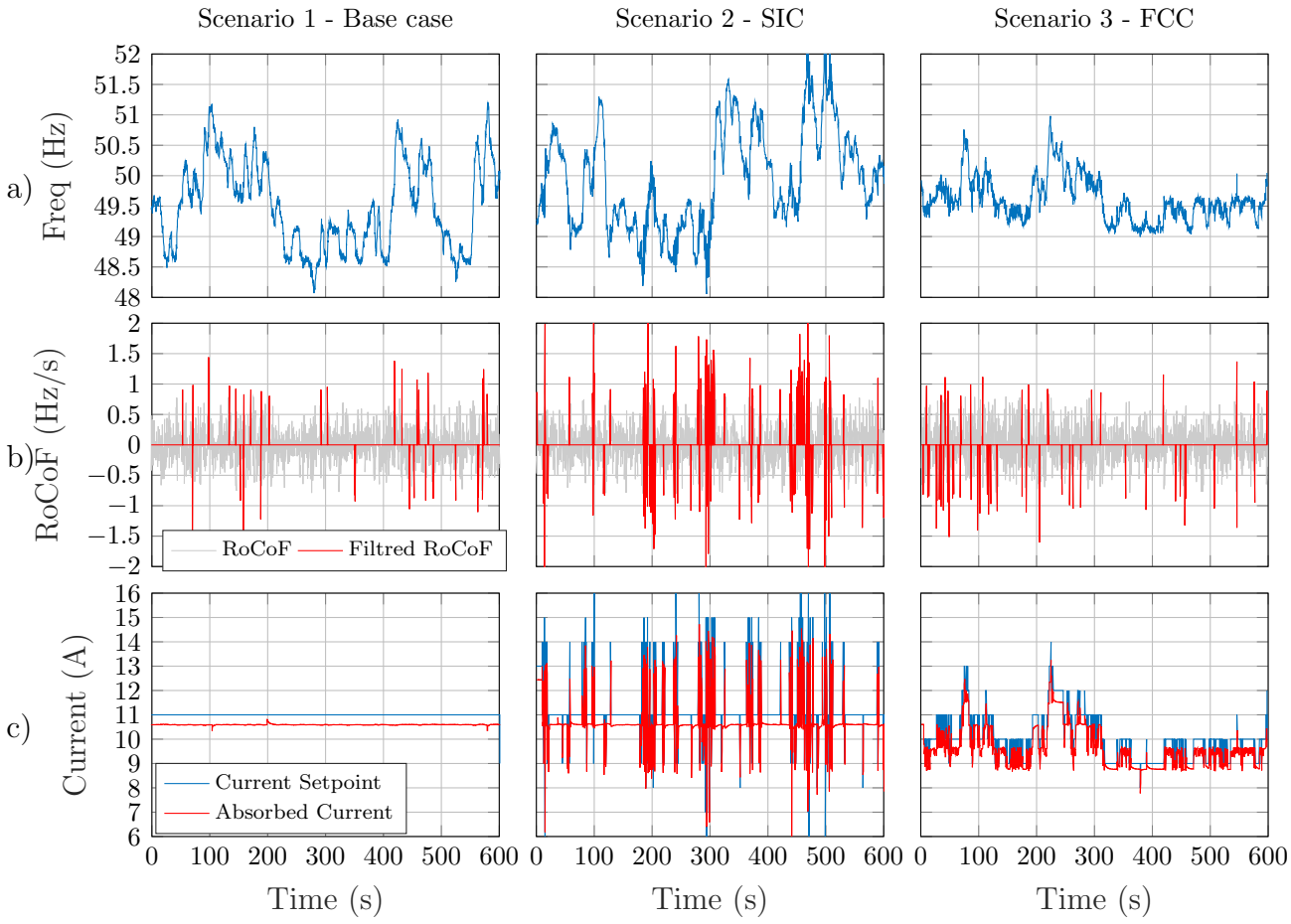

Figure 11: a)The grid frequency, b) The RoCoF, C)EV1's set-point vs absorbed current

Figure 11-a shows the grid frequency for the three scenarios. Figure 11-b shows the RoCoF measured over 200 ms in grey and the filtered signal after applying the deadband in red. In Figure 11-c the controllers' current set-point is plotted versus EVs' absorbed current. Since the three EVs are acting similarly, only the current of EV1 is presented.

The three scenarios were executed over a total time of 30 minutes. The average wind

production did not differ so much among the three scenarios: so that the different scenarios are still comparable. Figure 11-a shows that the FCC does have a remarkable effect in limiting the maximum frequency deviation.
Figure 11-b shows that applying the SIC, the RoCoF is outside the deadband more frequently.

To better compare the three scenarios, mean value and standard deviation of the wind production together with the standard deviation of the frequency and the RoCoF are calculated and presented in Table 4.

Table 4: SC2 - Standard deviation and normalised energy

	Wind Generation		RoCoF		Frequency
	Mean	SD	SD	Normalised Energy	SD
Base	3.5 kW	1.4	0.31	0.098	0.71
SIC	4.6 kW	1.68	0.45	0.2	0.83
FCC	3.1 kW	1.28	0.34	0.11	0.36

As mentioned before, due to the random wind production and the non replicability of the same conditions, the comparison is not perfect, especially in terms of RoCoF due to the continuous variation of the wind profile.
However, the mean value of the wind production among the three scenarios does not differ excessively, which allows us to compare the standard deviation of the frequency. Table 4 and Figure 11-a show the remarkable positive effect of FCC on the frequency.

5. Conclusion and Future Work

Starting from the presented research question: given the trend of decreasing system inertia, can fast frequency containment compensate or replace the need for synthetic inertia? Firstly, this work showed analytically the interdependency between frequency containment and synthetic inertia control on the transient frequency variation and the RoCoF. Secondly, on simulation level, it presented the ability of fast frequency control in improving the frequency in terms of nadir, steady state value and RoCoF. It also presented the ability of

synthetic inertia control in improving the frequency nadir and slope following an event. While it was acknowledged that EVs could quickly and almost precisely respond to fast changing current set-points, some technical limitation in employing EVs for such services were found. Finally, an experimental validation was conducted, presenting the capabilities and limitations of the two controllers under two different circumstances: following load events in both directions and exogenous wind generation profiles.

Employing the FCC, the simulations results showed the remarkable improvement of the frequency nadir and steady state value. It showed also a very limited improvement in terms of RoCoF. The controller did not limit the maximum RoCoF following the event but it did improve the overall behaviour compared to the base case. Similarly, the experiments showed the ability of FCC in limiting the maximum frequency deviation, both, following a series of load events or considering a wind power generation. Although in simulation the sensitivity analysis showed a very limited effect of the granularity, in the experimental phase, due the 1A granularity, the FCC controller caused the EV absorbed current to oscillate between two consecutive set points worsening the calculated RoCoF. To be mention, this oscillation was due the combination of 1A granularity, the implemented droop and the operating point. However, this effect can be limited by employing an hysteresis based algorithm.

Applying the SIC, the simulations presented the limited frequency improvements in terms of frequency nadir and frequency slope. It also showed that employing a smaller deadband allowed a better contribution, slightly improving frequency nadir and slope. On the other hand, the smaller deadband worsen the RoCoF trend compared to the base case. However, in both cases the controller did not limit the maximum RoCoF value. As mentioned, the SIC improved slightly the frequency slope but worsen the RoCoF. As interpretation of such unexpected phenomena, the authors believe that this might be due to the fact of using the same RoCoF signal both for control and examination purposes. In other words, the RoCoF used for control purpose should be calculated over a smaller time window of the one used by the RoCoF relay for detecting the variations. Nevertheless, considering the derivative characteristic of the SIC, its implementation might easily lead to frequency oscillation and limits the ability of exploiting the resource (e.g. large deadband). As for the

FCC, experiments investigations were conducted for two cases. Firstly following load events and secondly considering a wind power generation. In terms of frequency, the SIC effects were negligible for both cases. Regarding the first case, even if the EVs were able to follow the desired set points, the SIC did not show any noticeable improvement in terms of RoCoF. On the other hand, considering a wind power generation, the SIC had a very remarkable negative effects in terms of RoCoF. To be mention, this effect might have been limited by employing less steep droop parameters, which on the other hand would have limited the EVs participation (i.e. flexibility margin).

In general, employing faster response devices will allow exploiting better the resource capabilities. For example, this was shown in case of SIC where the smaller time response permitted the use of a narrower deadband. It can be clearly concluded that the actual series produced EVs are able to provide ancillary services in terms of fast frequency response and synthetic inertia solely relying on unidirectional charging. On the other hand the experiments show that with the actual EVs response time, a large deadband was needed for the SIC limiting its contribution. To achieve better performance, new requirements in terms of EVs response time need to be set. As future work, the authors recognise the importance of extending the analytical formulation of the interdependency of the two controllers on the system frequency. Moreover, it is of interest to expand the analysis over a larger number of flexible units employing different control attributes.

Acknowledgments

The work in this paper has been partly supported by the European Commission, under the FP7 project ELECTRA (grant no: 609687) and partly by the Danish research projects Parker (ForskEL kontrakt nr. 2016-1-12410) and Electra Top-up (grant: 3594756936313). The authors are also grateful to Nissan Denmark for providing the two Leafs used in the experiments.

References

[1] A. Adrees, P. N. Papadopoulos, J. V. Milanovi, A Framework to Assess the Effect of Reduction in Inertia on System Frequency Response, Power and Energy Society General Meeting (2016) 1–5doi:10.1109/PESGM.2016.7741695.

[2] A. Ulbig, T. Borsche, G. Andersson, Impact of Low Rotational Inertia on Power System Stability and Operation, in: The 19th World Congress ofthe International Federation of Automatic Control (IFAC14, 2014, pp. 1–12. arXiv:arXiv:1312.6435v2, doi:10.3182/20140824-6-ZA-1003.02615.

[3] ENTSO-E, Frequency Stability Evaluation Criteria for the Synchronous Zone of Continental Europe, Tech. rep., ENTSOE (2016).

[4] The Commission for Energy Regulation, Rate of change of frequency modification to the grid code, Tech. rep., CER (2014).

[5] E. Muljadi, V. Gevorgian, M. Singh, S. Santoso, Understanding inertial and frequency response of wind power plants, 2012 IEEE Power Electronics and Machines in Wind Applications (2012) 1–8doi:10.1109/PEMWA.2012.6316361.

[6] S. Sharma, S. H. Huang, N. D. R. Sarma, System inertial frequency response estimation and impact of renewable resources in ERCOT interconnection, IEEE Power and Energy Society General Meeting (2011) 1–6doi:10.1109/PES.2011.6038993.

[7] R. A. Walling, N. W. Miller, Distributed Generation Islanding Implications on Power System Dynamic Performance, in: Power Engineering Society Summer Meeting,, Chicago, 2002, pp. 92–96. doi:10.1109/PESS.2002.1043183.

[8] C. Ten, P. Crossley, Evaluation of ROCOF relay performances on networks with distributed generation, IET 9th International Conference on Developments in Power Systems Protection (DPSP 2008) 2008 (2008) 522–527. doi:10.1049/cp:20080092.

[9] Y. Mu, J. Wu, N. Jenkins, H. Jia, C. Wang, A Spatial-Temporal model for grid impact analysis of plug-in electric vehicles, Applied Energy 114 (February) (2014) 456–465. doi:10.1016/j.apenergy.2013.10.006.

[10] J. R. Pillai, B. Bak-Jensen, Impacts of electric vehicle loads on power distribution systems, IEEE Vehicle Power and Propulsion Conference, VPPC (2010) 6–11doi:10.1109/VPPC.2010.5729191.

[11] A. Foley, B. Tyther, P. Calnan, B. Ó. Gallachóir, Impacts of Electric Vehicle charging under electricity market operations, Applied Energy 101 (2013) 93–102. doi:10.1016/j.apenergy.2012.06.052.
URL http://dx.doi.org/10.1016/j.apenergy.2012.06.052

[12] K. Hedegaard, H. Ravn, N. Juul, P. Meibom, Effects of electric vehicles on power systems in Northern Europe, Energy 48 (1) (2012) 356–368. doi:10.1016/j.energy.2012.06.012.
URL http://dx.doi.org/10.1016/j.energy.2012.06.012

[13] M. H. Amini, M. Parsa, O. Karabasoglu, Simultaneous allocation of electric vehicles ' parking lots and distributed renewable resources in smart power distribution networks, Sustainable Cities and Society 28 (2017) 332–342. doi:10.1016/j.scs.2016.10.006.
URL http://dx.doi.org/10.1016/j.scs.2016.10.006

[14] M. H. Amini, M. P. Moghaddam, Probabilistic Modelling of Electric Vehicles ' Parking Lots Charging Demand, in: Electrical Engineering (ICEE), 2013 21st Iranian Conference, 2013, pp. 3–6. doi:10.1109/IranianCEE.2013.6599716.

[15] A. Molina-garcía, F. Bouffard, D. S. Kirschen, Decentralized Demand-Side Contribution to Primary Frequency Control, IEEE Transactions on Power Systems 26 (1) (2011) 411–419. doi:10.1109/TPWRS.2010.2048223.

[16] M. R. V. Moghadam, S. Member, R. T. B. Ma, Distributed Frequency Control in Smart Grids via Randomized Demand Response, IEEE Transactions on Smart Grid 5 (6) (2014) 2798–2809.

[17] W. Kempton, J. Tomić, Vehicle-to-grid power implementation: From stabilizing the grid to supporting large-scale renewable energy, Journal of Power Sources 144 (1) (2005) 280–294. doi:10.1016/j.jpowsour.2004.12.022.

[18] E. Sortomme, M. A. El-sharkawi, Optimal Scheduling of Vehicle-to-Grid Energy and Ancillary Services, IEEE TRANSACTIONS ON SMART GRID 3 (1) (2012) 351–359. doi:10.1109/TSG.2011.2164099.

[19] D. Wang, J. Coignard, T. Zeng, C. Zhang, S. Saxena, Quantifying electric vehicle battery degradation from driving vs . vehicle-to-grid services, Journal of Power Sources 332 (2016) 193–203. doi:10.1016/j.jpowsour.2016.09.116.
URL http://dx.doi.org/10.1016/j.jpowsour.2016.09.116

[20] K. Knezović, C. Træholt, M. Marinelli, P. B. Andersen, Katarina Knezović Active integration of electric vehicles in the distribution network theory , modelling and practice, Phd thesis, Technical University of Denmark (2017).
URL http://orbit.dtu.dk/files/131995291/Knezovic{_}PhDthesis{_}final.pdf

[21] Y. Mu, J. Wu, J. Ekanayake, N. Jenkins, H. Jia, Primary frequency response from electric vehicles in the Great Britain power system, IEEE Transactions on Smart Grid 4 (2) (2013) 1142–1150. doi:10.1109/TSG.2012.2220867.

[22] K. Knezović, S. Martinenas, P. B. Andersen, A. Zecchino, M. Marinelli, Enhancing the Role of Electric Vehicles in the Power Grid: Field Validation of Multiple Ancillary Services, IEEE Transactions on Transportation Electrification 7782 (c) (2016) 1–1. doi:10.1109/TTE.2016.2616864.

[23] W. Kempton, J. Tomic, Vehicle-to-grid power implementation: From stabilizing the grid to supporting large-scale renewable energy, Journal of Power Sources, J. Power Sources, J Power Sou, J Power Sources 144 (1) (2005) 280–294. doi:10.1016/j.jpowsour.2004.12.022.

[24] F. Teng, Y. Mu, H. Jia, J. Wu, P. Zeng, G. Strbac, Challenges on primary frequency control and potential solution from EVs in the future GB electricity system, Applied Energy 194 (2016) 353–362. doi:10.1016/j.apenergy.2016.05.123.

[25] A. Schuller, C. M. Flath, S. Gottwalt, Quantifying load flexibility of electric vehicles for renewable energy integration, Applied Energy 151 (2015) 335–344. doi:10.1016/j.apenergy.2015.04.004.

[26] P. Tielens, D. V. Hertem, The relevance of inertia in power systems, Renewable and Sustainable Energy Reviews 55 (2016) 999–1009. doi:10.1016/j.rser.2015.11.016.
URL http://dx.doi.org/10.1016/j.rser.2015.11.016

[27] IEC 61851-1:2010, Electric vehicle conductive charging system Part 1: General requirements (2010).

[28] M. Marinelli, S. Martinenas, K. Knezović, P. B. Andersen, Validating a centralized approach to primary frequency control with series-produced electric vehicles, Advances in Life Course Research 7 (2016) 63–73. doi:10.1016/j.est.2016.05.008.

[29] J. A. Suul, S. D. Arco, G. Guidi, Virtual Synchronous Machine-Based Control of a Single-Phase Bi-Directional Battery Charger for Providing Vehicle-to-Grid Services, IEEE Transactions on Industry Applications 52 (4) (2016) 3234–3244. doi:10.1109/TIA.2016.2550588.

[30] L. Martini, A. Morch, L. Radaelli, C. Caerts, C. Tornelli, S. Hänninen, H. Brunner, Electra IRP approch to voltage and frequency control for future power systems with high DER penetration, in: 23rd International Conference on Electricity Distribution CIRED, 2015, pp. 1–5.

[31] ENTSO-E, ENTSO-E, Continental Europe Operation Handbook, Tech. Rep. Cc, ENTSOE (2009).

[32] P. Kundur, J. Paserba, V. Ajjarapu, G. Andersson, A. Bose, C. Canizares, N. Hatziargyriou, D. Hill, A. Stankovic, C. Taylor, T. Van Cutsem, V. Vittal, Definition and Classification of Power System Stability, IEEE Transactions on Power Systems 21 (3) (2004) 1387–1401. doi:10.1109/TPWRS.2004.825981.

[33] P. Kundur, Power System Stability and Control, McGraw-Hill, 1994.

[34] A. Zecchino, M. Rezkalla, M. Marinelli, Grid Support by Single-Phase Connected Electric Vehicles without V2G Capability : Fast Primary Frequency Control, in: International Universities' Power Engineering Conference - UPEC, Coimbra, 2016, p. 6.

[35] M. Rezkalla, S. Martinenas, A. Zecchino, M. Marinelli, Implementation and Validation of Synthetic Inertia Support Employing Series Produced Electric Vehicles, in: International Conference on Electricity Distribution - CIRED, 2017, pp. 12–15, accepted for publication.

[36] M. Rezkalla, M. Marinelli, M. Pertl, K. Heussen, Trade-off analysis of virtual inertia and fast primary frequency control during frequency transients in a converter dominated network, in: 2016 IEEE Innovative Smart Grid Technologies - Asia (ISGT-Asia), 2016, pp. 890–895. doi:10.1109/ISGT-Asia.2016.7796503.

[G] Implementation and Validation of Synthetic Inertia Support Employing Series Produced Electric Vehicles

IMPLEMENTATION AND VALIDATION OF SYNTHETIC INERTIA SUPPORT EMPLOYING SERIES PRODUCED ELECTRIC VEHICLES

Michel REZKALLA, Sergejus MARTINENAS,
Antonio ZECCHINO, Mattia MARINELLI
Technical University of Denmark – Denmark
{mirez, smar, antozec, matm}@elektro.dtu.dk

Evangelos RIKOS
Center for Renewable Energy Sources – Greece
vrikos@cres.gr

ABSTRACT

The high integration of renewable energy resources (inverter connected) replacing conventional generation reduces the available rotational inertia in the power system. This introduces the need for faster regulation services including synthetic inertia services. These services could potentially be provided by electric vehicles due to their fast response capability. This work evaluates and experimentally shows the capability and limits of EVs in providing synthetic inertia services. Three series produced EVs are used during the experiment. The results show the performance of the EVs in providing synthetic inertia. It shows also that, on the contrary of synchronous inertia, synthetic inertia might lead to unstable frequency behavior.

INTRODUCTION

The displacement of conventional generation by converter connected resources reduces the available rotational inertia in the power system which leads to faster frequency dynamics and consequently a less stable frequency behaviour [1]. One of the main concerns of transmission system operators (TSOs) is the fast rate of change of frequency (RoCoF) which might lead to a cascade tripping of conventional and distributed generators connected by means of RoCoF relays [2], [3].
Traditionally, inertial response has not been considered as an ancillary service, but rather as a natural characteristic of the power system. Due to the high integration of converter connected resources, several TSOs began to recognize the value of synthetic inertia response [4], [5].
Simultaneously, the growing number of electric vehicles (EVs), on one hand is seen as an additional load on the grid from system operators' perspective. On the other hand, EVs are also one of the candidates for providing grid regulation services (i.e. frequency and voltage control) due to their fast response capability [6], [7]. In principle, they are able to provide fast regulating power in both directions in case of Vehicle-to-Grid (V2G), or just to modulate the charging power [8]. Nevertheless, EV's technical characteristics introduce different challenges such as limited individual power and energy ratings, single phase connection that imply potential source of unbalances and fast, but variable response time.

The total response time of the EV can be divided into different parts:

- Measurement time, which is the time necessary to the measurement device to measure the controller input signal.
- Communication time, which is the time required to send the control signal from the metering location to the location where the EVs are connected to the grid. The two locations can be identical, but it is possible actually to remotely control the EVs as explained in [7].
- EVs' response time, which is the time necessary for ramping up (or down) the power to meet the requested value by the controller.

In this study the V2G capability, which implies the possibility of reversing the power flow, is not considered and the service provision is possible only by controlling the charging current as defined by IEC 61851 standard [9]. The standard defines that EVs can be controlled by modulating the charging current between 6 and 16 A with 1-A steps. It also defines that EVs have to respond within 3 seconds and the current has to be limited to the set value. Because of the previous requirements and depending on the EV model and year of production EVs may show different performances (i.e. the EVs response can vary from under a second to few seconds) [10]. Since this study focuses on synthetic inertia support, the time response is of a crucial importance [11].
In this work three single phase EVs are employed to provide synthetic inertia and tested in one islanded configuration of the experimental low voltage grid SYSLAB PowerLabDK research infrastructure.

METHODOLOGY

Synthetic inertia in the power system could be emulated if the active power delivered (or absorbed) by the dedicated unit (EVs in this case) is controlled in inverse proportion to the variation of the grid frequency over the time ($\Delta f/\Delta t$) [12]. The experimental setup and power components are shown in Fig. 1 and detailed in the experimental layout.

Power components

The experiments are executed in the experimental infrastructure SYSLAB which is part of the PowerLabDK platform.

SYSLAB represents a small scale low voltage power system. It consists of a number of real power components interconnected by a three-phase 400 V AC power grid, distributed (more than 1 km) over the Risø campus of the Technical University of Denmark [7]. SYSLAB is also characterized by its communication and control nodes allowing a strong controllability over the grid and the ability of employing different control architecture (e.g. centralized architecture, distributed architecture). The following components are used during the experiment:

- Three controllable EVs: Two Nissan leaf – each equipped with single phase 16A charger and 30kWh lithium battery storage, both are produced in 2016 (addressed in this work as EV1 and EV3). One Nissan e-NV200 with single phase 16A charger and 24kWh lithium battery storage, produced in 2015 (addressed as EV2).
- Diesel gen-set equipped with a 60 kVA synchronous generator, capable of providing an active power output up to 48 kW.
- A controllable resistive load, named dumpload. The maximum load which is the sum of all the resistors is 78 kW.

All the devices are connected to the same bus-bar and the EVs' initial charging level is chosen so that there is room to increase and decrease the charging level equally [12].

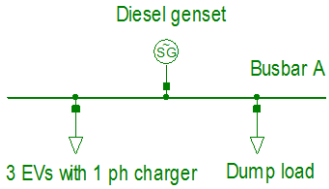

Fig. 1 The grid layout

EVs Controller description

The 3 single phase EVs are connected to the grid by means of 3 electric vehicle supply equipment (EVSE), each connected to a different phase. As the time of response is crucial for the synthetic inertia services and is dependent on the whole control loop, each EV/EVSE pair is controlled independently and in parallel using multithreading.

The communication and control setup are shown in Fig. 2 and detailed in [10].

It consists of the following components:

- Smart Charging Controller – receives the measurements from the power meter and sends control signals to the EVSE.
- DEIF MIC-2 – multi instrument measurement device for voltage, current and power measurements with 0.5% accuracy. The device is polled every 0.2 seconds.
- DEIF MTR-3 – multi instrument measurement device used here for fast frequency measurements.
- EVSE – Electric Vehicle Supply Equipment rated for 16A.
- EV – the 3 tested EVs.

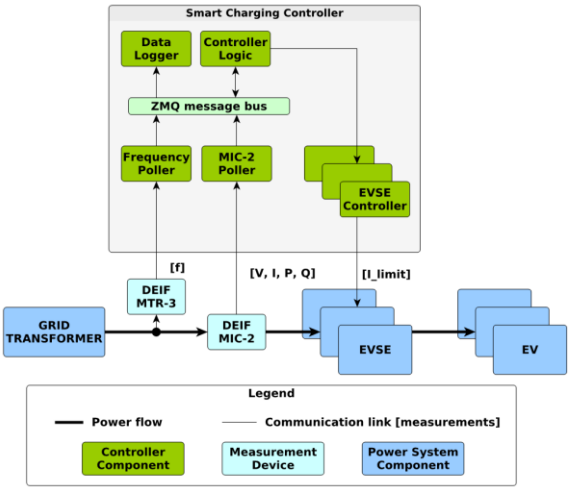

Fig. 2 Communication and control setup

- Grid – grid connection at the SYSLAB experimental facility.

The smart charging controller consists of many sub-components as described here:

- Controller logic – reads the latest frequency measurements from the message bus and determines the $\Delta f/\Delta t$. It calculates the set-points and sends control signals directly to the EVSE controller.
- EVSE controller – acts as an interface between the physical EVSE and the controller logic.
- Frequency poller – acts as an interface to the frequency measurement devices. In this case DEIF MTR-3 measurements instrument would be used for frequency sampling every 0.2 seconds with accuracy of ±10m Hz.
- MIC-2 poller – multi instrument interface.
- Data logger – monitors the data exchange on the message bus and logs it to the database.
- ZMQ message bus – message bus used for representing the data exchange between the various components.

EXPERIMENTAL SETUP AND RESULTS

The experiments are intended to test the EVs' capability of providing synthetic inertia support limiting the RoCoF in case of load variations. The experiments are executed in an islanded configuration where the frequency is set by the diesel generator. Three test scenarios are tested, where the frequency variation is triggered by several load events. The load events include an alternate load increase and decrease so that over and under frequency dynamics can be investigated. The amplitude of the load event in the three scenarios is equal to 40% of the installed power (i.e. 20 kW), which is 80 times more compared to the expected load step in the European synchronous area. The choice of this large event is to compensate the high inertia value of the diesel genset (2H = 50 s), allowing for the EVs the time to participate with synthetic inertia support. The diesel's moment of inertia is very high since it has been designed to operate in island mode.

In this study the primary frequency control is delivered by the diesel governor and automatically activated by the diesel internal controller, while the secondary frequency control has been disabled.
The three test scenarios are reported below and summarized in Table 1:

1) 20 kW load power steps from the dumpload to investigate the diesel response and the frequency behavior. No EVs are connected.
2) Load power steps with the EVs controlled by a synthetic inertia controller (controller's thresholds are ±1.5 Hz/s with a deadband (DB) of ±0.8 Hz/s, addressed as α droop).
3) Load power steps with the EVs controlled by a synthetic inertia controller (controller's thresholds are ±1 Hz/s with a DB of ±0.35 Hz/s, β droop).

Table 1 Components initial conditions and controller parameters

	Components initial conditions			EVs controller parameters	
	Diesel [kW]	**Load** [kW]	**3 EVs** [kW]	**Thresholds** [Hz/s]	**DB** [Hz/s]
Scen.1	28	28	-	-	-
Scen.2	35.5	28	7.5	±1.5	±0.8
Scen.3	35.5	28	7.5	±1	±0.35

Scenario 1

In this scenario only the dumpload and the diesel generator are connected. Since the experiments are performed in island configuration and the diesel governor is active, the scenario aims at investigating if the frequency dynamics are the same for the same load event. For example, investigating if the same load event applied several times implies the same frequency nadir, meaning a precise replicability of the conditions. It is important to note that the RoCoF is determined as Δf/Δt, where the frequency is measured every 0.2 seconds and therefore Δt is also 0.2 seconds.
The grid frequency, the RoCoF and the active power of diesel and dumpload are presented in Fig. 3.

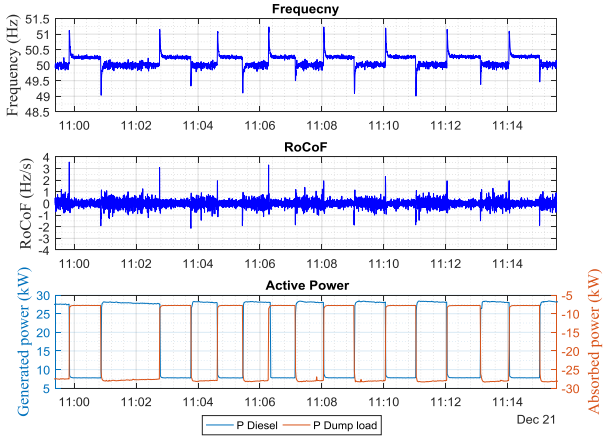

Fig. 3 Grid frequency, RoCoF and the absorbed and generated active power

One can notice that, the active power generation and consumption, respectively from the diesel and the dumpload, are varying with the same amplitude over the time. In theory this variation should case the same frequency change over the time.
However, frequency nadir and zenith are not the same over the time. This behavior is due to the mechanical dynamics of the diesel and small variation in the fuel injection rate during each cycle. Unfortunately, this behavior limits the possibility of performing a precise comparison of the EVs effects on the RoCoF with and without synthetic inertia support.
In other words, it is not possible to guarantee if the RoCoF improvement is due to the synthetic inertia or to the mechanical dynamics of the diesel. However, it is of high interest to investigate how EVs respond and if the controller and the communication infrastructure are properly designed rather than performing a numerical assessment of the frequency improvement.

Scenario 2

In this scenario the diesel generator, the dumpload and the three EVs are connected. The EVs are equipped with a synthetic inertia controller. The controller calculates the Δf/Δt and it changes the EVs' current setpoint in function of the applied droop. In this study two different droops are considered: α (the RoCoF limits are ±1.5 Hz/s with a DB of ±0.8 Hz/s) and β (RoCoF limits of ±1 Hz/s and DB of ±0.35 Hz/s). The two droops are RoCoF-Current droops and are presented in Fig. 4. The solid lines represent the 1-A step functions implemented in order to comply with the IEC 61851 standard.
The α droop is used in scenario 2 while the β droop is used in scenario 3. It is important to highlight that the voltage regulator of the diesel tries to maintain the voltage equal to 230 V, therefore setting the current is like setting the active power.

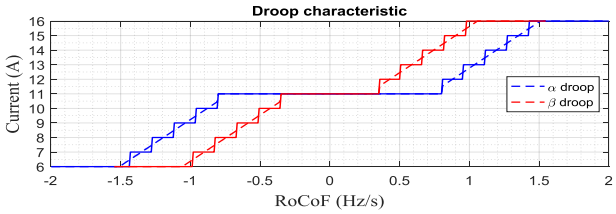

Fig. 4 Current – RoCoF droop characteristic

As for scenario 1, the load events include an alternate load increase and decrease of the same amplitude, so that over and under frequency dynamics can be investigated. The amplitude of the load event is 20 kW.
As it can be seen in Fig. 5, due to the mechanical dynamics, the large inertia value of the diesel and the limited number of EVs, it is not possible to appreciate improvements in the RoCoF.
However, in Fig. 6 it can be seen that the EVs' current setpoint is following the RoCoF variation as desired.

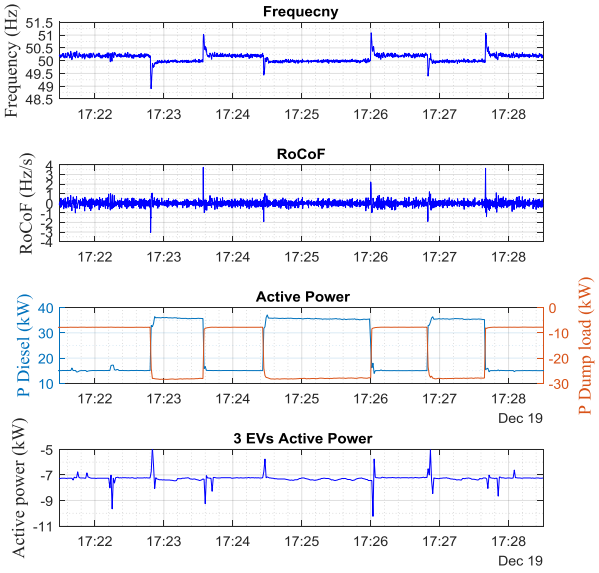

Fig. 5 Frequency and RoCoF dynamics and the absorbed and generated active power

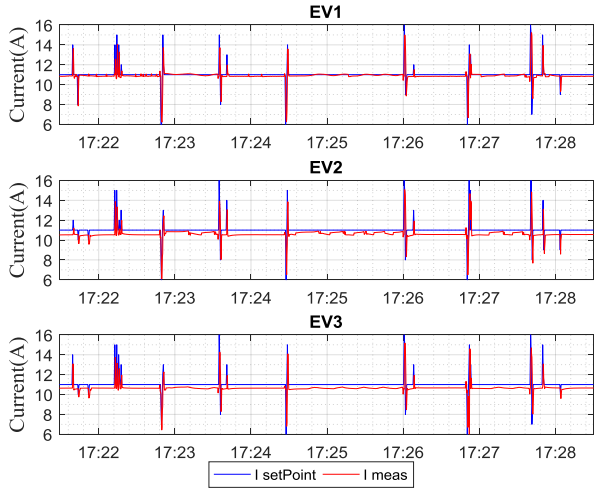

Fig. 6 EV's current setpoint sent by the controller and the EV's measured current

This variation can also be seen in Fig. 7, which shows a zoom of two consecutive load steps. In Fig. 7 only EV1's current is shown. The delay between the current setpoint and the absorbed one depends on the EV model and the year of production, in this case it is in the range of 200÷400 ms.

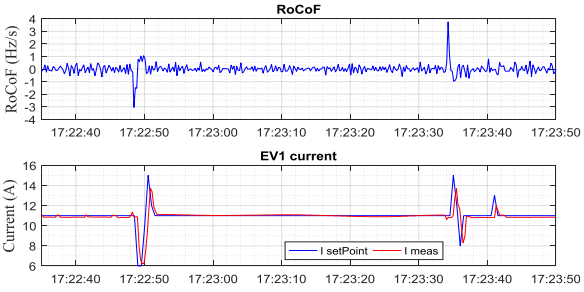

Fig. 7 RoCoF and EV's current

Scenario 3

This scenario aims at demonstrating the importance of choosing the appropriate controller's thresholds as well as the DB. In this scenario the authors decided to apply a higher gain and a smaller DB, namely β droop, to show that on the contrary of the synchronous inertia, synthetic inertia might lead to unstable frequency behaviour if the controller is not well tuned. The results are shown in Fig. 8 and Fig. 9, which show the frequency, the RoCoF and the absorbed and generated power.

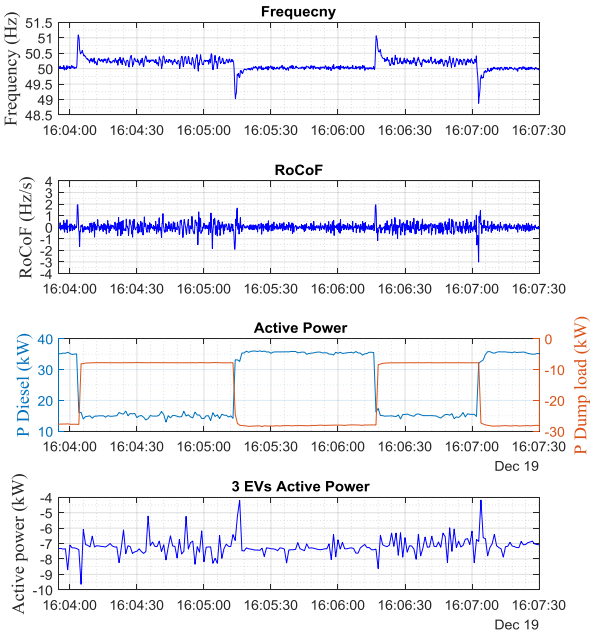

Fig. 8 Frequency and RoCoF and the absorbed and generated active power

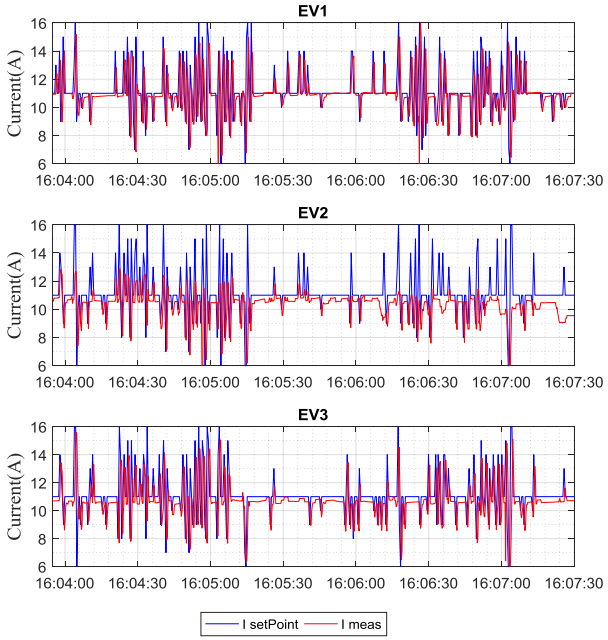

Fig. 9 EV's current setpoint sent by the controller and the EV's measured current

On the contrary of the previous scenario, one can notice that the RoCoF is larger which it can be also appreciated from the EVs' current setpoint. To prove so, the standard deviation for frequency and RoCoF for scenario 2 and 3 is calculated.
For scenario 2, it is equal 0.15 Hz and 0.32 Hz/s respectively, versus 0.19 Hz and 0.39 Hz/s for scenario 3.
To be mentioned, the grid frequency change and RoCoF are relatively limited due to the diesel large inertia. The smaller dead band and the higher gain induce more frequent changes in the current setpoint.
One can notice that, due to the different models and production year among the EVs, EV2 founds difficulty in following the setpoint as shown in Fig. 9. This difference can be seen as under or overshooting of the measured current as well as a delay between the current setpoint and the measured current.

CONCLUSION

The analysis showed the EVs' capability of providing synthetic inertia support. An experimental islanded microgrid has been set, and three series produced EVs have been controlled relying on synthetic inertia controllers. It was shown that on the contrary of synchronous inertia, more synthetic inertia (achieved by a higher gain and smaller dead band) does not guarantee a slower RoCoF and more stable behavior. Contrarily, the experiment showed that the higher gain and the smaller DB imposed the EVs to change the current set-point more frequently leading to faster RoCoF. The experiments demonstrated also that even if the EVs are all equipped by the same controller and the same standard (IEC 61851), they do not follow the setpoint in the same manner.
Further experiments will be carried out employing a higher number of EVs to appreciate more their effect on the RoCoF in case of high inertia system as well as low inertia system. Future work will also focus on comparing fast frequency control with synthetic inertia and on the capability of EVs in providing those two services. Namely, employing some EVs for fast frequency control and others for synthetic inertia. Consequently, testing the capability of providing synthetic inertia and fast frequency control from the same unit

ACKNOWLEDGMENTS

The work in this paper has been partly supported by the European Commission, under the FP7 project ELECTRA (grant no: 609687) and partly by the Danish research projects Parker (ForskEL kontrakt nr. 2016-1-12410).
The authors are also grateful to Nissan Denmark for providing the two Leafs used in the experiments.

REFERENCES

[1] A. Ulbig, T. Borsche, and G. Andersson,2014, "Impact of Low Rotational Inertia on Power System Stability and Operation," in *The 19th World Congress ofthe International Federation of Automatic Control*, 1–12.
[2] The Commission for Energy Regulation,2014, "Rate of Change of Frequency (RoCoF) Modification to the Grid Code,".
[3] R. A. Walling and N. W. Miller, 2002, "Distributed Generation Islanding – Implications on Power System Dynamic Performance," in *Power Engineering Society Summer Meeting*, , 92–96.
[4] EIRGRID and SONI, 2016,"RoCoF Alternative & Complementary Solutions Project".
[5] E. Muljadi, V. Gevorgian, and M. Singh, 2012, "Understanding Inertial and Frequency Response of Wind Power Plants," in *IEEE Symposium on Power Electronics and Machines in Wind Applications*, 1–8.
[6] K. Knezovic, S. Martinenas, P. B. Andersen, A. Zecchino, and M. Marinelli, 2016,"Enhancing the Role of Electric Vehicles in the Power Grid: Field Validation of Multiple Ancillary Services," *IEEE Trans. Transp. Electrif.*, vol. 99, 1–1.
[7] M. Marinelli, S. Martinenas, K. Knezovic, and P. B. Andersen, 2016,"Validating a centralized approach to primary frequency control with series-produced electric vehicles," *Jounal Energy Storage*, vol. 7, 63–73.
[8] W. Kempton and J. Tomić, 2005, "Vehicle-to-grid power implementation: From stabilizing the grid to supporting large-scale renewable energy," *J. Power Sources*, vol. 144, 280–294.
[9] IEC 61851-1, 2010, "Electric vehicle conductive charging system – Part 1: General requirements."
[10] S. Martinenas, M. Marinelli, P. B. Andersen, and C. Træholt, 2016, "Evaluation of Electric Vehicle Charging Controllability for Provision of Time Critical Grid Services", 1–5.
[11] M. Rezkalla, M. Marinelli, M. Pertl, and K. Heussen, 2016, "Trade-off Analysis of Virtual Inertia and Fast Primary Frequency Control During Frequency Transients in a Converter Dominated Network," in *IEEE PES Innovative Smart Grid Technologies – Asia*, 1–6.
[12] M. Rezkalla, A. Zecchino, M. Pertl, and M. Marinelli, 2016, "Grid Frequency Support by Single-Phase Electric Vehicles Employing an Innovative Virtual Inertia Controller," in *International Universities' Power Engineering Conference - UPEC*, 1–6.

[H] Augmenting System Inertia Through Fast Acting Reserve - A Power System Case Study with High Penetration of Wind Power

Augmenting System Inertia Through Fast Acting Reserve – A Power System Case Study with High Penetration of Wind Power

Michel Rezkalla, Mattia Marinelli
Center for Electric Power and Energy
Technical University of Denmark
Roskilde, Denmark
{mirez, matm}@elektro.dtu.dk

Hassan Qazi, Jon O'Sullivan
Innovation Team
EirGrid
Dublin, Ireland
{Hassan.Qazi, Jon.O'sullivan}@Eirgrid.com

***Abstract*—A number of jurisdictions across the world are committed to reducing their carbon emissions. A key route to decarbonisation is by raising the share of renewable generation. However, this will result in reduction of the system inertia and consequently deterioration of frequency stability. Fast acting reserve (FAR) is seen as a possible solution. Various approaches concerning the control of FAR (e.g. frequency gradient and frequency deviation based triggering) have previously been proposed. There is however a lack of clarity regarding the volume of FAR that can potentially compensates for reduction in system inertia. This paper carries out a quantitative assessment of FAR to limit the rate of change of frequency. All island power system of Ireland is adopted as a test case for analysis. The study concludes that FAR can mitigate the RoCoF and it presents also the quantitative relationship between FAR and conventional inertia which depends on system conditions.**

***Index Terms*—Fast acting reserves, Frequency stability, Low carbon system, Synthetic inertia.**

I. Introduction

The increasing share of distributed and inertia-less resources entails an increase upsurge in the requirement for balancing and system stabilisation services. The reduction of system inertia has mainly two implications with regards to system frequency stability: 1) Faster rate of change of frequency (RoCoF) - resulting in possible tripping of grid components, especially embedded renewable generation, conventional generation pole slipping and cascade tripping. 2) Higher frequency deviations (nadirs/zeniths) potentially leading to load shedding and in worst cases, system collapse. Moreover, the high volatility of renewable energy sources (RES) contributes to the frequency stability issue by changing the grid inertia over time and increasing the need for better planning due to higher uncertainty.

Michel Rezkalla is a Ph.D. student at the Technical University of Denmark (DTU) and is supported by the EU FP7 project ELECTRA (grant: 609687) and the Danish Research Project ELECTRA Top-up (grant: 3594756936313). More information at www.electrairp.eu

Various transmission system operators (TSOs) with limited AC interconnection have identified these issues to be of critical significance and have initiated mitigation measures. For example, the synchronous power system of the Republic of Ireland and Northern Ireland has an operational constraint of a minimum of 20000 Megawatt-seconds (MWs) of kinetic energy stored in rotating masses of the system, generally addressed as system inertia floor, which is the sum of each machine's rated power time relative inertia constant H ($E_K = \sum_{i=1}^{n} H_i S_i$ [MWs]) [1]. Instead of maintaining a minimum inertia floor, such as 20000 MWs, authors in [2] propose an economic dispatch strategy to dynamically calculate the minimum inertia level, leading to reduced inertia requirement in some cases, which still needs to be maintained by conventional plants. The Hydro-Quebec Transenergie's (HQT) transmission connection requirement stipulates in detail that wind power plants must be equipped with an inertia emulation system. HQT is now in the process of procuring and validating manufacturers' models integrating inertia emulation features [3]. Due to the high share of inertia-less resources, National Grid, UK TSO is procuring fast reserves to provides the rapid delivery of power through either increased output from a generator or a reduction in consumption from demand sources, to control frequency changes that might arise from sudden, and sometimes unpredictable, changes in generation or demand [4]. The Electric Reliability Council of Texas (ERCOT) recognises the need for a fast frequency response service (full response delivered within 0.5 seconds) to changing frequency to supplement the inherent inertial response from synchronous machines and thus helping with the implications of low system inertia. ERCOT also recognise the need of synthetic inertia response from inverter based wind turbines [5]. On the other hand, Energinet, the Danish TSO, have started to investigate the effect of synchronous condensers in mitigating the RoCoF and enhancing the frequency stability [6].

However, one can notice that the various solutions previously mentioned and employing inverter connected resources (e.g. energy storage, wind turbine etc..) do not define the quantitative relationship between MW of reserve and the

correspondent MWs of synchronous inertia that those will be able to replace. For example, how much MW of fast acting reserve (FAR) will compensate for the reduction of 1 MWs of synchronous inertia?

This work aims at investigating the ability of non-synchronous fast reserves to replace generators' inertia and assessing the quantitative relationship between FAR (MW) units (e.g. energy storage systems) and MWs of synchronous inertia. In this study, the FAR units are represented by a single equivalent unit which represents an aggregated number of units of the same characteristics (e.g. same response time). Two different control mechanisms are investigated, RoCoF based control, addressed further as synthetic inertia control (SIC) and frequency deviation based control, addressed as fast frequency control (FFC) [7], [8]. The analysis is applied on an equivalent model of the Republic of Ireland and Northern Ireland power system.

II. Methodology

A. Mathematical background

During any disturbance that causes an imbalance between the torques acting on the rotor (i.e. active power imbalance between generation and consumption), the net torque causing acceleration or deceleration is $T_a = T_m - T_e$, where T_m is the mechanical torque applied on the rotor and T_e is the electrical torque on the rotor. The simplest model of electro-mechanical swings in a power system is based on the so called swing equation [9]:

$$T_a = T_m - T_e = J\frac{d\omega_m}{dt} \tag{1}$$

where J is the combined moment of inertia of the generator and the turbine (kgm^2), and ω_m is the angular velocity of the rotor (rad/s).

Formulating the swing equation as in [7], it can be expressed as:

$$\frac{\mathrm{d}\bar{\omega}_e}{\mathrm{d}t} = \frac{\bar{T}_m - \bar{T}_{e_0} - (K_D + K_{FCC})\Delta\bar{\omega}_e}{2H + K_{SIC}} \tag{2}$$

where $\bar{\omega}_e$ is the angular velocity of the electrical rotor, K_D is a damping factor in per unit (pu), K_{FFC} and K_{SIC} are the FFC and SIC proportional control coefficients respectively and H is the inertia constant.

One can notice that FFC and SIC can affect the RoCoF variation during the transient. Note that due to the response time of FFC and SIC and the power ramp-rate limitations of the used resource (e.g. battery ramp-rate), it turns out to be a complex time-variant term. However, the presented swing equation shows clearly that mitigating the impact of power imbalances in terms of RoCoF can be achieved by increasing the system rotational inertia H, employing fast reserves with RoCoF based control and/or with frequency deviation based control.

B. System model and generating units

A single busbar equivalent model of the All Island Power System (AIPS), which is the synchronized power system linking the Republic of Ireland and Northern Ireland, has been considered as the study case system [10]. The AIPS system projected for the year 2020, and developed as a single bus bar dynamic mode1, has been employed to assess system frequency stability. This model is further addressed as the Single Frequency Model (SFM). The AIPS is an islanded system with two HVDC connections to Great Britain. An overview of the system installed capacity is represented in Table I. The system has a total dispatchable power of 10064 MW [11].

TABLE I
THE AIPS INSTALLED CAPACITY AND LOAD

Fuel Type	Installed capacity
Gas and/or distillate oil	6249 MW
Pumped storage hydro	292 MW
Milled peat and biomass	346 MW
Coal and/or Heavy fuel oil	1961 MW
Hydro	216 MW
DC interconnector	1000 MW
All Wind (partially/Non-dispatchable)	5000 MW
Peak load	6900 MW

The SFM is specifically used to examine the frequency behavior of the power system following the loss of the largest single infeed (LSI). The model had been previously developed on MATLAB/SIMULINK platform and more details can be found in [12]. The SFM employs a single bus which concentrates on the energy imbalance of the power system ignoring any of the transmission characteristics. The model assumes a single busbar and represents the dynamic interactions of turbines, governors, boilers and load. This model has been developed over many years for the power system of Ireland and Northern Ireland and has been validated based on manufacturer data and real event traces to provide accurate traces of the overall system frequency response in the first 30 s following significant generation/demand imbalance events [13], [14]. The model includes all the generators present in the AIPS fed by any desired dispatch. All generation units are assumed to be grid code compliant with droop settings of approximately 4%. Individual plant's characteristics such as plant inertia are based on data provided by the manufacturers. Fixed speed (FS) wind turbines and variable speed (VS) wind turbines are modelled separately to recognize the inertia contribution from the fixed speed turbines. A schematic layout of the single bus frequency model is shown Figure 1. The Plexos production cost modelling tool was used to simulate hourly dispatch schedules for the year 2020 [10]. Key assumptions of the Plexos 2020 model include:

- Installed wind generation of 5 GW.
- System peak load of 6900 MW.

In this study, 780 dispatches representative of different operational scenarios are used.

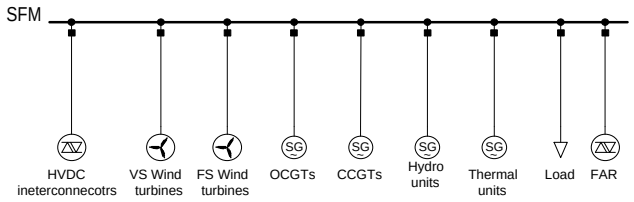

Figure 1. The single frequency model representation

C. Methodology

This study applies a bottom-up inductive approach for analysis of quantitative evaluation of synchronous inertia which can be potentially replaced by a specified magnitude of fast acting reserves. The inductive approach provides systematic set of procedures for analyzing data that can produce reliable and valid findings. The study employs two different control mechanism for FAR, namely SIC and FFC. The method consists in: firstly, examining the RoCoF following the loss of the LSI. Secondly, in removing one conventional plant and its associated inertia which it gets substituted with FAR. An equivalence is established when the RoCoF value from the pre-plant removal and post FAR addition equalize. This process will be done over a large number of dispatches. A flow chart of the applied method is presented in Figure 2 and the following procedure is applied:

1) Firstly, apply a simulated system dispatch (e.g. dispatch A) to the SFM and evaluate the system frequency and RoCoF following the loss of the LSI.

2) Dispatch A is modified by firstly removing a conventional plant and its associated inertia and secondly by redispatching the power of the removed plant over the remaining ones (dispatch A'). The LSI must remain the same as in dispatch A.

3) Add FAR reserves to the modified dispatch to compensate for the removed inertia. An equivalence between MW of FAR and MWs of synchronous inertia is established when the maximum average RoCoF from the pre-plant removal and post FAR addition equalize.

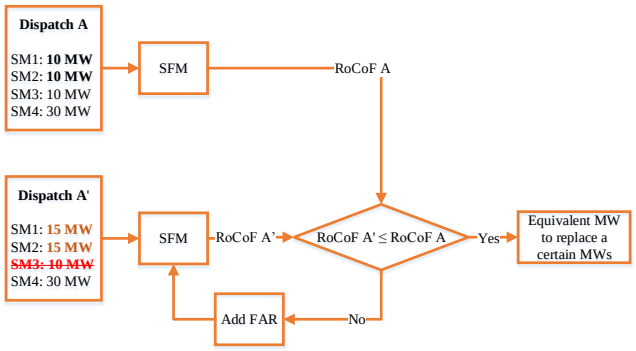

Figure 2. Applied methodology flow chart

It has been decided to calculate the RoCoF over a 500 ms moving window similar to the RoCoF relays' requirements in the Irish grid code [1].

The control diagram of the SIC and FFC are represented in Figure 3-a and Figure 3-b, respectively. The proportional control (K_{SIC} and K_{FFC}) are calculated through an iteration process to determine the needed amount of reserves able to compensate for the reduced synchronous inertia as previously explained in the methodology. The fast acting reserves' dynamics are represented through a transport delay and first order delay. The two values are determined based on various studies and energy storages' datasheets [15], [16]. For example, Sodium Sulphur batteries (NaS) are characterized by their fast response time and as claimed by certain manufactures, the response time is within 1 ms [17] .

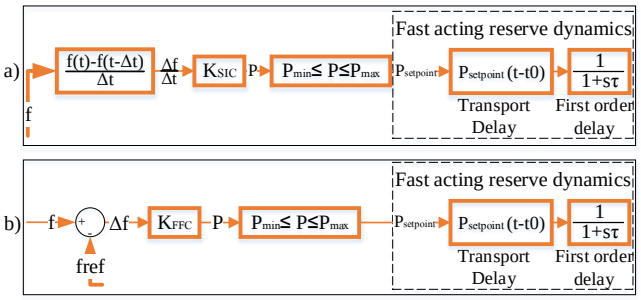

Figure 3. SIC and FFC control diagram

III. Results

Four different scenarios are analyzed. In the Four scenarios the system response is triggered by the loss of the LSI which varies over the different dispatches. In the following an overview of the different scenarios is presented:

- Sceanrio 1: The first scenario investigates the ability of SIC and FFC in mitigating the RoCoF and their effects on the system stability. Applying the proposed methodology, the scenario presents the performance of the two control mechanisms when two different dispatches are applied, respectively, high inertia and low inertia dispatches.

- Scenario 2: Using more than 700 dispatches and applying the proposed methodology, the second scenario determines the relation between MW of FAR and MWs of equivalent synchronous inertia.

- Scenario 3: The third scenario carries out a sensitivity analysis of the FAR's response time. It highlights the response time's effects on the system stability and on the relation between MW and MWs. Response times of 50 ms, 100 ms and 150 ms are used.

- Scenario 4: The fourth scenario carries out a sensitivity analysis of the deadband applied on the control signal. The following values are used for FFC: 80 mHz, 120 mHz and 300 mHz. Similarly, for the SIC the following values are used: 80 mHz/s, 120 mHz/s and 300 mHz/s.

A. Scenario 1

The first scenario analyses the capability of FFC and SIC in limiting the RoCoF and their effects on the system stability. The following deadbands are used 80 mHz and 80 mHz/s for FFC and SIC, respectively and 50 ms response time is applied. Using as a metric the system inertia, two different dispatches are investigated, high inertia case and low inertia case, respectively 36855 MWs and 16649 MWs. It should be noted that AIPS is currently not operated with such a low value of inertia. However, these values are considered low or high in relation to the AIPS. To be noted, the SFM does not consider the loads' inertia contribution and therefore the system inertia is composed only by the generations' inertia.

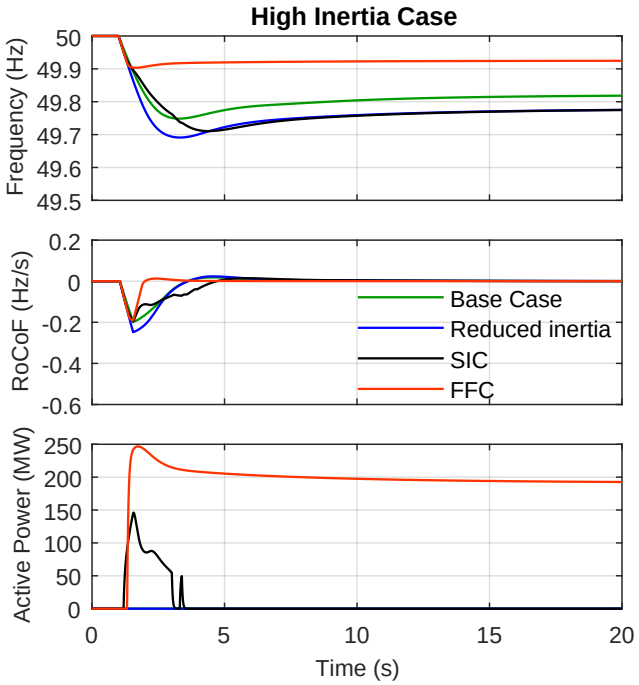

Figure 4. System frequency and RoCoF High inertia

As previously demonstrated in equation (2), Figure 4 shows the ability of the two controllers in mitigating the RoCoF. Due to the different control approaches (i.e. SIC and FFC) and the applied deadbands, different amounts of MW were needed to replace the same amount of MWs of synchronous inertia, this point will be further addressed in Scenario 2 and 3 employing more dispatches. One can notice that the FFC required roughly the double amount of MW compared to SIC which is due to the different deadbands. In fact, employing 80 mHz deadband for a high inertia case where the frequency deviation is relatively small, it delays the FFC participation. Due to this effect, the FFC starts responding when the frequency deviation is larger compared to the start point of SIC and therefore it requires a larger amount of MW. Applying 50 mHz deadband for the same study case, the FFC required only 63 MW of active power opposed to 108 MW with 80 mHz deadband.

The study does not aim at improving the system frequency (i.e. in terms of nadir and steady state value), however, one can notice the better performance of FFC compared to the SIC. In other words, the employment of FFC for mitigating the RoCoF will implicitly support the system frequency improving the overall system stability. In fact, Figure 4 shows that FFC continue to deliver power even after the mitigation of the RoCoF since it is a frequency deviation based control.

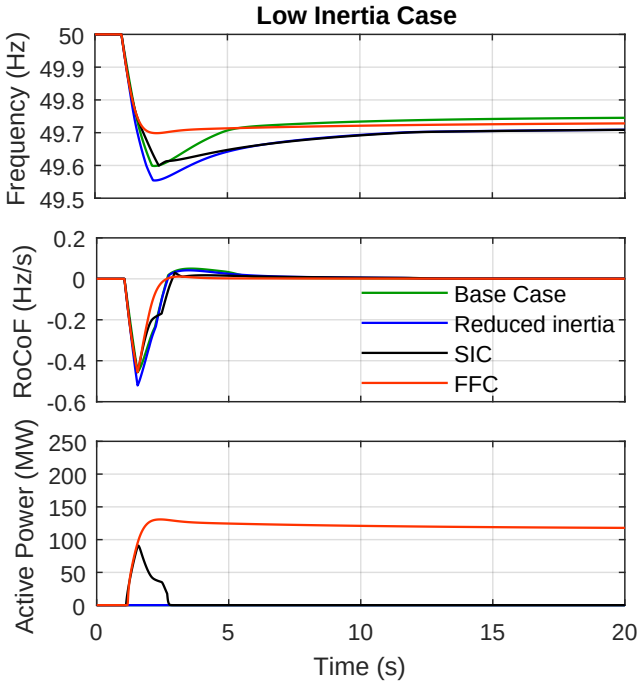

Figure 5. System frequency and RoCoF Low inertia

In the case of low generation inertia (i.e. 16649 MWs), Figure 5 shows the ability of FFC and SIC in mitigating the maximum average RoCoF value by compensating for the reduced generation's inertia. Due to the system low inertia, the frequency deviation was larger and steeper which led to faster activation of the FFC compared to the high inertia case. However, the FFC still requires a larger amount of MW to compensate for the reduced generators' inertia compared to the SIC. To be noted, also in this case the SIC was triggered before FFC due to the different deadband

B. Scenario 2

In the second scenario 780 dispatches are used. It aims at defining the relationship between 1 MW of FFC (or SIC) and MWs of synchronous inertia.

Applying the previously proposed methodology over the various dispatches, Figure 6 shows the relationship between MW to MWs and maximum average RoCoF (i.e. measured over 500 ms) for the FFC control approach. The Y axis represents the MWs that can be replaced by 1 MW of FFC while the X axis represents the pre-contingency maximum average RoCoF following the loss of the LSI. The blue dots

are the different dispatches. On one hand, the relation between MW to MWs is not constant over the different dispatches, however one can see a clear trend between the MW to MWs and the system maximum average RoCoF. Using MATLAB's fitting algorithm, it was possible to determine the 3rd order polynomial regression among the different dispatches, represented by the following function: $y = -3.3e03x^3 - 3.8e03x^2 - 1.4e03x - 1.2e02$.

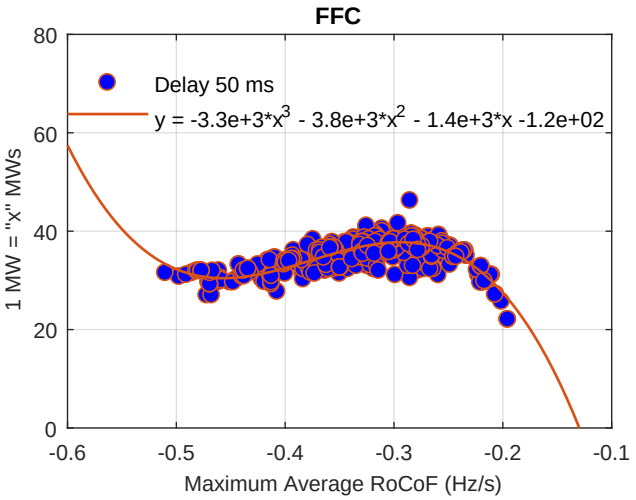

Figure 6. Relationship between MW/MWs and RoCoF FFC

One can notice that for low inertia cases and/or larger infeed loss (i.e. fast RoCoF), the equivalent MWs of inertia that can be substituted with 1 MW of FFC is getting lower. On the other hand, due to the applied deadband as shown and explained in Scenario 1, for high inertia cases and/or small infeed loss, the equivalent MWs of inertia to 1 MW of FFC is also getting lower.

Similarly, the same study was applied on the SIC controller. Figure 7 shows the relation between MWs to MW and the system maximum RoCoF for the SIC control approach. The same dispatches are used.

Likewise the FFC, for low inertia cases and/or larger infeed loss (i.e. fast RoCoF), the equivalent MWs of inertia that can be substituted with 1 MW of SIC is lower than for high inertia cases. On the contrary, for high inertia cases the equivalent MWs of inertia to 1 MW of SIC is not decreasing as for FFC. This behavior is due mainly to the different deadband between the two controllers. In other words, the 80 mHz/s deadband does not limit the SIC participation as the 80 mHz for FFC.

C. Scenario 3

To better understand the effects of the fast acting reserves' time response on the relation between MW and MWs and on the overall system stability, a sensitivity analysis of the device's response time is carried out. The following time delays (i.e. response time) are applied: 50 ms, 100 ms and 150 ms. The chosen values are inspired from different energy storage manufactures' data sheet [15]–[17].

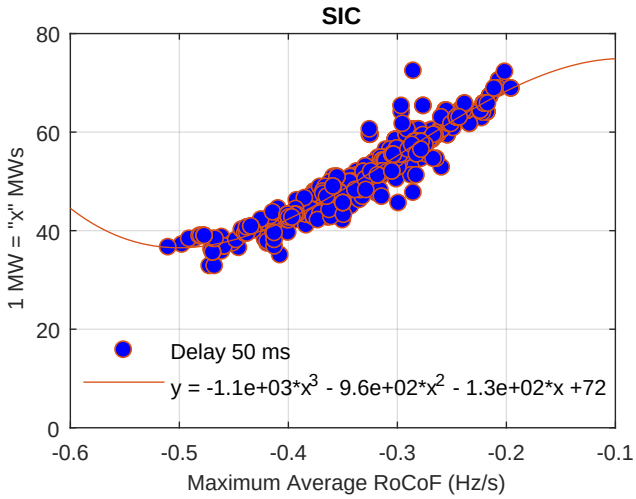

Figure 7. Relationship between MW/MWs and RoCoF SIC

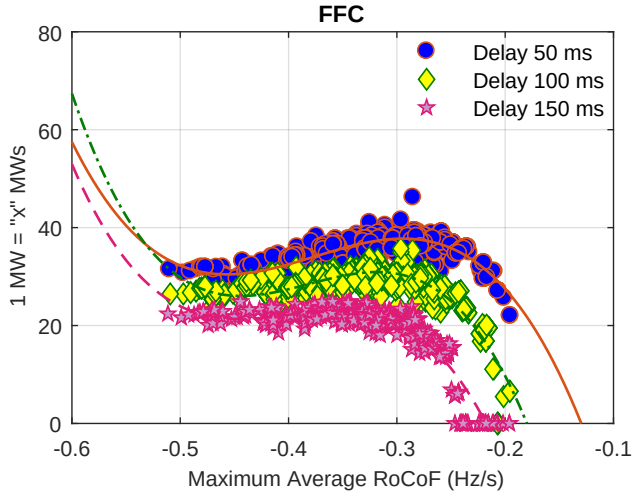

Figure 8. Response time sensitivity analysis - FFC

Figure 8 shows the time delay effect on the relationship between MW and MWs when FFC is applied. It can be noticed that the larger response time reduced the FFC effects on mitigating the RoCoF leading to the need of larger reserves. However, in some dispatches, the larger response time led to frequency oscillations and therefore no solution was found In fact, due to the delay, the controller is acting on system conditions that were occurring for example 150 ms in the past and not on the current conditions [18]. For dispatches with high inertia and/or small infeed loss, employing 150 ms delay with the 80 mHz deadband, the controller was not able to mitigate the maximum average RoCoF since it was occurring before the unit's response (i.e. represented by zero on the x axes). Figure 8 points out that the units' characteristics (e.g. response time, ramp rate etc...) will influence the 3rd order regression and therefore the method needs to be applied for each group of units of certain characteristics allowed to

participate in this grid service.

Similarly to the FFC, Figure 9 shows the time delay effects when the SIC is applied. Also in this case, the larger response time reduced the effect of SIC in improving the RoCoF, which it can be seen from the 3rd order polynomial regressions of the three utilized response times.

Due to the different deadband used by the two controllers, SIC was able to participate in mitigating the RoCoF for all the tested dispatches. On the other hand, applying SIC, the system was more vulnerable to oscillation in a much higher number of dispatches compared to FFC and the larger response time has amplified the amplitude of the oscillation.

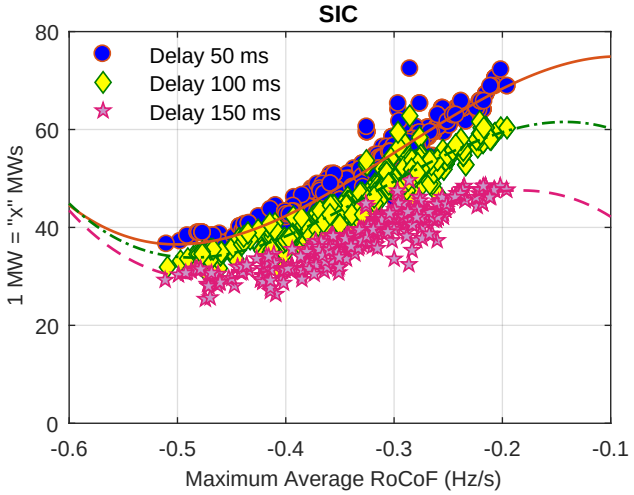

Figure 9. Response time sensitivity analysis - SIC

D. Scenario 4

To better investigate the effects of the used deadband on the controllers' performance and on the relation between MW and MWs, this scenario carries out a sensitivity analysis on the deadband applied on the control signal. Since this study assumes that this inertia service is a contingency based service, it has been decided to use deadband values relatively larger than the frequency deadband present on conventional generators and interconnectors established by the grid code [19]. For example, Republic of Ireland's grid code requires that a frequency deadband of no greater than +/- 15 mHz may be applied to the operation of the governor control system [20]. In this study the following deadband values are used for FFC: 80 mHz, 120 mHz and 300 mHz. Similarly, for the SIC the following deadband values are used: 80 mHz/s, 120 mHz/s and 300 mHz/s.

Fig. 11 shows that the larger deadband reduced the effects of FFC in mitigating the RoCoF. Employing 120 mHz deadband, for high inertia cases and/or small infeed loss, the controller was not able to influence the maximum average RoCoF since it was occurring within the applied deadband. Applying 300 mHz deadband, FFC was not able to participate in any of the dispatches since all the congestions were occurring within the deadband. On one hand, employing a large deadband will limit the FFC participation to large congestion cases avoiding its activation following normal load change On the other hand, Fig. 11 points out that employing a large deadband will reduce the equivalent MWs that can be replaced by 1 MW of FFC as might also make the controller completely useless as the case with 300 mHz deadband.

Fig. 12 shows that the larger deadband reduces the equivalent MWs that can be replaced by 1 MW of SIC. For low inertia cases and/or larger infeed loss (i.e. fast RoCoF), one can notice that applying 120 mHz/s deadband, the SIC performance did not differentiate so much from 80 mHz/s deadband. On the other hand, employing 300 mHz/s deadband limited the SIC participation for the majority of dispatches and imposed oscillation for the remaining ones.

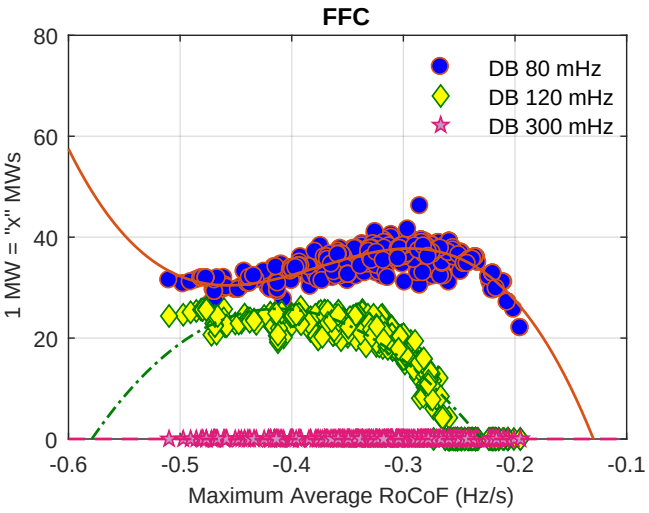

Figure 10. Deadband sensitivity analysis - FFC

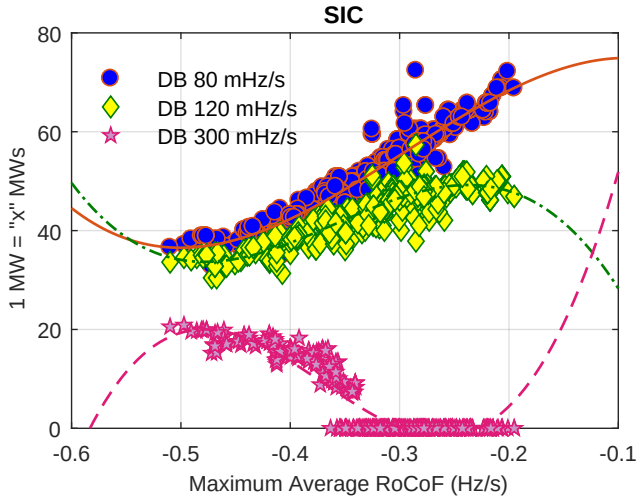

Figure 11. Deadband time sensitivity analysis - SIC

IV. Discussion

This study investigated the ability of FFC and SIC in mitigating the RoCoF and compensating for the system inertia reduction. To allow a generic result and to guaranty the applicability of the methodology on any system and by any FAR unit, a technology neutral approach was applied. It aims at allowing any technology that is capable of providing this service to be eligible. For example, this service may be provided by technologies such as HVDC interconnectors, energy storages and other emerging technologies. To be noted, the proposed methodology has been tested on an equivalent model of the Republic of Ireland and Northern Ireland power system but that does not limit its applicability on other systems since no direct connection between the equivalent model and the methodology is present.

The application of the presented methodology can assess the system operator in increasing the penetration of renewable energy by reducing the inertia floor while respecting the grid code constraint of maximum RoCoF. For example, during the dispatch phase, the system operator knows the maximum RoCoF by knowing the generation inertia and the LSI. Having access to the 3rd order polynomial regression, the operator will thus be able to find the relationship between MW and MWs and therefore he will be able to replace the desired amount of MWs by FFC or SIC.

The analysis showed that with the tested deadbands and response times, 1 MW of SIC was able to compensate for a higher amount of MWs compared to FFC. On the other hand it showed that SIC has a higher probability in leading to system oscillation compared to FFC. It also showed that FFC was able to improve the frequency nadir and the steady state value improving the overall system stability. However, it should be noted that although FAC can replace inertia from conventional plant, they are still need for synchronous torque and voltage stability. In fact, FAC will need to be used in conjunction with other technologies (e.g. rotating condensers) for large scale integration.

V. Conclusion and future works

This work showed the ability of fast acting reserves in mitigating the RoCoF when such reserves are controlled by frequency deviation based control or by RoCoF based control. Exploiting more than 700 simulated dispatches of the All Island power system, it was possible to define an analytical relationship between MW of reserve and MWs of synchronous inertia for the two applied control mechanisms (i.e. FFC and SIC). Future work will consider the activation of the reserves based on a threshold to analyse the effects and possibility of mitigating the RoCoF through a threshold based control using both FFC and SIC. Further analysis will also analyse the effects of measuring the RoCoF over a different time window on the controllers' performance and the frequency stability. Also, various control technique such as hysteresis control will be investigated to understand and counteract the frequency oscillation due to the implementation of the two controllers.

References

[1] DNV GL Energy Advisory, "RoCoF Alternative Solutions Technology Assessment," tech. rep., EIRGRID, 2015.

[2] P. Daly, D. Flynn, and N. Cunniffe, "Inertia Considerations within Unit Commitment and Economic Dispatch for Systems with High Non-Synchronous Penetrations," in *PowerTech IEEE*, (Eindhoven), pp. 1–6, 2015.

[3] J. Brisebois and N. Aubut, "Wind Farm Inertia Emulation to Fulfill Hydro-Québec's Specific Need," in *Power and Energy Society General Meeting IEEE*, vol. 7, pp. 1–7, 2011.

[4] National Grid, "Fast Reserve Service Description," Tech. Rep. April, 2013.

[5] ERCOT, "Future Ancillary Services in ERCOT," tech. rep., 2013.

[6] H. T. Nguyen, G. Yang, A. H. Nielsen, and P. H. Jensen, "Frequency Stability Improvement of Low Inertia Systems Using Synchronous Condensers," in *Smart Grid Communications IEEE*, pp. 1–6, 2016.

[7] M. Rezkalla, A. Zecchino, S. Martinenas, A. M. Prostejovsky, and M. Marinelli, "Comparison between Synthetic Inertia and Fast Frequency Containment Control Based on Single Phase EVs in a Microgrid," *Applied Energy*, pp. 1–12, 2017.

[8] M. Rezkalla, M. Marinelli, M. Pertl, and K. Heussen, "Trade-off Analysis of Virtual Inertia and Fast Primary Frequency Control during Frequency Transients in a Converter Dominated Network," in *Innovative Smart Grid Technologies - Asia (ISGT-Asia), IEEE*, (Melbourne, VIC, Australia), pp. 1–6, 2016.

[9] P. Kundur, J. Paserba, V. Ajjarapu, G. Andersson, A. Bose, C. Canizares, N. Hatziargyriou, D. Hill, A. Stankovic, C. Taylor, T. Van Cutsem, and V. Vittal, "Definition and Classification of Power System Stability," *IEEE Transactions on Power Systems*, vol. 21, no. 3, pp. 1387–1401, 2004.

[10] H. W. Qazi, Z. H. Rather, and D. Flynn, "Impact of Large Scale Demand Side Response on System Frequency- A Case Study," in *PowerTech IEEE*, (Eindhoven), pp. 1–6, 2015.

[11] EirGrid and SONI, "All-Island Generation Capacity Statement," tech. rep., 2017.

[12] J. O'Sullivan and M. O'Malley, "Identification and Validation of Dynamic Global Load Model Parameters for Use in Power System Frequency Simulations," *IEEE Transactions on Power Systems*, vol. 11, no. 2, pp. 851–857, 1996.

[13] J. O'Sullivan, A. Rogers, and A. Kennedy, "Determining and implementing an approach to system frequency and inertial response in the Ireland and Northern Ireland power system," in *Power and Energy Society General Meeting IEEE*, pp. 1–6, 2011.

[14] J. O'Sullivan, A. Rogers, D. Flynn, S. Member, P. Smith, A. Mullane, and M. O'Malley, "Studying the Maximum Instantaneous Non-Synchronous Generation in an Island System Frequency Stability Challenges in Ireland," *IEEE Transactions on Power Systems*, vol. 29, no. 6, pp. 2943–2951, 2014.

[15] International Electrotechnical Commission, "Electrical Energy Storage," tech. rep.

[16] US Department of Energy, "Grid Energy Storage," Tech. Rep. December, 2013.

[17] NGK INSULATORS, "Structure of NAS Energy Storage System Principle of NAS Battery," tech. rep.

[18] S. Donnelly, S. Mattix, D. Trundowski, and J. Deagle, "Autonomous Demand Response for Primary Frequency Regulation," Tech. Rep. January, U.S Department of Energy, 2012.

[19] N. W. Miller, M. Shao, S. Pajic, and R. D. Aquila, "Eastern Frequency Response Study," Tech. Rep. May, 2013.

[20] EirGrid, "System Services for Interconnectors," tech. rep., Dublin, 2012.

Department of Electrical Engineering
Center for Electric Power and Energy (CEE)
Technical University of Denmark
Elektrovej, Building 325
DK-2800 Kgs. Lyngby
Denmark

www.elektro.dtu.dk/cee
Tel: (+45) 45 25 35 00
Fax: (+45) 45 88 61 11
E-mail: cee@elektro.dtu.dk